Neuromodulatory inputs generate and optimize neural responses and behavioural perception to second-order natural sensory stimuli

Chengjie (Gary) Huang

Department of Physiology,
McGill University.
Montreal, Quebec, Canada

August 2018

A thesis submitted to the faculty of Graduate Studies and Research in partial fulfillment of the degree of Doctorate in Philosophy

To My Grandfather

Table of Contents

Abstract

Sensory systems have evolved to optimally encode stimuli found in the natural environment. In order to achieve this optimal coding, neural coding strategies in many sensory systems have been adapted to the natural scene statistics to efficiently encode sensory stimuli. Thus, neurons within sensory systems must perform numerous complex computations in a concerted manner in order to give rise to what we perceive as the external world. In this thesis, I studied how sensory neurons in the hindbrain encode and process natural second-order sensory stimuli in the weakly-electric fish. These neurons in the hindbrain area, electrosensory lateral line lobe (ELL) receive a multitude of inputs from both feedforward and feedback and it is unknown to date how these determine neural coding and behavioural perception.

I first characterized how second-order electrosensory signals are processed within the many subclasses of pyramidal neurons in the ELL. We hypothesized that the ELL of the weakly-electric fish utilizes the three different segments for parallel coding. Specifically, the pyramidal neurons will respond differentially to natural sensory stimuli in the three segments so as to preserve a copy of the stimulus containing all its redundancies in the bandpass filtering CMS segment, while the high-pass filtering LS segment temporally decorrelates the stimulus in order to remove the redundancies. When working in parallel and in combination with one another, stimulus information and its statistics could therefore be segregated, filtered, and recombined to be passed on to successive brain areas for higher-order processing. Using standard in vivo extracellular electrophysiology techniques, we recorded neurons from all subclasses of pyramidal neurons and found that there are differential tuning properties within the ELL to confirm our hypothesis. Indeed, LS neurons were able to perform temporal whitening, while CMS neurons preserved the stimulus statistics. This would lead to the idea that this is a feasible coding strategy in order to properly decode optimized information sent in parallel through temporally whitened responses based on context downstream of the ELL in higher brain areas.

Next, I explored further into how pyramidal neurons in the ELL perform temporal whitening. What kind of cellular machinery would enable the pyramidal neuron to achieve high-pass tuning to match and oppose those of decaying power-law natural stimulus statistics, and thus efficient neural coding? A highly likely candidate for this role is the small-conductance calcium-activated potassium (SK) channel. SK channels are specialized calcium-dependent

potassium channels commonly found in many brain regions and is crucial to many functions of the nervous system. We hypothesized that SK channels provide the underlying molecular mechanism which gives rise to power-law adaptation in pyramidal cells and hence optimal neural encoding of natural sensory stimuli. Furthermore, we hypothesized that SK channels could alter neural tuning in a way such that it also alters behavioural perception in a predictable manner. Using a combination of pharmacology, electrophysiology, and behavioural paradigms, we observed that SK channels do indeed determine the degree of high-pass tuning, and that altering the SK channel conductance changes neural tuning and behaviour of the animal in a predictable way. These results suggest that SK channels play a novel critical role in which the nervous system can implement efficient processing and perception of natural sensory input that is likely to be shared across systems and species.

Finally, I questioned whether efficient processing of second-order natural stimuli is due to a combination of both feedforward and feedback input. For this purpose, I initially asked how the envelope response in pyramidal cells is generated in the first place. By using a linearly increasing envelope stimulus, we aimed to determine exactly how low of a stimulus intensity is needed to generate an envelope response in different neurons along the electrosensory pathway. By performing extracellular electrophysiology recordings from electrosensory afferents (EAs), pyramidal cells in the ELL, stellate cells in the nucleus praeeminentialis (nP), in conjunction with pharmacological feedback block of the nP, we observed that feedback (in particular the direct feedback pathway) is necessary to generate the envelope response in pyramidal cells, and hence, the behavioural output for low contrast envelope stimuli. Subsequently, we also performed similar experiments exploring the role of feedback in determining the optimized neural tuning across envelope frequencies. Using a combination of electrophysiology, pharmacology, and behavioural paradigms, we observed that multipolar neurons in the nP, which are the source of the indirect feedback pathway, was necessary in shaping the high-pass tuning observed in the pyramidal neurons in the ELL. Our results from these studies thus provide the first experimental evidence that feedback generates and optimizes both neural and behavioral responses to low contrast stimuli that are commonly found in the natural environment.

Résumé

Les systèmes sensoriels ont évolué pour encoder de façon optimale les stimuli présents dans l'environnement naturel. Afin d'obtenir ce codage optimal, les stratégies de codage neuronal dans les systèmes sensoriels sont adaptées aux statistiques de la scène naturelle. Ainsi, les neurones des systèmes sensoriels doivent effectuer de nombreux calculs complexes de manière concertée afin de donner naissance à ce que nous percevons comme le monde extérieur. Dans cette thèse, j'ai étudié comment les neurones sensoriels primaires du cerveau postérieur codent et traitent les stimuli sensoriels naturels de deuxième ordre chez les poissons faiblement électriques. Ces neurones dans la région du cerveau postérieur, le lobe de ligne latérale électrosensorielle (ELL), reçoivent une variété d'entrées à la fois prospection et rétroaction et on ignore à ce jour comment ces entrées neuromodulatrices s'intègrent pour déterminer le codage neuronal et la perception comportementale.

J'ai d'abord caractérisé comment les signaux électrosensoriels de deuxième ordre sont traités dans les nombreuses sous-classes de neurones pyramidaux du ELL. Nous avons émis l'hypothèse que l'ELL du poisson faiblement électrique utilise les trois segments différents pour le codage parallèle. Spécifiquement, les neurones pyramidaux répondront différemment aux stimuli sensoriels naturels dans les trois segments de manière à conserver une copie du stimulus contenant toutes ses redondances dans le segment CMS filtrant la bande passante, tandis que le segment LS filtrant passe-haut décorrélera temporellement le stimulus afin de supprimer les redondances. En travaillant en parallèle et en combinaison les uns avec les autres, l'information de stimulus et ses statistiques pourraient donc être séparées, filtrées et recombinées pour être transmises à des zones cérébrales successives pour un traitement d'ordre supérieure. En utilisant des techniques standard d'électrophysiologie extracellulaire in vivo, nous avons enregistré des neurones provenant des sous-classes de neurones pyramidaux et nous avons trouvé qu'il y avait des propriétés sélectivité au sein de l'ELL pour confirmer notre hypothèse. En effet, les neurones LS étaient capables d'effectuer un blanchiment temporel, alors que les neurones CMS conservaient les statistiques de stimulus. Cela conduirait à l'idée qu'il s'agit d'une stratégie de codage réalisable permettant de décoder correctement les informations optimisées envoyées en parallèle à travers des réponses temporellement blanchies basées sur le contexte en aval de l'ELL dans les zones cérébrales supérieures.

Ensuite, j'ai exploré comment les neurones pyramidaux dans l'ELL effectuent un blanchiment temporel. Quel type de machinerie cellulaire permettrait au neurone pyramidal de réaliser un accord passe-haut pour faire correspondre et opposer ceux des statistiques de stimulus naturel de puissance décroissante, et donc un codage neural efficace? Un candidat très probable à ce rôle est le canal de potassium à faible conductance activé par le calcium (SK). Les canaux SK sont des canaux potassiques calcium-dépendants spécialisés que l'on trouve couramment dans de nombreuses régions du cerveau et qui sont cruciaux pour de nombreuses fonctions du système nerveux. Nous avons émis l'hypothèse que les canaux SK fournissent le mécanisme moléculaire sous-jacent qui donne lieu à une adaptation de la loi de puissance dans les cellules pyramidales et donc un codage neural optimal des stimuli sensoriels naturels. De plus, nous avons émis l'hypothèse que les canaux SK pourraient modifier l'accord neuronal d'une manière telle qu'il modifierait également la perception comportementale d'une manière prévisible. En utilisant une combinaison de pharmacologie, d'électrophysiologie et de paradigmes comportementaux, nous avons observé que les canaux SK déterminent en effet le degré d'accord passe-haut et que la modification de la conductance du canal SK modifie sélectivité neuronale et le comportement de l'animal de manière prévisible. Ces résultats suggèrent que les canaux SK jouent un nouveau rôle s'avérant critique. Grâce à ces canaux, le système nerveux pourrait effectuer un traitement d'information efficace ainsi permettrait la perception de l'apport sensoriel naturel susceptible d'être partagé entre les systèmes et les différentes espèces.

Enfin, je me suis demandé si le traitement efficace des stimuli naturels de second ordre était dû à une combinaison de prospection et de rétroaction. À cette fin, j'ai d'abord demandé comment la réponse de l'enveloppe dans les cellules pyramidales est générée en premier lieu. En utilisant un stimulus d'enveloppe augmentant linéairement, nous avons cherché à déterminer l'intensité minimale d'un stimulus permettant de générer une réponse d'enveloppe dans différents neurones le long de la voie électrosensorielle. En effectuant des enregistrements électrophysiologiques extracellulaires à partir d'afférences électrosensorielles (EA) de cellules pyramidales dans l'ELL et de cellules stellaire dans le noyau praeeminentialis (nP), en conjonction avec le blocage pharmacologique du nP, nous avons observé que cette rétroaction (en particulier la voie de rétroaction directe) est nécessaire pour générer la réponse d'enveloppe

dans les cellules pyramidales, et par extension, la réponse comportementale pour les stimuli d'enveloppe à faible contraste. Par la suite, nous avons également effectué des expériences similaires explorant le rôle de la rétroaction dans la détermination de l'optimisation neuronale à travers les différentes fréquences d'enveloppe. En utilisant une combinaison d'électrophysiologie, pharmacologie et paradigmes comportementaux, nous avons observé que les neurones multipolaires dans le nP, qui sont la source de la voie de rétroaction indirecte, étaient nécessaires pour façonner filtre passe-haut observé dans les neurones pyramidaux de l'ELL. Nos résultats de ces études fournissent ainsi la première preuve expérimentale que la rétroaction génère et optimise à la fois les réponses neuronales et comportementales à des stimuli à faible contraste qui sont couramment trouvés dans l'environnement naturel.

Acknowledgements

My experience as a graduate student at McGill University has been one that I will remember and treasure forever. Below, I would like to thank the people who I am indebted to, who have made this dissertation possible, and the people who have supported me every step of the way.

First and foremost, I would like to thank Dr. Maurice Chacron for the wonderful opportunity to work with him for the past 5 years. This has truly been a memorable experience and I have no regrets in joining his lab. Over the past 5 years, I have learned so much, not only about science, but also about life as an individual of society. With his dedicated guidance, I have matured into a capable and confident science, ready to take the next steps in my life. I thank Dr. Chacron for all the opportunities he has given me in my career, such as introducing me to many brilliant scientists both within and outside the field of weakly-electric fish research, as well as allowing me to become a teaching assistant for the prestigious Neural Systems & Behaviour Course at the Marine Biological Laboratory. I would also like to thank him for the incredible project ideas for which we worked on together over the course of my dissertation, many of which benefitted myself as a growing scientist and my future career as well. Dr. Chacron is and will always be one of the most important mentors of my entire life.

I would like to thank all the members of my supervisory committee Drs. Erik Cook, Christopher Pack, Alanna Watt, Kathleen Cullen, and Julio Martinez-Trujillo, who have sat through several years of my committee meetings, and provided guidance and constructive criticisms throughout this dissertation. I would like to also give special thanks to Dr. Eric Fortune for being a wonderful mentor as well for all these years and bestowing me his trusty laser pointer.

I would next like to thank Dr. John Orlowski and Dr. John White, first for the many Friday seminar classes and seminars I had to sit through, but also learned a wide variety of science pertaining to physiological systems that I would not have otherwise been exposed to; and second, both for serving as Chairs of the Physiology Department and signing the many forms I needed signed when necessary. I would also like to thank all those in the Physiology departmental staff, in particular Rosie Vasile, for putting up with all my questions and helping me make sure that I have completed all the requirements for this degree.

Next, I would like to thank both present and past members of Dr. Chacron's lab. I would like to especially thank Dr. Michael "Maso" Metzen, for whom has been a wonderful friend and mentor to me in the lab. Dr. Metzen taught me the necessary techniques such as surgery and electrophysiology, MATLAB coding, entirely from scratch. I would like to thank him for aiding in the projects in Chapters 4 and 5 of this thesis, which would not have been possible without his contributions and assistance. I would like to thank him for teaching me everything he knows, and I will always treasure the unforgettable lessons he has bestowed upon me. Finally, I would also like to thank him for the endless discussions, both scientific and non-scientific, and in helping me grow as a person.

I would like to also thank Dr. Volker Hofmann, for keeping me on my toes and being the critical voice that has helped me improve and have a "standard" for good science as well as figure making. I would also like to thank Dr. Hofmann for all the skills I have learned regarding electrical hardware, and having the patience to teach me how to work with all the tools in the lab to optimize my setups. Lastly, thank you for all the fruitful discussions and being a wonderful office mate for the past few years.

I would like to thank Mariana Marquez-Machorro, who has been an amazing friend and labmate. I would like to thank her for all our discussions about people, life, and science, as well as truly enlightening me to a different perspective on many things. I would also like to thank her for being an encouraging and positive individual in my life and always being there with unwavering support when I needed her. I only hope to have a labmate as great as her in the future, and I wish her all the best with the rest of her PhD and future in academia.

I would lastly like to thank the other members of the Chacron lab: Chelsea Kim, Michael Sproule, Dr. Diana Martinez, Dr. Rhalena Thomas, Teerawat Monnor, Zhubo (Drew) Zhang, Tristan Aumentado-Armstrong, Qixin Yang, and Yujing Zou for being amazing friends and labmates.

Outside of the Chacron Lab, I would like to especially thank my parents, Zhaohui Huang and Yan Xue, for supporting me throughout my entire academic career. I still think IB in high school was a bad idea, but I guess in the end I still ended up with a Doctorate degree many years later. Thank you both for working so hard to immigrate to Canada and allowing me the chance to

experience growing up in Canada and having the access to the best education in the world. I am truly privileged to be your son.

I would also like to thank all the wonderful friends I have made throughout my 8-year journey through undergraduate and graduate school here at McGill University: Andy Gao for giving me a place to live throughout my graduate studies, and for being one of my best friends I've had since first-year in undergrad, Nancy Shie, Linda Zhang, Mike Zou, Jeffrey Leung, Theresa Tang, Vanessa Chan, Charlie Chang, Echo Wang, Peter Lee, Joy Wang, Christina Qian, Calvin Liang, Morgan Yang, and Nicole Liu, for being some of the first and best friends I have made for a lifetime at McGill since the beginning, Jonathan Cote, who has kindly been my friend since the start of graduate school and special thanks for helping me translate my thesis abstract, Larissa Ferguson, Aimee Chan, Lawrence Chen, Yi Gao, Marisa Cressatti, Yuki Sato, Francis Wong, Victor Dumitru, Ryan Rys, Boyan Woychyshyn, Katarina Pessina, Miguel Romero Sepúlveda, Laurent MacKay, Alexis Dale, Diana Mitchell, Vanessa Chang, Sophie Park, Mat Leavitt, Giselle Boukhaled, Hannah Guak, and Soyoon Won, for being the greatest friends and brightest people I have met in graduate school.

Thank you all for everything.

Contribution of Authors

Chapter 2 (Manuscript)

Dr. Maurice J. Chacron designed research; Chengjie G. Huang performed research; Chengjie G. Huang analyzed data; Chengjie G. Huang and Dr. Maurice J. Chacron wrote the paper. This work was supported by the Fonds de recherche du Quebec–Nature et Technologies and the Canada Research Chairs (Maurice J. Chacron).

Chapter 3 (Manuscript)

Dr. Maurice J. Chacron designed research. Chengjie G. Huang and Zhubo D. Zhang performed research and analyzed the data. Chengjie G. Huang and Dr. Maurice J. Chacron wrote the paper. This research was supported by the Fonds de recherche du Quebec—Nature et technologies, the Canadian Institutes of Health Research, and the Canada research chairs (Maurice J. Chacron). We thank Dr. Rudiger Krahe for critical reading of the manuscript.

Chapter 4 (Manuscript)

This is a co-first authored manuscript. Michael G. Metzen and Chengjie G. Huang contributed equally to this work. Dr. Maurice J. Chacron designed research. Michael G. Metzen and Chengjie G. Huang performed research and analyzed the data. Michael G. Metzen, Chengjie G. Huang and Dr. Maurice J. Chacron wrote the paper. This research was supported by the McGill University Faculty of Medicine, Fonds de recherche du Quebec—Nature et technologies, the Canadian Institutes of Health Research, and the Canada research chairs (Maurice J. Chacron).

Chapter 5 (Manuscript under Review)

This is a co-first authored manuscript. Chengjie G. Huang and Michael G. Metzen contributed equally to this work. Dr. Maurice J. Chacron designed research. Chengjie G. Huang and Michael G. Metzen performed research and analyzed the data. Chengjie G. Huang, Michael G. Metzen, and Dr. Maurice J. Chacron wrote the paper. This research was supported by the McGill University Faculty of Medicine, Fonds de recherche du Quebec—Nature et technologies, the Canadian Institutes of Health Research, and the Canada research chairs (Maurice J. Chacron).

Chapter 1

General Introduction

The natural world which we experience is made up of nearly endless complex stimuli. The way we can interact with the natural world relies on our perception, and critically, our sensory systems. The transduction from seeing a red apple or hearing a bird sing into a series of electrical signals, called action potentials, also known as the neural code, is a central question of neuroscience investigation. The question of perception has sparked the curiosity of mankind since the time of Aristotle when he first claimed that there were "the five senses." Today, we know that cells in the central nervous system, called neurons, are able to integrate information received from peripheral sensory receptors and perform complex computations in order to give rise to our perception of the world and drive appropriate behavioural responses.

Despite our current knowledge, the complex computations which translate natural sensory stimuli to a series of action potentials remains a mystery, as solving the problem requires asking fundamental questions and understanding why and how neurons perform such computations in order to generate perception. One of the most important categories of sensory stimuli in our natural world are interaction signals with conspecifics. For humans, whether these are communication signals such as spoken or written language, sign language, or even traffic lights and signs, they are all processed by our brain to mean something, for us to understand one another. However, these interaction signals in nature often contain a complex and rich spatiotemporal structure, which must be processed by the neurons in sensory systems. One example of this type of natural stimuli is second-order stimuli, which corresponds to amplitude modulations in speech, contrast detection in vision, etc. Unfortunately, very little is known about how they are processed in biological systems. This is the fundamental and central question of this dissertation and I will attempt to investigate this question by approaching it using the electrosensory system of the weakly-electric fish. We will use the weakly-electric fish because it offers unique advantages such as its well-characterized anatomy and physiology, as well as the possibility to simultaneously capture *in vivo* neural activity and behaviour.

In this introductory chapter, I will first review how I addressed this question during my graduate studies by introducing the essential concepts such as the model animal of choice (weakly-electric fish), the types of electrosensory interaction signals between conspecifics, the neural anatomy and circuitry in which these signals are potentially processed, as well as possible efficient information coding mechanisms in the brain. These sections will provide the framework in which my dissertation is structured.

1.1 – Animal Model

The ideas presented above provide a general rationale as to why it is important to study the key questions pertaining to sensory processing of natural stimuli. However, our ultimate goal is to be able to tie all these concepts together and provide concrete links between molecular mechanisms, neural processing, and behavioural perception. Therefore, we proposed to use the electrosensory system in the weakly-electric fish to answer the questions in my dissertation. The electrosensory system offers several unique advantages to study the questions addressed above due to its well-characterized anatomy and physiology (see (Chacron et al., 2011; Clarke et al., 2015; Krahe and Maler, 2014; Maler, 2009a, b) for review). It should be noted that while weakly-electric fish are comprised of those who have either a discontinuous "pulse-type" EOD such as the African species, *Gnathonemus petersii*, belonging to the family *Mormyridae*, the focus of my studies are exclusively in the "wave-type" electric fish, who emit a continuous signal, belonging to the family *Gymnotidae* (Bennett, 1971); however, some Gymonotids are also pulse-type. These two families have independently evolved; however, the principle of an active electrosensory system remains common between these fish. The proposed species to perform the studies in my thesis is the South American wave-type weakly electric fish *Apteronotus leptorhynchus*, commonly known as the brown-ghost knifefish. The brown-ghost knife fish generates a continuous quasi-sinusoidal signal called the electric organ discharge (EOD), which it uses in order to sense the environment (Hitschfeld et al., 2009; Krahe and Maler, 2014). The EOD of these animals is sexually dimorphic, with frequencies typically in the 600-800 Hz range for females and higher in the 800-1500 Hz range for males (Krahe and Maler, 2014). The weakly-electric fish utilizes this unique sensory system to detect everything in its environment including objects such as rocks and plants, small prey items such as daphnia, as well as using it to communicate with other conspecifics.

1.2 – Electrosensory Conspecific Interaction Signals

1.2.1 – Amplitude Modulations: First Order

The wave-type weakly-electric fish generate an active electric field around the body in order to sense what is in the environment. However, it is the disturbance or perturbation of this electric field, which gives rise to a stimulus signal to the fish (Bennett, 1971). For example, if there is an object or another conspecific in proximity of the fish, the object or fish's difference in conductivity from the water will perturb the electric field lines causing frequency (FM) or amplitude modulations (AM) (Carlson and Kawasaki, 2006). Hence, we can refer to the EOD of the fish as the zeroth-order stimulus and the perturbations in the form of frequency or amplitude modulations as the first-order stimulus. It is important to note that the FMs and AMs are modulations of the fish's own EOD, and therefore carry the relevant signal. My studies focus on AMs exclusively, as FMs and AMs are processed independently by distinct electrosensory pathways, which will be described later below. While small objects and prey items such as daphnia (local stimuli) cause small AMs to the fish's otherwise constant EOD, the situation becomes more complex during interactions between two conspecific fish (global stimuli) (Nelson and MacIver, 1999; Zupanc and Maler, 1993). This is because in situations in which two conspecifics are in proximity of one another (<1m), their individual electric fields interact in such a way that there is constructive and destructive interference. Similar to sound waves, the resulting signal is a "beat", occurring at a frequency equal to the difference between the two fish's EOD frequencies. For example, if one fish has an EOD frequency of 900 Hz and a nearby fish has an EOD frequency of 910 Hz, the resulting AM would be a modulated signal occurring at 10 Hz (Fig. 1A). Previous literature include extensive studies in regards to AMs that arise from conspecific interactions (Bastian et al., 2002; Bastian and Nguyenkim, 2001a; Engler et al., 2000; Engler and Zupanc, 2001), both in terms of physiology and behaviour. One of the most remarkable behaviours is the jamming avoidance response (JAR). The JAR occurs when two fish are close enough in their emitted EOD frequencies (1-5 Hz difference) such that they are actively jamming each other's signals. This is a detriment to the fish as both fish are essentially blind to the environment. Thus, in order to stop the signal jamming, one of the fish will either increase its own EOD frequency, or in some cases, decrease their own EOD frequency in order to be able to detect what is in the environment again (Kawasaki, 1997; Stamper et al., 2012). In addition to

this, there have been a variety of studies characterizing other communication signals such as "chirps", which are transient increases in one fish's EOD frequency signalling agonistic behaviour, seen between two same-sex fish, as well as many others (Benda et al., 2005; Engler and Zupanc, 2001; Marsat and Maler, 2012).

1.2.2 – Amplitude Modulations of Amplitude Modulations: Second Order – Envelopes

The interaction signals described above are limited to the interactions of two stationary fish. In their natural environment, this is of course not true, as rarely two fish will stay stationary next to one another. Thus, when we introduce the movement of two interacting fish, the quantification of these signals become even more complex. One can simplify this process by first imagining one fish looming perpendicular to another stationary fish at a constant speed (Fig. 1B). The underlying first-order AM signal would still occur at 10 Hz (per our example above), but this constant amplitude 10 Hz signal would be further amplitude modulated at a lower frequency. Therefore, this "amplitude modulation of the amplitude modulation" of the 10 Hz signal can be referred to as a second-order signal, otherwise known as an envelope (Stamper et al., 2013; Stamper et al., 2012). The continuous random approaching and receding motion of the moving fish at a given speed would generate a second-order envelope of a range of frequencies that is much lower than the 10 Hz first-order AM (Fig. 1B). Thus, the envelope carries separate and distinct information about the movement of another moving fish (Metzen and Chacron, 2014; Stamper et al., 2013). Previous literature have looked at these "movement envelopes" in a variety of contexts (Stamper et al., 2013), and the general consensus is that these particular envelopes occur at lower frequencies in the range of as low as 0.03 Hz to 1 Hz. In addition, it is important to note that envelopes can also exceed 1 Hz, which have been previously classified as "social envelopes". These social envelopes are separately categorized because they correspond to when three or more fish are in close proximity and are stationary, the EODs sum and the combined signal which thus consists of two prominent AMs interact to form an overlying time-varying envelope. Such social envelopes do not require movement, but due to the fact that it is an interaction of multiple AMs, the resultant envelope is one which contains higher frequencies > 1 Hz (Stamper et al., 2013). Although there is a clear distinction between movement and social envelopes, the studies presented in this thesis are largely focused on movement envelopes, which occur < 1 Hz. Several studies have also characterized the movement envelope frequency power,

which is an indirect measure of how often these frequencies occur, and it was found that low frequencies occur the most and have the highest power, and higher frequencies occur less often with lowest powers across many orders of magnitude (Fotowat et al., 2013; Metzen and Chacron, 2014). It was also found that the decay in power from low to high envelope frequencies occur in a scale-invariant power-law fashion, a similar feature is found in most natural stimuli of other sensory modalities (Carriot et al., 2017; Lundstrom et al., 2010; Metzen and Chacron, 2014). Note that this is an extremely important feature of natural stimuli and will be discussed in detail throughout this thesis.

Envelopes are not exclusive to the electrosensory system, as the information carried by envelopes is vitally important in sensory processing across different modalities. For example, first-order AMs in the electrosensory system can be compared to sinewave gratings (alternating signals) in the visual system, as well as pure tones found in the auditory system. These first-order signals are all carrier signals of second-order envelope signals, as the envelope in the visual system corresponds to contrast, and amplitude modulations in speech in the auditory system (see (Clarke et al., 2015) for review). Therefore, envelopes carry behaviourally-relevant stimulus information that could be independently processed and are essential to drive neural responses in the brain and ultimately behavioural responses in an organism. Due to the complexity of this question, my thesis will utilize the electrosensory system in order to elucidate how envelope information decoded in the central nervous system.

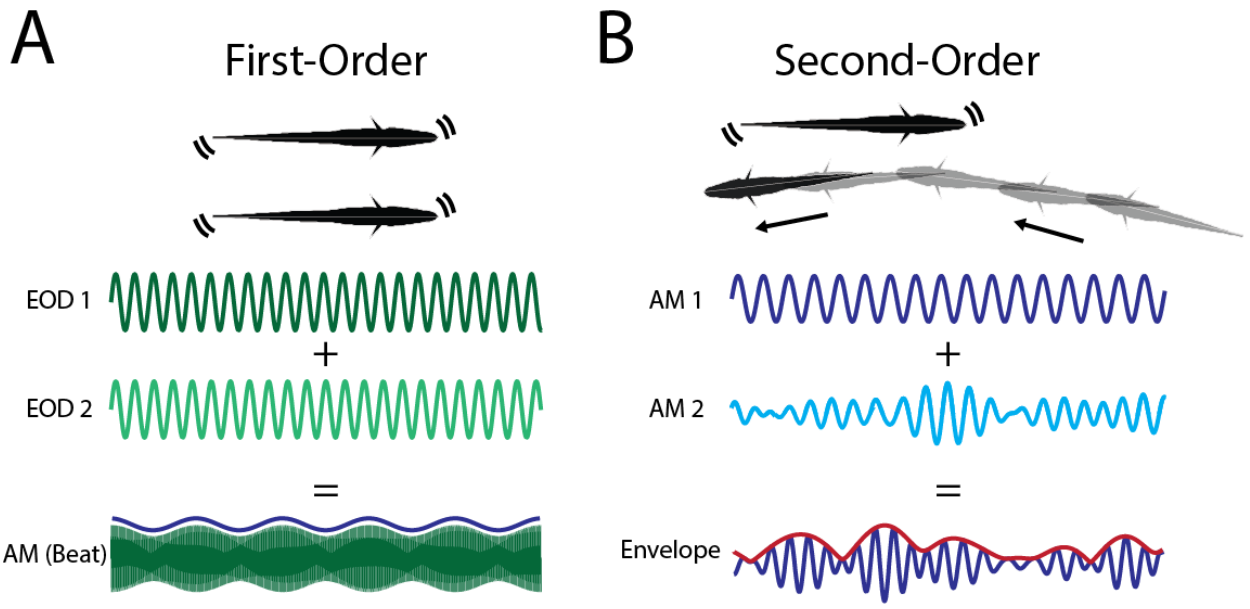

Figure 1. First- and second-order electrosensory interaction signals. A) Two stationary fish within proximity to one another <1 m (top) will each emit their own EOD at a particular frequency (dark green and light green, middle), which gives rise to an amplitude modulation of each fish's EOD frequency called the AM or beat (blue). The resulting AM is at a frequency equal to the difference in EOD frequencies between the two fish. B) One stationary fish and another fish approaching and receding away from the fish (top) will give rise to an amplitude-modulation of the beat (middle), resulting in a second-order stimulus called the envelope (bottom, red). This envelope overlaying on top of the beat is of lower amplitude and frequency compared to the beat.

What is known and what remains to be discovered? While much is known about how first-order signals are processed, relatively little is known regarding second-order signal processing. Much of the electrosensory system literature have focused on first-order signals and it was not until recently that it was found that second-order signals are behaviourally-relevant signals that elicit a behavioural response (Metzen and Chacron, 2014). It is unclear where the envelope response is generated in the electrosensory system and other studies have investigated this. It was shown that both movement envelopes (Metzen and Chacron, 2015) and social envelopes (Savard et al., 2011) do elicit a neural response in peripheral electroreceptor afferents, while other studies did not find this response and instead claim that the envelope response is generated by an inhibitory interneuron in the hindbrain (Middleton et al., 2006). Furthermore, it is likely that envelope responses are generated in the periphery, as another study has found that the midbrain area

contains subsets of neurons which also respond selectively to envelopes (McGillivray et al., 2012). Thus, while we do know there are neural and behavioural responses to envelopes, it is unknown how they are processed in the brain and the underlying mechanisms associated with these processes. Therefore, the focus of my studies in my thesis will answer the fundamental questions in regards to envelopes, and understand how these important signals are processed in the brain in order to give rise to behavioural responses.

1.3 - Neural Anatomy of the Weakly Electric fish – From Receptors to Behaviour

1.3.1 – Peripheral Electroreceptors and Electroreceptor Afferents

The weakly-electric fish offers a unique opportunity to study these questions due to its well-characterized brain anatomy and physiology. As mentioned above, the fish receives both FM and AM signals due to modulations in its EOD. Changes in EOD frequency or amplitude are encoded by tuberous electroreceptors, which are located in pores all over the fish's skin. These pores contain epithelial cells which are connected to an afferent nerve through an excitatory synapse, and thus elicit action potentials to signal changes in EOD frequency or amplitude (Bullock et al., 2005). In wave-type fish, two classes of tuberous electroreceptors exist: the T-type (time coders) which exclusively code the phase and hence frequency of the EOD, and P-type (probability coders), which exclusively code the amplitude of the EOD (Carlson and Kawasaki, 2006; Chacron, 2006; Wessel et al., 1996). Since I am primarily interested in AM and envelope signals, the remainder of the thesis will focus on the encoding from the P-type electroreceptors. The electrosensory afferent nerve (EA) carries information from the electroreceptors up to the brain to the first brain area for electrosensory processing (Krahe et al., 2008), otherwise known as the electrosensory lateral line lobe (ELL) in the hindbrain.

1.3.2 – The Electrosensory Lateral Line Lobe

The ELL serves as the first brain area in which AM information coming from the EAs terminate in a feedforward manner. Anatomically, the ELL is divided into three major segments: the lateral segment (LS), centrolateral segment (CLS), and centromedial segment (CMS). There is an additional segment called the medial segment (MS), which exclusively processes information coming from ampullary electroreceptors, which will not be discussed in this thesis. The EAs from the tuberous electroreceptors trifurcate as they approach the ELL (Fig. 2) (Krahe et al.,

2008), which means that each of the three major segments receive the same incoming information. LS is the smallest and CMS is the largest area, while receptive fields of pyramidal neurons in the LS have the largest size and in the CMS the smallest size (Maler, 2009a; Shumway, 1989). Furthermore, the ELL has largely a cerebellar-like laminar structure which can be divided into eight layers: deep fiber layer (DFL), deep neuropil layer (DNL), granular cell layer (GCL), plexiform layer (PIL), pyramidal cell layer (PCL), stratum fibrosum (StF), Ventral molecular layer (VML) and dorsal molecular layer (DML). The ELL contains sensory neurons called pyramidal cells, whose somata are located in the PCL (Maler, 1979).

The pyramidal neurons can be divided into ON-type cells, which receive direct synaptic input from EAs, and OFF-type cells, which indirectly receive input from EAs via an inhibitory interneuron (Fig. 2). The ON-type cells are named due to their responses to increases in EOD amplitude (i.e. rising or peaks of first-order AM stimuli), while OFF-type cells are named due to their responses to decreases in EOD amplitude (i.e. falling or troughs of first-order AM stimuli)(Maler, 1979; Saunders and Bastian, 1984). These subclasses are similarly typically found in other sensory systems such as primary sensory areas in the visual system, auditory system, etc. Furthermore, the pyramidal cells are arranged in columns such that along each column, pyramidal cells are further subdivided into depth classes: superficial, intermediate, and deep cells. Superficial cells typically have large and extensive apical dendrites, and typically have a spontaneous firing rate of <15 Hz. Intermediate neurons have smaller apical dendrites and typically have a spontaneous firing rate of 15 – 25 Hz. Finally, deep neurons have small apical dendrites and typically have high spontaneous firing rates of >25 Hz (Bastian et al., 2004; Bastian and Nguyenkim, 2001a; Chacron et al., 2005c).

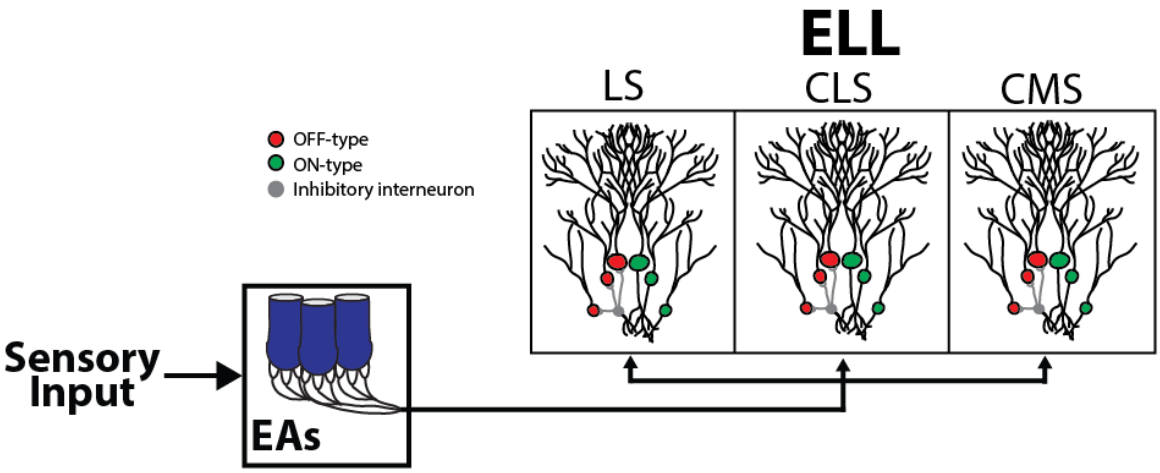

Figure 2. Tuberous electroreceptors project to the Electrosensory lateral line lobe. Tuberous electroreceptors (blue) send projections via afferents (EAs), which trifurcate to synapse onto pyramidal neurons in each of the three major segments: lateral segment (LS), centrolateral segment (CLS), and centromedial segment (CMS). The EAs synapse onto superficial, intermediate, and deep pyramidal neurons, characterized by the arborisation of their dendritic tree, in each segment. Each segment also contains ON- (green) and OFF-type (red) pyramidal neurons, which either synapse directly with EAs or indirectly through an inhibitory interneuron (grey) respectively.

1.3.3 – Beyond the ELL – Higher Brain areas and Feedback

While pyramidal cells are quite similar across the ELL segments, each segment's neurons process incoming feedforward input from EAs very differently. The pyramidal cells are the sole output projection cells of the ELL and thus play a fundamental role in information processing. In addition to the feedforward input from the EAs, the ELL pyramidal cells also receive massive excitatory and inhibitory feedback input from higher brain areas. Neurons from all three segments project to the higher brain area Torus semicircularis (TS) located in the midbrain (Maler, 1979). The TS further projects to even higher brain areas and gives rise to the behaviour we see in the form of changes in EOD frequency such as the JAR. The TS also projects to a major feedback area called the nucleus praeeminentialis (nP), also located in the midbrain (Bastian and Bratton, 1990; Bratton and Bastian, 1990). The nP contains two classes of neurons: stellate cells and multipolar cells. Stellate cells and multipolar cells can be distinguished by their spontaneous firing rate as well as tuning to first-order AM stimuli. Stellate cells typically have

<5 Hz spontaneous firing rate and are tuned to low AM frequencies (<16 Hz) and do not respond to higher frequencies beyond 16 Hz. On the other hand, multipolar cells have high spontaneous firing rates ~80 – 100 Hz, and are tuned to high AM frequencies (>32 Hz). Stellate cells in the nP are responsible for the direct feedback pathway and project directly back to the ELL pyramidal cell proximal dendrites via the StF. Multipolar cells in the nP are instead responsible for the indirect feedback pathway such that they project via the praeeminential tract (PET) first to the Eminentia granularis posterior (EGP), where granule cells in the EGP project back to the apical dendrites of the pyramidal cells in ELL (Bastian and Bratton, 1990; Bratton and Bastian, 1990).

As mentioned in the above sections, the ELL is a fundamental sensory processing area that receives both feedforward and extensive feedback inputs (Summary in Fig. 3). As with other sensory systems, feedback largely outweighs the incoming feedforward inputs, and therefore suggests a functional role for sensory processing. Thus, the ELL pyramidal cells are the primary focus of the studies presented in this thesis with investigations of the inputs coming from surrounding areas in the electrosensory pathway. In the following section, I will describe more in detail the known functions of sensory processing in the ELL as well as present outstanding problems which will set up the rationale for questions of the presented studies in this thesis.

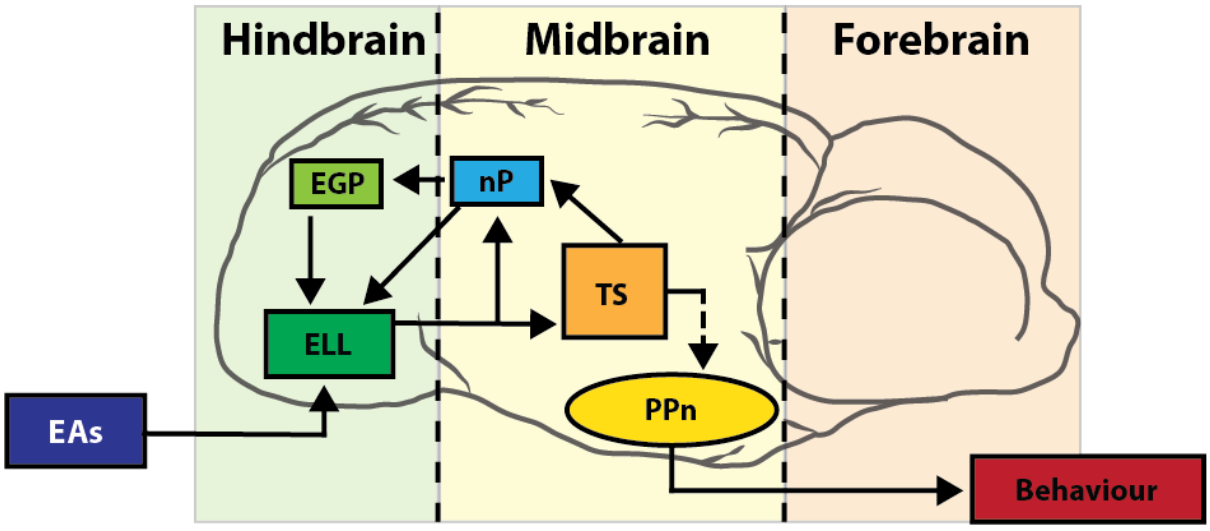

Figure 3. Summary of the electrosensory system pathways. The electroreceptor afferents (EAs) are the sole source of feedforward input to the hindbrain area electrosensory lateral line lobe (ELL), where

pyramidal neurons are located. The pyramidal neurons of the ELL project further downstream via the lateral lemniscus (LL) to the midbrain area Torus semicircularic (TS), which eventually gives rise to behaviour via the pre-pacemaker nucleus (PPn). The TS also sends descending feedback projections to the nucleus praeeminentialis (nP), where stellate and multipolar cells are located. The stellate cells of the nP project through the direct feedback pathway back to the ELL via the stratum fibrosum (StF). The multipolar cells project indirectly back to the ELL via the praeeminential tract (PET) to the Eminentia granularis posterior (EGP), where granule cells in the EGP project back to the apical dendrites of the pyramidal cells in ELL.

1.4 – Functional roles in the ELL and Sensory Processing of Electrosensory Stimuli

1.4.1 – Background

ELL pyramidal cells can be divided into several subclasses based on segment (LS, CLS, CMS) and depth (superficial, intermediate, deep), and can be further classified into ON- and OFF-type cells. There is extensive literature on the sensory processing of first-order AM stimuli, including tuning curves from cells in all 9 subclasses (Chacron et al., 2005c) as well as detailed functional roles of each of the three major ELL segments. Generally, CMS is largely responsible for processing the JAR (Krahe et al., 2008; Metzner and Juranek, 1997). CLS has been shown to be extensively involved in generating the negative image to cancel out signals generated by the fish's own movement in a cerebellar-like fashion (Sawtell, 2017). Finally, LS is known to be responsible for the processing of global stimuli (i.e. interaction and communication signals) between conspecifics (Deemyad et al., 2013; Marsat and Maler, 2012). Several behavioural studies have shown that lesions of LS decrease and attenuate aggressive signals by the fish in response to conspecific electrocommunication signals. On the other hand, lesions of CLS and CMS have no effect on these aggressive signals, thus demonstrating that LS is primarily responsible for electrocommunication (Metzner and Juranek, 1997). Many of the studies presented in this thesis are thus focused on the ELL pyramidal neurons of the LS.

Much of what we have described in the sections up until now deal with first-order AM stimuli, such as "beats" which are simply the sinusoidal amplitude modulation of the fish's EOD occurring at the frequency which is equal to the difference in frequency between two conspecific fish, and "chirps", which are the transient frequency increases in the beats which signal aggression between two conspecifics. Much of the previous studies have focused on these two

categories of stimuli and much is known about how they are processed by pyramidal neurons in the ELL. In addition, we have introduced the concept of "envelopes" which are second-order amplitude-modulated stimuli, and are vastly more complex in their spatial and temporal features. This is because envelopes contain important information about the relative distance and movement between two conspecific fish, adding an additional dimensionality for sensory processing. Although there has been extensive literature on first-order AM stimuli, much less is known about responses to second-order stimuli such as envelopes. However, there are studies which have characterized the natural stimulus statistics of envelopes and observed that the stimulus power is highest at low envelope frequencies and several magnitudes lower at high frequencies, and that this decay in power follows a power-law (Fotowat et al., 2013; Metzen and Chacron, 2014), making it scale-invariant. In addition, we know that playing sinusoidal envelope stimuli to the fish results in a unique behavioural response. In this case, the fish's EOD responds with an increase in frequency (offset), and actually modulates its EOD on top of this offset in a sinusoidal fashion 1:1 to the envelope stimuli (Metzen and Chacron, 2014). Therefore, we know that envelopes elicit a behavioural response, and thus there must be sensory processing happening at the neural level.

1.4.2 – Sensory Processing of envelopes at the periphery

To begin looking at the neural processing side, one recent study has observed envelope responses in the peripheral EAs. It was found that EAs respond to envelopes ranging from 0.05 Hz – 1 Hz in a broadband manner such that all frequencies resulted in similar gain values with a flat tuning curve. However, the EAs displayed wide heterogeneities and only tracked the envelope when the firing rate was saturated or rectified. A linear-nonlinear model was used to explain the gain and phase responses of the EAs, and was able to accurately match up with the experimental data (Metzen and Chacron, 2015). It was theorized that the heterogeneity could increase information transmission, and perhaps this would be true at the next stage of sensory processing in the ELL. Another study demonstrated that correlated activity between EAs could also encode envelopes to an extent, which would also be in line with the fact that hundreds of EA units synapse onto a single pyramidal cell (Metzen et al., 2015). Despite these studies in the EAs, it is unknown whether the pyramidal cells actually respond to envelopes in the manners predicted by the model and experimental data, and further studies were needed in order to confirm these hypotheses. The

question of information transmission also comes into play in a regard that due to the power-law nature of natural envelope stimuli, stimulus information must be efficiently processed further downstream of the EAs to drive behaviour. One interesting point to note is that both the behavioural gain and the stimulus power of the envelope decay as a power-law with similar exponents, and this has been observed experimentally in the studies mentioned above (Metzen and Chacron, 2014). This prompts the question of what exactly happens downstream of EAs in the ELL pyramidal neurons and how exactly their integration of both feedforward and feedback input drive behaviour.

1.4.3 – Sensory Processing Strategies and Efficient Coding Mechanisms

While we do not know how the ELL will respond to envelopes, we can make some predictions based on the anatomy of the ELL itself. Firstly, we know that EAs trifurcate to synapse onto pyramidal cells of each of the three segments. This is important because each ELL segment is receiving the same electrosensory stimuli information and could possibly process them in very different ways similar to how first-order stimuli are processed (McGillivray et al., 2012). The architecture of the ELL also sets up the perfect candidate for parallel processing, similar to what is observed for the dorsal and ventral stream or how the cochlear nucleus is subdivided into segments in the visual and auditory systems respectively (Rauschecker, 2015). Therefore, it is likely that each ELL segment, as well as each of the subclasses of ELL pyramidal cells within each segment, can give rise to different neural responses and tuning curves to envelope stimuli. This opens up the possibility that a variety of differential responses could efficiently encode the various statistics found in the natural envelope stimuli.

Optimal coding theory also posits that neural systems should be adapted to encode stimuli in order to maximize information transmission and reduce redundancy (Barlow, 2001; Barlow, 1961). One such strategy would be to temporally decorrelate or temporally whiten the information in the decaying power-law statistics found in natural environments of the fish. In order to achieve this, one would need a subset of pyramidal neurons, which are high-pass tuned (i.e. neural gain increases as a function of envelope frequency) in order to match and counter-oppose the decaying power-law stimulus statistics (Fig. 4). The concept of neural tuning matching the stimulus statistics is also found across sensory systems (Dan et al., 1996; Pozzorini et al., 2013; Wang et al., 2003), and there has been extensive evidence that neurons in early

sensory processing stages serve as a filter in order to only detect transient changes and reduce redundant stimuli as well as maximize the information transmission in the brain (Lundstrom et al., 2010; Lundstrom et al., 2008). Thus, it is a likely possibility that temporal whitening can occur in the electrosensory system as well to efficiently encode natural second-order stimuli.

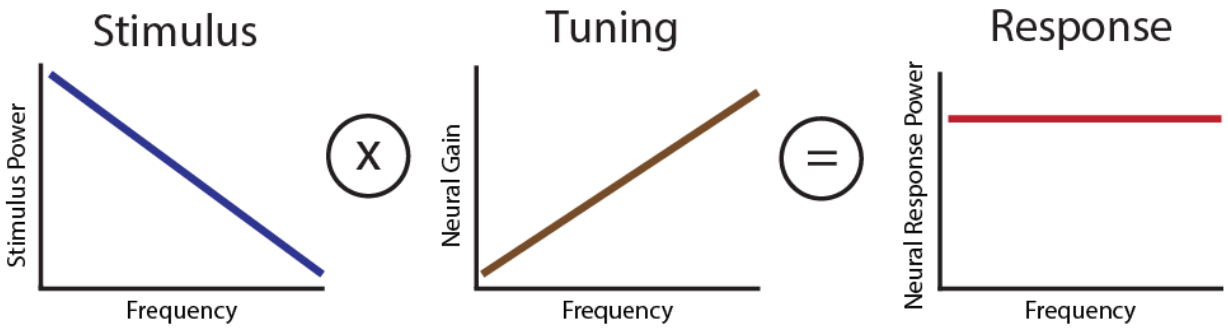

Figure 4. Temporal whitening. Schematic showing that, in order to optimize coding, the tuning curve (middle) must oppose stimulus statistics (left) in order to give rise to a neural response power that is independent of frequency (right).

1.4.4 – SK Channels

How could these strategies be achieved? The cellular and molecular machinery in pyramidal cells are complex on their own merit. There are a variety of channels and receptors which could serve to aid in efficient sensory processing. One such candidate which can explain differences in sensory processing across segments for first-order AM stimuli are small-conductance calcium-activated potassium (SK) channels. . SK channels (Fig. 5A) share common structural similarities with other members in the potassium channel family in that they have six transmembrane domains as well as a pore region found in traditional voltage-gated potassium channels between S5 and S6. Due to the lack of a functioning voltage sensor, SK channels are not voltage-gated but are instead activated by increases in the intracellular calcium concentration. SK channels are hence named for their high calcium sensitivity as well as their small conductance of approximately 10-14 pS (Hirschberg et al., 1998; Kohler et al., 1996). The binding of small concentrations of calcium onto calmodulin leads to an important conformational change of the SK channel, causing an inward rectification of potassium in the outward direction. SK channels

regulate cellular excitability by controlling the afterhyperpolarization (AHP) following action potential firing (Deemyad et al., 2011; Ellis et al., 2007). This would then influence how fast the neuron recovers before it can fire the next action potential, and in turn affect how often a neuron can fire given a particular stimulus (Fig. 5B).

In particular, it was found that SK type 2 (SK2) channels gives rise to differential adaptation responses as well as a tendency to be tuned to different beat frequencies. This is due to the differential expression pattern of SK2 channels in pyramidal cell somata across the segments, where LS contained the most SK2, whereas CMS contained the least (Ellis et al., 2008). When LS SK2 channels were antagonized, the adaptation responses of LS neurons became more like those found in CMS, and tuning shifted to the lower AM beat frequencies found in CMS (Deemyad et al., 2012; Ellis et al., 2007). However, it is important to note that this effect is only found in ON-type cells, and not OFF-type cells. SK1 channels, which are found in the dendrites of pyramidal cells, also follow a similar expression pattern to the SK2 channels, such that LS contains the most SK1 channels and CMS contains the least. However, it is important to note that unlike the SK2 channels, SK1 channels are found in both ON- and OFF-type pyramidal cell dendrites. Thus, it is a possibility that SK1 channels could serve as a mechanism to give rise to similarly differential tuning curves and adaptation responses to second-order stimuli such as envelopes.

Previous studies have shown that blocking SK channels with apamin or UCL-1684 results in a loss of AHP and thus the cells become more excitable, leading to more burst firing (Faber and Sah, 2003). In contrast, SK channel activity can also be increased with pharmacological agonists such as 1-EBIO, which increases the AHP, leading to lower excitability (Fig. 5C). The differential expression of SK channels across segments could therefore also control the degree of high-pass tuning via changes in conductance to give rise to a subset of neurons which can perform temporal whitening. In conjunction with the fact that SK1 channels are located in the dendrites, where feedback input from higher brain areas such as the nP terminate, it is likely that there are integration mechanisms worth investigating which could lead to efficient coding strategies of second-order stimuli.

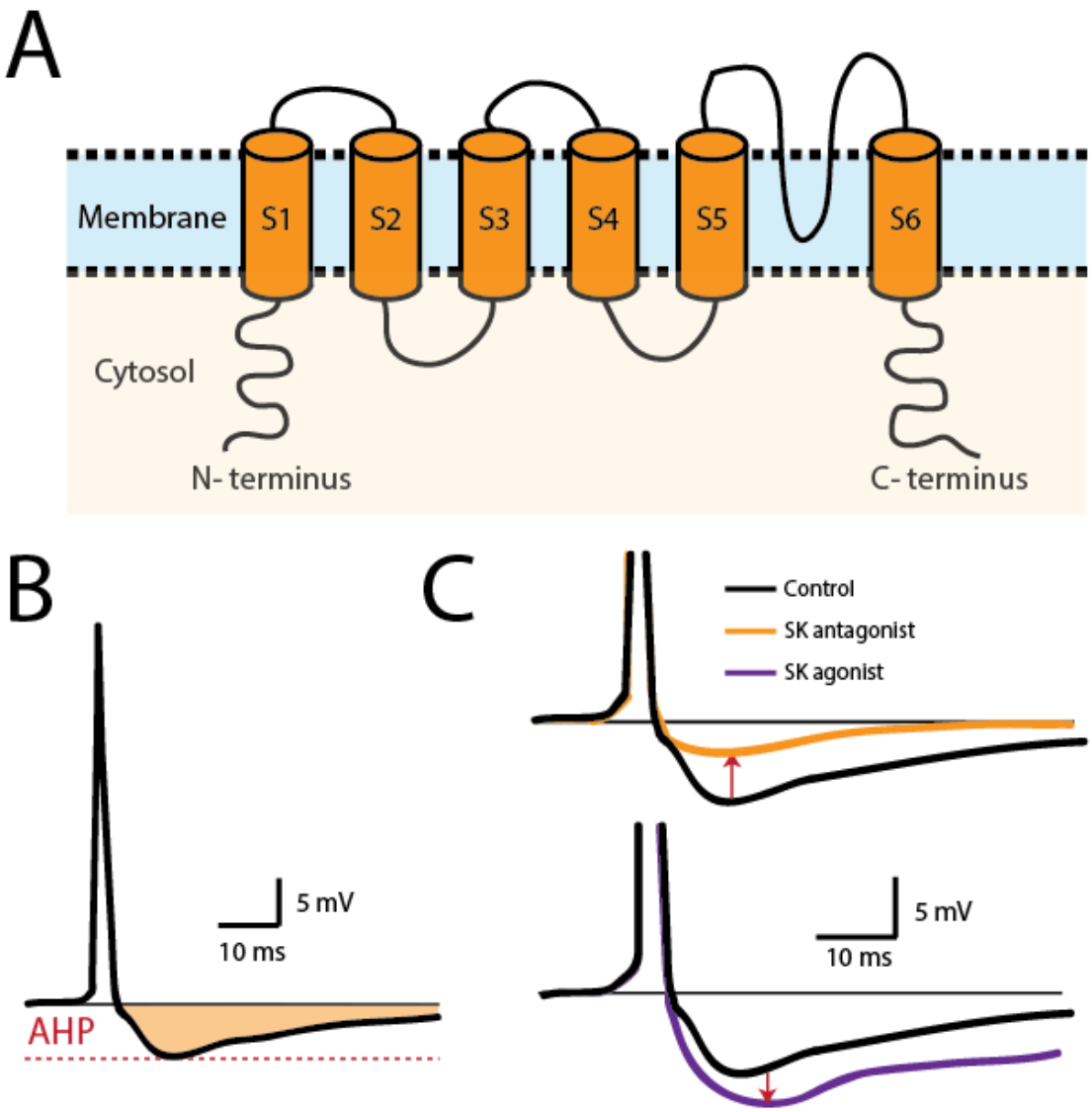

Figure 5. SK channels determine neural excitability. A) Schematic of an SK Channel showing its basic structure consisting of 6 transmembrane domains. B) SK channels are activated by increases in the intracellular calcium concentration following action potential firing and give rise to an after-hyperpolarization (AHP) (shaded region). C) SK channel antagonist application reduces the AHP, leading to increased neural excitability, while SK channel agonist application instead increases the AHP, leading to decreased neural excitability. Figure adapted from (Huang and Chacron, 2017).

1.4.5 – Summary

In this section, I had first introduced the animal model of the weakly-electric fish and presented arguments as to why it is an attractive model to study questions of sensory processing, then introduced the types of electrosensory signals that we are primarily interested in investigating,

outlined the neural anatomy and what is known about sensory processing of related electrosensory signals, and presented a series of possibilities in which efficient coding and processing of the electrosensory signals (i.e. envelopes) I am interested in investigating. In summary, the above sections provide a general outline of the key unresolved questions and provide potential hypotheses and approaches to unraveling these mysteries. In the final section below, I will present the goals of each of the studies in this thesis.

1.5 – Goals of the present studies

The electrosensory system will allow me to elucidate if and how this system is able to process second-order natural stimuli. Due to the fact that little is known about envelope responses in the brain, the first goal of the study presented in Chapter 2 will be to characterize all the heterogeneous responses in all 9 subclasses pyramidal neurons according to ELL segments and depth, as well as investigate differences in the responses between two primary classes of ON- and OFF-type pyramidal neurons in the ELL. A secondary goal of this study would be to elucidate if parallel processing is a possibility in the ELL as an efficient coding strategy. I propose that there will be differential responses across the ELL pyramidal cell population and that parallel processing serves as a primary strategy which is to be used in higher brain areas such as the TS in order to decode envelope stimuli information

Chapter 3 will investigate whether and how ELL pyramidal cells can perform temporal decorrelation or temporal whitening in order to maximize information transmission and optimally reduce redundancy in natural second-order stimuli. I propose that ELL pyramidal cells utilize temporal whitening in order to optimally encode envelope information such that tuning gives rise to matched behaviour to the stimulus statistics. I also hypothesize that this optimal coding will be mediated by the SK channels and I will additionally test if this system can be altered and investigate whether changes in neural tuning can directly lead to predictable changes in optimal coding and matched behaviour. This will be done by altering SK channels with pharmacological drugs to induce changes in neural tuning.

Chapter 4 will investigate whether it is truly feedforward or feedback which drives neural responses to envelopes. This will be achieved by playing linearly ramping envelope stimuli and

looking at the phase locking responses with vector strength, as well as firing rate responses across the electrosensory pathway. Furthermore, we will test whether feedback plays a critical role by blocking the direct and indirect feedback pathways to see how exactly envelope responses arise at low envelope stimulus intensities as well as what is being decoded downstream in the closed-feedback loop with the ELL pyramidal cells at the centre.

Finally, Chapter 5 will investigate the role of feedback in neural tuning and whether the direct or indirect feedback pathways play critical roles in determining the neural tuning of ELL pyramidal cells. We will again test this by blocking the direct and indirect feedback pathways to see how exactly envelope responses change. Due to the termination points of both feedback pathways in proximity with SK1 channels, I propose that both feedback pathways play a role in generating and optimizing the neural responses of ELL pyramidal cells.

Chapter 2

Characterization of Envelope Responses in Pyramidal Cells of the ELL

In this chapter, we aim to outline a complete neural tuning characterization of envelope responses in pyramidal cells of the ELL using a range of envelope frequencies mimicking the movement of another fish. As mentioned in the introduction, we know the responses of the peripheral EAs and how both single EAs and correlated EAs, hence population activity, encode for envelopes across the spectrum of low frequencies encompassing movement information. Here we explore the hub of electrosensory processing in the first downstream brain area where these EAs terminate. We performed a complete characterization of each class and subclass of pyramidal neurons: the difference (or lack thereof) between ON and OFF-type pyramidal neurons, neural responses in each of the three ELL segments, as well as superficial, intermediate, and deep neurons within each segment. This chapter is adapted from: Chengjie G. Huang, Maurice J. Chacron. Optimized parallel coding of second-order stimulus features by heterogeneous neural populations. *Journal of Neuroscience* 36: 9859-9872, 2016.

2.1 – Abstract

Efficient processing of sensory input is essential to ensure an organism's survival in its natural environment. Growing evidence suggests that sensory neurons can optimally encode natural stimuli by ensuring that their tuning opposes stimulus statistics, such that the resulting neuronal response contains equal power at all frequencies (i.e. is "white"). Such temporal decorrelation or whitening has been observed across modalities but the effects of neural heterogeneities on determining tuning and thus responses to natural stimuli have not been investigated. Here we investigated how heterogeneities in sensory pyramidal neurons organized in three parallel maps representing the body surface determine responses to second-order electrosensory stimulus

features in the weakly electric fish *Apteronotus leptorhynchus*. While some sources of heterogeneities such as ON and OFF-type responses to first-order stimuli did not affect responses to second-order electrosensory stimulus features, other sources of heterogeneity within and across the maps strongly determined responses. We found that these cells effectively performed a fractional differentiation operation on their input with exponents ranging from zero (no differentiation) to 0.4 (strong differentiation). Varying adaptation in a simple model explained these heterogeneities and predicted a strong correlation between fractional differentiation and adaptation. Using natural stimuli, we found that only a small fraction of neurons implemented temporal whitening. Rather, a large fraction of neurons did not perform any significant whitening and thus preserved natural input statistics in their responses. We propose that this information is needed in order to properly decode optimized information sent in parallel through temporally whitened responses based on context.

2.2 – Introduction

Understanding how the brain processes sensory input, thereby leading to behavior (i.e. the neural code) remains a central problem in neuroscience. Growing evidence suggests that the brain's coding strategies are adapted to the statistics of stimuli found in the natural environment, thereby making the use of natural stimuli paramount towards understanding the neural code (Attneave, 1954; Barlow, 1961; Laughlin, 1981; Simoncelli and Olshausen, 2001). In particular, it has been proposed that sensory neurons can efficiently encode time varying natural stimuli by removing redundant information and therefore maximizing information transmission (Rieke et al., 1996), leading to a neural response with equal power at all frequencies (i.e. "white"). Experiments have provided evidence that sensory neurons achieve such temporal decorrelation or whitening of natural stimuli by matching their tuning properties to natural stimulus statistics across modalities (visual: (Dan et al., 1996; Wang et al., 2003); auditory: (Rodriguez et al., 2010); somatosensory: (Pozzorini et al., 2013); electrosensory: (Huang et al., 2016)). However, strong heterogeneities have been observed in neural populations (Bannister and Larkman, 1995a, b; Goldberg, 2000), even for a given cell type (Marder and Goaillard, 2006; Schulz et al., 2006). While heterogeneities can benefit coding (Mejias and Longtin, 2012; Padmanabhan and Urban,

2010; Tripathy et al., 2013), how these influence optimized coding of natural stimuli through temporal whitening has not been investigated to date.

Gymnotiform wave-type weakly electric fish offer an attractive model system for studying the coding of natural stimuli because of its well-characterized neural circuits and natural stimulus statistics. These fish sense amplitude modulations (AMs) of their self-generated quasi-sinusoidal electric organ discharge (EOD) through peripheral electroreceptors found on their skin. Electroreceptors send afferents that trifurcate to contact sensory pyramidal neurons within three parallel maps of the body surface (lateral segment: LS; centro-lateral segment: CLS; centro-medial segment: CMS) within the electrosensory lateral line lobe (ELL) that subsequently project to higher brain areas, thereby mediating perception and behavioral responses (see (Chacron et al., 2011; Krahe and Maler, 2014; Marsat et al., 2012) for review). ELL pyramidal cells display large and well-known heterogeneities. First, there are two pyramidal cell types: ON cells that respond to increases in EOD amplitude and OFF cells that instead respond to decreases in EOD amplitude (Saunders and Bastian, 1984). Second, pyramidal cells within a given map display large heterogeneities in both morphology and physiology (Avila-Akerberg et al., 2010; Bastian et al., 2002, 2004; Bastian and Nguyenkim, 2001a; Chacron, 2006; Chacron et al., 2005a; Chacron et al., 2005c). Third, pyramidal cells across the three ELL maps display strong response heterogeneities (Krahe et al., 2008; Shumway, 1989).

As in other sensory modalities, natural electrosensory stimuli consist of a fast time varying waveform (i.e. the EOD AM which is a first-order attributes) whose amplitude (i.e. the envelope which is a second-order attribute) varies more slowly (Stamper et al., 2013). It is important to note that the animal's EOD is a carrier and that the time varying EOD AM is the meaningful stimulus here. Thus, the first- and second-order features of the stimulus correspond to the second- and third-order features of the full signal received by the animal, respectively. Envelopes carry behaviorally relevant information and are processed within the brain as they give rise to behavioral responses (Metzen and Chacron, 2014; Stamper et al., 2012). While much is known about how heterogeneities in ELL pyramidal cells influence responses to AMs (see (Krahe and Maler, 2014; Maler, 2009a) for review), almost nothing is known about their influence on responses to envelopes. ELL pyramidal cells can respond to envelopes (McGillivray et al., 2012; Middleton et al., 2006) and a recent study has shown that LS pyramidal cells efficiently process

envelopes through temporal whitening by matching their tuning properties to natural statistics (Huang et al., 2016). However, the effects of pyramidal cell heterogeneities within as well as across the ELL maps on their responses to envelopes have not been investigated to date.

2.3 – Methods

2.3.1 – Animals

The weakly electric fish *Apteronotus leptorhynchus* was used exclusively in this study. Animals of either sex were purchased from tropical fish suppliers and were acclimated to laboratory conditions according to published guidelines (Hitschfeld et al., 2009). All procedures were approved by McGill University's animal care committee and were performed in accordance with the guidelines of the Canadian Council on Animal Care.

2.3.2 – Surgery

Surgical procedures have been described in detail previously (Chacron et al., 2003; Metzen et al., 2015; Toporikova and Chacron, 2009). Briefly, 0.1-0.5 mg of tubocurarine (Sigma) was injected intramuscularly in order to immobilize the fish for electrophysiology experiments. The fish was respirated through a mouth tube at a flow rate of ~10 mL/min when placed in the recording tank. To stabilize the head during electrophysiology recordings, a metal post was glued to the exposed area of the skull. A small hole of ~ 2 mm^2 was drilled over the caudal lobe of the cerebellum above the ELL in order to gain access to the pyramidal neurons.

2.3.3 – Electrophysiology

We used well-established techniques to perform extracellular recordings with Woods metal electrodes from pyramidal cells (Frank and Becker, 1964). Cells were assigned to each segment based on recording depth and medio-lateral placement of the electrode on the brain surface as done previously (Khosravi-Hashemi and Chacron, 2014; Krahe et al., 2008). Extracellular recordings were digitized using CED 1401-plus hardware and Spike II software at 10 kHz sampling rate.

2.3.4 – Stimulation

The electric organ discharge of *A. leptorhynchus* is neurogenic, and therefore is not affected by injection of curare. All stimuli consisted of amplitude modulations (AMs) of the animal's own EOD and were produced by triggering a function generator to emit one cycle of a sinewave for at each zero crossing of the EOD as done previously (Bastian et al., 2002). The frequency of the emitted sinewave was set slightly higher (~ 30Hz) than that of the EOD, which allowed the output of the function generator to be synchronized to the animal's discharge. The emitted sinewave was subsequently multiplied with the desired AM waveform (MT3 multiplier; Tucker Davis Technologies) and resulting signal was isolated from ground (A395 linear stimulus isolator; World Precision Instruments). The isolated signal was then delivered through a pair of chloridized silver wire electrodes placed ~15 cm on either side of the recording tank perpendicular to the fish and, depending on polarity, either added or subtracted from the animal's own discharge. The stimulus intensity was adjusted to give rise to changes in EOD amplitude that were ~20% of the baseline level as in previous studies (Aumentado-Armstrong et al., 2015; Deemyad et al., 2013; Metzen et al., 2016a; Simmonds and Chacron, 2015b) as measured using a small dipole placed close to the animal's skin. The typical stimulus intensity used was ~ 0.2 mV/cm. The stimuli consisted of a 4Hz sine wave AM with a constant envelope to test pyramidal cell responses to first-order stimuli. Moreover, we used stimuli consisting of two noisy AM waveforms with frequency contents 5-15 Hz and 60-80 Hz whose envelopes were modulated sinusoidally with frequencies ranging from 0.05 Hz to 1 Hz mimicking those frequencies found in movement envelopes (Huang et al., 2016; Metzen and Chacron, 2014, 2015). We also used noisy envelopes whose spectrum decayed as a power law with exponent -0.8 mimicking signals seen under natural conditions (Metzen and Chacron, 2014).

2.3.5 – Fractional Differentiation Model

Fractional differentiation is a linear operation that can be described simply as d^{α}/dt^{α}, in which the order of differentiation α is a non-integer number. In the frequency domain, fractional differentiation of order α corresponds to filtering by a transfer function *H(f)* given by:

$$H(f) = (2\pi f)^{\alpha} \exp\left(i\frac{\alpha\pi}{2}\right)$$

The gain G(f) and phase ϕ(f) of the model can then be written as:

$$G(f) = |H(f)| = (2\pi f)^{\alpha}$$

$$\phi(f) = \arctan\left(\frac{Im[H(f)]}{Re[H(f)]}\right) = \frac{\alpha\pi}{2}$$

where $Im[H(f)]$ and $Re[H(f)]$ are the imaginary and real parts, respectively. We fitted a fractional differentiation model to our data using the Grunwald-Letnikov definition, which was adapted to use a vectorization method to pass signals through a spectrum of fractional derivative values between 0 and 1 from which we obtained the fractional differential exponent α_{neuron}.

2.3.6 – Neuron Model

In order to model the pyramidal neural responses to the stimuli used in this study, we implemented a leaky integrate-and-fire model (Lapicque, 1907) with a power-law adaptation:

$$C\frac{dV}{dt} = -g_{leak}(V - E_{leak}) - z_1(t) + I + \sigma_{noise}\,\xi(t) + \sigma_{stim}\,s(t)$$

where C is the membrane capacitance, g_{leak} is the leak conductance, E_{leak} is the leak reversal potential, I is a constant bias current, $\xi(t)$ is gaussian white noise with zero mean and standard deviation unity, σ_{noise} is the noise intensity, $s(t)$ is the stimulus which was taken to have the same statistics as for the data, σ_{stim} is the stimulus intensity, V is the membrane potential, and $z_1(t)$ is the adaptation current. Each time the membrane potential reaches the threshold θ, it is reset to V_{reset} and an action potential is said to have occurred at that time. We approximated the power law adaptation using M variables $z_1 \ldots z_M$ that obeyed the following system of differential equations (Drew and Abbott, 2006):

$$\frac{dz_i}{dt} = \frac{-z_i(t) + z_{i+1}(t)}{\tau_i} + b\,\gamma^{1-i}\sum_j \delta(t - t_j) \text{ for i} = 1 \text{ to M} - 1$$

$$\frac{dz_M}{dt} = \frac{-z_M(t)}{\tau_M} + b\,\gamma^{1-M}\sum_j \delta(t - t_j)$$

$$\tau_i = \tau_{\min}\gamma^{i-1}$$

where t_j are the spikes times, $\delta(t)$ is the delta function, and b and γ are constants that determine the strength and power law exponent α_{neuron} of the neural sensitivity, respectively. The model was simulated using an Euler-Maruyama integration with timestep dt=0.025 ms. Unless

otherwise stated, we used parameter values C=1 μF/cm^2, g_{leak}=0.36 μS/cm^2, E_{leak}=-70 mV, I= 7 μA/cm^2, σ_{noise}= 5 μA/cm^2, M=40, b=0.2, γ=1.1253, τ_{min}=100 ms, θ=-50 mV, V_{reset}=-70 mV, C=1 μF/cm^2. We note that we varied parameters b (the adaptation strength) as well as I (the bias current) in order to reproduce the heterogeneities seen across segments as well as within each segment when considering the different cell classes (i.e. superficial, intermediate, and deep).

2.3.7 – Data Analysis

Superficial, intermediate, and deep pyramidal cells were segregated based on the baseline (i.e. in the absence of stimulation but in the presence of the animal's unmodulated EOD) firing rate, as done previously (Avila-Akerberg et al., 2010; Chacron, 2006; Chacron et al., 2005c). Cells whose baseline firing rate was less or equal to 15 Hz were classified as superficial, cells whose baseline firing rate was greater or equal to 35 Hz were classified as deep, cells whose baseline firing rate was between 15 and 35 Hz were classified as intermediate.

In order to quantify the neural responses and relate the responses to the stimulus envelope, we used linear systems identifications techniques to compute the gain and phase relationships. The recorded neural activity was first high-pass filtered (100 Hz; eighth-order Butterworth). Spike times were defined as the times at which this signal crossed a given threshold value from below. A binary sequence R(t) was constructed from the spike times by discretizing time into bins of width 0.1 ms and setting the content of a given bin to 10000 if a spike occurred within it or 0 otherwise. The time varying firing rate was obtained by low-pass filtering R(t) using a second-order Butterworth filter with cutoff frequencies 0.2 Hz, 0.35 Hz, 0.75 Hz, 1.5 Hz, 2.5 Hz, and 3.5 Hz for envelope frequencies 0.05, 0.1, 0.2, 0.5, 0.75, and 1 Hz, respectively. Using linear systems identification techniques, the response gain was calculated as the ratio of the amplitude of the filtered firing rate response and the amplitude of the stimulus obtained from the dipole during the recording. The response phase was calculated as the average phase at which the filtered firing rate waveform reached its maximum value relative to the peak values of the stimulus waveform over each cycle/period of 2π. We note that computing response gain from the phase histogram gave values that were not significantly different than those obtained using the filtered firing rate (data not shown).

The whitening index was calculated by taking the area under the power spectrum curve of the spiking response using a trapezoidal method and dividing by that obtained by replacing all values by the maximum value in the power spectrum. The whitening index ranges between 0 and 1, where 1 indicates complete whitening (i.e. a power spectrum that is independent of temporal frequency), as done previously (Huang et al., 2016).

2.4 – Results

We recorded from ELL pyramidal cells within the CMS, CLS, and LS maps. Our stimuli consisted of sinusoidal AMs with constant amplitude as well as noisy EOD AMs whose envelope: 1) varied sinusoidally at different frequencies spanning the behaviorally relevant range or, 2) mimicked the frequency spectrum of natural envelopes. Fig. 1A shows example traces of the AM (magenta), envelope (blue), and the full signal received by the animal (green) with their respective temporal frequency contents. Previous results have shown that cells whose somata are found most superficially within the pyramidal cell layer (i.e. superficial pyramidal cells) tend to have the largest dendritic trees. In contrast, cells whose somata are found most deeply within the pyramidal cell layer (i.e. deep pyramidal cells) tend to have the smallest dendritic trees. Finally, cells whose somata are located at intermediate levels within the pyramidal cell layer (i.e. intermediate pyramidal cells) have properties in between those of their superficial and deep counterparts. Importantly, previous anatomical work has shown that ELL pyramidal cells are organized in columns within each map (Maler, 2009a). Each column consists of six cells (ON and OFF-type deep, intermediate, and superficial) receiving almost identical input from peripheral receptors (Fig. 1B). Previous studies have shown a strong correlation between the baseline (i.e. in the absence of stimulation) firing rate and the location of the soma within the pyramidal cell layer (Bastian et al., 2004; Bastian and Nguyenkim, 2001a). We thus used the baseline firing rate to distinguish between these cell classes, as done previously (Avila-Akerberg et al., 2010; Chacron, 2006; Chacron et al., 2005c).

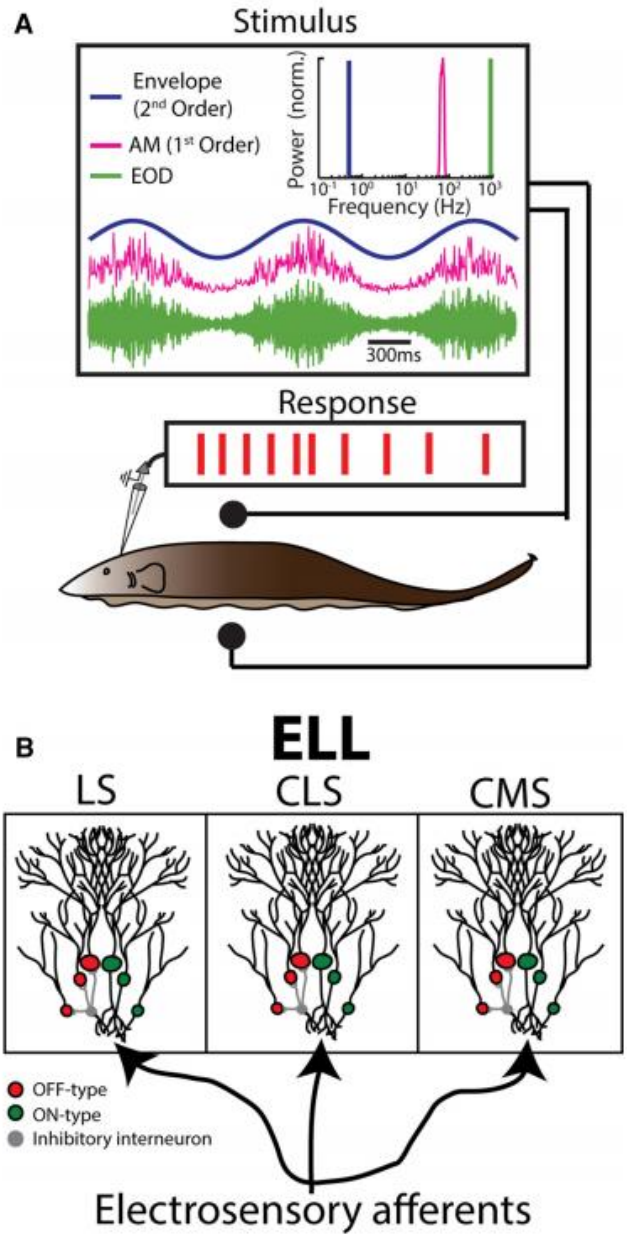

Figure 1. Experimental setup and relevant anatomy. A) Schematic representation showing the awake-behaving preparation where a stimulus is presented to the animal while neural activity is being recorded via extracellular Woods Metal electrodes. Shown on the right are: example AM waveform (magenta), its envelope (blue), and the full signal received by the animal (green) with their respective frequency contents. B) Schematic showing anatomy where peripheral electrosensory afferents trifurcate to make synaptic contact with pyramidal cells with three parallel maps of the body surface: the lateral segment (LS), the centro-lateral segment (CLS), and the centro-medial segment (CMS). Within each segment pyramidal cells are organized into columns each consisting of six cells: three ON-type (deep, intermediate, superficial) and three OFF-type (deep, intermediate, superficial).

2.4.1 – ON- and OFF-type pyramidal neurons display similar responses to envelopes

We first investigated how ON and OFF-type ELL pyramidal cells responded to EOD AMs. ON and OFF-type pyramidal cells have different morphologies and can easily be distinguished based on their responses to AM stimuli (Bastian et al., 2002; Maler, 1979; Maler et al., 1981; Saunders and Bastian, 1984). Indeed, in the case of a 4 Hz sinusoidal AM, ON-type cells tend to respond during the stimulus upstroke and near the peak (Fig. 2A). In contrast, OFF-type cells tend to respond during the stimulus downstroke and near the trough (Fig. 2B). As such, ON (n=46) and OFF-type (n=45) cells in our dataset responded to opposite phases (Figs. 2C,D) of the AM. The distribution of preferred phases of all recorded neurons was clearly bimodal (Hartigan's dip test, p=0.01) (Fig. 2E), consistent with previous results (Bastian et al., 2002; Saunders and Bastian, 1984).

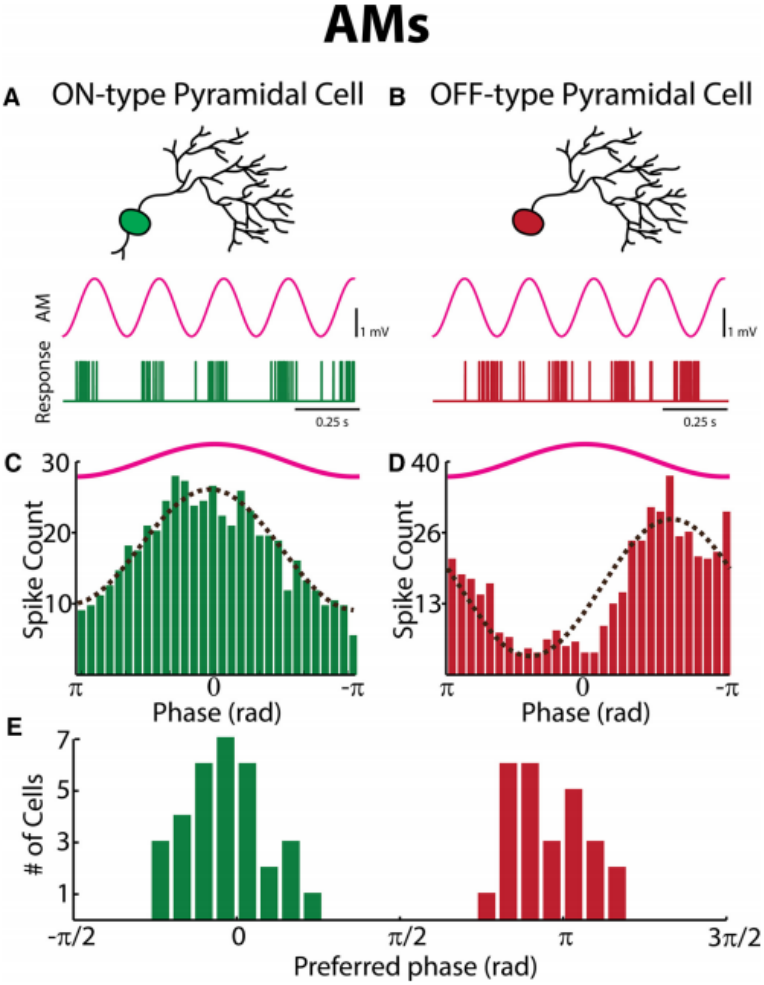

Figure 2. ON- and OFF-type pyramidal neurons respond in opposite fashion to EOD AMs (i.e. first-order). A) Top: Schematic showing the morphology of an ON-type pyramidal cell with its distinctive basilar dendrite receiving excitatory input from peripheral afferents. Bottom: sinusoidal EOD AM stimulus with frequency 4 Hz and the spiking response of an example ON-type pyramidal neuron. B) Top: Schematic showing the morphology of an OFF-type pyramidal cell. Note the lack of a basilar dendrite as the cell instead receives di-synaptic inhibition from peripheral afferents on its soma through a local interneuron (not shown). Bottom: sinusoidal EOD AM stimulus with frequency 4 Hz and the spiking response of an example OFF-type pyramidal neuron. C) Phase histogram showing the preferred phase response from this same neuron shown in A with the best-fit sinusoid (dashed black). D) Phase histogram showing the preferred phase response from this same neuron shown in B with the best-fit sinusoid (dashed black). E) Distribution of preferred phases for ON (green) and OFF (red) ELL pyramidal cells in our dataset. The entire distribution was clearly bimodal (Hartigan's dip test, p=0.01) and both modes could easily be separated.

We next investigated how ON and OFF-type ELL pyramidal cells responded to envelopes. Surprisingly, we found that both ON and OFF-type ELL pyramidal cells displayed similar responses (Figs. 3A,B) to these by firing preferentially during the envelope upstroke (Figs. 3C,D). Similar results were seen across our dataset as the distributions of preferred phases largely overlapped between ON and OFF-cells (Fig. 3E). Similar sensitivity and phases for envelope responses were observed when using either low (5-15 Hz) or high (60-80 Hz) frequency AMs (Kruskal-Wallis test, p=0.85). Responses obtained for either low or high frequency AMs were thus pooled in all subsequent analyses. We thus conclude that ON and OFF-type pyramidal cells, despite responding in opposite fashion to AMs, actually respond similarly to envelopes.

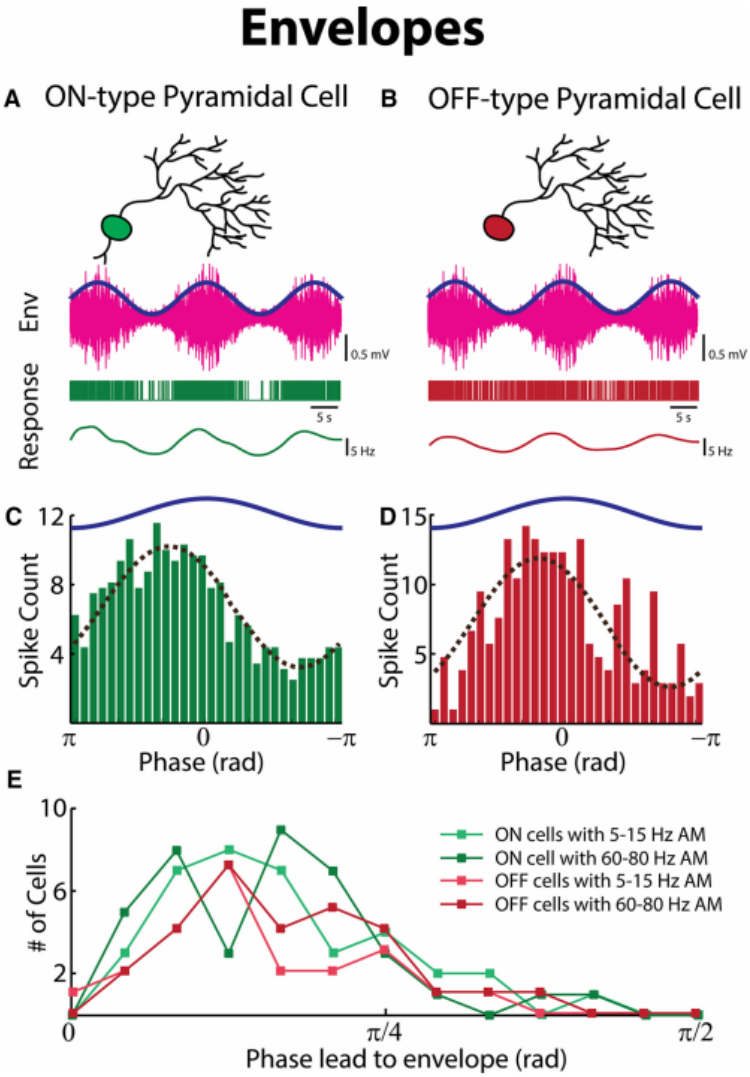

Figure 3. ON- and OFF-type pyramidal neurons respond similarly to envelopes (i.e. second-order). A) Top: Stimulus consisting of a noisy EOD AM (magenta) whose envelope (blue) is modulated sinusoidally. Bottom: spiking and time-varying firing rate response from an example ON-type LS pyramidal cell to this stimulus. B) Top: Stimulus consisting of a noisy EOD AM (magenta) whose envelope (blue) is modulated sinusoidally. Bottom: spiking and time-varying firing rate response from an example OFF-type LS pyramidal cell to this stimulus. C) Phase histogram from this same LS ON-type example neuron shown in A to the envelope with the best-fit sinusoid (dashed black). D) Phase histogram from this same LS OFF-type example neuron shown in B to the envelope with the best-fit sinusoid (dashed black). E) Distribution of preferred phases for ON (green) and OFF (red) ELL pyramidal cells in our dataset across the CMS, CLS, and LS maps for 5-15 Hz (light green and red) and 60-80 Hz (dark green and red) EOD AMs. All distributions were not significantly different from one another (Kruskal-Wallis test, p=0.89)

2.4.2 – Pyramidal cell populations of different ELL segments display differential tuning to envelopes

Previous studies have shown important differences between the responses of ELL pyramidal cells across the three maps to AM stimuli (Krahe et al., 2008; Mehaffey et al., 2008; Shumway, 1989) and have suggested different functional roles for each map (Metzner and Juranek, 1997). Thus, one possibility is that one ELL map is specialized to process envelope stimuli. If that were the case, then we would expect that only pyramidal neurons within that map would respond to envelopes. Another possibility is that ELL pyramidal neurons across the three maps are tuned differentially to envelopes, as is observed for AMs (Krahe et al., 2008; Shumway, 1989).

We thus investigated how ELL pyramidal cells within the LS (ON: n=21, OFF: n=14), CLS (ON: n=15, OFF: n=14), and CMS (ON: n=12, OFF: n=15) maps respond to envelopes. Since sinusoidal envelope stimulation elicited sinusoidal modulations in firing rate at the same frequency, we used linear systems identification techniques (see Methods) to quantify the gain and phase relationship between the envelope and neural response. We found that, for both ON and OFF-type LS pyramidal cells, gain increased as a power law as a function of increasing envelope frequency (Fig. 4A, green and red filled circles) while phase was largely independent of envelope frequency (Fig. 4A, green and red open circles), which is characteristic of fractional differentiation (Lundstrom et al., 2008; Pozzorini et al., 2013). We thus fitted a fractional differentiation model to our data (see Methods) and found excellent agreement (Fig. 4A, compare circles with dashed lines). We obtained similar fractional differentiation exponents (which is equal to the power law exponent describing the increase in gain) for ON and OFF-type LS pyramidal cells LS (ON: $\alpha=0.31\pm0.04$; OFF: $\alpha=0.27\pm0.04$; One-way ANOVA, $p=0.52$).

We found qualitatively similar results for CLS pyramidal cells in that the gain also increased as a power law as a function of increasing envelope frequency and that the phase lead was also independent of envelope frequency for both ON and OFF-type CLS neurons (Fig. 4B, compare filled and open red and green circles). Our data for CLS pyramidal cells were also well fit by a fractional differentiation model (Fig. 4B, compare circles with dashed lines). However, we found that the rate of increase of the gain as well as the phase lead were smaller in magnitude than those observed for LS pyramidal cells, as confirmed by smaller fractional differentiation

exponents that were similar for ON and OFF-type cells but lower than those observed in LS (ON: α=0.22±0.02; OFF: α=0.17±0.04; One-way ANOVA, p=0.29).

We next investigated how CMS pyramidal cells responded to envelopes. While ON and OFF-type cells also display similar response profiles, our data shows that CMS pyramidal cells respond to envelopes in a qualitatively different manner than their CLS or LS counterparts. This is because we found that response gain was independent of envelope frequency and that these cells displayed little or no phase lead (Fig. 4C, compare filled and open red and green circles). Our data was also well fit by a fractional differentiation model (Fig. 4C, compare circles and dashed lines) but the obtained fractional differentiation exponents (i.e. the power-law exponent), while similar for ON and OFF-type cells (ON: α=0.06±0.05; OFF: α=0.04±0.04; One-way ANOVA, p=0.82), were not significantly different than zero (ON: t-test, p=0.29; OFF: t-test, p=0.25), indicating that CMS pyramidal cells performed little or no filtering on the envelope stimulus.

Our results thus show that ELL pyramidal cells within all three maps responded to envelopes, thereby providing strong evidence against the hypothesis that there is only one ELL map that processes these. Rather pyramidal cells across the ELL maps were differentially tuned to envelopes. We conclude that pyramidal cell heterogeneities across the ELL maps significantly influence their response properties to envelopes. LS pyramidal cell responses displayed the strongest fractional differentiation exponent followed by their CLS counterparts with CMS pyramidal performing little or no fractional differentiation (Fig. 4D, One-Way ANOVA with Tukey's HSD correction, $p<0.05$). We note that, since we found no significant differences between ON and OFF-type cells across all three segments, data from each cell class were pooled in all subsequent analyses.

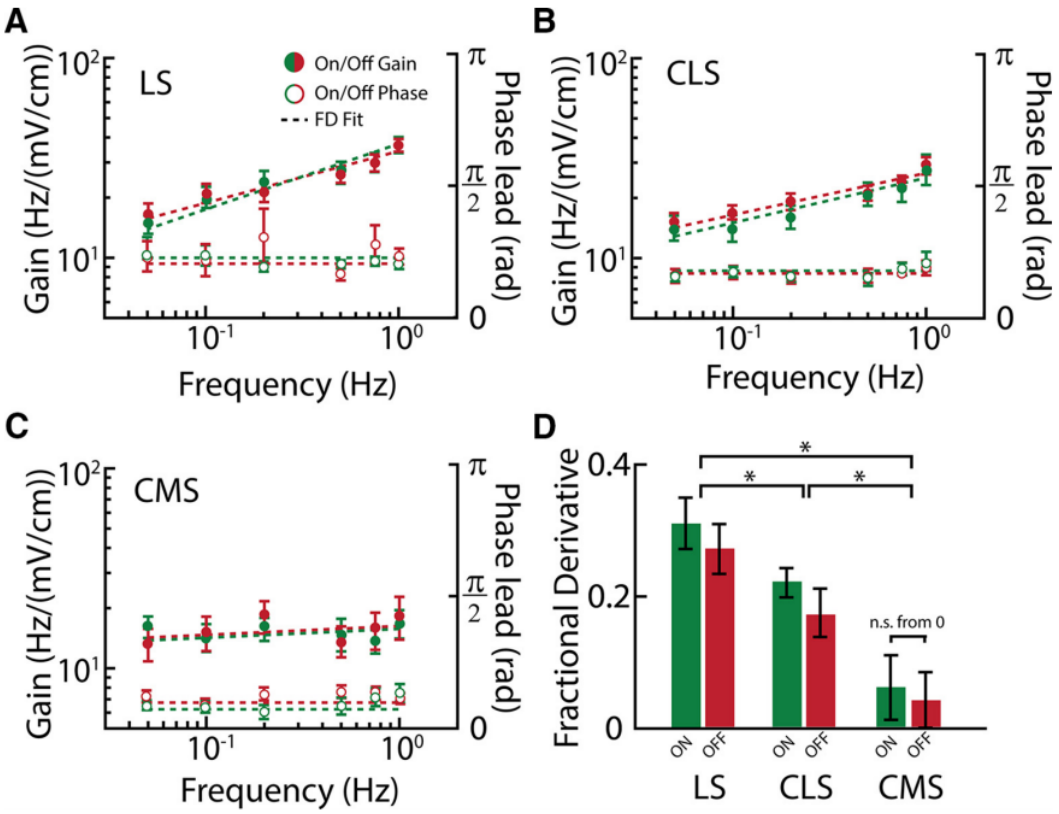

Figure 4. ELL pyramidal cells across the three ELL maps display differential responses to envelopes. A) Population-averaged gain (filled circles) and phase (open circles) relating the neural response to the envelope for LS ON (green) and OFF (red) pyramidal neurons with fractional differentiation (FD) fits (dashed lines). B) and C) Same as A but for CLS and CMS cells, respectively. D) Population-averaged fractional differentiation exponents for ON (green) and OFF (red) pyramidal cells in LS (left), CLS (middle), and CMS (right). For each map, the fractional differentiation exponents of ON and OFF-type cells were not significantly different from one another (one-way ANOVA's, $p \geq 0.29$ in all three cases). In contrast, the fractional differentiation exponents were significantly different between maps and decreased from LS to CMS. "" indicates significant difference at $p<0.05$ level using a one-way ANOVA with Tukey's LSD correction. Error bars indicate ± 1 SEM.*

2.4.3 – A simple LIF model predicts that differential degrees of adaptation can explain the observed response heterogeneities across ELL maps to second-order electrosensory stimuli

How can the observed differences between the responses of LS, CLS, and CMS pyramidal cells to envelopes be explained? Previous studies have shown that spike frequency adaptation can lead to high-pass filtering of the neuronal response (Benda and Hennig, 2008; Benda et al., 2005; Deemyad et al., 2012). Importantly, pyramidal cells display spike frequency adaptation in response to envelope steps, with the degree of adaptation strongest in LS and weakest in CMS

(Zhang and Chacron, 2016). Thus, we hypothesized that the different response profiles across the ELL maps could be explained by the fact that ELL pyramidal cells display different degrees of adaptation. To test this hypothesis, we used a simple model based on the leaky integrate-and-fire formalism that included an adaptation current (Fig. 5A, see Methods). We found that, with high adaptation, our model could successfully reproduce the gain and phase of LS pyramidal cells (Fig. 5B). By decreasing the adaptation strength in our model, we were able to successfully reproduce the gain and phase of CLS pyramidal cells (Fig. 5C). Finally, with no adaptation, our model successfully reproduced the gain and phase of CMS pyramidal cells (Fig. 5D). In all cases, our model simulation data was well fit by a fractional differentiation model whose exponent matched that observed experimentally (Fig. 5E) (LS: t-test, p=0.10; CLS: t-test, p=0.40; CMS: t-test, p=0.73). These results demonstrate that, by manipulating the degree of adaptation, we can reproduce the experimentally observed heterogeneities in the responses of ELL pyramidal cells across the three maps. Our model thus predicts that it is the degree of adaptation that determines a cell's response profile to envelopes.

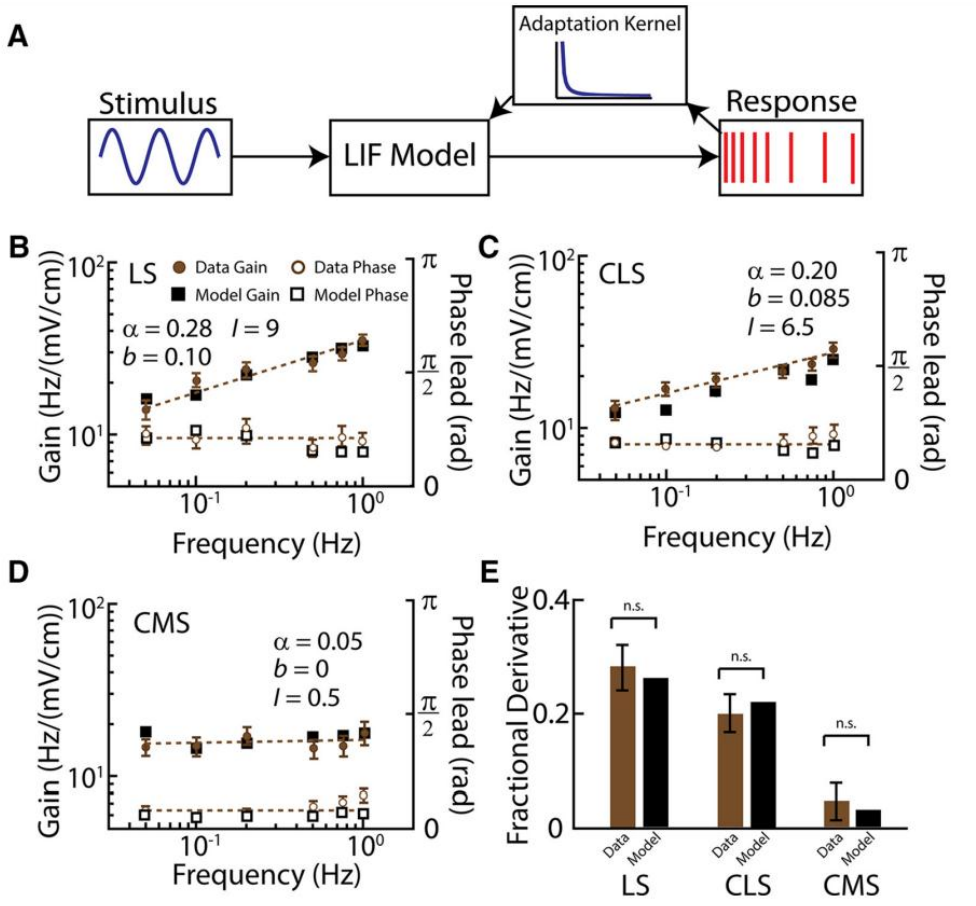

Figure 5. A simple leaky integrate-and-fire model with power-law adaptation successfully reproduces the experimentally-observed heterogeneities seen across ELL maps. A) Model schematic representation in which the stimulus (blue) is fed to a leaky integrate-and-fire (LIF) neuron model with an adaptation kernel that decays as a power law as a function of time. We chose a power law since a previous study has shown that LS pyramidal cells displayed power law adaptation in response to envelope stimuli (Huang et al., 2016). B) Population-averaged gain (filled circles) and phase (open circles) for our experimental data in LS. Also shown are the gain (filled black squares) and phase (open black squares) from our LIF model. C) and D) Same as B but for our CLS and CMS datasets, respectively. Note that I was decreased in order to maintain the baseline (i.e. in the absence of stimulation) constant across all segments, as observed experimentally (Krahe et al., 2008). E) Population-averaged fractional differentiation exponents for our experimental data (brown) and model (black) for LS (left), CLS (middle), and CMS (right). For all three maps, the fractional differentiation exponents obtained experimentally and from the model were not significantly different from one another. n.s. indicates not significant at the $p<0.05$ level. Error bars indicate ± 1 SEM.

2.4.4 – Our simple LIF model also predicts that differential degrees of adaptation can explain the observed response heterogeneities within each ELL map

We next tested whether pyramidal cell class (i.e., superficial, intermediate, or deep) influenced responses to envelopes. To do so, we segregated cells within each segment into deep (LS: n=9, CLS: n=9, CMS: n=10), intermediate (LS: n=12, CLS: n=11, CMS: n=9), and superficial (LS: n=14, CLS: n=8, CMS: n=8) using the baseline firing rate as done previously (Avila-Akerberg et al., 2010; Chacron, 2006; Chacron et al., 2005c). We found that, within LS, superficial cells displayed the greatest degree of fractional differentiation, followed by intermediate, and with deep cells displaying the least degree of fractional differentiation (Fig. 6A). Qualitatively similar results were obtained in CLS (Fig. 6B). Importantly, we found that, within CMS, deep, intermediate, and superficial pyramidal cells all displayed little to no fractional differentiation (Fig. 6C).

We then tested using our model whether differential degrees of adaptation could explain the different levels of fractional differentiation performed by superficial, intermediate, and deep cells across all three ELL maps. We found that, by suitably varying the adaptation strength in our model, we could reproduce the response heterogeneities within each segment (Fig. 6, compare circles and squares in each panel). We thus conclude that our simple mathematical model could reproduce all the response heterogeneities seen in the data. Our model thus makes the important prediction that the differential levels of fractional differentiation seen across ELL maps and

across pyramidal cell class can both be explained by differences in the level of adaptation. The implications of this result as well as the nature of the underlying mechanisms are discussed below.

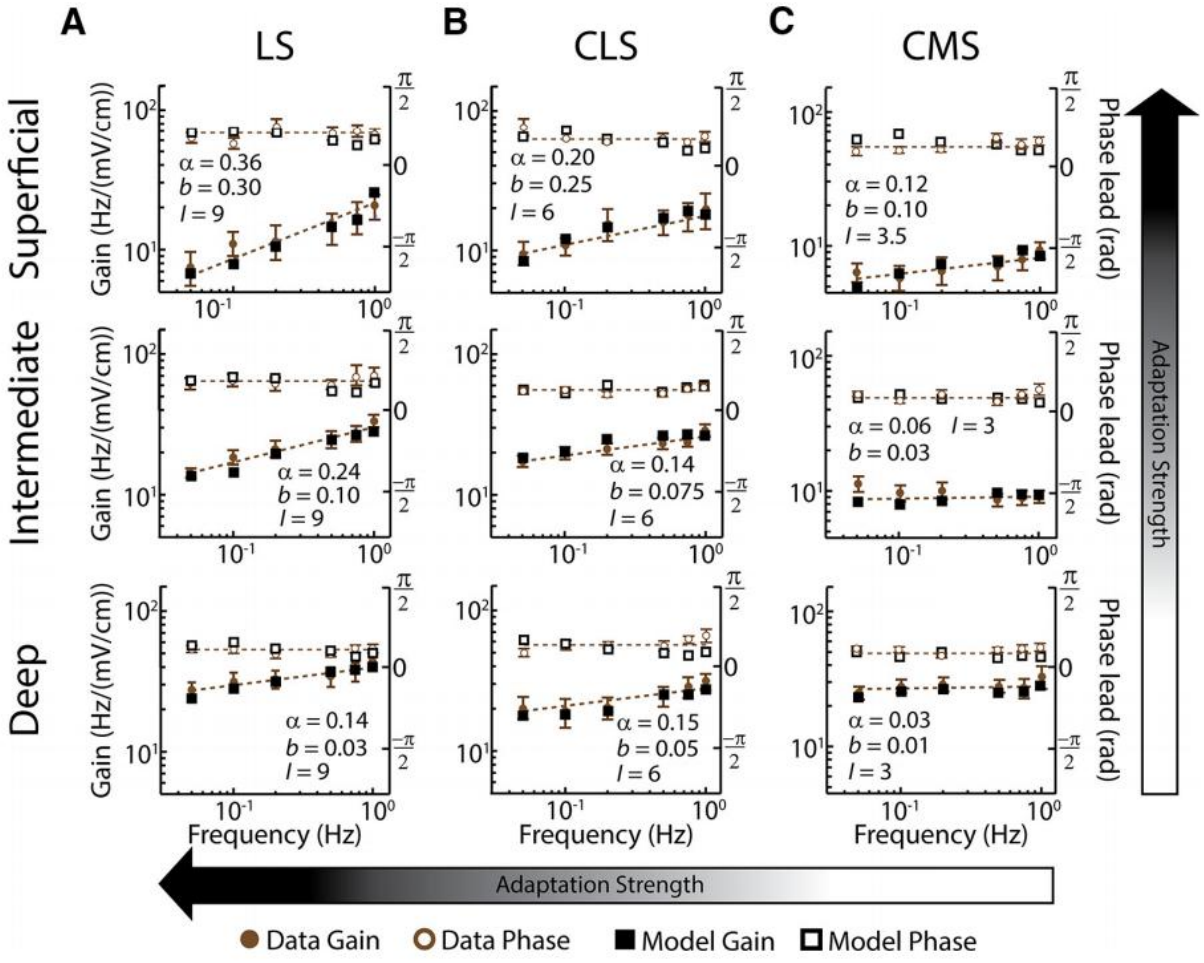

Figure 6. Pyramidal cell classes within each ELL map display differential responses to envelopes. A) Population-averaged gain (filled brown circles) and phase (open brown circles) for our experimental data for superficial (top), intermediate (middle), and deep (bottom) LS cells. Also shown are the gain (filled black squares) and phase (open black squares) from the model in each case with corresponding fractional differentiation exponent α and adaptation strength value b. B) and C) same as A, but for CLS and CMS neurons, respectively. Note that, for CMS, deep, intermediate, and superficial CMS neurons all displayed similar fractional differentiation exponents that were all not significantly different from 0. Our LIF model could reproduce heterogeneities in envelope responses by decreasing adaptation strength going from LS to CMS for a given cell class (i.e. deep, intermediate, or superficial) as well as going from superficial to deep within a given ELL map (i.e. CMS, CLS, or LS). The values of model parameter b and I_{bias} (in microamperes per square centimete) used in each case are shown.

2.4.5 – Coding of natural envelope stimuli by ELL pyramidal cells

It is important to note that we have, so far, used artificial sinusoidal envelope stimuli to characterize the responses of ELL pyramidal cells across maps. However, natural envelope stimuli are not sinusoidal in nature and are instead characterized by a whole spectrum of temporal frequencies (Fotowat et al., 2013; Metzen and Chacron, 2014; Yu et al., 2012b). Importantly, as natural envelope stimuli are scale invariant (i.e. are self-similar when looked at different timescales), their power spectrum decays according to a power law as a function of envelope temporal frequency (Fig. 7A). As mentioned above, in order to maximize information transmission, a neuron's tuning curve should oppose this decaying power such that response power is independent of frequency (i.e. temporal decorrelation or whitening).

We thus investigated how different ELL pyramidal cell subtypes (i.e. deep, intermediate, and superficial) across maps (i.e. CMS, CLS, and LS) responded to natural envelope stimuli. Within LS, we found that the response power spectra of superficial pyramidal cells were independent of frequency (Fig. 7B, top panel). That of intermediate pyramidal cells decayed as a function of frequency (Fig. 7B, middle panel) while that of deep pyramidal cells showed an even more pronounced decay (Fig. 7B, bottom panel). We quantified the degree of temporal decorrelation or whitening by computing a white index whose value is 1 if the response power spectrum is constant. White index values were greatest for LS superficial pyramidal cells, followed by intermediate pyramidal cells, and smallest for deep pyramidal cells (Fig. 7E).

In contrast, superficial cells within CLS did not perform as much temporal decorrelation of natural envelope stimuli as their LS counterparts as quantified by a lower white index (Fig. 7C, top panel). Superficial CLS pyramidal cells nevertheless displayed larger white index values than their intermediate counterparts (Fig. 7C, compare top and middle panels). Deep CLS cells performed even less temporal decorrelation (Fig. 7C, bottom panel). Interestingly, superficial, intermediate, and deep CMS pyramidal cells did not perform any significant temporal decorrelation or whitening of natural envelope stimuli (Fig. 7D, top, middle, and bottom panels and Fig. 7E). Indeed, the white index values computed from the neural responses were not significantly different than those obtained for the stimulus power spectrum (Fig. 7E), indicating that these cells instead preserve the statistics of natural input in their responses.

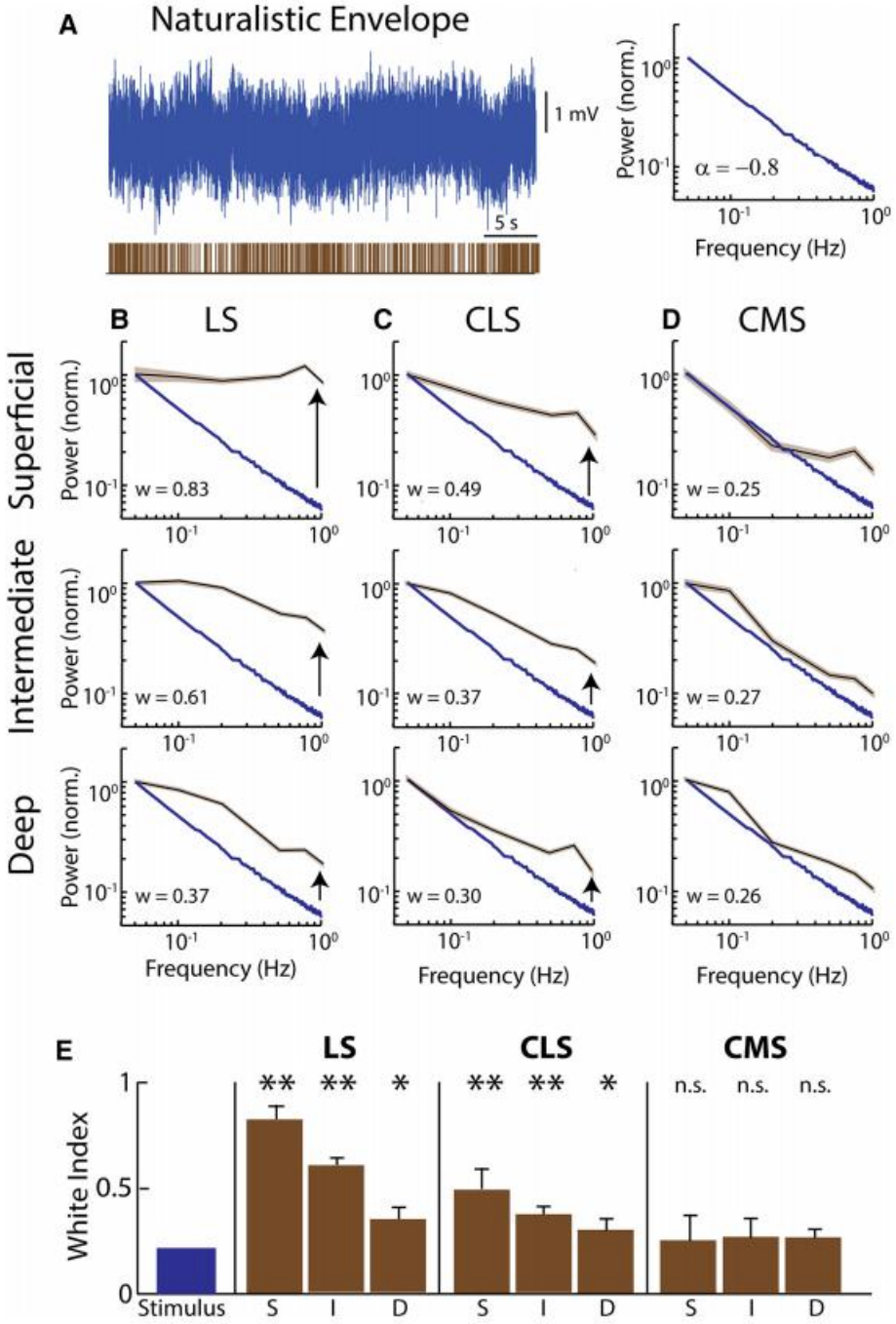

Figure 7. Different pyramidal cell classes across the three ELL maps perform different degrees of temporal whitening in response to natural envelope stimuli. A) Example time series of a natural envelope stimulus (top left), its power spectrum (top right) that decays as a power law with exponent -0.8 as a function of temporal frequency, and the spiking response from an example pyramidal neuron (bottom left). B) Stimulus (blue) and population-averaged response (black) power spectra for superficial (top), intermediate (middle), and deep (bottom) LS pyramidal cells. C) and D) same as B, but for CLS and CMS pyramidal cells, respectively. E Population-averaged whitening indices for the stimulus (blue) and for superficial (S), intermediate (I), and deep (D) pyramidal cells within the LS (left), CLS (middle), and CLS

(right) maps. "" indicates significance at the p<0.05 level, "**" indicates significance at the p<0.01 level. n.s. indicates not significant at the p<0.05 level. Error bands indicate ± 1 SEM.*

2.4.6 – Summary

Fig. 8 shows a summary of our results. A previous study has shown that most peripheral receptors do not perform significant filtering of envelopes and thus faithfully relay information about their detailed structure to ELL pyramidal cells (Metzen and Chacron, 2015). Overall, ON and OFF-type pyramidal cells displayed similar responses to envelopes. Using artificial sinusoidal envelopes, we further found that LS cells displayed, on average, the strongest degree of fractional differentiation to envelope stimuli. CLS cells displayed, on average, intermediate degrees of fractional differentiation while CMS cells displayed little or no fractional differentiation (Fig. 8). Within the CLS and LS segments, deep pyramidal cells performed little to no fractional differentiation while superficial pyramidal cells displayed the greatest degree of fractional differentiation. Overall, a mathematical model showed that differential levels of adaptation could explain the experimentally observed heterogeneities in tuning. Using natural stimuli, we found that superficial pyramidal cells within LS and CLS performed temporal decorrelation or whitening while all CMS cells instead preserved natural stimulus statistics. Thus, our results have shown that a significant proportion of ELL pyramidal cells (deep cells for LS and CLS as well as all cells within CMS) perform little to no filtering of envelope stimuli. As all pyramidal cells project to higher brain areas, our results have important implications for understanding envelope coding as discussed further below.

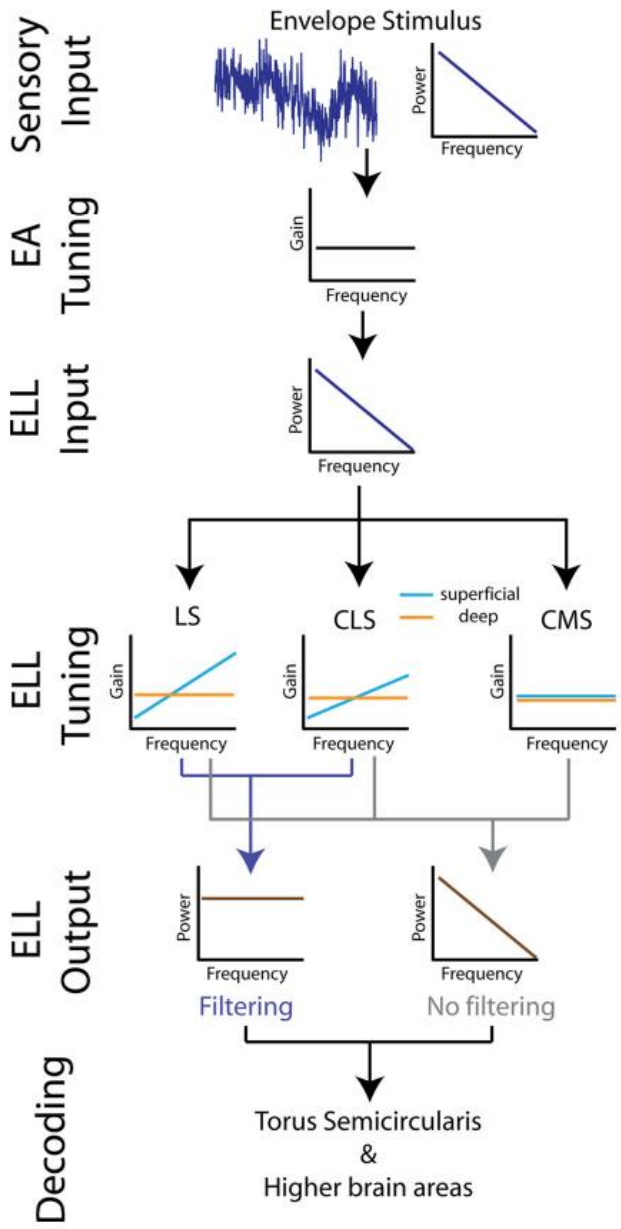

Figure 8. Summary of envelope processing by ELL pyramidal neurons. Natural envelope stimuli are first processed by peripheral electroreceptor afferents (EAs) that perform little to no filtering (Metzen and Chacron, 2015), thereby preserving stimulus statistics. EAs then relay this information to pyramidal cells within the three ELL maps. Superficial pyramidal cells (cyan) within the LS perform the most temporal whitening of these natural stimuli (middle left), followed by superficial CLS pyramidal neurons (middle). Within CMS, all cells displayed little to no temporal whitening and instead preserve natural envelope stimulus statistics. Also, within the CLS and LS maps, deep pyramidal cells (orange) perform little to no temporal whitening and instead preserve natural envelope stimulus statistics. ELL pyramidal cells can thus be segregated into two groups: those that do not perform filtering (gray) and those that do (navy blue). Information transmitted by those two groups is decoded by TS neurons before being transmitted to higher brain areas.

2.5 – Discussion

2.5.1 – ELL pyramidal cell heterogeneities and coding of second-order electrosensory attributes

We investigated how ELL pyramidal cell heterogeneities influence their responses to envelopes. We found that heterogeneities either did not or strongly influenced envelope responses. Specifically, the responses of ON and OFF-type ELL pyramidal cells, despite being out of phase with one another when first-order electrosensory stimulus features were considered, were actually in phase with one another when second-order electrosensory stimulus features were instead considered. Such relative homogeneity is surprising given that peripheral afferents providing feedforward input to ELL pyramidal cells display strong heterogeneities in their responses to second-order features (Metzen and Chacron, 2015; Savard et al., 2011). Indeed, responses to envelopes were in phase for 66% of afferents and out of phase for the remaining 34%. One possibility is that afferents whose responses are out of phase with the envelope do not synapse directly onto pyramidal cells but rather indirectly through local inhibitory interneurons, thereby making the input in phase with the envelope and potentially explaining why ON and OFF-type ELL pyramidal cells display similar responses to envelopes.

We also found that responses to envelopes were cell class (i.e. superficial, intermediate, or deep) as well as map specific. However, as the connectivity pattern from ELL to Torus semicircularis (TS), while preserving somatotopy, appears to be random with respect to cell class or map (Krahe and Maler, 2014), we argue that the different envelope response profiles observed in ELL constitute heterogeneities from the point of view of the decoder. Our simple mathematical model further showed that different levels of adaptation could reproduce our experimental data. Importantly, our model predicts a strong correlation between the observed fractional differentiation exponent and the strength of adaptation across cell classes and across ELL maps. A previous study has shown that LS pyramidal cells display stronger adaptation to envelope steps than their CMS counterparts (Zhang and Chacron, 2016), thereby supporting our hypothesis. We further hypothesize that the differences in envelope response profiles observed across ELL maps and cell class are both primarily if not exclusively due to differences in the level of SK channel expression. This is because: 1) SK channels strongly influence adaptation in ELL pyramidal cells (Deemyad et al., 2012; Ellis et al., 2007) and; 2) the strongest SK channel expression in pyramidal cells was observed in LS and decreased going to CLS, with CMS

showing little to no expression (Ellis et al., 2008; Ellis et al., 2007). Moreover, within LS and CLS, the strongest level of SK channel expression was observed for superficial, decreased for intermediate, and was almost negligible for deep pyramidal cells (Maler, 2009a). Thus, experimentally observed variations in the fractional differentiation exponent were very well correlated with known levels of SK channel expression across cell classes and across ELL maps. Together with previous results showing that pharmacological manipulation of SK channels can directly alter LS pyramidal cell tuning to envelopes (Huang et al., 2016), these results strongly suggest that SK channel expression determines a pyramidal cell's response to envelopes.

ELL pyramidal cell receptive fields (RFs) have a classic antagonistic center-surround organization. There is a tradeoff between the relative sizes of the RF center and surround across the ELL maps. Indeed, while RF center size decreases from CMS to LS, RF surround size instead increases (Maler, 2009a; Shumway, 1989). Moreover, superficial cells have the largest surround while deep cells have little to no surround (Bastian et al., 2002). Thus, while RF size differences across maps are linked to differences in tuning to AM temporal frequency (see (Krahe and Maler, 2014) for review), there does not appear to be such a link when envelopes are instead considered. One important caveat however, is that ELL pyramidal cell RFs were all measured using AMs and not envelopes. Further studies are needed to map pyramidal cell RFs to envelopes and determine whether the spatial structure is coordinated with the temporal response profile.

2.5.2 – Functional role of pyramidal cell heterogeneities in coding of first and second-order electrosensory stimulus attributes

Our results have shown that, within the LS and CLS segments, deep pyramidal cells performed little to no filtering of envelope stimuli as indicated by their gains that were independent of envelope frequency and negligible phase leads. As such, their responses closely resembled that of most peripheral afferents (Metzen and Chacron, 2015). An important question is thus, what is the functional role of having central neurons whose responses are virtually identical to those of most peripheral receptors? One potential explanation is that deep cells exclusively project to the nucleus praeminentialis and provide feedback to their superficial and intermediate counterparts indirectly via parallel fibers originating from cerebellar granule cells within the eminentia granularis posterior (Bastian et al., 2004). We hypothesize that the lack of filtering by LS and

CLS deep cells is necessary to provide feedback to their superficial and intermediate counterparts, thereby determining their response properties to envelopes.

Interestingly, all pyramidal cells within the CMS performed no significant filtering of envelope stimuli because their gains did not depend on envelope frequency and they displayed negligible phase leads. As such, their response profiles closely resemble those of most peripheral receptor afferents (Metzen and Chacron, 2015). What is then the functional role of CMS pyramidal neurons in envelope processing? One possibility is that the observed responses to envelopes are not behaviorally relevant, as downstream brain areas do not decode them. While this possibility cannot be ruled out, we argue that it is unlikely to be true. First, the CMS is by far the largest segment and it does not appear efficient to effectively "waste" such a large amount of resources on the coding of behaviorally relevant stimuli. Rather, as all three ELL maps project to downstream brain areas such as the midbrain TS, we hypothesize that the responses of CMS cells are necessary to properly decode the filtered responses of superficial and intermediate LS and CLS pyramidal cells. The lack of fractional differentiation observed for CMS neurons could provide the contextual information necessary in order to properly decode the optimized representation of natural envelope stimuli provided by superficial LS pyramidal neurons in downstream areas.

Alternatively, it is also possible that the lack of filtering by CMS pyramidal cells serves to provide reliable responses to the prominent low-frequency components of natural envelope stimuli, while the high-pass filtering through fractional differentiation would serve to enhance responses to the weak high-frequency components that could easily be contaminated by noise, as proposed originally by Barlow (Barlow, 2001). We note that such high-pass filtering cannot extend to arbitrarily large frequencies where stimulus power is negligible, as it would then lead to noise magnification. As such, neural sensitivity should increase over the frequency range for which stimulus power is significant and decrease for higher frequencies. Such band-pass tuning has been observed in the retina and is thought to provide an efficient strategy for coding natural scenes (Atick and Redlich, 1992). In the electrosensory system, natural envelopes can contain significant power for frequencies up to ~10 Hz (Fotowat et al., 2013; Stamper et al., 2013; Stamper et al., 2012). Further studies using envelope frequencies higher than those used here are needed to test whether the sensitivity of ELL pyramidal cells to these will decrease. It is also

possible that neurons in higher brain areas low-pass filter input from ELL pyramidal cells, thereby removing noise. Further studies focusing on how TS neurons receiving input from ELL pyramidal cells are tuned to envelopes are necessary to test this hypothesis and are beyond the scope of this paper. However, we note that previous studies have found that a significant fraction of TS neurons displayed responses that were similar to that of ELL neurons and that these project to higher brain areas (Sproule et al., 2015; Vonderschen and Chacron, 2011). It is thus very likely that the information transmitted by CMS pyramidal cells about envelopes is preserved in the electrosensory brain and contributes to determining observed behavioral responses (Metzen and Chacron, 2014).

2.5.3 – Implications for other systems

It is likely that our results will be applicable to other systems. First, we note that natural stimuli across sensory modalities frequently consist of a fast time varying waveform whose envelope varies more slowly. For example, in the auditory system, envelopes carry behaviorally relevant information relating to timbre for music as well as speech recognition (Heil, 2003; Shannon et al., 1998) and are also characterized by a power spectrum that decays as a power law (Theunissen and Elie, 2014). Studies of auditory processing of natural sounds suggest that the auditory system efficiently encodes them through whitening (Lewicki, 2002; Rodriguez et al., 2010). Other sensory systems also perform whitening of natural stimuli (Dan et al., 1996; Wang et al., 2003) and our proposed mechanism involving SK channels, which are expressed ubiquitously in the central nervous system and are major determinants of adaptation (Adelman et al., 2012), could explain the observed high-pass filtering properties of these sensory neurons to artificial stimuli, thereby explaining whitened responses to natural stimuli whose spectra decay as a function of frequency.

Chapter 3

SK Channels enable temporal whitening in pyramidal cells

We had established in chapter 2 that pyramidal cells can respond to envelope stimuli, to differential degrees depending on the segment and depth they are located in. In particular, the curious case of LS superficial pyramidal cells had been predicted to give rise to temporal whitening or temporal decorrelation of the natural movement envelope stimulus statistics. In Chapter 3, we will confirm this prediction by observing responses to natural envelopes within this subset of neurons. We will extend our LIF model to make predictions on how the degree of high-pass tuning is determined, and test these predictions using pharmacological agents to test whether the molecular candidate, SK channels, are actually responsible for establishing optimal coding. Finally, we will link the changes in neural tuning directly to changes in behavioural responses at the organismal level. This chapter is adapted from: Chengjie G. Huang, Zhubo Zhang, Maurice J. Chacron. Temporal decorrelation by SK channels enables efficient neural coding and perception of natural stimuli. *Nature Communications.* 7: 11353, 2016.

3.1 – Abstract

It is commonly assumed that neural systems efficiently process natural sensory input. However, the mechanisms by which such efficient processing is achieved, and the consequences for perception and behavior remain poorly understood. Here we show that small conductance calcium-activated potassium (SK) channels enable efficient neural processing and perception of natural stimuli. Specifically, these channels allow for the high-pass filtering of sensory input, thereby removing temporal correlations or, equivalently, whitening frequency response power. Varying the degree of adaptation through pharmacological manipulation of SK channels reduced efficiency of coding of natural stimuli, which in turn gave rise to predictable changes in behavioral responses that were no longer matched to natural stimulus statistics. Our results thus

demonstrate a novel mechanism by which the nervous system can implement efficient processing and perception of natural sensory input that is likely to be shared across systems and species.

3.2 – Introduction

Understanding the key computations by which neurons process incoming natural sensory stimuli, thereby giving rise to perception and behavior, remains a central problem in neuroscience. There is growing evidence that sensory systems developed coding strategies to suit a dynamic range of statistics in natural sensory stimuli (Attneave, 1954; Barlow, 2001; Dong and Atick, 1995; Laughlin, 1981; Simoncelli and Olshausen, 2001). Indeed, sensory systems can efficiently process input by matching their adaptation properties to natural scene statistics, thereby removing redundant information and thus maximizing information transmission in the presence of noise (Brenner et al., 2000; Fairhall et al., 2001; Maravall et al., 2007). Specifically, efficient neural coding can be achieved by ensuring that the neural tuning function is inversely proportional to stimulus intensity as a function of frequency, thereby achieving a neural response that is decorrelated in the temporal domain or, equivalently, whose amplitude is independent of frequency (Rieke et al., 1996). Such "temporal whitening" has been observed across species and systems (Dan et al., 1996; Wang et al., 2003). However, the mechanisms giving rise to efficient neural processing and, importantly, whether, and if so how, this information is decoded downstream in order to mediate perception and behavior remains poorly understood to this day. Here we show that SK channels, which are found ubiquitously in the brain (Faber and Sah, 2003), mediate efficient processing of natural stimuli by sensory neurons through temporal decorrelation and, importantly, how such processing ensures that perception is matched to natural scene statistics at the organismal level.

Gymnotiform wave-type weakly electric fish sense amplitude modulations of their self-generated quasi-sinusoidal electric organ discharge (EOD) through peripheral electroreceptors found on their skin. These electroreceptors in turn send afferents onto sensory pyramidal neurons within the electrosensory lateral line lobe (ELL) that subsequently project to higher brain areas, thereby mediating perception and behavioral responses (Chacron et al., 2011; Krahe and Maler, 2014). Natural electrosensory stimuli have complex spatiotemporal characteristics(Fotowat et al., 2013; Nelson and MacIver, 1999) and, as in other systems, display both first and second order attributes that vary independently of one another and whose intensity decreases as a power law

as a function of temporal frequency under natural conditions (Fotowat et al., 2013; Stamper et al., 2013). First order stimulus attributes consist of changes in the animal's EOD amplitude caused by objects with conductivity different than that of the surrounding water (e.g. prey, plants, rocks, other fish) (Fotowat et al., 2013; Nelson and MacIver, 1999). In contrast, the second order stimulus attributes occur exclusively during social interactions with conspecifics. For example, when two fish come into close proximity to one another, interference between both EODs gives rise to a sinusoidal stimulus (i.e. a beat or first order) whose frequency is equal to the difference between the two EOD frequencies. The beat amplitude (i.e. the envelope or second order) then depends on the relative distance and orientation between both fish and is therefore a time varying signal under natural conditions that carries behaviorally relevant information and elicits robust behavioral responses (Fotowat et al., 2013; Metzen and Chacron, 2014; Stamper et al., 2013; Stamper et al., 2012).

The responses of electrosensory neurons to first order electrosensory stimulus attributes have been well characterized (see (Chacron et al., 2011; Clarke et al., 2015; Krahe and Maler, 2014; Marquez et al., 2013) for review). Importantly, peripheral receptor afferents display high-pass filtering characteristics of time-varying first order attributes that oppose the strongly decaying intensity as a function of temporal frequency seen under natural conditions (Bastian, 1981; Chacron et al., 2005b; Fotowat et al., 2013; Xu et al., 1996). These afferents are thus thought to efficiently process natural first order natural electrosensory stimulus attributes by temporal whitening (Fotowat et al., 2013). Each afferent trifurcates and makes synaptic contact onto pyramidal cells within three parallel maps (lateral segment: LS; centrolateral segment: CLS; centromedial segment: CMS) of the body surface within the ELL (Heiligenberg and Dye, 1982). Pyramidal cells are the sole output neurons of the ELL and project to higher brain areas (Maler, 1979). Parallel processing occurs at the level of the ELL as pyramidal cells within each map extract different features of first order attributes in part through differential frequency tuning (Krahe et al., 2008; Marsat et al., 2009; Shumway, 1989) that are necessary to elicit appropriate differential behavioral responses at the organismal level (Metzner and Juranek, 1997).

In contrast, much less is known about coding strategies used for the processing of second order electrosensory stimulus attributes. In particular, previous studies have shown that peripheral afferents can faithfully encode these both at the single neuron and population levels

(Metzen and Chacron, 2015; Metzen et al., 2015; Savard et al., 2011). However, because their tuning was found to be independent of temporal frequency, afferents do not efficiently process natural second order electrosensory stimulus attributes through temporal whitening (Metzen and Chacron, 2015). While previous studies have shown that ELL pyramidal cells can respond to second order electrosensory stimulus attributes (McGillivray et al., 2012), their temporal frequency tuning to these has not been investigated to date. It is therefore not known whether and, if so, how, processing of second order electrosensory stimulus attributes by these cells is constrained by natural scene statistics.

We found that ELL pyramidal neurons efficiently process natural second order electrosensory stimulus attributes through temporal whitening. Indeed, neural responses were characterized by weak correlations and by constant power for envelope frequencies spanning three orders of magnitude. Further experimentation and modeling revealed that such temporal whitening is achieved because pyramidal neurons display time-scale invariant adaptation to envelope stimuli. This adaptation enables high-pass filtering of the input through a fractional derivative operation whose exponent is matched to natural stimulus statistics. We further show that small conductance calcium-activated potassium (SK) channels mediate adaptation to envelopes in pyramidal neurons. Indeed, both pharmacological activation and inactivation of these channels altered the degree of fractional differentiation and tuning to envelope stimuli, thereby reducing efficiency of processing of natural stimuli. Importantly, these manipulations caused predictable changes in behavioral responses to natural stimuli by inducing a mismatch between behavioral sensitivity and natural scene statistics. Our results therefore reveal a general mechanism by which SK channels can enable efficient processing and perception of natural stimuli through scale invariant adaptation.

3.3 – Methods

3.3.1 – Animals

The weakly electric fish *Apteronotus leptorhynchus* was used exclusively in this study. Animals were purchased from tropical fish suppliers and were acclimated to laboratory conditions according to published guidelines (Hitschfeld et al., 2009). All procedures were approved by McGill University's animal care committee.

3.3.2 – Surgery

0.1-0.5 mg of tubocurarine (Sigma) was injected intramuscularly in order to immobilize the fish for experiments. The fish was respirated through a mouth tube at a flow rate of ~10 mL/min when placed in the recording tank. To stabilize the head during recording, a metal post was glued to the exposed area of the skull. A small hole of ~ $2mm^2$ was drilled over the caudal lobe of the cerebellum above the ELL in order to gain access to the pyramidal neurons.

3.3.3 – Electrophysiology

We used well-established techniques to make extracellular recordings with Woods metal electrodes from pyramidal cells within the lateral segment (LS) of the ELL (Krahe et al., 2008). We used CED 1401-plus hardware and Spike II software to record the resulting signal with resolution 0.1 ms.

3.3.4 – Pharmacology

The composition of the vehicle/control saline is as follows (all chemicals were obtained from Sigma): 111 mM NaCl, 2 mM KCl, 2 mM $CaCl_2$, 1 mM $MgSO_4$, 1 mM $NaHCO_3$, 0.5 mM NaH_2PO_4. The pH of the saline solution was 6.8. Glutamate (Sigma), UCL-1684 Ditrifluoroacetate hydrate (Sigma), and 1-EBIO 1-Ethyl-2-benzimidazolinone (Sigma) were dissolved in saline for application as before (Toporikova and Chacron, 2009). Drug application electrodes were two-barrel KG-33 glass micropipettes (OD 1.5 mm, ID=0.86 mm, A-M Systems) pulled by a vertical micropipette puller (Stoelting Co.) to a fine tip and subsequently broken to attain a tip diameter of ~10 μm. The two barrels were used for separate application of either UCL-1684 (100 μM) or 1-EBIO (2.5 mM) and glutamate (1 mM). During recordings, we first used excitatory responses to glutamate application via PicoSpritzer to confirm that we were within proximity of the pyramidal neuron we were recording from as done previously (Deemyad et al., 2013). UCL-1684 and 1-EBIO were then applied as done previously (Toporikova and Chacron, 2009).

3.3.5 – Behavior

Animals were immobilized and set up in the recording tank similarly to the method described above. However, both ELLs were exposed and two glass micropipettes loaded with saline

control solution, UCL-1684 (100 μM), or 1-EBIO (2.5mM) solution were inserted into the LS segment using previously established techniques (Deemyad et al., 2013; Larson et al., 2014). Simultaneous bilateral injection of either saline, UCL-1684, or 1-EBIO into the LS region of the ELL molecular were delivered via a PicoSpritzer (Pressure=10 psi, Pulse duration=140 ms). Sinusoidal waveforms with frequency of 4 Hz below the animal's baseline EOD frequency and with intensity of 2 mV/cm with duration of 50 s were presented. Previous studies have shown that such stimuli will reliably elicit a jamming avoidance response (JAR) and/or transient EOD frequency excursion (i.e. chirp) responses in *A. leptorhynchus* (Deemyad et al., 2013). The JAR magnitude was defined as the maximum frequency elicited during stimulation minus the baseline (i.e., without stimulation) value and was used as a positive control to confirm that UCL-1684 had an effect. Envelope stimuli were then subsequently played and saline or UCL injected two or three times before each stimulus presentation. Behavioral sensitivity was measured as the ratio between the amplitude of the envelope stimulus as extracted by the dipole, and the response, which was quantified by the average extracted change in EOD frequency of the fish over the course of the stimulus. The phase relationship was quantified by determining the difference between the phase at which the maximum peak of the envelope stimulus occurred and the phase at which the maximum peak of the average extracted change in EOD frequency. $\alpha_{behavior}$ was obtained by fitting a power law to the behavioral sensitivity as a function of frequency.

3.3.6 – Stimulation

The electric organ discharge of *A. leptorhynchus* is neurogenic, and therefore is not affected by injection of curare. All stimuli consisted of amplitude modulations (AMs) of the animal's own EOD and were produced by triggering at the zero crossing of each EOD cycle as done previously (Bastian et al., 2002). This allowed the train of sinusoid stimuli to be synchronized to the animal's discharge and depending on the polarity, either added or subtracted from the animal's own discharge. The modulated waveform was subsequently multiplied (MT3 multiplier; Tucker Davis Technologies) and the resulting signal was isolated from ground (A395 linear stimulus isolator; World Precision Instruments). The signal was then delivered through a pair of chloridized silver wire electrodes placed ~15cm on either side of the recording tank perpendicular to the fish. The stimulus intensity was adjusted to give rise to changes in EOD amplitude that was ~20% of the baseline level as in previous studies (Bastian et al., 2002) that

were measured using a small dipole placed close to the animal's skin. The stimuli consisted of two noisy AM waveforms with frequency contents 5-15Hz and 60-80Hz whose envelopes were modulated, sinusoidally with frequencies ranging from 0.05Hz to 1Hz (Fotowat et al., 2013) or in a stepwise fashion at frequencies 0.05, 0.1, 0.25, 0.5, 1, 2, and 4 Hz for 5-15 Hz and 0.05, 0.1, 0.25, 0.5, 1, 2, 4, 8, and 16 Hz for 60-80 Hz (note that the step duration is then half of the stimulus period). Stimuli also consisted of envelope stimulus waveforms obtained under natural conditions (Metzen and Chacron, 2014) as well as noisy waveforms whose power spectrum decayed as a power law with exponent α_{stim}=-0.8 and whose phase varied uniformly. The slope of the spike triggered average computed in response to the noisy AM waveform was used to assign each cell as either ON of OFF-type as done previously (Chacron et al., 2005c).

3.3.7 – Fractional Differentiation model

Fractional differentiation (Podlubny, 1999) can be described simply as the differentiation operation, d^{α}/dt^{α}, in which the order of differentiation, is a non-integer number. In the frequency domain, fractional differentiation of order α corresponds to filtering by a transfer function *H(f)* given by:

$$H(f) = (2\pi f)^{\alpha}\exp\left(i\alpha\frac{\pi}{2}\right)$$

The gain G(f) and phase ϕ(f) of the model can then be written as:

$$G(f) = |H(f)| = (2\pi f)^{\alpha}$$

$$\phi(f) = \arctan\left(\frac{Im[H(f)]}{Re[H(f)]}\right) = \alpha\frac{\pi}{2}$$

where $Im[H(f)]$ and $Re[H(f)]$ are the imaginary and real parts, respectively. We fitted a fractional differentiation model to our data using the Grunwald-Letnikov definition which was adapted to use a vectorization method to pass signals through a spectrum of fractional derivative values between 0 and 1 from which we obtained α_{neuron} (Podlubny, 1999).

3.3.8 – Matching response sensitivity to stimulus statistics in order to ensure temporal decorrelation

Linear response theory(Risken, 1996) posits that the response power spectrum $P_{rr}(f)$ is related to the gain *G(f)* and the stimulus power spectrum $P_{ss}(f)$ by the following equation:

$$P_{rr}(f) \approx G^2(f) P_{ss}(f)$$

Thus, if the stimulus power spectrum decays as a power law with exponent α_{stim} and if the neural gain increases as a power law with exponent α_{neuron}, then we have:

$$P_{rr}(f) \approx f^{2\alpha_{neuron}+\alpha_{stim}}$$

The response power spectrum will then be independent of frequency *f* if $2\alpha_{neuron}+\alpha_{stim}=0$ or, equivalently, if:

$$\alpha_{neuron} = -\frac{\alpha_{stim}}{2}$$

3.3.9 – Relationship between neural tuning and behavior

We assume that the neural tuning exponent α_{neuron} and the behavioral exponent $\alpha_{behavioral}$ are related by:

$$\alpha_{behavior} = -\alpha_{neuron} - 0.4$$

We then have:

$$\Delta\alpha_{behavior} = -\Delta\alpha_{neuron}$$

where $\Delta\alpha$ is the change in exponent α resulting from pharmacological manipulation of SK channels.

3.3.10 – Neuron Model

In order to model the responses of the pyramidal neurons to the stimuli used in this study, we implemented a leaky integrate-and-fire model with power-law adaptation:

$$C\frac{dV}{dt} = -g_{leak}(V - E_{leak}) - z_1(t) + I + \sigma_{noise}\,\xi(t) + \sigma_{stim}\,s(t)$$

where *C* is the membrane capacitance, g_{leak} is the leak conductance, E_{leak} is the leak reversal potential, *I* is a constant bias current, $\xi(t)$ is gaussian white noise with zero mean and standard deviation unity, σ_{noise} is the noise intensity, $s(t)$ is the stimulus which was taken to have the same statistics as for the data, σ_{stim} is the stimulus intensity, V is the membrane potential, and $z_1(t)$ is the adaptation current. Each time the membrane potential reaches the threshold θ, it is reset to V_{reset} and an action potential is said to have occurred at that time. The adaptation current is then incremented

We approximated the power law adaptation using N variables $z_1 \ldots z_N$ that obeyed the following system of differential equations (Drew and Abbott, 2006):

$$\frac{dz_i}{dt} = \frac{-z_i(t) + z_{i+1}(t)}{\tau_i} + b\,\gamma^{1-i} \sum_j \delta(t - t_j) \text{ for i = 1 to N} - 1$$

$$\frac{dz_N}{dt} = \frac{-z_N(t)}{\tau_N} + b\,\gamma^{1-N} \sum_j \delta(t - t_j)$$

$$\tau_i = \tau_{\min}\gamma^{i-1}$$

where t_j are the spikes times, $\delta(t)$ is the delta function, and b and γ are constants that determine the strength and power law exponent α_{neuron} of the neural sensitivity, respectively. The model was simulated using an Euler-Maruyama integration with timestep dt=0.025 ms. We used parameter values C=1 μF/cm^2, g_{leak}=0.36 μS/cm^2, E_{leak}=-70 mV, I= μA/cm^2, σ_{noise}= μA/cm^2, N=40, b=0.2, γ=1.1253, θ=-50 mV, V_{reset}=-70 mV, C=1 μF/cm^2. For these parameter values, we obtained α_{model}=0.4.

3.3.11 – Data Quantification

We used several Methods in order to quantify our experimental data. Correlation time was measured as the duration of time it took to decay to 5% of maximum autocorrelation value. White index was measured by taking the normalized area under the power spectrum curve using a trapezoidal method and dividing by the maximum normalized area to achieve a value between 0 and 1. The match between behavior and natural stimulus statistics was obtained as 1-(α_{stim}-$\alpha_{behavior}$) and thus is maximum when the two power-law exponents and match. This method was used in order to quantify the optimality of the animal's behavior during the pharmacology experiments. For step envelope stimuli, we constructed peri-stimulus time histograms (PSTHs) by averaging over each step onset and offset and typically used 50 bins for a given step duration.

3.4 – Results

3.4.1 – Fractional differentiation enables temporal whitening

We recorded ELL pyramidal neuron responses to stimuli (n=14) in awake and behaving animals (Figs. 1A). Our stimuli consisted of a fast time varying waveform (first-order) with a slow time

varying amplitude (i.e. the envelope or second-order) as encountered under natural conditions (Fotowat et al., 2013; Metzen and Chacron, 2014). Fig. 1A shows an example AM waveform (magenta), its envelope (blue), as well as the full signal received by the animal (green) with respective frequency content. It is important to realize that the animal's unmodulated EOD is a carrier and that the meaningful stimulus here is the EOD AM. Thus, we note that the first- and second-order features of the stimulus actually correspond to the second- and third-order features of the full signal received by the animal, respectively.

We considered envelope waveforms that either varied sinusoidally or whose timecourse mimicked of that seen under natural conditions (Fig. 1B, see Methods). Specifically, for the latter case, the envelope autocorrelation decayed over a time window of 400 ms (Fig. 1C, inset) while the envelope power decayed as a power law with exponent α_{stim}=-0.8 (Fig. 1C). We found that pyramidal neurons displayed robust responses to such stimuli (Fig. 1B, bottom). Interestingly, further analysis revealed that pyramidal neurons perform temporal decorrelation of natural envelope stimuli. Indeed, the response autocorrelation function decayed to zero much faster than that of the stimulus over a time window of 27.5 ms (Fig. 1C, inset) as quantified by significant differences in correlation time (see Methods, Fig. 1D, left). Moreover, the response power spectrum was constant for frequencies spanning three orders of magnitude (Fig. 1C), indicating whitening. Indeed, the population-averaged neural whitening index was significantly larger than that of the stimulus (Fig. 1D, right). We note that ELL pyramidal cells can be classified as either ON or OFF-type based on whether they respond with increases or decreases in firing rate to increases in EOD AM (i.e. first order), respectively (Saunders and Bastian, 1984). Cells in our dataset could be easily identified as either ON or OFF-type based on responses to sinusoidal AMs (Supplementary Figures 1A, 1B). We however found no significant differences between ON and OFF-type pyramidal cell responses to envelope stimuli (Supplementary Figures 1C, 1D). Data from each cell class were thus pooled in subsequent analyses.

How is temporal whitening of natural stimuli by pyramidal neurons achieved? Theory posits that such whitening is achieved by ensuring that the neuron's tuning curve is matched to the statistics of natural input (Rieke et al., 1996). Neural sensitivity should then be highest for frequencies at which stimulus power is lowest. A simple derivation (see Methods) predicts that, in order to achieve temporal whitening of stimuli whose power decreases with exponent α_{stim}= -

0.8, neural sensitivity should increase as a power law with exponent $\alpha_{neuron}=-\alpha_{stim}/2=0.4$ (Fig. 2A).

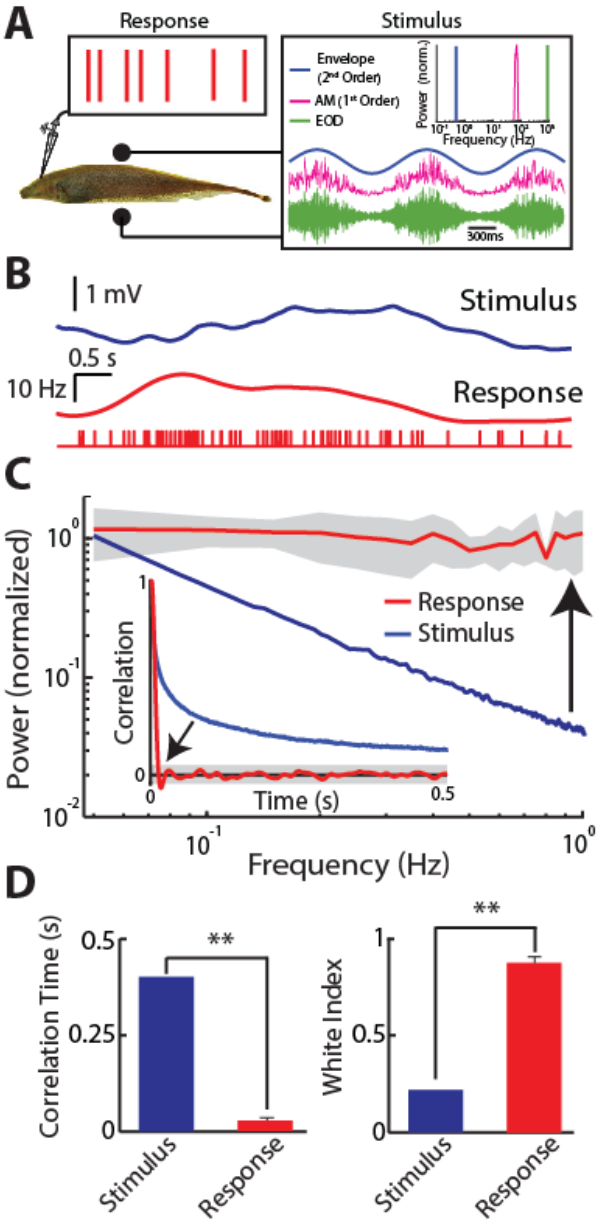

Figure 1. Temporal decorrelation of natural stimuli by electrosensory pyramidal neurons. A) Schematic showing the awake behaving preparation where a stimulus is presented to the animal while neural activity is being recorded. Shown on the right are: example AM waveform (magenta), its envelope (blue), and the full signal received by the animal (green) with their respective frequency contents. B) Natural envelope stimulus (blue) as well as the firing rate (middle) and spiking (bottom) response of a typical ELL pyramidal neuron. C) Stimulus (blue), and population-averaged (red) neural response power spectrum. Note the flattening of the response spectrum (black arrow). The gray band shows one SEM. Inset: Stimulus (blue), and population-averaged (red) neural response autocorrelation function. Note that the neural autocorrelation function decays to zero much faster than that of the stimulus (black arrow).

*The gray band shows the 95% confidence interval around zero. D) Left: Correlation time for the stimulus (blue) and neural response (red). Right: White index for the stimulus (blue) and neural response (red). "**" indicates statistical significance at the p=0.01 level using a Wilcoxon rank-sum test with N=14.*

To verify this prediction, we recorded pyramidal neuron responses (n = 14) to sinusoidal envelope stimuli with frequencies spanning the behaviorally relevant range (0.05-1 Hz). We found that pyramidal neurons responded to such stimuli through sinusoidal modulations in firing rate that increased in amplitude as a function of frequency (Fig. 2B). We then used linear systems identification and plotted the sensitivity and phase relationships between stimulus and neural response as a function of frequency (Fig. 2C). Our results show that sensitivity indeed increased as a power law as a function of frequency with exponent 0.4 (Fig. 2C, top), while the phase remained constant (Fig. 2C, bottom). Such phase constancy is typical of fractional differentiation, a mathematical operation that is thought to be advantageous for coding (Lundstrom et al., 2008). Fractional differentiation in the time domain is equivalent to linearly filtering by a transfer function with gain $(2\pi f)^{\alpha}$ and phase $\alpha\pi/2$ (see methods), where f is the frequency and α is the order of differentiation. We thus fitted a fractional derivative model with α=0.4 to our data (see Methods) and found an excellent fit (Fig. 2C). Importantly, this simple model correctly predicted temporal decorrelation and whitening seen in response to naturalistic envelope stimuli (Fig. 2D) as quantified by both correlation time (Fig. 2E) and whitening index (Fig. 2F). We conclude that temporal whitening of natural envelopes occurs because pyramidal neurons high-pass filter the input stimulus through fractional differentiation whose exponent is precisely matched to natural scene statistics.

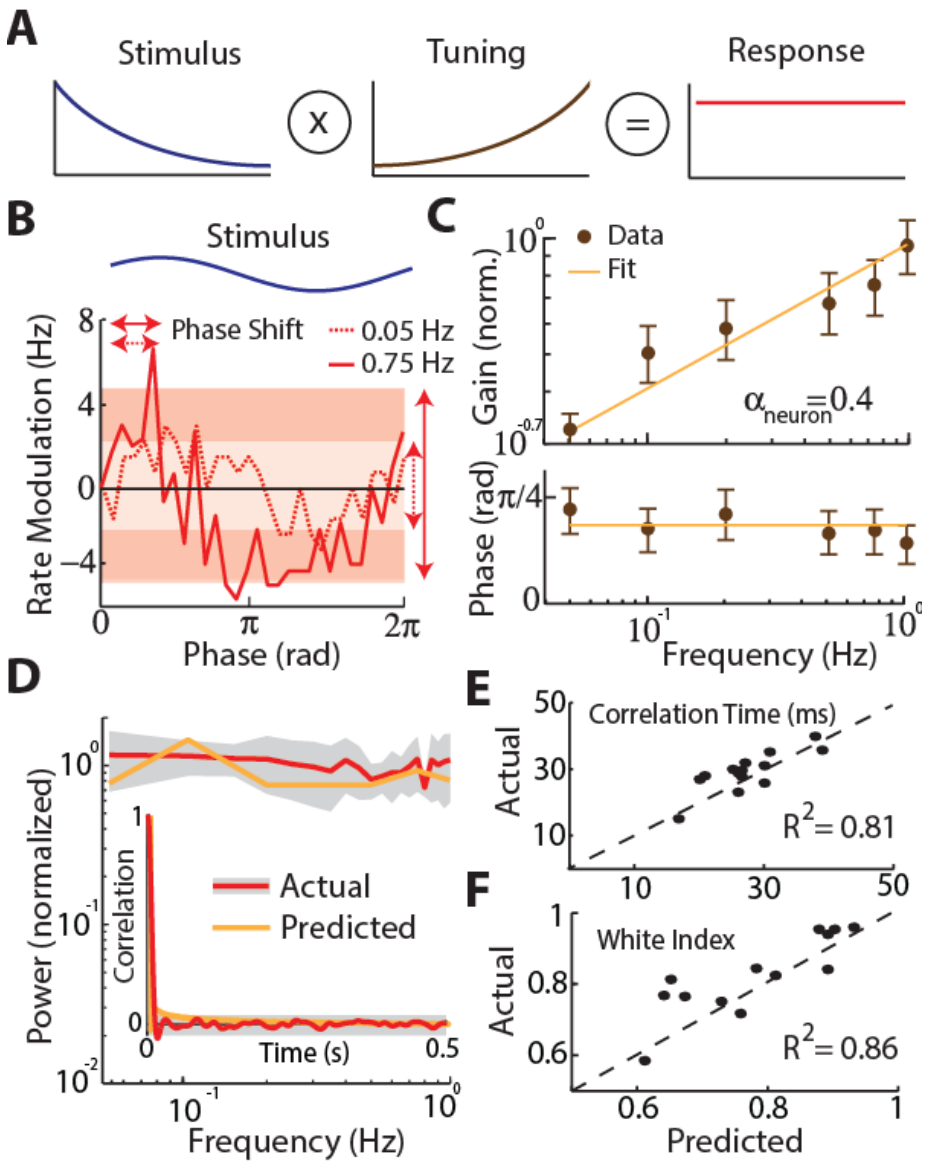

Figure 2. Fractional differentiation by electrosensory pyramidal neurons achieves temporal decorrelation. A) Schematic showing that the neural tuning function (middle) must oppose the decay in the stimulus power (left) in order to achieve a neural response that is constant (right). B) Phase histograms showing the firing rate modulation in response to the stimulus (blue) for low (dashed red) and high (solid red) envelope frequencies. The bands and vertical arrows show the amplitudes of the best sinusoidal fits (not shown for clarity) for both frequencies, which are used to compute gain. The horizontal arrows show the phase shift between the stimulus and the firing rate modulation signal. C) Population-averaged (brown) sensitivity (top) and phase (bottom) obtained from sinusoidal stimuli (N=14). The solid orange lines show the gain and phase of the best-fit fractional derivative. D) Predicted (orange) and actual (red) response power spectra to natural stimuli (N=14). The grey band shows 1 SEM. Inset: Predicted (orange) and actual (red) response autocorrelation function. The grey band shows the 95% confidence interval around zero. E,F) Predicted as a function of actual correlation time and white index, respectively.

3.4.2 – A simple model reproduces experimental data

In order to gain insight into the mechanism which enables pyramidal neurons to efficiently process natural stimuli through fractional differentiation, we built a simple model based on the leaky integrate-and-fire formalism that included a spike-activated adaptation current that decayed as a power law in the absence of firing (Drew and Abbott, 2006), see Methods (Fig. 3A). The output model spike train was analyzed in the same way as our experimental data. Numerical simulation revealed that this simple model accurately reproduced our experimental data (compare Figs. 3B and 2B). Indeed, the model neuron's sensitivity and phase closely matched those obtained experimentally (Fig. 3C). Importantly, the model also accurately reproduced temporal whitening in response to naturalistic stimuli (Fig. 3D) as quantified by correlation time (Fig. 3E) and white index (Fig. 3F).

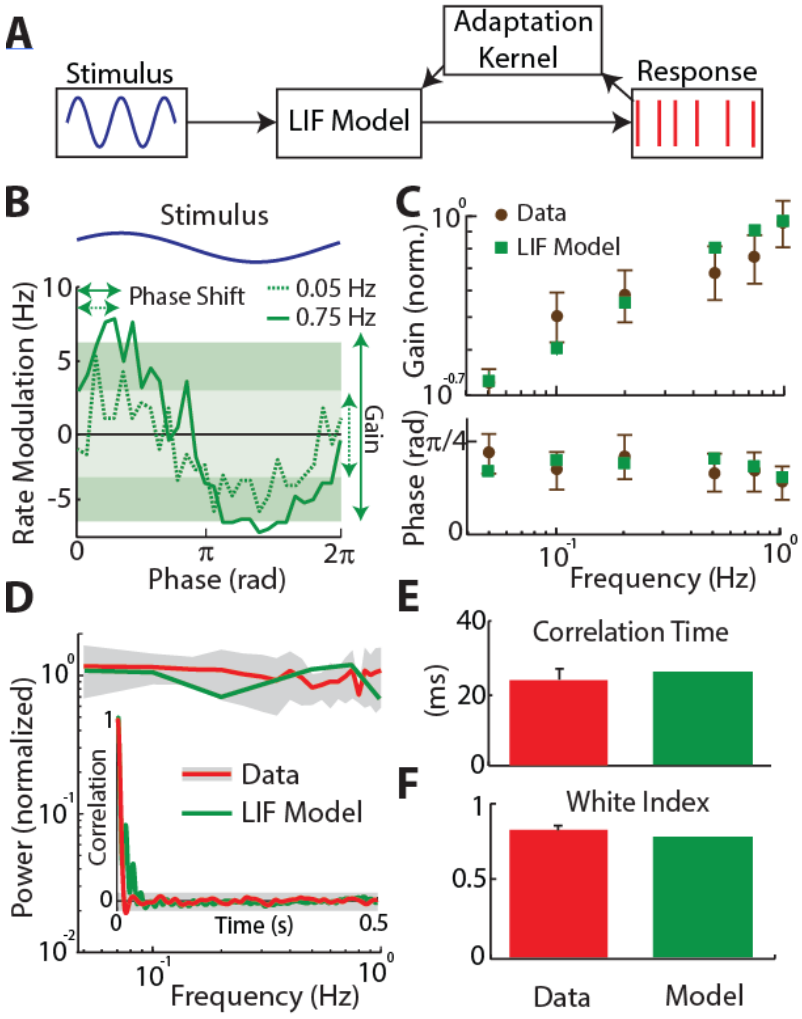

Figure 3. A simple model with power law adaptation implements temporal decorrelation by fractional differentiation. A) Model schematic in which the stimulus (blue) is fed to a leaky integrate-and-fire (LIF) neuron model with an adaptation kernel that decays as a power law as a function of time. The spiking output of the model (red) was analyzed in the same manner as the experimental data. B) Phase histograms showing the firing rate modulation in response to the stimulus (blue) for low (dashed green) and high (solid green) envelope frequencies. The bands and vertical arrows show the amplitudes of the best sinusoidal fits (not shown for clarity) for both frequencies, which are used to compute gain. The horizontal arrows show the phase shift between the stimulus and the firing rate modulation signal. C) Population-averaged sensitivity (top) and phase (bottom) for the data (brown) and our LIF model (green) obtained for sinusoidal stimuli. D) Response power spectra to natural stimulation for our experimental data (red) and LIF model (green). The grey band shows 1 SEM for the experimental data. Inset: Response autocorrelation function to natural stimulation for our experimental data (red) and LIF model (green). The grey band shows the 95% confidence interval around zero for the experimental data. E,F) Population-averaged values obtained from experimental data (red) and for our LIF model (green) for correlation time and white index, respectively.

To understand how adaptation can lead to efficient processing of natural stimuli, we next systematically varied the strength of the adaptation current in our model. We found that, without adaptation, our model displayed constant sensitivity and no phase lead in response to envelope stimuli (light green curves in Figs. 4A, B). Increasing the adaptation strength led to sensitivity curves which increased more steeply as a function of frequency and furthermore increased phase lead (compare light and dark green curves Figs. 4A, B), consistent with increases in the neural exponent α_{neuron} (Fig. 4C). These results have important implications as they predict that, for a given adaptation strength, our model can only achieve temporal decorrelation/whitening of stimuli whose power decays with a given exponent. This was verified by plotting the whitening index for naturalistic envelope stimuli (i.e. α_{stim}=-0.8) as a function of the adaptation strength. Indeed, both lower and higher adaptation strength led to tuning curves that were not matched to natural stimulus statistics and lowered coding efficiency as quantified by lower white index values (Fig. 4D).

Our model therefore makes two important predictions. The first is that, in order to observe temporal whitening of scale invariant natural stimuli through fractional differentiation, neurons must display adaptation that is also scale invariant (i.e. decay as a power law). The second is that temporal whitening is only achieved for a given adaptation strength. Thus, increases or decreases in the adaptation strength will alter neural tuning and lead to sub-optimal processing of natural stimuli.

3.4.3 – Pyramidal neurons display power law adaptation

To test whether pyramidal neurons display scale invariant adaptation, we recorded their responses to step changes in envelopes (Fig. 5A). We found that pyramidal neurons responded to such stimuli by a rapid increase in firing rate followed by a slower decay following the step onset, which is characteristic of spike frequency adaptation (Fig. 5A). If adaptation displays a characteristic timescale (i.e. is not scale invariant), then we expect that the peristimulus time histogram (PSTH) responses to step onset with different duration will all be well-fit by an exponential curve with the same time constant whereas a power law will instead give a poor fit. If adaptation is instead scale invariant, then we expect that PSTH responses to step onset with different duration will all be well fit by a power law curve with the same exponent. The apparent decay time constant of adaptation as quantified by fitting an exponential will then be inversely proportional to the step duration (Fairhall et al., 2001; Lundstrom et al., 2010).

To test our hypothesis, we plotted the time-dependent firing rate in response to steps with different durations. The curves obtained did not overlap and were each well fit by exponentials but with different time constants (Fig. 5B). Rescaling both the firing rate and time led to strong overlap between the curves that were all well fit by power laws with the same exponent (Fig. 5C). We note that rescaling both firing rate and time will not alter the power law exponent. Thus, our results suggest that the time course of adaptation in ELL pyramidal cells follows a power law rather than an exponential. We next systematically varied the step duration and found that, while the exponential time constant varied strongly as a function of step duration (Fig. 5D, left), the power law exponent was instead relatively independent of step duration (Fig. 5D, right). We conclude that pyramidal neurons indeed display scale invariant (i.e. power law) adaptation in response to envelopes as predicted by our model.

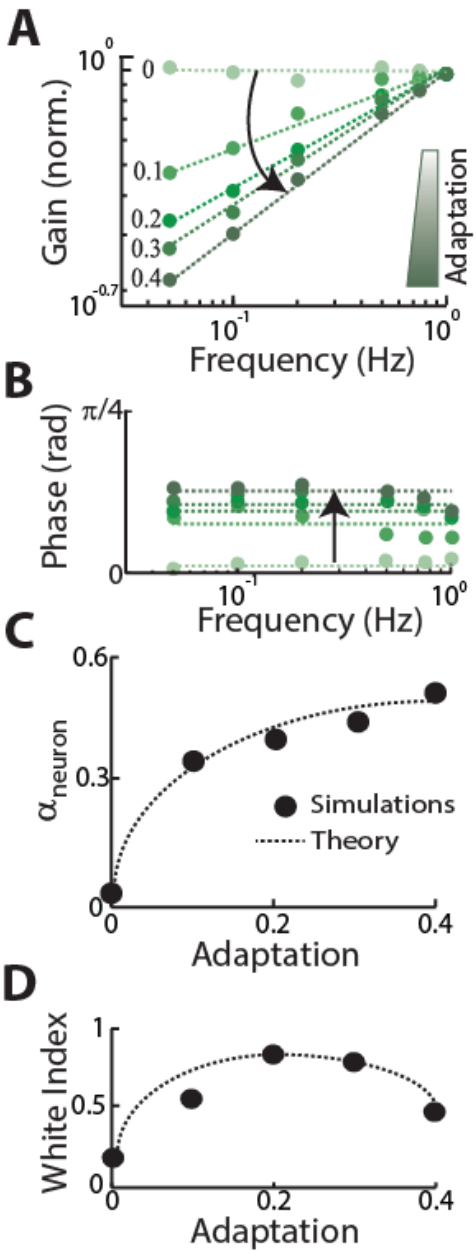

Figure 4: Our model predicts that adaptation strength is critical to ensure efficient processing of natural stimuli. A,B) Model gain and phase as a function of frequency for different amounts of adaptation, respectively. For each amount of adaptation, the circles show the values obtained from numerical simulation and the dashed lines those from the best-fit fractional derivative model. Note the progressive steepening of the gain curve as well as the increase in phase as adaptation is increased (black arrows). C) Neural exponent α_{neuron} as a function of adaptation showing values obtained from numerical simulation (black circles) and theoretical prediction (dashed line). D) White index computed in response to a natural stimulus with exponent α_{stim}=-0.8 as a function of adaptation showing values obtained from numerical simulation (black circles) and theoretical prediction (dashed line).

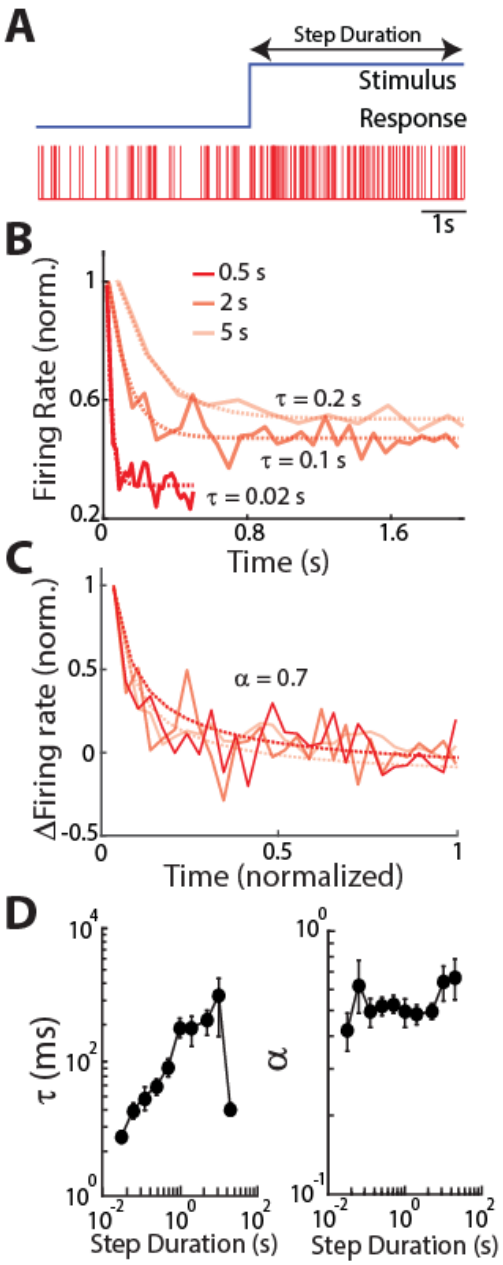

Figure 5: Electrosensory pyramidal neurons display power law adaptation in response to step changes in envelopes. A) Top: Step stimulus that switches from a low to a high value (onset) with duration indicated by the black arrow. Bottom: Spiking response from a typical electrosensory pyramidal neuron to this stimulus. B) Time dependent firing rate following the step onset (solid red) for three different step durations and corresponding best exponential fits (dashed red). The numbers give the time constants of these fits: note the different values obtained for different step durations. We note that firing rate normalization does not affect the value of the fitted exponential time constants. C) Normalized change in firing rate as a function of normalized time following the step onset (solid red) for the same three different step durations and corresponding power law fits (dashed red). Note that the curves now superimpose and are thus well fit by power laws with similar exponents. D) Left: Population-averaged exponential time constant τ as a function of step duration. Right: Population-averaged power law exponent α as a function of step duration (N = 23).

3.4.4 – SK channels promote efficient coding of natural stimuli

So far, we have shown that ELL pyramidal neurons can efficiently process natural stimuli through temporal decorrelation because of fractional differentiation, which ensures that the neural tuning increases as a power law with exponent α_{neuron} that is precisely related to the power law exponent of the stimulus α_{stim}. Our model predicted that such fractional differentiation can

be explained by including an adaptation current whose timecourse follows a power law which was confirmed experimentally. Importantly, our model also predicted that changing the level of adaptation can strongly affect α_{neuron}, which should decrease coding efficiency. Thus, we next tested experimentally whether modifying adaptation in pyramidal neurons will alter their tuning exponent α_{neuron}, and whether this will decrease coding efficiency as quantified by the white index.

We focused on small conductance calcium-activated potassium (SK) channels. This is because previous results have shown that pharmacologically activating and inactivating these currents will increase and decrease adaptation in ELL pyramidal neurons, respectively (Deemyad et al., 2011; Ellis et al., 2007). We thus hypothesized that pharmacological activation and inactivation of SK channels will increase and decrease fractional differentiation by pyramidal neurons, respectively, thereby altering tuning. Both manipulations are then predicted to decrease efficient coding of natural stimuli by temporal whitening. We thus micro-injected the SK channel antagonist UCL-1684 (UCL) as well as the SK channel agonist 1-EBIO (EBIO) in the ELL using well-established methodology (Bastian 1993; Deemyad et al. 2013; Supplementary Figure 2A, see Methods) (Fig. 6A). We note that previous studies have shown that injection of saline alone using this methodology does not alter pyramidal neuron activity (Bastian, 1993; Deemyad et al., 2013). Consistent with previous results (Ellis et al., 2007; Toporikova and Chacron, 2009), we found that UCL and EBIO application both strongly altered pyramidal neuron activity in the absence of stimulation (Supplementary Figures 2B,C,D).

If our hypothesis is true, then we expect that UCL application will decrease the neural tuning exponent α_{neuron} as neural sensitivity should then increase less steeply as a function of frequency when using sinusoidal stimuli. In contrast, we expect that EBIO application will increase the neural tuning exponent α_{neuron} as neural sensitivity should then increase more steeply as a function of frequency. Consistent with these predictions, neural sensitivity indeed became relatively independent of frequency following UCL application as quantified by a decrease in α_{neuron} (Fig. 6B, compare red and purple). Neural sensitivity increased more steeply as a function of frequency after EBIO application as quantified by an increase in α_{neuron} (Fig. 6B, compare red and cyan).

We next tested whether changes in neural tuning do indeed decrease coding efficiency when instead using natural stimuli. To do so, we next plotted the response power spectra before and after application of either UCL or EBIO. We found that, after UCL application, the response power spectrum decayed as a function of frequency (Fig. 6C, compare red and purple). In contrast, the response power spectrum increased as a function of frequency after EBIO application (Fig. 6C, compare red and cyan). The changes in power spectra observed were in agreement with predictions from our simple model (Fig. 6C, compare dashed and solid curves) that were based solely on the changes in α_{neuron} (Fig. 6D). Importantly, confirming our prediction; UCL and EBIO application both significantly reduced coding efficiency as quantified by the white index (Fig. 6E).

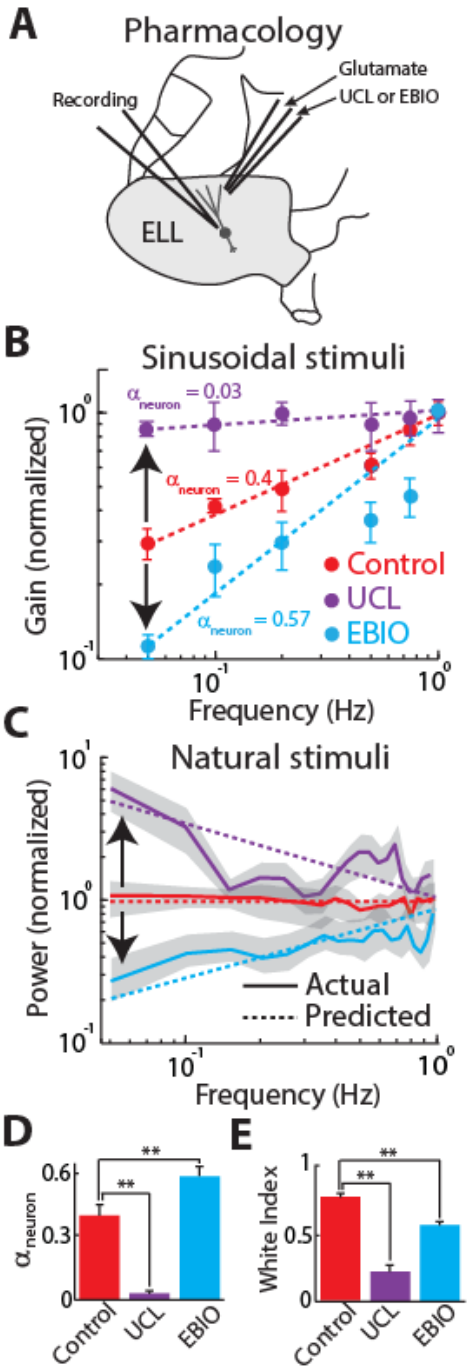

*Figure 6: Pharmacological inactivation and activation of SK channels alter neural sensitivity and both reduce coding efficiency of natural stimuli. A) Schematic showing how a double-barrel electrode approaches and can eject glutamate as well as either UCL (SK channel antagonist) or EBIO (SK channel agonist) in the near vicinity of the pyramidal neuron being recorded from. B) Normalized gain as a function of frequency obtained for sinusoidal stimuli under control (red), after UCL application (purple), and after EBIO application (cyan). The circles show the experimental data and the dashed lines the best power law fits with exponents α_{neuron} given in the figure. UCL and EBIO application decreased and increased the steepness of the curve, respectively (black arrows). C) Response power spectra to natural stimuli under control (solid red), after UCL application (solid purple), and after EBIO application (solid cyan). The dashed lines show the predicted values obtained from the power law fits in B). UCL and EBIO application led to response power spectra that were no longer independent of frequency (black arrows). D) Population-averaged neural exponent α_{neuron} under control (red), after UCL application (purple) (N=6), and after EBIO application (cyan) (N=8). E) Population-averaged white index values under control (red), after UCL application (purple) (N=6), and after EBIO application (cyan) (N = 8). "**" indicates statistical significance at the p=0.01 level using a one-way ANOVA with post-hoc Bonferroni correction.*

3.4.5 – SK channels in ELL determine behavioral responses

Information transmitted by neurons is only useful to an organism if it is actually decoded downstream. Thus, we next investigated how efficient coding of natural stimuli by ELL

pyramidal neurons mediates perception. To do so, we took advantage of the fact that weakly electric fish display robust behavioral responses to envelope stimuli (Metzen and Chacron, 2014, 2015) (Fig. 7A). These consist of changes in the animal's EOD frequency that follows the stimulus' detailed timecourse but whose magnitude decreases with increasing frequency (Fig. 7B). Behavioral response sensitivity is matched to natural stimulus power (Fig. 7C). Indeed, both curves decreased as a power law with exponents $\alpha_{behavior}$ and α_{stim} that were not significantly different from one another (Fig. 7C, inset). This matching ensures that behavioral sensitivity is greatest for stimulus frequencies that tend to occur most frequently in the natural environment (Metzen and Chacron, 2014; Simoncelli and Olshausen, 2001).

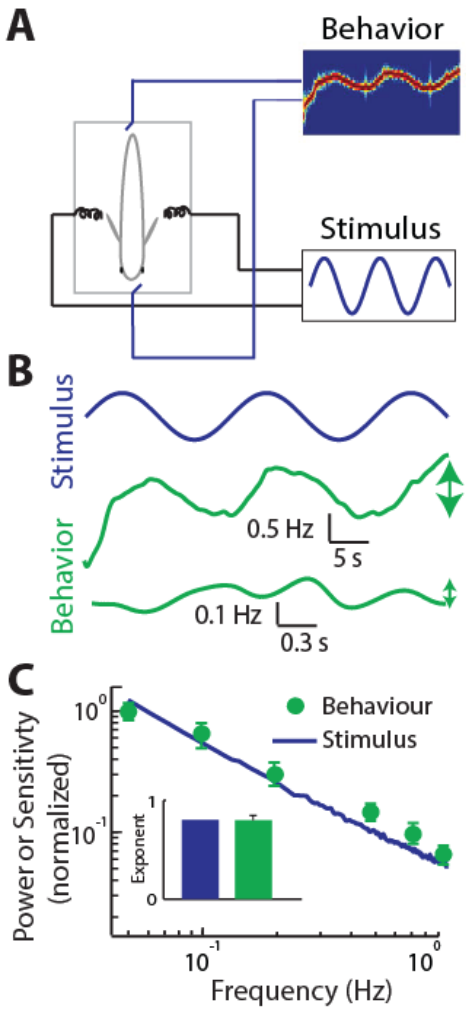

Figure 7: Weakly electric fish display behavioral responses that are matched to natural scene statistics. A) Schematic showing the behavioral setup in which the animal's behavioral responses to stimuli are recorded by continuously monitoring its EOD whose spectrogram indicates the time varying frequency. B) Stimulus (blue) and time varying EOD frequency responses (green) to 0.05 Hz (middle) and 0.75 Hz (bottom) sinusoidal stimuli. Note the smaller changes in EOD frequency in response to the 0.75 Hz stimulus (vertical green arrows). C) Behavioral response sensitivity (green) is matched to the power spectrum (blue) of natural envelope stimuli. Inset: Population-averaged power law exponents from behavioral sensitivity (green) and from natural envelope stimuli (blue).

We hypothesized that behavioral sensitivity is directly related to ELL pyramidal neuron tuning. Thus, changing the neural tuning exponent α_{neuron} should cause changes in the behavioral exponent $\alpha_{behavior}$ (Fig. 8A) and a simple model predicts that $\Delta\alpha_{behavior}=-\Delta\alpha_{neuron}$ (see Methods). To test our hypothesis, we injected UCL and EBIO bilaterally into the ELL (Fig. 8B) (Deemyad et al., 2013; Larson et al., 2014) (see Methods). As a control, injection of saline alone had no significant effect on behavioral responses (Supplementary Figure 3). In contrast, UCL and EBIO injection both strongly altered behavioral sensitivity (Fig. 8C). Indeed, behavioral sensitivity decreased more steeply following UCL application as quantified by a greater behavioral exponent $\alpha_{behavior}$ (Fig. 8C, compare red and purple, Fig. 8C, inset). In contrast, behavioral sensitivity decreased less steeply after EBIO application as quantified by a lesser behavioral exponent $\alpha_{behavior}$ (Fig. 8C, compare red and cyan, Fig. 8C, inset). Importantly, behavioral sensitivity was no longer matched to natural stimulus statistics after both UCL and EBIO application (Fig. 8D). Consistent with our simple model, changes in behavioral tuning $\alpha_{behavior}$ following UCL and EBIO application were consistent with predictions made from changes in α_{neuron} (Fig. 8E). Thus, we conclude that efficient processing of natural envelope stimuli by ELL pyramidal neurons does indeed ensure that behavioral sensitivity at the organismal level is matched to natural scene statistics.

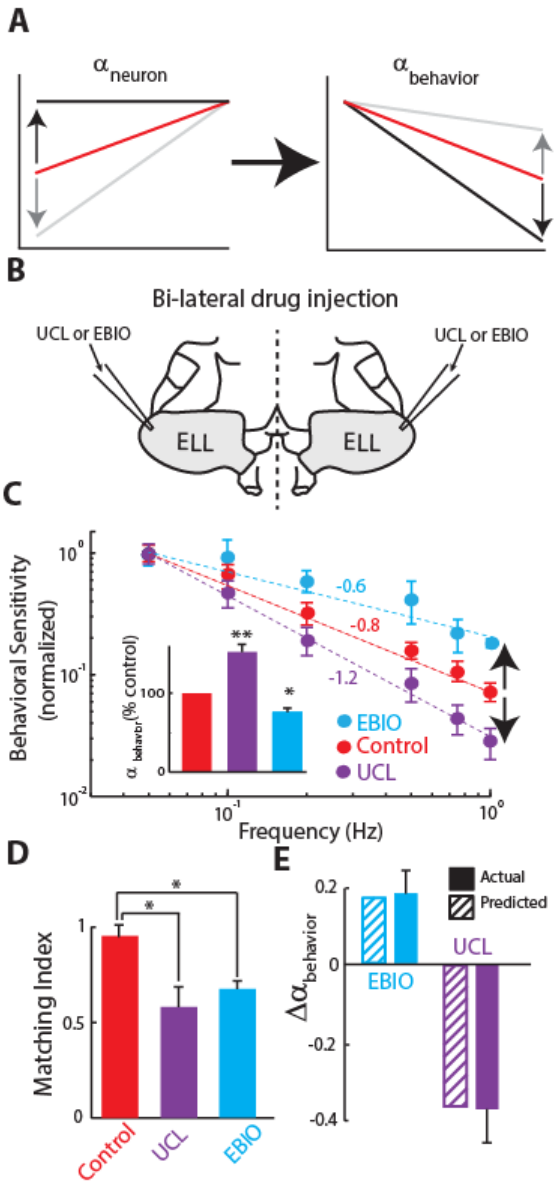

Figure 8: *Changes in neural sensitivity caused by pharmacologically manipulating SK channels cause predictable changes in behavioral responses.* ***A)*** *Schematic showing how changes in the neural tuning characterized by exponent* α_{neuron} *are predicted to cause changes in behavioral sensitivity characterized by exponent* $\alpha_{behavior}$. ***B)*** *Schematic of the bilateral ELL drug injection setup by which UCL or EBIO is injected simultaneously in both ELL's on each side of the brain via two electrodes.* ***C)*** *Population-averaged normalized behavioral sensitivities under control (red), after UCL application (purple), and after EBIO application (cyan). The circles show the experimental data and the dashed lines the best power law fits with exponents* $\alpha_{behavior}$ *given in the figure. Inset: Population-averaged* $\alpha_{behavior}$ *values under control (red), after UCL application (purple), and after EBIO application (cyan).* ***D)*** *Population-averaged matching index between behavioral response and natural stimulus statistics under control (red), after UCL application (purple) (N=6), and after EBIO application (cyan) (N=6). Both drugs significantly decreased the matching index value.* ***E)*** *Actual (solid) and predicted (striped) changes in exponent* $\alpha_{behavior}$ *caused by UCL (purple) and EBIO (cyan) application. The changes were predicted solely from the changes in neural*

*tuning exponent α_{neuron} shown in Fig. 6D. "**" and "*" indicate statistical significance a using a one-way ANOVA with post-hoc Bonferroni correction at the p=0.01 and 0.05 levels, respectively.*

3.5 – Discussion

3.5.1 – Efficient coding of natural second-order stimuli depend on SK1 channels

Envelopes constitute a critical component of the natural electrosensory environment as they carry information about the relative positions between conspecifics as well as their identities (Fotowat et al., 2013; Stamper et al., 2013). In particular, envelopes can arise during movement between two conspecifics as well as from the static interactions between the electric fields of three of more fish. While the former movement envelopes generally tend to contain low (<1 Hz) temporal frequencies (Fotowat et al., 2013; Metzen and Chacron, 2014; Stamper et al., 2013), the latter "social" envelopes tend to instead contain higher (>1 Hz) temporal frequencies (Fotowat et al., 2013; Stamper et al., 2013). Behavioral studies have shown that weakly electric fish can perceive both categories of envelopes (Metzen and Chacron, 2014; Stamper et al., 2012). While it is known that electrosensory neurons respond to mimics of social envelope stimuli (McGillivray et al., 2012; Savard et al., 2011; Vonderschen and Chacron, 2011), little is known about the coding of movement envelope stimuli.

Here we have shown that ELL pyramidal neurons receiving direct synaptic input from peripheral afferents optimally process natural movement envelope stimuli because of scale invariant adaptation. Such adaptation leads to high-pass filtering of envelopes through fractional differentiation whose exponent is matched to natural scene statistics, thereby removing temporal correlations in the response or, equivalently, whitening the response power across frequencies. By whitening the response power across frequencies, the brain should be able to encode the most important information in natural sensory stimuli while discarding any redundancies, most often found in the high-power, low frequencies range. This agrees with efficient coding theory, which states that optimality is achieved by adapting to the natural scene statistics, and by completely removing any correlations which are potentially present in the signals to be encoded(Barlow, 1961). This process was shown to critically depend on SK channels. It was previously shown that SK2 channels are located on the somata of ON-type pyramidal neurons while SK1 channels are instead located on the apical dendrites of both OFF and ON-type pyramidal neurons (Ellis et

al., 2008). Despite these differences, even when we segregated pyramidal neurons into ON and OFF types, the temporal whitening of natural second-order scene statistics did not differ significantly. Furthermore, when we applied the SK channel antagonist and agonist in the apical dendritic tree, we observed that each of their effects were similar in ON and OFF-type pyramidal neurons. We therefore hypothesize that SK1 channels are sufficient to give rise to optimized envelope processing and perception. Pyramidal neurons receive large amounts of feedback on their apical dendrites (Sas and Maler, 1983) that help refine responses to electrosensory stimuli (Bastian et al., 2004; Chacron et al., 2005a; Simmonds and Chacron, 2015b) and previous studies have shown that pharmacological inactivation of SK1 channels strongly disrupted responses to first-order electrosensory stimuli (Toporikova and Chacron, 2009). It is therefore likely that SK1 channels optimize processing of movement envelope stimuli by altering feedback input to ELL pyramidal neurons but further studies are needed to gain more understanding of the underlying mechanisms. We also note that, while our results make it clear that disrupting pyramidal neuron responses to envelopes leads to predictable changes in behavior, further studies are needed to understand how downstream targets of pyramidal neurons will respond to this behaviorally relevant stimulus feature.

Our results suggest a novel mechanism by which neural responses can be adaptively optimized to process natural stimuli. Indeed, our modeling and pharmacological manipulations suggest that SK channel conductance is critical for optimizing processing of natural stimuli with given statistics. If true, then regulating SK channel conductances could serve as a dynamic control for adaptive optimized processing of stimuli following changes in the environment. In particular, we predict that exposing the animals to envelope stimuli whose power law exponents differ from those seen in the natural environment will give rise to changes in SK channel conductance, thereby altering ELL pyramidal neuron tuning in order to optimize processing of these new stimuli through temporal decorrelation/whitening, thus altering and optimizing perception and behavior. Dynamic regulation of SK channel conductance could come from serotonergic modulation as previous studies have shown that elevating serotonin levels inhibits SK channels in ELL pyramidal neurons (Deemyad et al., 2011; Deemyad et al., 2013). Finally, it should be noted that our simplistic model predicts a direct link between the ELL pyramidal neurons and behavior. These behavioral responses are likely to result from further processing of ELL by several downstream areas possibly including forebrain. In this context, the observed

match between changes in ELL neural and behavioral responses induced by pharmacologically manipulating SK might thus appear surprising. This match should not, however, be taken as evidence that downstream brain areas always merely relay information carried in ELL pyramidal cell spike trains. Rather, it is likely that these are involved in other aspects of behavioral responses to envelopes that were not considered in the current study such as the previously described habituation to repeated presentations of the same envelope stimulus (Metzen and Chacron, 2014). Further studies are needed to test these interesting hypotheses to demonstrate how processing and perception of natural stimuli are dynamically optimized based on input statistics, but are clearly beyond the scope of this paper.

3.5.2 – Implications for differential sensory coding of first- and second-order stimulus attributes in the electrosensory system

We first note that our results showing that the electrosensory system efficiently process second order natural electrosensory stimulus attributes in no way imply that other stimulus attributes (e.g. first order) are not also processed efficiently. This is because previous studies have shown that both first and second order attributes are processed in parallel by different subset of neurons in higher order areas (McGillivray et al., 2012). However, both attributes must first be processed by the same neurons in more peripheral areas prior to reaching these. In particular, peripheral receptor afferents respond to both first and second order electrosensory stimulus attributes but display differential frequency tuning to each attribute. Indeed, while afferents are preferentially tuned to higher temporal frequencies for first order attributes (Bastian, 1981; Chacron et al., 2005b; Xu et al., 1996), their tuning to second order attributes is instead independent of temporal frequency (Metzen and Chacron, 2015). For first order statistics, the power law exponent characterizing the rate at which sensitivity increases is matched to the power law exponent characterizing the rate at which stimulus power decays as a function of frequency; afferents are thus thought to efficiently encode the first order natural electrosensory stimulus attributes through temporal whitening (Fotowat et al., 2013). However, no such match was observed for second order attributes as the sensitivity does not increase as a function of temporal frequency in order to oppose the rate at which envelope power decays as a function of frequency (Metzen and

Chacron, 2015). Thus, peripheral afferents do not efficiently process natural second order electrosensory stimulus attributes through temporal whitening.

Our results show that efficient processing instead emerges at the level of the ELL and requires SK channels. It is important to note here that we only recorded from pyramidal cells within LS, which displays the greatest SK channel expression (Ellis et al., 2007). Since pyramidal cells within CLS and CMS display considerably less expression, we predict that these will not efficiently process natural second order electrosensory stimulus attributes through temporal whitening. This is not a problem as pyramidal cells within CLS and CMS have been shown to be involved in the processing other stimulus attributes (Chacron et al., 2003; Metzner and Juranek, 1997). These include those encountered during prey capture. Indeed, weakly electric fish display robust behavioral responses showing that they can reliably and accurately detect the presence the underlying weak stimuli as they then execute a series of movements to capture the prey (Nelson and MacIver, 1999). Such behavior is likely to require multisensory integration as the animal then experiences simultaneous stimulation of its active electrosensory, passive electrosensory, and lateral line systems (Nelson et al., 2002). In particular, the passive electric sense is likely to make a substantial contribution to allow the animal to first successfully detect the presence of a prey as ampullary electroreceptors are exquisitely sensitive to the resulting small amplitude exogenous electric fields (Fotowat et al., 2013). The perturbations of the animal's own electric field caused by the prey during the detection phase are very weak and will in turn cause very small perturbations in the activities of tuberous electroreceptors (Nelson and MacIver, 1999). While these can theoretically be decoded (Nesse et al., 2010), further studies are needed to understand whether and, if so, how neural circuits of the active electric sense actually decode these faint signals in the presence of substantial variability. It is thought that the active electric sense makes an important contribution to give the animal sensory feedback as to the prey's location as it is executing a series of movements to bring the prey close to its mouth. ELL pyramidal cells within CLS and CMS are then likely to be involved as both their frequency tuning (Chacron et al., 2003; Krahe et al., 2008; Shumway, 1989) and receptive field organization (Maler, 2009a, b) are optimized to the statistics of the input. Importantly, we note that LS pyramidal cells, which were the focus of the current study, do not solely process second order electrosensory stimulus attributes. Indeed, previous results have shown that these cells respond to natural communication calls consisting of high frequencies transients (Marsat et

al., 2009). Since SK channels are major determinants of frequency tuning in LS pyramidal cells (Deemyad et al., 2012; Ellis et al., 2007), it is likely that these will also contribute to shaping responses to natural communication stimuli. It is then conceivable that SK channel expression would be not only constrained to optimally process second order electrosensory stimulus attributes as shown here but might also be constrained to optimally process natural communication stimuli as well.

Thus, it is likely that electrosensory coding strategies are constrained to efficiently process natural stimuli. However, these will differ depending on the subset of natural stimuli considered and are likely to involve multiple sensory modalities. A complete understanding of these will require further studies and is clearly beyond the scope of this paper that only considered second order electrosensory stimulus attributes.

3.5.3 – Implications for other sensory systems

It is very likely that our results will be applicable to other systems. First, we note that SK channels found in weakly electric fish display ~86% sequence identity with those found in mammals (Ellis et al., 2007). SK channels are furthermore expressed ubiquitously in the brain and are key determinants of spike frequency adaptation (Faber and Sah, 2003). Second, natural stimuli have been shown to also exhibit power spectra that decay as a power law in the visual (Dong and Atick, 1995; Ruderman and Bialek, 1994) and auditory (Theunissen and Elie, 2014) systems and also display first and second order attributes. Third, growing evidence suggests that neural coding strategies are adapted to natural scene statistics by optimizing neural responses via temporal decorrelation/whitening across systems and species (Dan et al., 1996; Wang et al., 2003). In particular, adaptation to second order stimulus attributes is widely observed (Brenner et al., 2000; Maravall et al., 2007; Smirnakis et al., 1997). Further, our proposed mechanisms underlying temporal decorrelation/whitening, namely high-pass filtering by fractional differentiation as mediated by scale invariant adaptation, are also generic and have been observed in other systems including cortex (Lundstrom et al., 2010; Pozzorini et al., 2013). Thus, our results provide a general mechanism by which SK channel can optimize neural responses to natural stimuli through temporal decorrelation/whitening, which in turn optimizes behavioral responses by making them best tuned to stimuli that occur most frequently in the natural environment. Optimized coding and perception of natural stimuli mediated by SK

channels is thus likely to be a universal feature of sensory processing that is shared amongst systems and species.

Chapter 4

How are envelope responses generated in the first place?

The chapters up until now have characterized responses to second-order natural stimuli and elucidated that SK channels are responsible for determining high-pass tuning to enable efficient encoding via temporal whitening to elicit matched behaviour to the natural stimulus statistics. However, our LIF model largely predicts a feedforward model in which the spike-frequency adaptation power-law kernel allows pyramidal neurons to perform these complex operations. The matter of the fact remains that there are additional possibilities to just feedforward. We know that EAs do not perform any temporal whitening and can only respond to envelopes when stimulus intensity reaches an amplitude which elicits either saturation or rectification. If the pyramidal neurons receive feedforward exclusively, then envelope stimuli must be of sufficient intensity to be detected at all. Therefore, in this chapter, we tested this question by recording from both EAs and pyramidal neurons to see just how low of an intensity is needed to elicit an envelope response, either by phase locking or firing rate modulation. We hypothesized that it is not only feedforward which plays a role in generating an envelope response in pyramidal cells, and that feedback also plays a critical role in the envelope response at weak or low stimulus intensities. This chapter is adapted from: Michael G. Metzen, Chengjie G. Huang, Maurice J. Chacron. Descending pathways generate perception of and neural responses to weak sensory input. *PLoS Biology* 16: e2005239.

4.1 – Abstract

Natural sensory stimuli frequently consist of a fast time-varying waveform whose amplitude or contrast varies more slowly. While changes in contrast carry behaviorally relevant information necessary for sensory perception, their processing by the brain remains poorly understood to this day. Here, we investigated the mechanisms that enable neural responses to and perception of low-contrast stimuli in the electrosensory system of the weakly electric fish *Apteronotus leptorhynchus*. We found that fish reliably detected such stimuli via robust behavioral responses.

Recordings from peripheral electrosensory neurons revealed stimulus-induced changes in firing activity (i.e., phase locking) but not in their overall firing rate. However, central electrosensory neurons receiving input from the periphery responded robustly via both phase locking and increases in firing rate. Pharmacological inactivation of feedback input onto central electrosensory neurons eliminated increases in firing rate but did not affect phase locking for central electrosensory neurons in response to low-contrast stimuli. As feedback inactivation eliminated behavioral responses to these stimuli as well, our results show that it is changes in central electrosensory neuron firing rate that are relevant for behavior, rather than phase locking. Finally, recordings from neurons projecting directly via feedback to central electrosensory neurons revealed that they provide the necessary input to cause increases in firing rate. Our results thus provide the first experimental evidence that feedback generates both neural and behavioral responses to low-contrast stimuli that are commonly found in the natural environment.

4.2 – Introduction

Understanding how sensory information is processed by the brain in order to give rise to perception and behavior (i.e., the neural code) remains a central problem in systems neuroscience. Such understanding is complicated by the fact that natural sensory stimuli have complex spatiotemporal characteristics. Specifically, these frequently consist of a fast time-varying waveform whose amplitude (i.e., the "envelope" or contrast) varies more slowly (Attias and Schreiner, 1997; Joris et al., 2004; Theunissen and Elie, 2014). Envelopes are critical for perception (Shannon et al., 1995; Shannon et al., 1998), yet their neural encoding continues to pose a challenge to investigators because their extraction (i.e., signal demodulation) requires a nonlinear transformation (Rosenberg and Issa, 2011; Stamper et al., 2013).

It is generally thought that peripheral sensory neurons implement such demodulation through phase locking, in which action potentials only occur during a restricted portion of the stimulus cycle, and that such signals are further refined downstream to give rise to perception. Indeed, in the auditory system, peripheral auditory fibers respond to amplitude-modulated sounds because of phase locking (Joris and Yin, 1992) with the most sensitive units displaying detection thresholds similar to those of the organism (see (Joris et al., 2004) for review). Sensitivity to amplitude modulations (AMs) increases in higher-level areas (e.g., cochlear nuclei,

inferior colliculus, auditory cortex), thereby exceeding that seen at the periphery, but the underlying mechanisms remain poorly understood (Joris et al., 2004; Krishna and Semple, 2000; Malone et al., 2010; Sayles et al., 2013; Zhao and Liang, 1997). The common wisdom is that these are feedforward in nature and involve integration of afferent input from the sensory periphery. Here, we show that refinement of neural sensitivity to AMs that occurs in central brain areas is not due to integration of afferent input but is rather mediated by feedback pathways, thereby mediating perception and behavior.

Wave-type weakly electric fish generate a quasi-sinusoidal signal called the electric organ discharge (EOD) around their body, which allows exploration of the environment and communication. During interactions with conspecifics, each fish experiences sinusoidal AMs as well as phase modulations (PMs) of its EOD (i.e., a beat). This beat can interfere with electrolocation of other objects when the frequency is low. Specifically, such stimuli elicit a jamming avoidance response (JAR) in which both fish shift their EOD frequencies in order to increase the beat frequency to higher values that do not interfere with electrolocation. The neural circuitry giving rise to the JAR is well understood and involves feedforward integration of AM and PM information that is processed in parallel by separate neural pathways that later converge (see (Heiligenberg, 1991) for review), although JAR behavior can sometimes be elicited by stimuli consisting of AMs or PMs only. In particular, neural sensitivities to AM and PM components increase in higher level areas, thereby explaining the animal's remarkable behavioral acuity (Kawasaki, 1997).

Experiments focusing on the JAR have typically but not always used beats with constant depth of modulation (i.e., the envelope or contrast). More recent studies have focused on studying how time-varying contrasts, which carry information as to the distance and relative orientation between both fish (Fotowat et al., 2013; Yu et al., 2012a), are processed by the AM neural pathway to give rise to behavioral responses that consist of the animal's EOD frequency tracking the detailed time course of the envelope (Huang and Chacron, 2016, 2017; Huang et al., 2016; Martinez et al., 2016; McGillivray et al., 2012; Metzen and Chacron, 2014, 2015, 2017; Metzen et al., 2016b; Middleton et al., 2006; Savard et al., 2011; Stamper et al., 2013). P-type peripheral electrosensory afferents (EAs) scattered over the animal's skin surface encode EOD amplitude, but not PMs, and synapse onto pyramidal cells (PCells) within the electrosensory

lateral line lobe (ELL). PCells are the sole output neurons of the ELL and project to higher brain areas that mediate behavior. Moreover, PCells receive large amounts of input from descending pathways (i.e., feedback) (Bastian and Bratton, 1990; Berman and Maler, 1999; Bratton and Bastian, 1990) that have important functional roles such as gain control (Bastian, 1986a, b), adaptive stimulus cancellation (Bastian, 1996a, b; Bastian, 1998; Bastian, 1999; Bastian et al., 2004; Bol et al., 2011; Bol et al., 2013; Mejias et al., 2013), coding of natural electro-communication signals (Marsat and Maler, 2012), synthesizing neural codes for moving objects (Clarke and Maler, 2017), as well as shifting the tuning properties of PCells contingent on the stimulus' spatial extent (Chacron, 2006; Chacron et al., 2003; Chacron et al., 2005c). However, whether and how feedback input determines PCell responses to time-varying contrasts have not been investigated to date. Moreover, while previous studies have focused on studying neural and behavioral responses to high-contrast stimuli (Huang and Chacron, 2016, 2017; Huang et al., 2016; Martinez et al., 2016; McGillivray et al., 2012; Metzen and Chacron, 2014, 2015, 2017; Metzen et al., 2016b; Middleton et al., 2006; Savard et al., 2011; Stamper et al., 2013), we instead focused on low-contrast stimuli that are more commonly found in the natural environment (Fotowat et al., 2013).

4.3 – Methods

4.3.1 – Animals

The wave-type weakly electric fish, *Apteronotus leptorhynchus* was used exclusively in this study. Animals of either sex were purchased from tropical fish suppliers and were housed in groups (2-10) at controlled water temperatures (26-29°C) and conductivities (300-800 $\mu S*cm^{-1}$) according to published guidelines (Hitschfeld et al., 2009). All procedures were approved by McGill University's animal care committee and were performed in accordance with the guidelines of the Canadian Council on Animal Care.

4.3.2 – Surgery

Surgical procedures have been described in detail previously (Chacron et al., 2003; Metzen et al., 2015; Toporikova and Chacron, 2009). Briefly, 0.1-0.5 mg of tubocurarine (Sigma) was injected intramuscularly to immobilize the fish for electrophysiology and behavioral experiments. The

fish was then transferred to an experimental tank (30 cm x 30 cm x 10 cm) containing water from the animal's home tank and respired by a constant flow of oxygenated water through their mouth at a flow rate of 10 $mL*min^{-1}$. Subsequently, the animal's head was locally anesthetized with lidocaine ointment (5%; AstraZeneca, Mississauga, ON, Canada), the skull was partly exposed, and a small window was opened over the recording region (hindbrain for ELL or midbrain for nP).

4.3.3 – Stimulation

The electric organ discharge of *A. leptorhynchus* is neurogenic, and therefore is not affected by injection of curare. All stimuli consisted of AMs of the animal's own EOD were produced by triggering a function generator to emit one cycle of a sine wave for each zero crossing of the EOD as done previously (Bastian et al., 2002). The frequency of the emitted sine wave was set slightly higher (30 Hz) than that of the EOD, which allowed the output of the function generator to be synchronized to the animal's discharge. The emitted sine wave was subsequently multiplied with the desired AM waveform (MT3 multiplier; Tucker Davis Technologies), and the resulting signal was isolated from the ground (A395 linear stimulus isolator; World Precision Instruments). The isolated signal was then delivered through a pair of chloridized silver wire electrodes placed 15 cm away from the animal on either side of the recording tank perpendicular to the fish's rostro-caudal axis. Depending on polarity, the isolated signal either added or subtracted from the animal's own discharge. It is important to realize that these stimuli mimic the EOD AMs but not the FMs generated during encounters with conspecifics. This is not an issue here as these FMs do not elicit responses from the neurons considered here. Further, previous studies have shown that the behavioral responses considered here (see below) do not require FMs (Metzen and Chacron, 2014).

In order to obtain behavioral and neural (periphery: EAs; hindbrain: PCells; midbrain: STCells) detection thresholds we used a stimulus consisting of either a 5 Hz sinusoidal or a 5-15 Hz noise (4^{th} order Butterworth) carrier waveform whose depth of modulation computed with respect to the animal's unperturbed EOD amplitude increased from 0% to 100%. We found that EA detection thresholds were similar for both sinusoidal (n = 15) and noisy (n = 39) stimulus waveforms (Kruskal-Wallis, df = 2, p = 0.13). Thus, detection threshold values for EAs were pooled. We only used the 5 Hz sinusoidal waveform for determining detection thresholds for

ELL PCells, nP stellate cells, and behavior. We characterized each ELL pyramidal cell as either 'ON' or 'OFF' type using a noisy AM stimulus with frequency content of 0-120 Hz, as done previously (Hofmann and Chacron, 2017; Martinez et al., 2016). In this case, the standard deviation of the AM was adjusted as in previous studies (Aumentado-Armstrong et al., 2015; Deemyad et al., 2013; Metzen et al., 2016a; Simmonds and Chacron, 2015a), as measured using a small dipole placed close to the animal's skin in the middle of the animal's rostro-caudal and dorso-ventral axes (typically 0.2 $mV*cm^{-1}$). We note that it is likely that some of the variations in threshold values obtained for EAs are due to the location of the pore on the animal's skin relative to the stimulus.

4.3.4 – Pharmacology

The composition of the vehicle/control saline was as follows (all chemicals were obtained from Sigma): 111 mM NaCl, 2 mM KCl, 2 mM $CaCl_2$, 1 mM $MgSO_4$, 1 mM $NaHCO_3$ and 0.5 mM NaH_2PO_4. The pH of the saline solution was 6.8. Glutamate (Sigma), Lidocaine (Astra Pharmaceuticals) and CNQX 6-cyano-7-nitroquinoxaline-2,3-dione (CNQX, Sigma) were dissolved in saline before application as done previously (Huang et al., 2016). Drug application electrodes were made using two-barrel KG-33 glass micropipettes (OD 1.5 mm, ID 0.86 mm, A-M Systems) and pulled by a vertical micropipette puller (Stoelting Co.) to a fine tip and subsequently broken to attain a tip diameter of ~5 μm for each barrel. The two barrels were used for separate application of either Lidocaine (1 mM) or CNQX (1 mM), as well as glutamate (1 mM) or saline. During ELL recordings where the EGP indirect feedback was blocked with CNQX, we first used excitatory responses to glutamate application to confirm that we were within proximity of the pyramidal neuron we were recording from as done previously (Deemyad et al., 2013). CNQX was then applied to the neuron to ensure a local effect. Complete feedback inactivation was achieved by inserting two pipettes containing Lidocaine bilaterally into nP. In order to block the direct feedback from the midbrain area Torus semicircularis (TS), we performed unilateral injections of Lidocaine on the contralateral TS while recording from PCells within the ipsilateral ELL. Injection locations were guided by the *Apteronotus* brain atlas (Maler et al., 1991), and determined based on somatotopic mappings. We inserted a glass pipette (20-30 μm tip) and pressure injected Lidocaine at a few depths between 1000 – 1500 μm with 4-5 puffs each at a pressure of 15-20 psi and 130 ms of injection time as done previously (Clarke and

Maler, 2017). We note that this manipulation also blocks ascending input to higher order brain areas mediating behavior. As such, we did not investigate the effects of injecting Lidocaine within TS on behavioral responses. For behavioral recordings, injections of Lidocaine, saline, and CNQX were performed bilaterally in nP and ELL, respectively, as done previously (Deemyad et al., 2013; Huang et al., 2016). All pharmacological injections were performed using a duration of 130 ms at 15-20 psi using a Picospritzer (General Valve). Indirect feedback inactivation was assessed by comparing the baseline firing rates of pyramidal cells before and after drug application as shown in a previous study (Bastian and Nguyenkim, 2001a).

4.3.5 – Electrophysiology

Sharp glass micropipette electrodes (20 – 40 MΩ) backfilled with 3 M KCl were used to record *in vivo* from electrosensory afferents (EAs) within the deep fiber layer of ELL as described in previous studies (Bastian, 1981; Chacron et al., 2005b; Metzen and Chacron, 2017). EAs can be easily identified based on their high baseline (i.e., in the absence of stimulation) firing rates as well as from the fact that their probability of firing increases with increasing EOD amplitude (Gussin et al., 2007; Scheich et al., 1973). The recording electrode was advanced into the ELL with a motorized microdrive (IW-711; Kopf). We used well-established techniques to perform extracellular recordings with Woods metal electrodes from pyramidal cells (Frank and Becker, 1964) located within the lateral segment of the ELL based on recording depth and mediolateral placement of the electrode on the brain surface as done previously (Hofmann and Chacron, 2017; Huang and Chacron, 2016; Krahe et al., 2008).

Similarly, we performed extracellular recordings with Woods metal electrodes from stellate cells in nP. Stellate cells were confirmed based on the recording depth as well as their low spontaneous firing rate and response tuning curves to sinusoidal amplitude modulations based on previous characterization (see S5 Fig) (Bratton and Bastian, 1990). All recordings were digitized at 10 kHz sampling rate using CED 1401 plus hardware and Spike2 software (Cambridge Electronic Design) and stored on a computer hard disk for offline analysis.

4.3.6 – Behavior

Animals were immobilized by an intramuscular injection of 0.1-0.5 mg tubocurarine and set up in the recording tank similarly to the method described above. Depending on which feedback

pathway was pharmacologically inactivated, different surgeries were performed. Briefly, to inactivate the nP direct feedback pathway, both sides of the midbrain were exposed rostrally to T0 (Maler et al., 1991) and double barrel pipettes containing saline and lidocaine were inserted into the nP (1000-1250 μm). To inactivate the EGP indirect feedback pathway, both sides of the hindbrain ELL were exposed to the caudal-lateral edge where pipettes containing CNQX were inserted superficially (100-400 μm). Multiple injections (typically 3-5) were performed to ensure that both hemispheres of nP and ELL were sufficiently affected by the pharmacological agents. Stimuli were then presented as described above in order to elicit behavioral responses. The animal's behavior was recorded through a pair of electrodes located at the rostrum and tail of the animal. The fish's time-varying EOD frequency was extracted either by computing a spectrogram of the recorded signal or from the zero-crossings of the recorded EOD signal. For the former, the EOD frequency was then determined as the frequency with the highest power near the 4th harmonic of the fish's baseline EOD frequency and the extracted frequency was then divided by 4 in order to get the true EOD frequency of the fish. For the latter, the zero-crossings were used to generate a binary sequence as described above that was low-pass filtered (2^{nd} order Butterworth filter with 0.05 Hz cut-off frequency) to obtain the time-varying EOD frequency. Quantitatively similar results were obtained using either methodology.

4.3.7 – Data Analysis

All data analysis was performed offline using custom written codes in MATLAB software (MathWorks). The recorded electrical activity were first high-pass filtered (100 Hz; 8^{th} order Butterworth). Spike times were defined as the times at which the signal crossed a given threshold value from below. A binary sequence $R(t)$ was then constructed from the spike times of each P-unit in the following manner: time was first discretized into bins of width dt=0.1 ms. The value of bin i was set to 1 if there was a spike at time t_j such that $i*dt<t_j<(i+1)*dt$ and to 0 otherwise. Note that, since the bin width dt is smaller than the absolute refractory period of the neuron, there can be at most one spike time that can occur within any given bin. The firing rates were obtained by filtering the binary sequence using a 2^{nd} order Butterworth filter with 0.05 Hz cut-off frequency. Both neural and behavioral response detection threshold values to the stimulus were characterized by the intensity at which the firing rate or EOD frequency crossed a response level that corresponded to the 95% confidence interval established during the absence of stimulation.

We note that changing the significance in order to determine the response level did not change the detection threshold values significantly, as shown for a subset of our data (S7 Fig).

4.3.8 – Time-varying vector strength

To determine the degree of a neuron's phase locking to the AM stimulus, we computed a time-varying vector strength until the end of stimulation was reached. Therefore, spike trains where accumulated as cycle histograms and the response was quantified using the vector strength *(r)*, which measures the degree of phase locking and ranges between 0 (random spiking) and 1 (perfect phase locking) (Mardia and Jupp, 1999). Vector strength is defined as:

$$r = \frac{1}{N}\sqrt{(\sum_i \cos\theta_i)^2 + (\sum_i \sin\theta_i)^2} \qquad (1)$$

where *N* is the number of spikes during one cycle of stimulation. The time-varying vector strength was computed by averaging the vector strength *r* over a time window *T* of 1 s:

$$VS = \frac{\sum_i r_i}{T} \qquad (2)$$

where r_i is the vector strength obtained during one cycle of stimulation and *T* is a time-window of 1 s (i.e., 5 cycle periods). The Rayleigh statistics ($r^2N \geq 3.5$) was used to determine significance. Varying the time-window length between 0.6 and 2 s did not alter our results significantly.

4.3.9 – Correlation

To correlation between detection threshold values of PCells and behavior obtained simultaneously during repetitive stimulation (n = 10, three repetitions each) was assessed using the Pearson's correlation coefficient. The correlation between the residuals were computed by first subtraction the mean detection threshold value obtained for PCells and behavior over the three repetitions.

4.3.10 – Statistics

Statistical significance was assessed through a non-parametric Kruskal-Wallis test with Bonferroni correction or Wilcoxon sign rank test for paired measures at the $p = 0.05$ level. Values are reported as boxplots unless otherwise stated. Errorbars indicate ± SEM. On each box, the central mark indicates the median, and the bottom and top edges of the box indicate the 25th and 75th percentiles, respectively. The whiskers extend to the most extreme data points not considered outliers, and the outliers are plotted individually using the '•' symbol.

4.4 – Results

The goal of this study was to understand how behavioral responses to low-contrast stimuli are generated by neural circuits in the animal's brain. To do so, we used an awake-behaving preparation in which the immobilized animal is respirated within an otherwise empty tank (Fig. 1A). The animal's behavioral response is determined from its EOD, which is being continuously recorded (Fig. 1A, upper left) during stimulation (Fig. 1A, upper right). The relevant neural circuitry is shown in Fig. 1B. EAs make direct excitatory synaptic contact and indirect inhibitory synaptic contact with ON- and OFF-type ELL PCells, respectively. PCells project directly to torus semicircularis (TS) neurons, which in turn project to higher brain areas mediating behavioral responses. However, some TS neurons also project back to ELL via stellate cells (STCells) within the nucleus praeeminentialis (nP), thereby forming a closed feedback loop (Fig. 1b, cyan). Our stimuli consisted of AMs of the animal's own EOD that mimicked those encountered during interaction with a same-sex conspecific. Specifically, interference between the two EODs gives rise to a sinusoidal AM (Fig. 1C, blue) whose depth of modulation (i.e., the envelope, red) is inversely related to the relative distance between both fish. It is important to realize that the animal's EOD is a carrier and that the AM is the relevant stimulus here. We are considering both first- (i.e., AM) and second-order (i.e., envelope or contrast) features of the stimulus and note that these correspond to the second- and third-order features of the full signal received by the animal, respectively. Thus, the first- and second-order features correspond to the time-varying mean and variance of the stimulus, respectively. The AM, envelope, and full-signal waveforms with their respective frequency contents are shown in Fig. 1C. Our stimuli consisted

of a 5 Hz sinusoidal waveform (blue) whose contrast (red) increased linearly as a function of time.

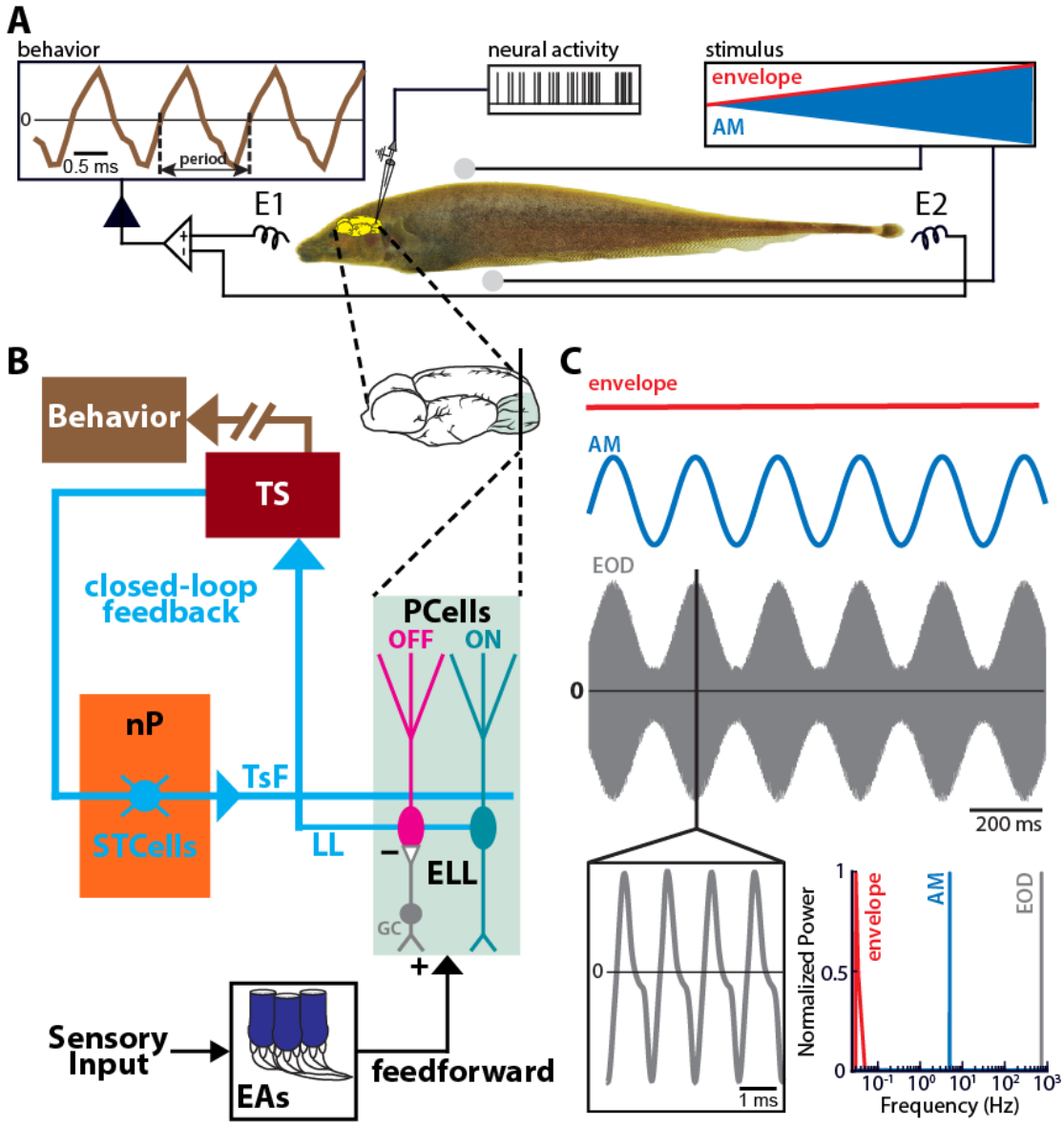

Figure 1. Weakly electric fish display low behavioral contrast detection thresholds. A) Relevant anatomy diagram showing the main brain areas considered. B) Top: EOD spectrogram (i.e., time varying power spectrum showing frequency as a function of time) obtained under baseline conditions (i.e., in the absence of stimulation but in the presence of the animal's unmodulated EOD). We found that the frequency at which there is maximum power (i.e., the EOD frequency) fluctuated as a function of time, which was used to compute a response level (white dashed line) to determine whether behavioral responses obtained under stimulation were significantly above than those obtained in the absence of stimulation. Middle: Stimulus waveform (blue) and its envelope (red) showing contrast as a function of time. Bottom: EOD spectrogram in response to the stimulus. It is seen that the EOD frequency increases after stimulus onset. The detection threshold is the contrast corresponding to the earliest time after

stimulus onset for which the EOD frequency was above the response level (black circle and white dashed line). Inset: Population-averaged detection threshold values for behavior (n = 35, brown).

4.4.1 – Weakly electric fish give behavioral responses to low contrasts

We first investigated behavioral responses to increasing contrast (Fig. 2A). To do so, we first quantified behavioral responses in the absence of stimulation by looking at the time-varying EOD frequency (Fig. 2B, top). Plotting the EOD spectrogram (i.e., the time-varying power spectrum of the measured EOD trace) revealed that the frequency at which there was maximum power (i.e., the EOD frequency) fluctuated slightly (Fig. 2B, top) around a mean value. We used these fluctuations to compute a probability distribution and to determine the interval of values that contains 95% of this distribution (Fig. 2B, white dashed lines, see Materials and methods). During stimulation, we found that the animal's EOD frequency increased more or less linearly as a function of time (Fig. 2B, bottom). The detection threshold was computed as the contrast corresponding to the smallest time after stimulus onset for which the EOD frequency was outside the range of values determined in the absence of stimulation (Fig. 2B, bottom, black circle and white dashed lines). We found that fish could reliably detect weak contrasts as evidenced from low detection thresholds (n = 35 fish, 8.8% ± 1.1%, min: 1.1%, max: 27.6%, Fig. 2B, bottom, inset). The detection threshold values obtained were furthermore robust to large changes in filter settings (S1 Fig).

Our behavioral results show that electrosensory neural circuits must extract the time-varying stimulus contrast (i.e., implement signal demodulation). We thus next investigated how electrosensory neurons respond to increasing contrast.

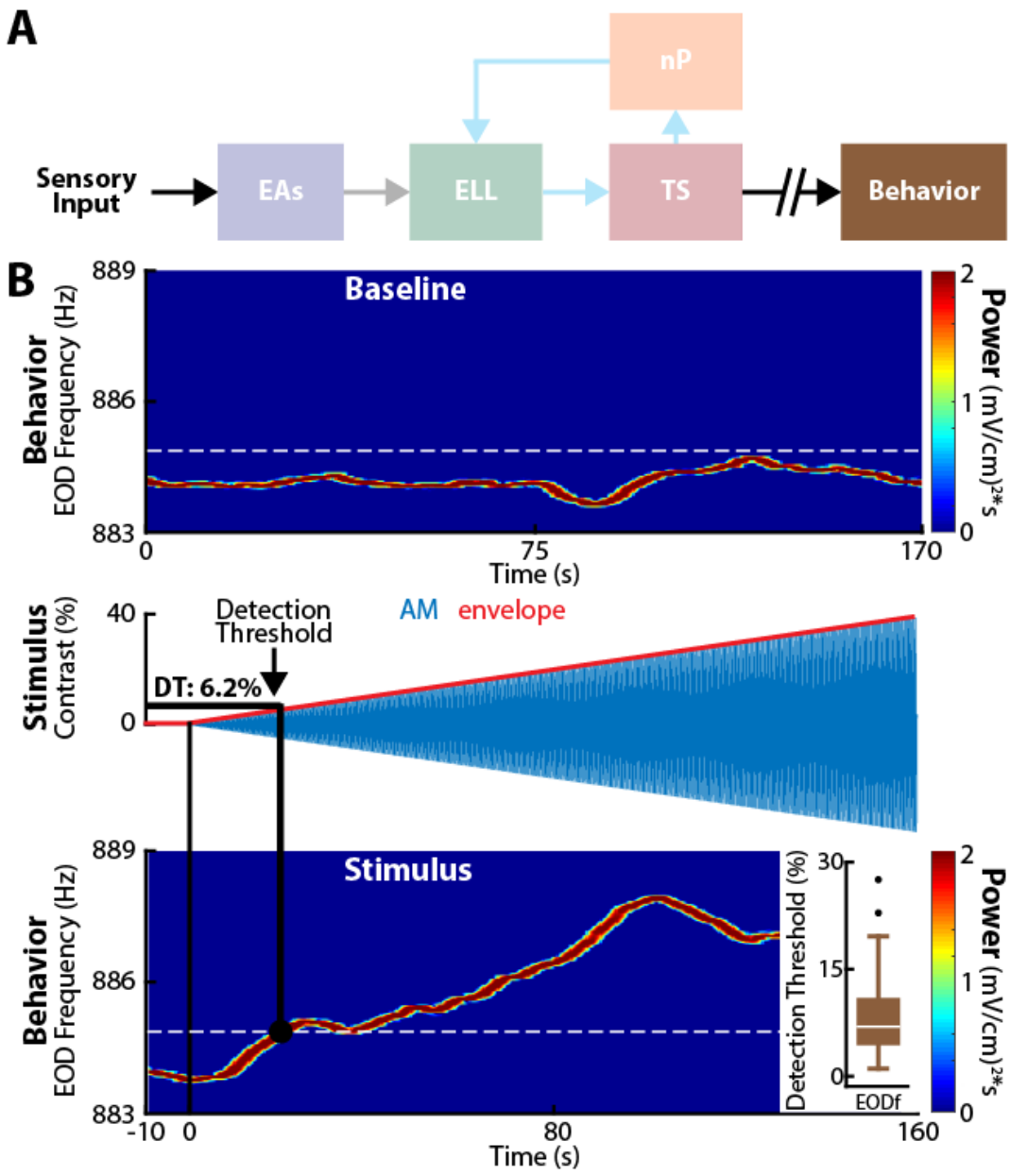

***F**igure 2. Weakly electric fish display low behavioral contrast detection thresholds**.** A) Relevant anatomy diagram showing the main brain areas considered. B) Top: EOD spectrogram (i.e., time varying power spectrum showing frequency as a function of time) obtained under baseline conditions (i.e., in the absence of stimulation but in the presence of the animal's unmodulated EOD). We found that the frequency at which there is maximum power (i.e., the EOD frequency) fluctuated as a function of time, which was used to compute a response level (white dashed line) to determine whether behavioral responses obtained under stimulation were significantly above than those obtained in the absence of stimulation. Middle: Stimulus waveform (blue) and its envelope (red) showing contrast as a function of time. Bottom: EOD spectrogram in response to the stimulus. It is seen that the EOD frequency increases after stimulus onset. The detection threshold is the contrast corresponding to the earliest time after stimulus onset for which the EOD frequency was above the response level (black circle and white dashed line). Inset: Population-averaged detection threshold values for behavior (n = 35, brown).*

4.4.2 – Peripheral EAs provide information about low contrasts through phase locking but not through firing rate

We first recorded from peripheral EAs (Fig. 3A). EAs are characterized by high baseline firing rates in the absence stimulation within the range of 200-600 spk*s^{-1} (Gussin et al., 2007; Metzen and Chacron, 2015). Our dataset confirms these previous results as the baseline firing rates were all within this range (population average: 400.8±18.0 spk*s^{-1}, n = 54, N = 5 fish). As done for behavior, we used the baseline activity of EAs to determine whether the observed neural activity was due to stimulation. We note that this is physiologically realistic as, in order to be detected, a stimulus must perturb the ongoing baseline activity of EAs. Overall, we found that EA activity was phase locked to the stimulus waveform for both low (Fig. 3B, left inset) and high (Fig. 3B, right inset) contrasts. Notably, for high contrasts, we observed stronger phase locking in that there was cessation of firing activity during some phases of the stimulus cycle (Fig. 3B, right inset). We quantified EA responses to stimulation using standard measures of firing rate (see Materials and methods) and phase locking (i.e., the vector strength [VS], see Materials and methods). Overall, the time-varying VS quickly became significantly different from baseline (i.e., in the absence of stimulation) after stimulus onset (Fig. 3B, dashed blue), leading to low phase locking detection threshold values (Fig. 3B, left black circle). However, the mean firing rate (Fig. 3B, solid blue) only became significantly different from baseline for larger contrasts, leading to higher firing rate detection threshold values (Fig. 3B, right black circle). We note that, while there is no complete dichotomy between phase locking and firing rate, our results above do show that it is possible to increase phase locking without increasing firing rate for low contrasts.

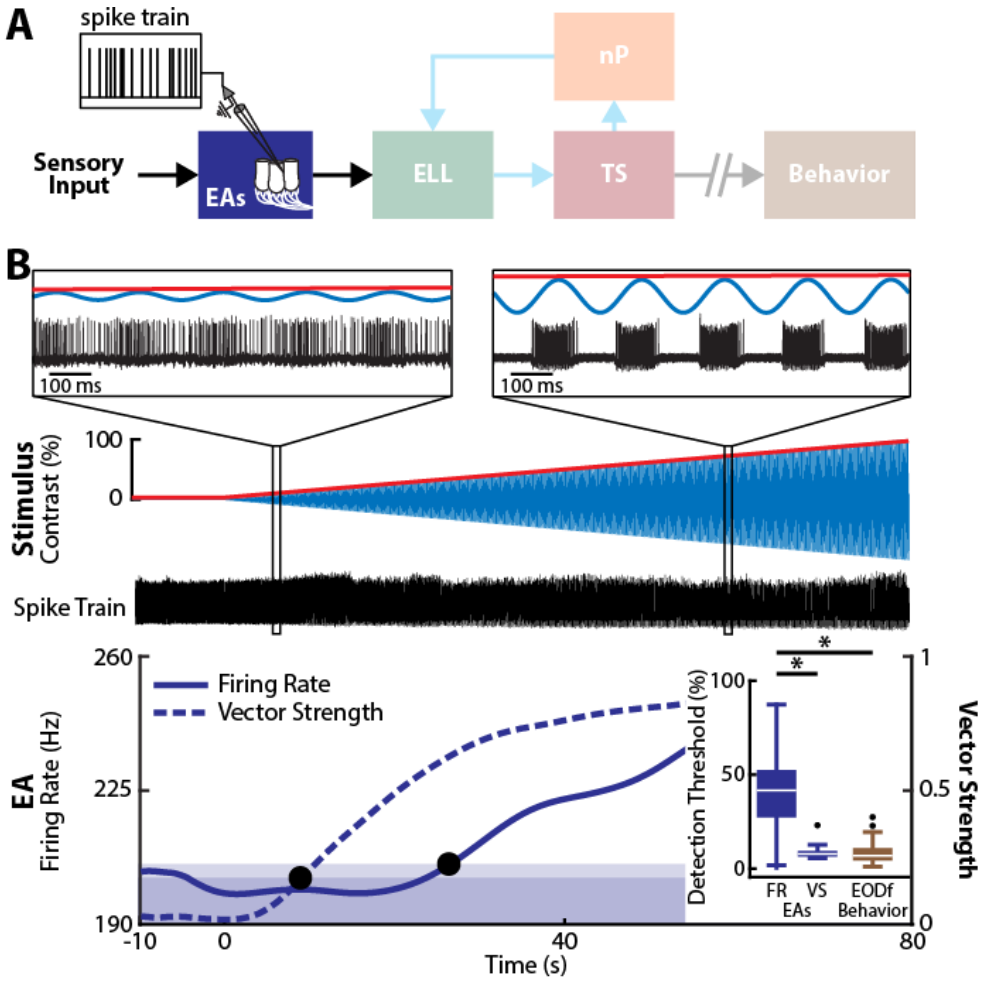

Fig 3. EAs reliably detect low-contrast stimuli through phase locking but not through overall changes in firing rate. *A) Relevant anatomy diagram showing the main brain areas considered. Recordings were made from individual EAs. B) Top: Stimulus waveform (blue) and its envelope (red) showing contrast as a function of time. Middle: Spiking activity (black) from a representative example EA. The insets show magnification at two time points. In both cases, the spiking response is modulated. Bottom: Double y-axis plot showing the mean firing rate (solid blue) and VS (dashed blue) of this EA as a function of time. The bands delimit the upper range of values determined from this EA activity in the absence of stimulation for VS (dark blue) and firing rate (light blue). The detection threshold obtained from VS (leftmost black circle) was much lower than that obtained from the mean firing rate (rightmost black circle). Inset: The population-averaged detection thresholds obtained from firing rate (left) was significantly higher than those obtained from VS (middle) and behavior (right) (Kruskal-Wallis, df = 2, FR-VS: $p = 2.6 \times 10^{-9}$; FR-Behavior: $p = 8.9 \times 10^{-5}$). The population-averaged detection threshold obtained from VS was not significantly different than that obtained from behavior (Kruskal-Wallis, df = 2, p = 1). "*" indicates significance at the p = 0.05 level.*

Similar results were seen across our dataset in that EA phase locking thresholds were low and comparable to behavioral values (EA VS: 9.1% ± 1.1%, behavior: 8.8% ± 1.1%, Kruskal-

Wallis, df = 2, $p = 0.99$), whereas those computed from firing rate were much higher than behavioral thresholds (38.2% ± 3.1%; Kruskal-Wallis, df = 2, $p = 8.9 \times 10^{-5}$; Fig. 3B, inset). Neural detection threshold values obtained were also robust to large changes in filter settings (S1 Fig). Thus, our results show that, for low contrasts (i.e., <15%), EA firing rate modulations (i.e., phase locking) carry the information necessary to implement signal demodulation. However, such demodulation must occur downstream of EAs, as their mean firing rates were effectively unchanged relative to baseline conditions. For high contrasts (i.e., >40%), our results show that EAs implement signal demodulation, as their firing rates are then different from baseline.

4.4.3 – ELL PCells provide downstream brain areas information about low contrasts through both their firing rates and phase locking

We next recorded from the downstream targets of EAs: PCells within the ELL (Fig. 4A). ELL PCells have much lower baseline firing rates than EAs, which are typically within the 5–45 Hz range (Krahe et al., 2008). Baseline firing rates of our PCell data were all within this range (population average: 13.2±0.8 spk*s^{-1}, n = 59, $N = 27$ fish). We found that, like EAs, ELL PCell spiking activity was phase locked to the stimulus shortly after stimulus onset (Fig. 4B, dashed green curve and Fig. 4B, insets). Phase locking was seen for both low and high contrasts in that spiking only occurred during a restricted portion of the stimulus cycle (Fig. 4B, compare left and right panels). However, PCells responded in a qualitatively different fashion than EAs in that their firing rates also became significantly different from baseline shortly after onset (Fig. 4B, solid green curve). Thus, firing rate detection threshold values for PCells were comparable to those found for behavior (PCells FR: 7.0% ± 0.9%; Kruskal-Wallis, df = 2, $p = 0.23$; Fig. 4B, bottom inset), whereas phase locking detection thresholds for PCells were significantly lower than firing rate and behavioral detection thresholds (VS: 3.9% ± 0.6%; Kruskal-Wallis, df = 2, FR-VS: $p = 0.0054$; VS-Behavior: $p = 1.1 \times 10^{-5}$; Fig. 4B, bottom inset). We further tested the relationship between neural and behavioral detection thresholds by plotting values obtained from neurons in different individual fish. Overall, there was a strong correlation between neural and behavioral detection threshold values (S2A Fig, $n = 10$, $N = 10$ fish, 3 repetitions each; r = 0.93; $p = 4.6 \times 10^{-7}$), indicating that neurons with low detection thresholds were primarily found in fish with low behavioral detection thresholds. There was, however, no correlation between the

trial-to-trial variabilities of neural and behavioral detection thresholds to repeated stimulus presentations (S2B Fig, $n = 10$, $N = 10$ fish, 3 repetitions each; $r = -0.14$; $p = 0.48$), indicating that fluctuations in the activity of a single ELL PCell do not significantly influence behavior. Overall, our results show that, for low contrasts (i.e., <15%), PCell phase locking and firing rate both carry information about contrast. As such, either phase locking or firing rate could be decoded by downstream brain areas in order to give rise to behavior.

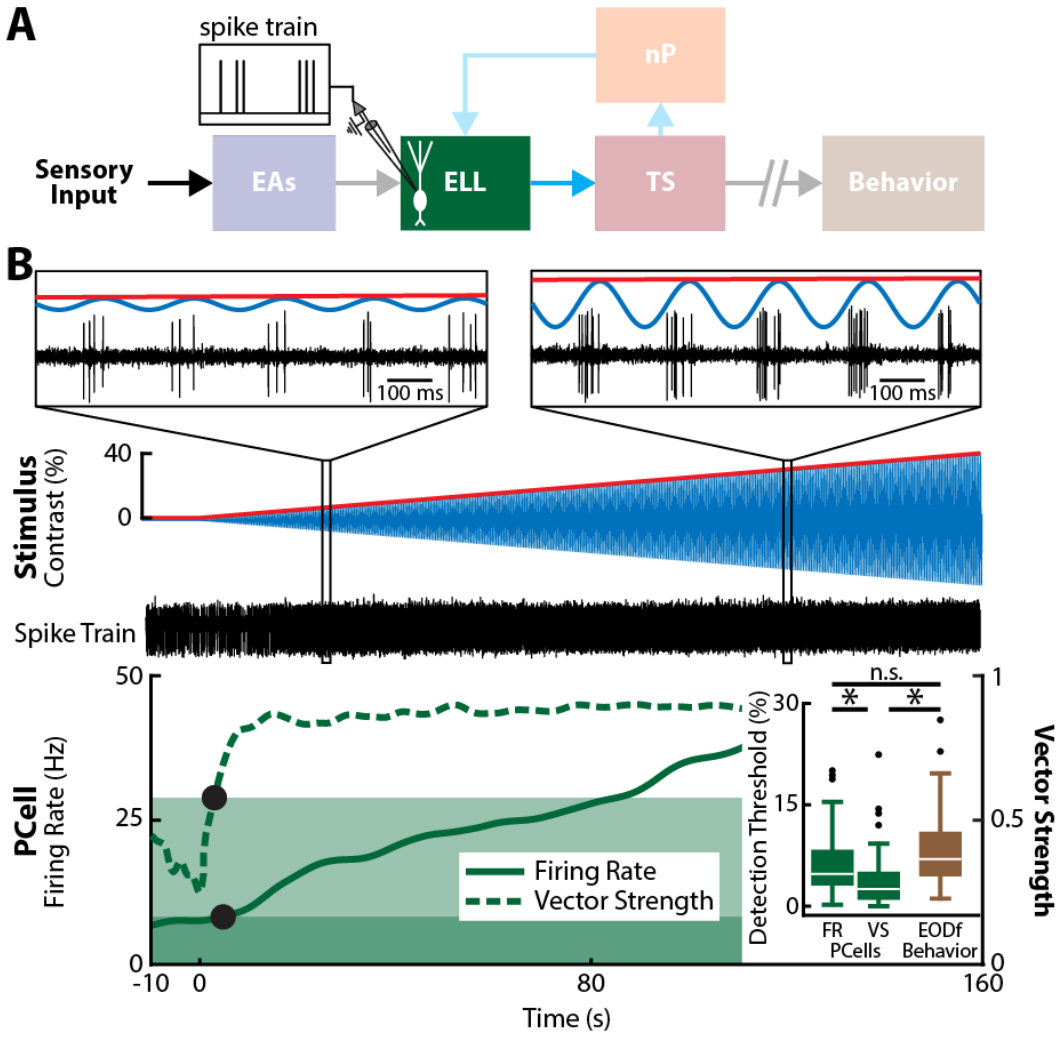

Figure 4. ELL PCell responses display low firing rate and phase locking detection threshold values that are comparable to behavior. A) Relevant anatomy diagram showing the main brain areas considered. Recordings were made from individual PCells. B) Top: Stimulus waveform (blue) and its envelope (red) showing contrast as a function of time. Middle: Spiking activity (black) from a representative example PCell. The insets show magnification at two time points. In both cases, the PCell activity strongly phase locked to the stimulus, but the average number of spikes per stimulus cycle increased with contrast. Bottom: Double y-axis plot showing the mean firing rate (solid green) and vector strength (dashed green) of this PCell as a function of time. The bands show the response levels determined from this PCell's

*activity in the absence of stimulation. The detection threshold obtained from firing rate (rightmost black circle) was similar to that obtained from vector strength rate (leftmost black circle). Inset: The population-averaged detection thresholds obtained from firing rate (left) were not significantly different from behavior (Kruskal-Wallis, df = 2, p = 0.23). The population-averaged detection thresholds obtained from vector strength (middle) were significantly lower compared to those obtained from firing rate or behavior (right) (Kruskal-Wallis, df = 2, FR-VS: p = 0.0054; VS-behavior: p = 1.1*10^{-5}).*

4.4.4 – Feedback input to PCells causes increases in firing rate, while feedforward input causes increased phase locking for low contrasts

Perhaps the simplest explanation for why PCells phase lock to stimuli with low contrasts is that they simply linearly integrate feedforward input from EAs, which are already phase locked to these. What then causes PCells to increase their firing rates in response to stimuli with low contrasts? Unlike the explanation above for increased phase locking, this cannot be due to linear integration of feedforward input from EAs. This is because our results show that, for low contrasts, EA firing rates are not significantly different from baseline values. One possibility is that increases in PCell firing rate result from nonlinear integration (e.g., half-wave rectification) of feedforward input from EAs. Another possibility is that increases in firing rate are due to feedback input. To determine the relative roles of feedforward and feedback inputs, we pharmacologically inactivated all feedback input onto ELL PCells by injecting lidocaine, a sodium channel antagonist, bilaterally into nP (n = 10 cells, N = 4 fish, see Materials and methods, Fig. 5A). Importantly, this manipulation does not alter feedforward input onto ELL PCells, since EAs do not receive feedback input. Thus, if increases in firing rate are due to feedforward input, then we would expect that PCell responses will be relatively unaffected and that the firing rate detection threshold will remain the same as under control conditions. If, on the other hand, increases in firing rate are due to feedback input, then we would expect that, after complete feedback inactivation, PCells will no longer respond to low-contrast stimuli through increases in firing rate, thereby significantly increasing the firing rate detection threshold.

We found that complete feedback inactivation strongly altered ELL PCell responses to stimuli with increasing contrast (Fig. 5B). Indeed, PCell firing rate only became significantly different from baseline for much higher contrasts (Fig. 5B, middle, compare dark and light solid green curves). Consequently, PCell firing rate detection threshold values were much higher after feedback inactivation (control: 8.4% ± 2.9%; lidocaine: 29.7% ± 6.3%, Fig. 5B, middle inset).

We note that this was not due to changes in the integration of feedforward input, as phase locking was unaffected (Fig. 5b, bottom, compare dark and light dashed green curves). Indeed, phase locking threshold values were similar before and after complete feedback inactivation (control: 5.2% ± 2.1%; lidocaine: 5.1% ± 2.0%, Fig. 5B, bottom inset). We note that vehicle injection (i.e., saline) did not affect ELL PCell firing rate (n = 7, N = 3 fish, control: 9.4% ± 1.0%; saline: 9.3% ± 0.7%, S3 Fig) or phase locking (control: 5.4% ± 1.7%; saline: 4.8% ± 1.5%, S3 Fig) detection thresholds. Thus, while increases in PCell firing rate were no longer observed for low (<15%) contrasts after complete feedback inactivation, such inactivation did not affect phase locking. These results show that it is possible to alter firing rate without altering phase locking. We conclude that, during low-contrast stimulation, increased PCell firing rate is due to feedback input, while increased phase locking is instead due to feedforward input from EAs.

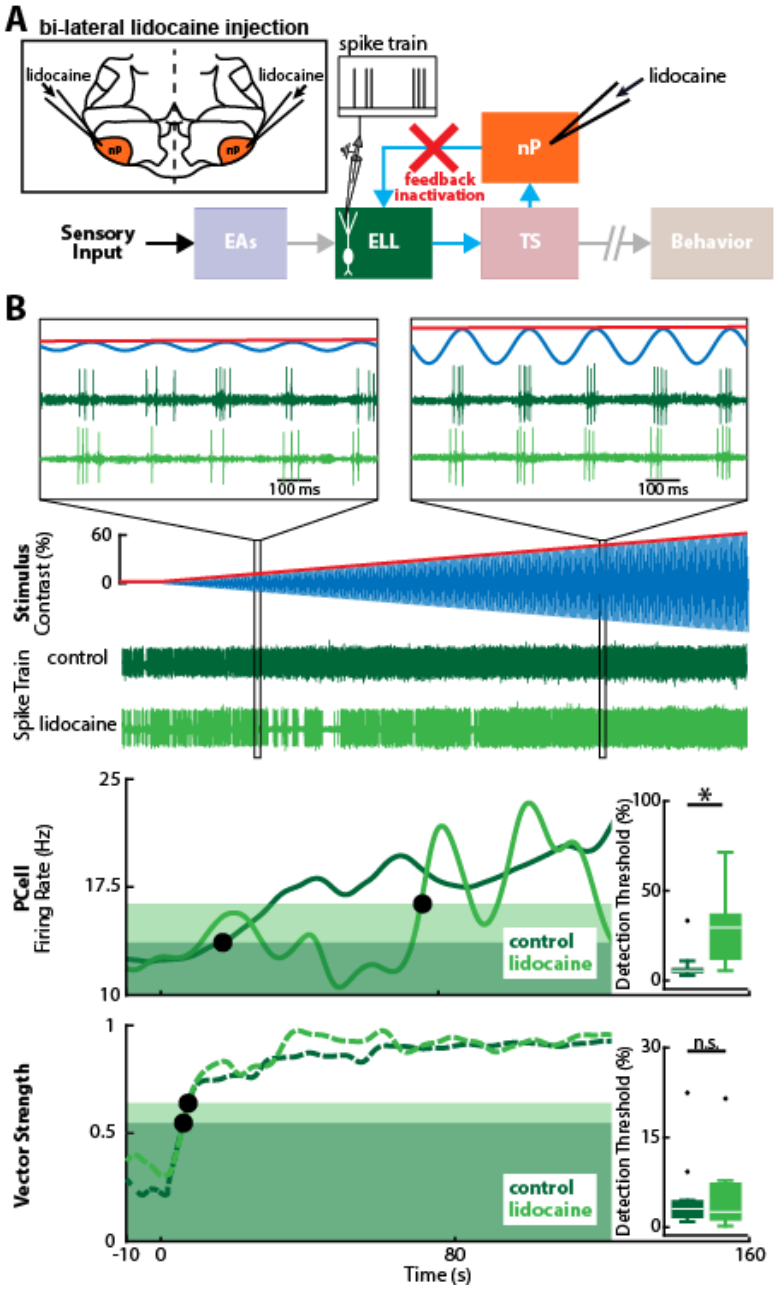

Figure 5. Feedback inactivation strongly increases PCell detection thresholds computed from firing rate but does not affect those computed from phase locking. A) Relevant anatomy diagram showing the main brain areas considered. Recordings were made from individual PCells while lidocaine, a sodium channel antagonist, was injected bilaterally into nP (top left inset), which will inactivate feedback input (red cross). B) Top: Stimulus waveform (blue) and its envelope (red) showing contrast as a function of time. Middle Top: Spiking activities of a representative example PCell before (dark green, top) and after (light green, bottom) feedback inactivation. The insets show magnification at two time points. PCell activity was strongly phase locked to the stimulus before and after feedback inactivation, indicating a strong response to feedforward input from EAs even for low stimulus contrasts. Middle bottom: Mean firing rates before (solid green) and after (light green) feedback inactivation. The detection threshold of this cell strongly increased after feedback inactivation (compare the position of the leftmost and rightmost

black circles). Inset: The population-averaged firing rate detection thresholds were significantly increased after feedback inactivation (Wilcoxon sign rank test, p = 0.0039). Bottom: Vector strength curves as a function of time before (solid green) and after (light green) feedback inactivation for this same cell. The phase locking detection thresholds (black circles) before and after feedback inactivation were similar to one another. Inset: The population-averaged phase locking detection threshold was not significantly altered by feedback inactivation (Wilcoxon sign rank test, p = 0.92).

4.4.5 – Changes in PCell firing rate, but not phase locking, determine behavioral responses

Our results so far show that the increase in PCell firing rate shortly after stimulus onset (i.e., to low contrasts) is due to feedback, while increased phase locking is instead due to feedforward input from EAs. As mentioned above, in theory, either PCell firing rate or phase locking could be used to determine behavioral responses. If the former, then increases in EOD frequency shortly after stimulus onset are due to increases in PCell firing rate. If the latter, then nonlinear integration of PCell input by downstream neurons would give the information necessary to drive behavior. To test which of PCell firing rate or phase locking is relevant for determining behavior, we investigated how complete feedback inactivation affected behavioral responses, as this manipulation does not affect ascending pathways from TS to higher brain areas mediating behavior (Fig. 6A). On the one hand, if phase locking is necessary to elicit behavior, then we would expect that feedback inactivation will not affect behavioral responses to low contrasts and thus that behavioral detection threshold values will be largely unaffected. On the other hand, if changes in PCell firing rate are necessary to elicit behavioral responses, then we would expect that feedback inactivation will cause cessation of behavioral responses to low contrasts, thereby increasing the behavioral detection threshold.

We found that complete feedback inactivation gave rise to significant changes in behavioral responses (N = 15 fish). Indeed, behavioral responses to low contrasts (<15%) were no longer present, as the EOD frequency remained below the response level (Fig. 6B, compare light and dark brown curves). EOD frequency only became significantly different from baseline for much larger contrasts than under control conditions, leading to significantly larger behavioral detection threshold values (control: 12.2% ± 2.3%; lidocaine: 34.2% ± 6.3%, Wilcoxon sign rank test, $p = 6.1 \times 10^{-5}$, Fig. 6C, brown boxes). We note that vehicle injection (i.e., saline) did not significantly affect behavioral detection thresholds (N = 10 fish, control: 13.9% ± 1.5%; saline: 14.1% ± 1.9%, S3 Fig). Thus, our results show that, for low contrasts, the information carried by

PCell phase locking is not decoded by downstream areas to determine behavior. Rather, it is the increase in PCell firing rate that is necessary to elicit behavioral responses. Interestingly, complete feedback inactivation increased PCell firing rate and behavioral detection thresholds to values that were similar to those obtained for the firing rate of single EAs (Fig. 6C). Thus, not only do our results show that feedforward input from EAs is sufficient to elicit changes in PCell firing rate for high (>40%) contrasts, but they also suggest that it is the changes in EA firing rate that are then necessary to elicit behavioral responses to high contrasts, rather than phase locking. We will return to this point below.

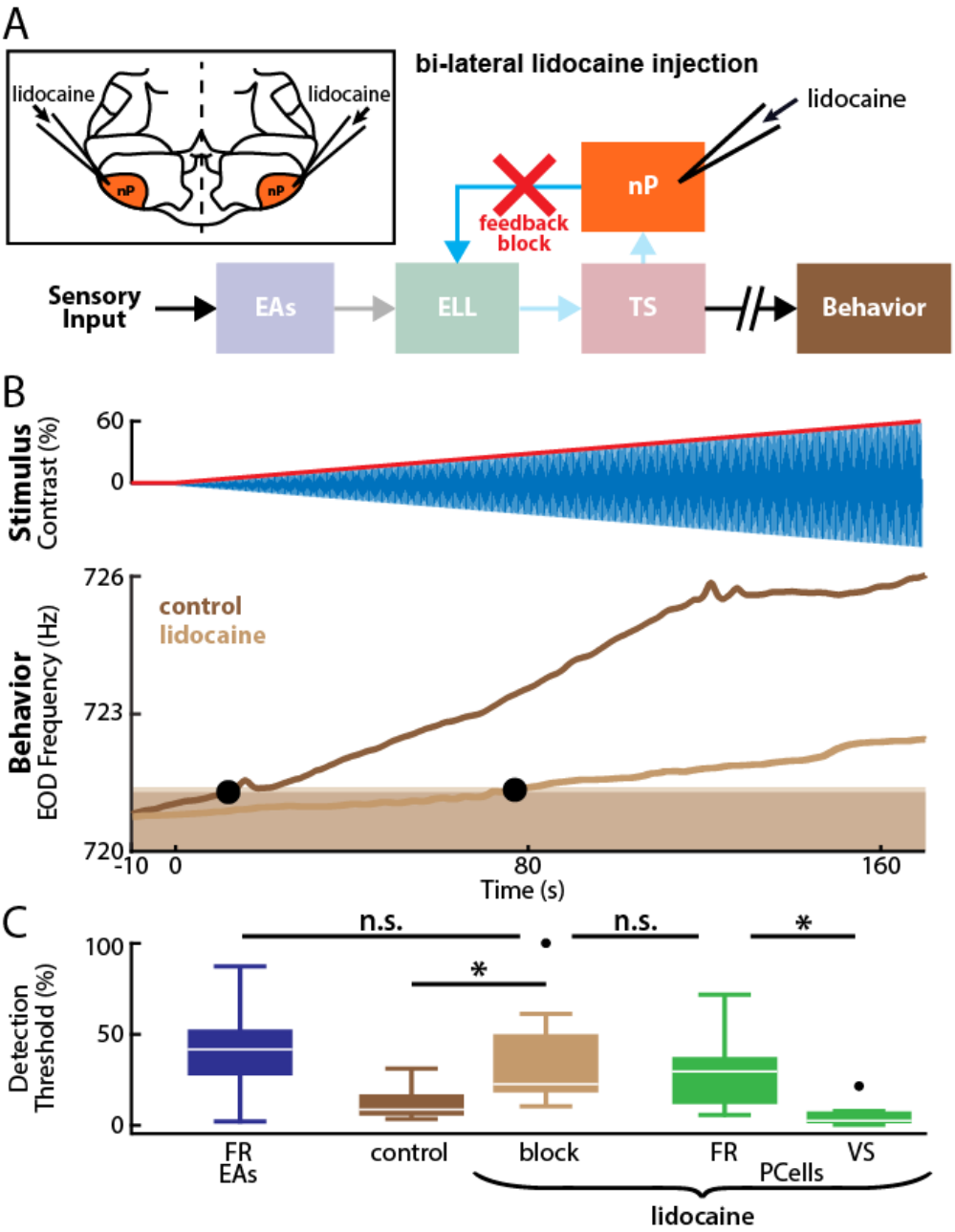

Figure 6. Feedback inactivation strongly increases behavioral detection thresholds. A) Relevant anatomy diagram showing the main brain areas considered. Behavioral responses were recorded before and after lidocaine, a sodium channel antagonist, was injected bilaterally into the nPs (top left inset), which will inactivate feedback input onto ELL PCells (red cross). B) Top: Stimulus waveform (blue) and its envelope (red) showing contrast as a function of time. Bottom: EOD frequency from a representative example individual fish before (dark brown) and after (light brown) feedback inactivation. The behavioral detection threshold strongly increased after feedback inactivation (compare the position of the leftmost and rightmost black circles). C) Whisker-box plots comparing population-averaged detection thresholds computed from behavior before (dark brown) and after (light brown) feedback inactivation to those obtained from PCells after feedback inactivation computed using firing rate (green, left) and phase locking (green, right) and to those computed from firing rate in EAs (blue). Overall, PCell firing rate was a

much better predictor of behavior than phase locking. The similarity of detection thresholds obtained from EA and PCell firing rate to that of behavior after feedback inactivation strongly suggests that, for low contrasts (<15%), phase locking in EAs is detected by PCells but is not decoded by downstream brain areas to give rise to behavior. "" indicates significance at the p = 0.05 level using a Wilcoxon sign rank or Kruskal-Wallis test (behavior).*

4.4.6 – Closed-loop direct feedback input mediates changes in ELL PCell firing rate

ELL PCells receive two sources of feedback input. One source originates directly from nP and forms a closed loop with ELL PCells, while the other instead originates indirectly from nP and goes through the eminentia granularis posterior (EGP) (S4 Fig). To test which pathway mediates changes in PCell firing rate responses, we performed two additional manipulations. The first was selectively blocking the indirect pathway by injection of 6-cyano-7-nitroquinoxaline-2,3-dione (CNQX) within the ELL, which did not significantly alter PCell firing rate or phase locking, as well as behavioral responses (S4 Fig). The second was to selectively inactivate direct feedback by injecting lidocaine unilaterally within the TS, which gave rise to similar changes in PCell activity as those observed with complete feedback inactivation (compare S5 Fig to Fig. 5). Thus, these results show that it is closed-loop feedback that causes increases in PCell firing rate in response to low-contrast stimuli.

4.4.7 – nP stellate cells providing direct feedback input to ELL pyramidal cells increase their firing rates with increasing contrast

How does closed-loop feedback input enable increases in PCell firing rate for low-stimulus contrasts? To answer this question, we recorded from nP STCells (n = 10, N = 3 fish) that provide direct feedback input to ELL PCells in response to increasing contrast (Fig. 7A). We used previously established criteria (Bratton and Bastian, 1990) to identify STCells (S6 Fig). Overall, STCells were mostly silent in the absence of stimulation and started firing shortly after stimulus onset (Fig. 7B, bottom, solid orange line). Overall, their firing rate detection thresholds were comparable to those of PCells under control conditions as well as behavior (STCells: 4.6% ± 0.7%, min: 2.0%, max: 7.6%; Fig. 7B, inset). We also found that STCells phase locked to the stimulus at the onset of firing (Fig. 7B, bottom, dashed orange line). Consequently, their phase locking detection thresholds were also low (6.5% ± 0.9%; Fig. 7B, inset). Thus, our results show

that STCells, by increasing their firing activity in response to low-contrast stimuli, provide the necessary input to drive increases in ELL PCell firing rates.

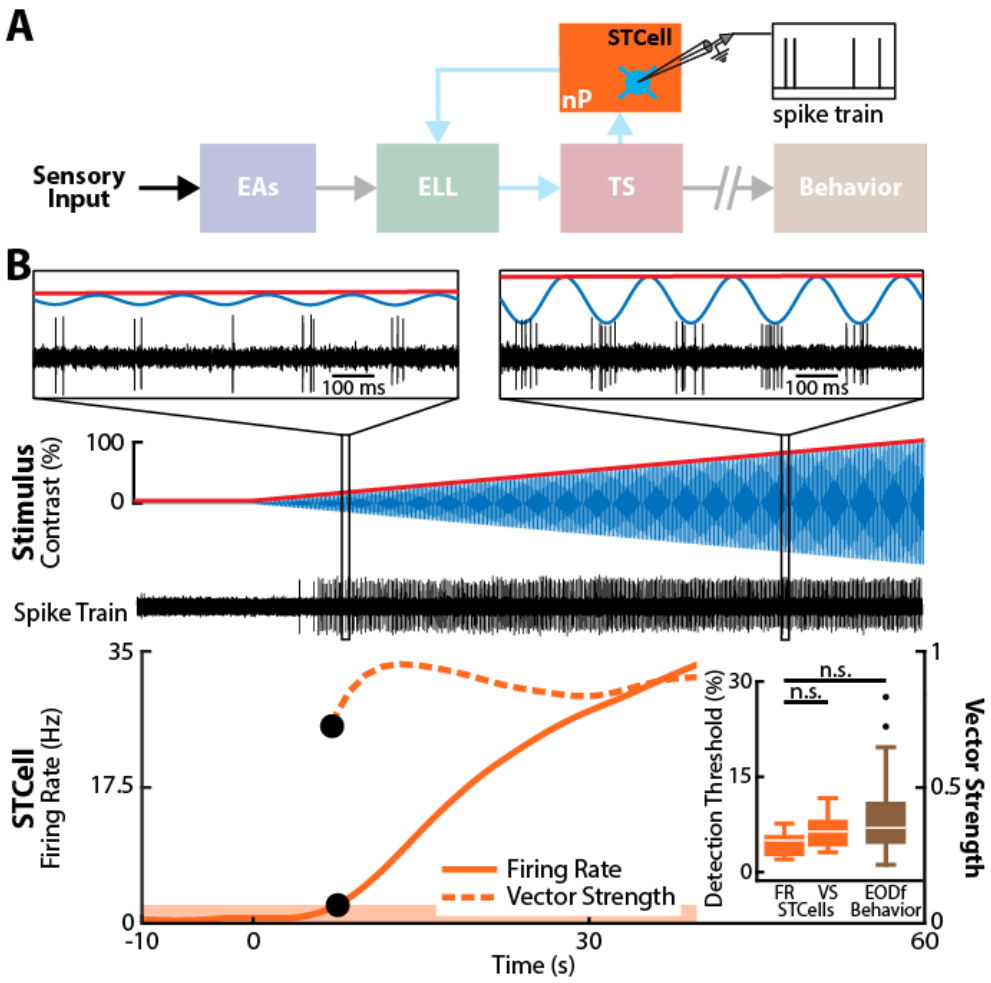

Figure 7. STCells within nP display low detection thresholds that are comparable to behavior. A) Relevant anatomy diagram showing the main brain areas considered. Recordings were made from individual STCells. B) Top: Stimulus waveform (blue) and its envelope (red) showing contrast as a function of time. Middle: Spiking activity from a representative STCell. The insets show magnification at two time points. In both cases, the STCell activity strongly phase locked to the stimulus, but the average number of spikes per stimulus cycle increased with contrast, similar to that observed for PCells under control conditions. Bottom: Double y-axis plot showing the mean firing rate (solid orange) and vector strength (dashed orange) of this STCell as a function of time. The band shows the response levels determined from this STCell's firing rate in the absence of stimulation. Because STCells tended to not fire action potentials in the absence of stimulation, it was not possible to compute a threshold level for the vector strength. The vector strength detection threshold (upper black circle) was thus set to the lowest contrast for which the STCell reliably fired action potentials for at least 5 consecutive stimulus cycles (see Methods). Inset: The population-averaged detection thresholds obtained from firing rate (left) and vector strength (middle) were not significantly different from one another of from behavior (Kruskal-Wallis, df = 2; FR-VS: p = 0.51; FR-behavior: p = 0.06; VS-behavior: p = 1).

4.4.8 – Summary

Fig. 8 shows the proposed contributions of feedforward and feedback inputs towards determining behavioral responses to increasing stimulus contrast. Overall, EAs phase lock to low contrasts, which causes ELL PCells to in turn phase lock to these. While the information carried by PCell phase locking is necessary to extract the contrast (i.e., implement signal demodulation), our results show that this information is not directly decoded by downstream brain areas to give rise to behavior (Fig. 8A). Rather, PCell phase locking is integrated via a closed-feedback loop that is necessary to elicit increases in PCell firing rate for low contrasts, which in turn elicit behavioral responses. For high contrasts, and in the absence of feedback, our results suggest that it is changes in EA firing rate that is carried over to ELL pyramidal cells, which in turn elicit behavioral responses (Fig. 8B).

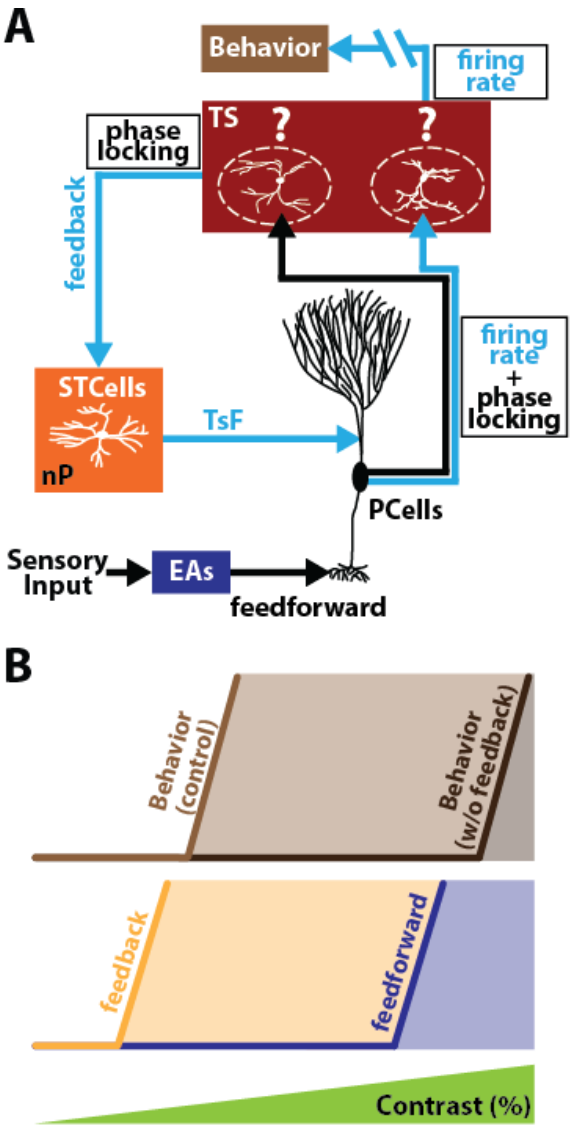

Figure 8. Summary of results. A) Relevant circuitry showing ELL PCells receiving feedforward input from EAs and projecting to TS. It is assumed that some neurons within TS decode information carried by PCell firing rate and in turn project to higher brain areas to give rise to behavior. It is further assumed that a separate group of neurons within TS project back to ELL via nP STCells and receive phase locking information from PCells, thereby forming the closed feedback loop that is necessary to elicit increases in firing rate and behavioral responses to low contrasts. B) Summary of the relative contributions of feedback and feedforward inputs towards determining behavioral responses as a function of contrast. For low contrasts (<15%) and under control conditions, feedback is necessary to elicit changes in PCell firing rate and behavior. However, for higher (>30%) contrasts, feedforward input is sufficient to elicit increases in PCell firing rate and behavior. This is because our results show that, after complete feedback inactivation, both PCell and behavior tended to be only elicited for contrasts for which EAs increased their mean firing rates.

4.5 – Discussion

4.5.1 – Summary of results

Here, we investigated how weakly electric fish process and perceive stimuli with different contrasts. Contrary to previous studies, we focused specifically on behavioral responses and the underlying neural mechanisms to low (<15%) contrasts. We found that behavioral detection thresholds were low on average (9%). Overall, peripheral EAs responded through phase locking and thus transmitted the necessary information to extract contrast to downstream areas. However, changes in EA firing rate were only elicited for much higher (approximately 40%) contrasts. ELL PCells receiving input from EAs responded to low contrasts through both increased phase locking as well as firing rate: the detection threshold values computed from either were lower than those for EAs (7% and 4%, respectively) and matched behavior (9%). Pharmacological inactivation of feedback input revealed that, while such input was necessary to elicit increases in firing rate for low contrasts, increases in phase locking were caused by feedforward input from EAs. Analysis of behavioral responses after feedback inactivation revealed that it was changes in PCell firing rate and not phase locking that determined behavior. Finally, we recorded from nP STCells that provide direct feedback input to PCells. STCells increase their firing activity shortly after stimulus onset and thus displayed low detection thresholds (5%) that matched those of PCells and behavior under control conditions. Our results thus provide the first experimental evidence showing that feedback is necessary to give rise to neural and behavioral responses to weak sensory input that would not be detected otherwise.

4.5.2 – Direct feedback generates neural responses to low contrasts

Our results show that behavioral and ELL PCell firing rate responses to low contrasts are generated because of closed-loop feedback. These results have strong implications for the electrosensory system as well as other systems, as described below. We note that information about low-stimulus contrast is carried by PCell phase locking and is due to feedforward input from EAs and does not require feedback. Theoretical studies have shown that it is possible to directly extract this information (e.g., by performing a nonlinear operation such as half-wave rectification followed by low-pass filtering (Rosenberg and Issa, 2011)). However, our results

show that downstream brain areas that mediate behavior do not decode information carried by PCell phase locking. This is because we showed that feedback inactivation strongly increased behavioral thresholds but did not alter PCell phase locking. We also note that some EAs displayed firing rate detection thresholds (approximately 2%) that are lower than those obtained at the organismal level (approximately 9%). The input from these EAs could theoretically be used to elicit behavioral responses to low contrasts. Moreover, as EAs display negligible correlations between their baseline firing rate variabilities (Chacron et al., 2005b; Metzen et al., 2016a; Metzen et al., 2015), it is then theoretically possible to improve the signal-to-noise ratio (SNR) by linearly integrating their activities (Zohary et al., 1994). Anatomical studies have shown that the PCells considered here receive input from many (600-1400) EAs (Maler, 2009a), which should give rise to substantial improvement in SNR, according to theory. However, it is unlikely that the lower firing rate thresholds of PCells are due to either selectively responding to input from the most sensitive EAs or to improving the SNR. This is because our results show that, under complete feedback inactivation, PCell firing rate threshold values were similar to those of single EAs (40%). We hypothesize that this is because heterogeneities within the EA population counteract the potential beneficial effects of summing afferent activities. Indeed, previous studies have shown that EAs display large heterogeneities, particularly in terms of their baseline firing rates (Gussin et al., 2007), which can strongly influence how they respond to envelopes (Metzen and Chacron, 2015).

It is well known that ELL pyramidal cells receive both direct and indirect sources of feedback (Berman and Maler, 1999). However, the functional role of the direct pathway has remained largely unknown until recently (Clarke and Maler, 2017). Indeed, previous studies have hypothesized that this pathway could act as a sensory searchlight that enhances salient features of sensory input as originally hypothesized by Crick (Crick, 1984). Our results provide the first experimental evidence that such feedback serves to generate sensory neural responses and perception of behaviorally relevant features of sensory input that would otherwise not be processed in the brain, which is in line with this hypothesis. In particular, nP STCells providing direct feedback input to ELL PCells have firing properties that are ideally suited for detecting low contrasts. Indeed, these cells display little to no spiking activity in the absence of stimulation (Bratton and Bastian, 1990), which is unlike ELL PCells (Bastian and Nguyenkim, 2001a; Saunders and Bastian, 1984) or multipolar cells that instead give rise to indirect feedback input

onto ELL pyramidal cells (Bastian and Bratton, 1990). Our results suggest that it is the increase in firing rate of STCells that is likely needed to increase PCell firing rate to low contrasts, thereby eliciting behavioral responses. We note that our results show that feedback plays an active role in generating increases in PCell firing rate, rather than changing how they integrate feedforward input. This is because PCell phase locking was unaffected by feedback inactivation, strongly suggesting that the response to feedforward input is similar under both conditions. This novel function for feedback is thus quite different than previously uncovered functions for feedback input such as gain control (Bastian, 1986a). We further note that our stimuli consisting of a sinusoidal waveform whose amplitude increases with time will roughly mimic the spatially diffuse AM stimulation caused by a looming conspecific (Yu et al., 2012a). The resulting stimulation is quite different than that caused by a looming object (e.g., a prey), which instead gives rise to spatially localized stimulation consisting of changes in EOD amplitude with no envelope. However, we note that a spatially localized envelope would be also generated if an oscillating motion would be superimposed on top of the looming motion. A previous study has shown that the direct feedback pathway played an important role in determining neural responses to receding but not looming objects (Clarke and Maler, 2017), strongly suggesting that responses to looming objects are primarily determined by feedforward input. Here, we have instead shown that the direct feedback pathway generates neural and behavioral responses to stimuli mimicking a looming conspecific. While previous studies have shown that lateral motion can give rise to changes in EOD frequency (Carlson and Kawasaki, 2007), how looming objects affect EOD frequency should be the focus of future studies.

An important question pertains to how feedback generates increased PCell firing rate responses to low contrasts. Such studies will require recording from the TS neurons that receive input from ELL PCells and project back to nP STCells. Previous studies have shown that there are about 50 cell types within the TS (Carr and Maler, 1985; Carr and Maler, 1986) that display highly heterogeneous responses to electrosensory stimulation (Chacron and Fortune, 2010; Chacron et al., 2009; Khosravi-Hashemi and Chacron, 2012; Khosravi-Hashemi et al., 2011; Sproule and Chacron, 2017; Sproule et al., 2015; Vonderschen and Chacron, 2011). In particular, some cell types in TS (i.e., so-called ON-OFF neurons) respond selectively to stimulus contrast because of balanced input from ON- and OFF-type ELL PCells (McGillivray et al., 2012). Specifically, these neurons respond to both increases and decreases in the stimulus and are thus

ideal to generate behavioral responses. This is because they will simply increase their firing rates with increasing contrast (see (Stamper et al., 2013) for review). Other cell types within TS respond to contrast in a manner similar to that of ELL PCells (i.e., through changes in phase locking and firing rate) (McGillivray et al., 2012). We hypothesize that it is these latter neurons that project back to nP and provide input to STCells. It is, however, important to note that all previous studies of TS neural responses used high contrasts. As such, future studies that are beyond the scope of this paper are needed to understand how different cell types within TS respond to the low contrasts considered here and mediate both ELL PCell and behavioral responses to these. Such studies should focus on brain areas downstream of TS, where it is expected that variability in the responses of single neurons would correlate with behavior, as observed in other sensory modalities (Pitkow et al., 2015).

What is the relationship between our observed behavioral responses to stimuli with time-varying contrasts and those previously observed using stimuli with constant contrasts? Previous studies have focused on studying the JAR behavior in response to stimuli with constant contrast. In particular, the JAR and the underlying neural circuitry have been extensively studied in the weakly electric fish species *Eigenmannia virescens* (Heiligenberg, 1991). This species shows exquisite sensitivity to AM stimuli, as these generate behavioral responses with contrasts as low as 0.1% (Carlson and Kawasaki, 2007). The JAR behavior in *Apteronotus* is less sensitive than for *Eigenmannia* (Dye, 1987), which is most likely due to the fact that the former species is less gregarious than the latter (Hagedorn, 1986; Hagedorn and Heiligenberg, 1985; Stamper et al., 2010). Further, there are important differences between the JAR behavior as well as the underlying neural circuitry in *Apteronotus* and *Eigenmannia* that have been reviewed extensively (Heiligenberg et al., 1996; Metzner, 1999; Rose, 2004). Most notably, *Apteronotus* tend to always increase their EOD frequency in response to low-frequency jamming stimuli with constant amplitude, which does not require the presence of PMs (Bastian et al., 2001; Zakon et al., 2002). Specifically, the EOD frequency will rise and saturate to a higher value. What is the role of feedback input onto ELL PCells in determining the JAR behavior? Previous studies have shown that lesioning both indirect and direct feedback onto ELL PCells increases their phase locking responses to low-frequency sinusoidal stimuli for high but not for low contrasts (Bastian, 1986a). Further studies have shown that this effect was mediated primarily, if not exclusively, by the indirect feedback pathway (Bastian et al., 2004; Chacron et al., 2005c). Our results showing

that selectively blocking the direct pathway does not alter phase locking in ELL PCells are consistent with these. Although the effects of complete feedback inactivation on the JAR have, to our knowledge, not been tested in *Apteronotus*, manipulations that enhanced phase locking by ELL PCells to low-frequency stimuli also led to an enhanced JAR (i.e., a greater increase in EOD frequency) (Deemyad et al., 2013). We thus predict that complete feedback inactivation would enhance the JAR and that this would be primarily, if not exclusively, due to the indirect pathway. If true, then this would imply that the role of feedback in determining JAR behavior in response to stimuli with constant contrast and our observed behavioral responses to stimuli with time-varying contrasts are qualitatively different. While the indirect feedback pathway is involved in determining the JAR magnitude via gain control, we have instead shown here that the direct feedback pathway is necessary in order to elicit increases in ELL PCell firing rate that in turn elicit increases in EOD frequency. It is nevertheless possible that the direct pathway could play a role in generating the initial increase in EOD frequency during the JAR, or in setting the latency. Further studies are needed to test these predictions.

Finally, our results show that feedback is only necessary to generate neural and behavioral responses to low contrasts. Indeed, our results show that EAs will change their firing rates for high (>40%) contrasts, which are then sufficient to elicit changes in PCell firing rate and, in turn, behavioral responses. An important question is thus: why generate responses to low contrasts through feedback when such responses could, in theory, be generated by feedforward pathways? To answer this question, one must first consider that the sinusoidal stimuli with different contrasts considered here, while behaviorally relevant, are by no means the only behaviorally relevant stimuli that must be encoded by the electrosensory system. For example, prey stimuli (Nelson and MacIver, 1999) as well as intraspecific communication stimuli (Marsat et al., 2012) must also be encoded. Secondly, one must consider the actual mechanism by which EAs can encode contrast, which involves static nonlinearities (e.g., rectification and/or saturation) during which the firing activity is constant and thus cannot encode sensory input. Thus, responses to envelopes in EAs comes at a cost. This is because these neurons then cannot respond as well to other sensory input, as the firing rate is constant (either at zero or at its maximum value) for some portion of the stimulus. We thus hypothesize that generating responses to low contrast at the level of feedback pathways does not compromise ELL PCell responses to other behaviorally relevant sensory input (e.g., caused by prey). While further

studies are needed to test this hypothesis, we note that ELL PCells display large heterogeneities, with some PCells receiving much less feedback than others (Bastian et al., 2004; Bastian and Nguyenkim, 2001b). It is also conceivable that these latter PCells, which also project to higher brain areas, help mediate perception of other behaviorally relevant stimuli.

4.5.3 – Implications for other sensory systems

Processing of AMs is behaviorally relevant in multiple sensory modalities (auditory: (Joris et al., 2004); visual: (Mareschal and Baker, 1998); vestibular: (Carriot et al., 2017; Metzen et al., 2015); somatosensory: (Lundstrom et al., 2010; Lundstrom et al., 2008)). As mentioned above, AMs found in natural auditory stimuli (e.g., speech) are particularly necessary for perception (Shannon et al., 1995; Shannon et al., 1998). There exist important parallels between processing of amplitude-modulated stimuli in both the auditory and electrosensory systems. Our results show that behavioral detection thresholds in weakly electric fish (approximately 9%) are similar to those found in the auditory system (approximately 4%) (Klump and Okanoya, 1991; Kohlrausch et al., 2000; Viemeister, 1979). The processing of amplitude-modulated sounds by the auditory system has been extensively studied. In particular, single peripheral auditory fibers will respond to AMs because of phase locking (Joris and Yin, 1992) with the most sensitive neurons displaying detection thresholds that are similar to perceptual values (Klump and Okanoya, 1991) (see (Joris et al., 2004) for review). Sensitivity to AMs also increases in higher-level areas (e.g., cochlear nuclei, inferior colliculus, auditory cortex) (Joris et al., 2004; Krishna and Semple, 2000; Malone et al., 2010; Sayles et al., 2013; Zhao and Liang, 1997). Thus, it has been commonly assumed in the auditory system that the lower detection thresholds seen centrally are the result of integration of afferent input from the periphery, as predicted from mathematical models (Hewitt and Meddis, 1994; Wang and Sachs, 1995). We hypothesize that the lower detection thresholds seen in more central areas are instead due to feedback. Further studies investigating the effects of feedback onto central auditory neurons are needed to validate this hypothesis.

Finally, we note that it is frequently assumed that behavioral responses are determined by feedforward integration of afferent input (Liu et al., 2013; Pitkow and Angelaki, 2017; Pitkow et al., 2015). However, anatomical studies in several systems have shown that feedback projections

from higher centers often vastly outnumber feedforward projections from the periphery (Cajal, 1909; Hollander, 1970; Ostapoff et al., 1990; Sherman and Guillery, 2002), and a recent review has highlighted the need for further studies focusing on the role of feedback projections in determining how sensory information gives rise to behavioral responses (Cumming and Nienborg, 2016). Previous studies have demonstrated that feedback is involved in predictive coding (Meyer and Olson, 2011; Meyer et al., 2014; van Kerkoerle et al., 2014) (see (Bastos et al., 2012) for review) or combined with feedforward input in order to amplify neuronal responses (Hupe et al., 1998). Instead, we provide here the first experimental evidence that closed-loop feedback actually generates responses to and perception of weak or low-intensity sensory input. Our results are thus timely in that they show for the first time how feedback pathways mediate sensory neural responses to and perception of behaviorally relevant stimulus features. Important commonalities between the electrosensory system and the visual, auditory, and vestibular systems of mammals (see (Bullock et al., 2005; Clarke et al., 2015) for review) suggest that similar mechanisms will be found in these systems as well.

Chapter 5

Feedback plays an essential role in optimizing neural responses and behavioural perception of second-order natural stimuli

Chapter 4 outlines how important it is to have feedback in generating envelope responses, particularly at low stimulus intensities, which occur frequently in the fish's natural environment. While we now know that this is mainly due to the effect of the direct feedback, it raises the question of what the indirect feedback is actually doing in regards to envelope responses. In this chapter, we therefore set out to observe frequency tuning to movement envelopes to elucidate exactly how feedback can give rise to the high-pass tuning that perfectly opposes the stimulus statistics seen in pyramidal cells to lead to temporal whitening. We hypothesized that the indirect feedback pathway plays a similar role as their effects on first-order AM stimuli such that they would attenuate the lower second-order envelope frequencies to give rise to high-pass tuning. To confirm this, we additionally recorded from neurons in the nP directly in order to validate our predictions. This chapter is adapted from: Chengjie G. Huang, Michael G. Metzen, Maurice J. Chacron. Feedback optimizes neural coding and perception of natural stimuli. This manuscript is currently under review at *eLife*.

5.1 – Abstract

A common assumption in systems neuroscience is that sensory neurons achieve optimal encoding by matching their tuning properties to the statistical structure of natural stimuli. However, the nature of the underlying mechanisms remains unclear. Here we demonstrate that feedback pathways originating from higher brain areas mediate optimized coding of natural stimuli via temporal whitening. Specifically, direct descending input enhances sensory neural

responses independently of frequency while indirect descending input instead selectively attenuates neural responses to low frequencies. The combined effect of descending direct and indirect pathways is thus to generate a high-pass neural tuning curve that opposes the decaying spectral power content of natural stimuli in order to optimize their encoding. Finally, we recorded from two populations of higher brain neurons giving rise to both direct and indirect descending inputs. While one population displayed broadband tuning, the other instead displayed high-pass tuning and performed temporal whitening. Thus, our results demonstrate a novel function for descending input in optimizing neural responses to sensory input through temporal whitening that is likely to be conserved across systems and species.

5.2 – Introduction

How sensory neurons process incoming sensory input thereby leading to perception and behavior remains a central question in systems neuroscience. There is growing evidence showing that neural systems can efficiently process natural sensory input by matching their tuning properties to natural stimulus statistics, thereby removing redundancy and thus maximizing information transmission (Brenner et al., 2000; Fairhall et al., 2001; Maravall et al., 2007). Theory posits that efficient coding is achieved by ensuring that the neural tuning function is inversely proportional to stimulus intensity as a function of frequency, thereby achieving a neural response whose amplitude is independent of frequency (Rieke et al., 1996). While such "whitening" has been observed across species and systems (Dan et al., 1996; Huang et al., 2016; Pitkow and Meister, 2012; Pozzorini et al., 2013; Wang et al., 2003), the nature of the underlying mechanisms remains unclear.

Weakly electric fish offer an attractive model system for studying the mechanisms underlying optimized coding of natural stimuli because of well-characterized anatomy and physiology (Berman and Maler, 1999; Chacron et al., 2011; Clarke et al., 2015). These fish generate a quasi-sinusoidal signal called the electric organ discharge (EOD) around their body, thereby allowing them to explore the environment and communicate with conspecifics. When two conspecifics are located close (<1 m) to one another, each fish experiences an amplitude modulation of its own EOD (i.e., a beat or first-order) whose amplitude (i.e., envelope or second-order) is a function of the distance and relative orientation between two conspecifics (Fotowat et al., 2013; Yu et al., 2012a) (see (Stamper et al., 2013) for review. Natural electrosensory

envelopes due to movement measured in freely moving animals display scale invariance in that their spectral power decays as a power law as a function of increasing temporal frequency (Fotowat et al., 2013; Metzen and Chacron, 2014). Furthermore, information as to their detailed timecourse is retained in the brain in order to give rise to behavioral responses (Metzen and Chacron, 2014). Envelopes and other electrosensory stimuli are sensed by electroreceptor afferents (EAs) that are scattered over the animal's skin. EAs project to pyramidal cells within the electrosensory lateral line lobe (ELL) which in turn project to higher brain structures, thereby giving rise to behavior.

While ELL pyramidal cell responses to beats and other first-order electrosensory stimuli are well characterized (see (Chacron et al., 2011; Clarke et al., 2015; Huang and Chacron, 2017; Krahe and Maler, 2014; Marsat et al., 2012) for review), comparatively much less is known about their responses to envelopes (Huang and Chacron, 2017; Middleton et al., 2006; Stamper et al., 2013). Moreover, all ELL pyramidal cells respond to envelopes, and their frequency tuning curves are determined by type 1 small conductance calcium-activated potassium (SK1) channels (see (Huang and Chacron, 2017) for review). Specifically, cells with large SK1 channel expression performed significant filtering of envelopes, as evidenced from high-pass tuning curves (Huang and Chacron, 2016) that effectively oppose the decaying spectral power content of natural envelopes, thereby making the resulting response independent of frequency (i.e., temporally whitened) (Huang and Chacron, 2016; Huang et al., 2016; Martinez et al., 2016; Zhang and Chacron, 2016). In contrast, cells with small or no SK1 channel expression performed minimal filtering of envelopes, as evidenced from broadband tuning curves (Huang and Chacron, 2016) that resembled those of EAs (Metzen and Chacron, 2015), and did not display temporally whitened responses to natural envelopes (Huang and Chacron, 2016). While previous studies have shown that SK1 channels are necessary to mediate temporal whitening of natural envelope stimuli by ELL pyramidal cells, the nature of the underlying mechanisms remains unknown to this day. One possibility is that, through SK1 channels, pyramidal cells filter incoming ascending input from EAs (i.e., feedforward) in order to achieve temporal whitening of natural envelopes, which is supported by modeling predictions (Huang et al., 2016). However, pyramidal cells also receive large amounts of descending inputs (i.e., feedback) from higher brain centers which emanate from the nucleus praeeminentialis (nP) (Berman and Maler, 1999; Sas and Maler, 1983,

1987). Thus, another possibility is that optimized coding of envelopes results from processing of descending (i.e., feedback) input by ELL pyramidal cells.

Here we used a systems level approach to investigate how feedback input mediates optimized processing of natural envelope stimuli by ELL pyramidal cells. Pharmacological inactivation of both direct and indirect sources of descending input strongly reduced pyramidal cell and behavioral responses to envelopes. However, pyramidal cell responses to high frequencies were relatively more attenuated than those at low frequencies, such that the resulting tuning was no longer high-pass but independent of frequency, which compromised optimized coding of natural stimuli by temporal whitening. In contrast, pharmacological inactivation of the indirect feedback pathway strongly increased both pyramidal cell and behavioral sensitivity to envelopes. However, enhancement was primarily seen for low envelope frequencies, such that the resulting pyramidal cell tuning curve was broadband, which also compromised optimized coding of natural stimuli by temporal whitening. Finally, we recorded from two different groups of nP neurons that project either directly or indirectly back to ELL pyramidal cells. The former displayed broadband envelope frequency tuning curves and thus did not perform temporal whitening. In contrast, the latter displayed high-pass envelope frequency tuning curves that effectively opposed the decaying envelope stimulus spectral power content, thereby enabling temporal whitening. Our results demonstrate clear but distinct functional roles for the direct and indirect feedback pathways in determining how ELL pyramidal cells respond to envelopes. While the direct pathway enhances responses to envelopes independently of frequency, the indirect pathway instead selectively attenuates responses to low frequencies, thereby giving rise to the high-pass tuning that is necessary to optimize coding of natural envelopes via temporal whitening. Interestingly, our results also show that indirect feedback input to ELL is already temporally whitened. Our results thus demonstrate an important new function for descending input onto sensory neurons in optimizing their responses to natural stimuli and their perception at the organismal level.

5.3 – Methods

5.3.1 – Animals

The wave-type weakly electric fish *Apteronotus leptorhynchus* was used exclusively in the present study. Fish were supplied by tropical fish suppliers and were housed in groups of 2-10 at

appropriate water temperatures and water conductivities similar to their natural habitats according to published guidelines (Hitschfeld et al., 2009). All procedures were approved by McGill University's animal care committee and were performed in accordance to the guidelines set out by the Canadian Council of Animal Care.

5.3.2 – Surgery

0.1-0.5 mg of tubocurarine (Sigma) was injected intramuscularly in order to immobilize the fish for both electrophysiology and behavioral experiments. Experiments were performed in a tank (30 cm x 30 cm x 10 cm) filled with the fish's home tank water. The fish were respired using a constant flow of 10 mL/min of oxygenated water over its gills for the duration of the experiment. A 2 mm^2 hole was then exposed over either the hindbrain and/or midbrain near T0 to gain access to either ELL pyramidal neurons or nP neurons respectively for electrophysiology and/or drug injection. Bilateral exposure of the brain was performed for experiments requiring bilateral drug injections.

5.3.3 – Stimulation

The electric organ discharge of *A. leptorhynchus* is neurogenic, and therefore is not affected by injection of curare. All stimuli consisting of AMs of the animal's own EOD were produced by triggering a function generator to emit one cycle of a sine wave for each zero crossing of the EOD as done previously (Bastian et al., 2002). The frequency of the emitted sine wave was set slightly higher (30 – 40 Hz) than that of the EOD, which allowed the output of the function generator to be synchronized to the animal's discharge. The emitted sine wave was subsequently multiplied with the desired AM waveform (MT3 multiplier; Tucker Davis Technologies), and the resulting signal was isolated from ground (A395 linear stimulus isolator; World Precision Instruments). The isolated signal was then delivered through a pair of chloridized silver wire electrodes placed 15 cm away from the animal on either side of the recording tank perpendicular to the fish's rostro-caudal axis. Depending on polarity, the isolated signal either added or subtracted from the animal's own discharge. The resultant signals which arrives at the fish's skin was approximated using a dipole with 1 mm of distance between the two poles to simulate what the electroreceptors would pick up.

Both neural and behavioral experiments utilized stimuli consisting of a 5 – 15 Hz noise (4^{th} order Butterworth) carrier waveform (i.e., AM) whose amplitude was further modulated (i.e., envelope) at frequencies ranging from 0.05 – 1 Hz, a behaviorally relevant range of frequencies which mimicked the envelope signals due to relative movement between two fish (Metzen and Chacron, 2014; Stamper et al., 2013). The depth of modulation for the envelope was approximately 20% of the baseline EOD amplitude as in previous studies (Deemyad et al., 2013; Metzen and Chacron, 2017; Metzen et al., 2016a). This was confirmed using the dipole recording mentioned above.

We note that movement envelopes, which are the focus of the current study, are fundamentally different than so-called "social" envelopes that are instead due to interaction between the EODs of three of more fish (Stamper et al., 2013) and which have been the focus of previous studies (McGillivray et al., 2012; Middleton et al., 2006; Savard et al., 2011; Stamper et al., 2012). Indeed, for social envelopes, the frequency content of the envelope is mostly determined by the frequencies of the three EODs. This is because the envelope frequency is given by the difference between the two resulting beat frequencies. In contrast, for movement envelopes occurring during interactions between two conspecifics, the envelope frequency content is not determined by the two EOD frequencies or the resulting beat frequency. Rather, it is determined solely by the relative movements of both fish (Fotowat et al., 2013; Metzen and Chacron, 2014). We further note that field studies have shown that Apteronotid species tend to encounter movement envelopes much more frequently than social envelopes: this is because they tend to be found in groups of 2 much more frequently than in groups of 3+ (Stamper et al., 2010). It is expected that social envelopes will be more relevant for weakly electric fish species that tend to be more gregarious (e.g., *Eigenmannia virescens*).

5.3.4 – Pharmacology

The composition of the vehicle/control saline was as follows: (all chemicals were obtained from Sigma): 111 mM NaCl, 2 mM KCl, 2 mM $CaCl_2$, 1 mM $MgSO_4$, 1 mM $NaHCO_3$ and 0.5 mM NaH_2PO_4. The pH of the saline solution was 6.8. Glutamate (Sigma), lidocaine (Astra Pharmaceuticals) and CNQX 6-cyano-7-nitroquinoxaline-2,3-dione (CNQX, Sigma) were dissolved in saline for application as done before (Deemyad et al., 2013; Huang et al., 2016). Drug application electrodes were made using either two-barrel KG-33 glass micropipettes (OD

1.5 mm, ID 0.86 mm, A-M Systems) pulled by a vertical micropipette puller (Stoelting Co.) or single barrel pipettes to a fine tip and subsequently broken to attain a tip diameter of ~5 μm for each barrel.

The two barrel pipettes were used for separate application of either lidocaine (1 mM) or CNQX (1 mM), as well as glutamate (1 mM) or saline. In order to block the indirect feedback, we injected CNQX into the ELL in proximity of a pyramidal neuron we were recording from, which we confirmed by using the excitatory response to glutamate application, as done previously (Deemyad et al., 2013). We also blocked the indirect feedback pathway by injecting lidocaine into the praeeminential electrosensory tract (PET) (behavior: bilateral; neurons: ipsilateral) projecting to the ipsilateral EGP rostral to ELL, as done previously (Bastian, 1986a). We then compared ELL neural and behavioral responses before and after injection. In order to block both the direct and indirect feedback pathways, we instead inserted two pipettes containing lidocaine into both the ipsilateral and contralateral nPs. Again, both ELL neural and behavioral responses were compared before and after injection. Bilateral injections of lidocaine were performed in order to completely silence the respective feedback pathways to directly observe the effect on neural responses and behavior, as done previously (Deemyad et al., 2013; Huang et al., 2016). In some cases, lidocaine was injected into the contralateral nP while recording from a pyramidal cell within the ipsilateral ELL (Figure S1). Saline controls were performed in the nP and we observed that there was no effect of the microinjection itself on either electrophysiology or behavior (see Figure S2). All pharmacological injections were performed using a duration of 130 ms at 103 - 138 kPa using a Picospritzer (General Valve).

5.3.5 – Electrophysiology

We used well-established techniques to perform extracellular recordings with Woods metal electrodes from pyramidal cells (Frank and Becker, 1964) located within the lateral segment of the ELL based on recording depth and mediolateral placement of the electrode on the brain surface as done previously (Huang and Chacron, 2016; Krahe et al., 2008). We recorded pyramidal cells for control in conjunction with their responses after either lidocaine (nP injections: n = 7; PET injections: n = 9), CNQX (n = 8), or saline (n = 8) injections. In addition, by tailoring the tip shape of our Woods metal electrodes, we also performed extracellular recordings from nP stellate (n = 11) and multipolar cells (n = 8) in the midbrain. We confirmed

the identity of each cell type based on recording depth, spontaneous baseline firing rates, and AM tuning curves (see Fig. S7). While stellate cells have low spontaneous firing rates (1.37±0.42 Hz) and do not respond to high AM frequencies, multipolar cells have high spontaneous firing rates (55.53±8.05 Hz and do respond well to high AM frequencies >32 Hz. These results match the results found in the literature (Bastian and Bratton, 1990; Bratton and Bastian, 1990), confirming our recordings were appropriate. All recordings were digitized at 10 kHz sampling rate using CED 1401 plus hardware and Spike2 software (Cambridge Electronic Design), and stored on a computer hard disk for offline analysis.

5.3.6 – Behavior

Animals were immobilized by an intramuscular injection of 0.1-0.5 mg tubocurarine and set up in the recording tank similarly to the method described above. Different surgeries were performed depending on the pharmacology protocol. Both nPs or both ELLs were exposed on either side of the head in order to bilaterally inject lidocaine (nP injection: n = 9; PET injection: n = 8), saline (n = 8) or CNQX (n = 7), respectively. Pipettes containing lidocaine/saline were placed approximately 1000 – 1250 μm below the surface where the nP is located, while pipettes containing CNQX were placed superficially at about 200 – 300 μm below the surface of the hindbrain where the EGP feedback terminates on the apical dendrites of pyramidal cells. Additionally, lidocaine injections were performed 50-100 μm below the brain surface adjacent to the rostral end of the ELL, where the PET is located terminating on the EGP, in order to block indirect feedback. Multiple injections (typically 3-5) were performed to ensure that both hemispheres of nP and ELL were sufficiently affected by the pharmacological agents. Stimuli were then presented as described above in order to elicit behavioral responses before and after drug application. The animal's behavior was recorded through a pair of electrodes located at the rostrum and tail of the animal. The zero-crossings of the recorded EOD signal were used to generate a binary sequence as described above that was low-pass filtered (2nd order Butterworth filter with 0.05 Hz cut-off frequency) to obtain the time-varying EOD frequency.

5.3.7 – Data Analysis

Data obtained from ELL pyramidal neurons were pooled as there is no difference in envelope response between ON- and OFF-type pyramidal cells (Huang and Chacron, 2016). All data analysis was performed offline using custom written codes in MATLAB software (MathWorks).

The recorded electrical activity were first high-pass filtered (100 Hz; 8th order Butterworth). Spike times were sorted using Spike2 software and defined as the times at which the signal crossed a given threshold value from below. To quantify the neural responses and relate them to the stimulus envelope, we used linear systems identifications techniques to compute the gain relationships to envelope frequency. We approximated the gain by averaging over the cycles of the stimulus and fitting a sinewave to the resultant cycle histogram to determine the firing rate modulation. We then divided the amplitude of the firing rate modulation to the stimulus envelope amplitude observed in the dipole to obtain the gain to any given envelope frequency. Our filtered firing rates were obtained using a second-order Butterworth filter with cutoff frequencies of 0.2, 0.35, 0.75, 1.5, 2.5, and 3.5 Hz for envelope frequencies 0.05, 0.1, 0.2, 0.5, 0.75, and 1 Hz, respectively, as done in previous studies (Huang and Chacron, 2016). Gain values calculated for behavior was performed using similar methods.

Responses to AMs were calculated using standard techniques by determining the spike-triggered average (STA) change in amplitude of the AM stimuli. The STA is the mean stimulus waveform that triggers an action potential and was obtained by averaging the stimulus waveforms within a 2 s time window surrounding each spike. We used the same envelope stimuli containing 5-15 Hz AM in order to calculate our STAs and determine the response to AMs. The response was then quantified as the peak-to-peak amplitude of each STA change in amplitude and was compared before and after drug application. We then quantified the change before and after drug application as a percentage of control, where the control STA was normalized to 100%.

Temporal whitening performed by ELL pyramidal neurons and nP neurons were calculated based on their observed tuning properties by squaring the gain at a given envelope frequency and multiplying it by the power of the natural stimulus whose spectrum decays as a power law with exponent $\alpha = -0.8$. The result provided us with an accurate estimation of the response power of the neuron across the range of frequencies we investigated. Indeed, previous studies have shown that an accurate approximation of the response power spectrum could be correctly predicted using the tuning function with this transfer function, as a change in the tuning curve of the neuron directly caused changes in the response power experimentally (Huang and Chacron, 2016; Huang et al., 2016). From the temporal whitening response power curves, the

whitening index was calculated by taking the area under the power spectrum curve of the spiking response using a trapezoidal method and dividing by that obtained by replacing all values by the maximum value in the power spectrum. The whitening index ranges between 0 and 1, where 1 indicates complete whitening (i.e., a power spectrum that is independent of temporal frequency), as done previously (Huang et al., 2016). Finally, the change in sensitivity between control and/or drug conditions were calculated using the following formula:

$$\frac{G_{Drug} - G_{Control}}{G_{Control}} \times 100\%$$

where G_{Drug} is the gain response of the neuron after drug injection at a given envelope frequency and $G_{Control}$ is the gain response of the neuron under control conditions at the same given envelope frequency. We then pooled the changes in sensitivity across envelope frequencies in order to obtain the case individually for neuron and behavior.

5.3.8 – Statistics

Statistical significance was assessed through a non-parametric Kruskal-Wallis ANOVA test if the data was unpaired or Wilcoxon signed-rank test for paired measures at the $p = 0.05$ level. Data is presented as mean ± standard error (SEM). For the whisker boxplot in figure S7, the central mark indicates the median, and the bottom and top edges of the box indicate the 25th and 75th percentiles, respectively. The whiskers extend to the range of data points.

5.4 – Results

We investigated the mechanisms that enable ELL pyramidal cells to optimally encode envelope stimuli. To do so, we performed recordings from these in awake behaving animals (Fig. 1A). Data obtained from ON- and OFF-type ELL pyramidal neurons were pooled as, consistent with previous studies (Huang and Chacron, 2016), we found no overall difference between their responses to envelopes. Our stimuli consisted of sinusoidal AMs with constant amplitude as well as noisy EOD AMs whose envelope varied sinusoidally at different frequencies. The left panel of figure 1A shows example traces of the AM (blue, first-order), envelope (red, second-order), and the full signal (cyan) received by the animal with their respective temporal frequency contents. It is further important to realize that the animal's EOD is a carrier and that the meaningful stimulus

here is the EOD AM. Thus, both first- and second-order features of the stimulus correspond to the second- and third-order features of the full signal received by the animal, respectively. We recorded both the neural activity as well as the animal's behavioral responses that consist of changes in the EOD frequency (Fig. 1A). As explained above, previous studies have shown that ELL pyramidal cells can optimally encode natural envelope stimuli because their high-pass tuning curves (Fig. 1B, middle panel) are set such as to counter the decaying stimulus spectral power (Fig. 1B, left panel). The resulting response spectrum is thus independent of frequency (Fig. 1B, right panel) which optimizes information transmission (Huang and Chacron, 2016; Huang et al., 2016) (see (Huang and Chacron, 2017) for review).

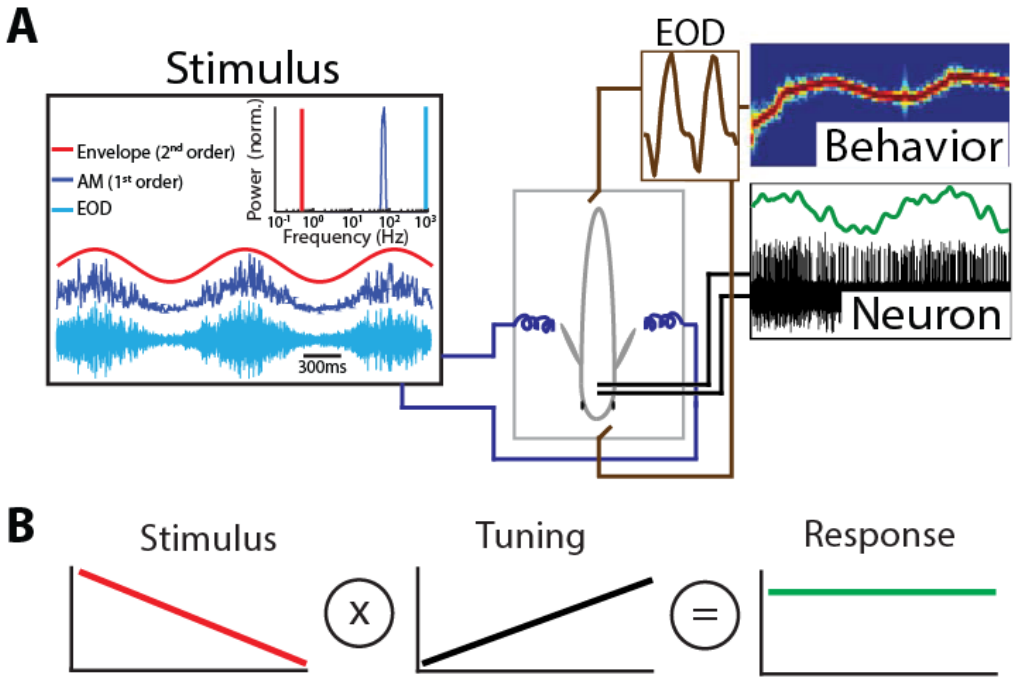

Figure 1. A) Schematic of the experimental setup showing the awake-behaving preparation where a stimulus (left) is presented to the animal while neural (bottom right) and behavioral (upper right) responses are recorded simultaneously. The stimuli consisted of amplitude modulations of the animal's own EOD: shown are an example AM waveform (blue), its envelope (red), and the full signal received by the animal (cyan) with their respective frequency contents. B) Principle of whitening by which the neural tuning curve (center) increases in order to effectively compensate for the decaying power spectrum of natural envelope stimuli (left), such that the resulting response power is independent of frequency (i.e., "whitened", right).

5.4.1 – Descending input shapes neural responses and perception of envelopes

In order to elucidate the role of feedback input, we injected the voltage gated sodium-channel antagonist lidocaine bilaterally into the nuclei praeeminentialis (nP) from which descending inputs onto ELL pyramidal cells originate (Figs. 2A, 2E). One pathway projects directly from nP to ELL (i.e., the direct feedback pathway, Fig. 2A, cyan) while the other projects indirectly from nP via the eminenatia granularis posterior (EGP) to ELL (i.e., the indirect feedback pathway, Fig. 2A, orange). We found that pharmacological inactivation of both feedback pathways strongly attenuated ELL pyramidal neural responses to envelopes (Fig. 2B, compare blue and purple). Under control conditions, cells typically responded vigorously to the sinusoidal envelope (Fig. 2B, top panel, red) through changes in firing rate (Fig. 2B, bottom panel, blue). However, after bilateral lidocaine injection, responses to the envelope were strongly reduced (Fig. 2B, bottom panel, purple). We note that unilateral injection of lidocaine within the contralateral nP gave rise to similar changes in ELL pyramidal neural responses to envelopes (Fig. S1), while injection of saline alone had no effect (Fig. S2). Bilateral lidocaine injection had no significant effect on ELL pyramidal cell responses to AMs (Fig. S3).

We next varied the envelope frequency and investigated the effects of feedback inactivation on tuning. Under control conditions, the frequency tuning of ELL pyramidal cells is high-pass, such that neural gain increases as a power law when envelope frequency is increased (Fig. 2C, blue). Further, the power law exponent is set such as to oppose the decay of the spectrum of natural envelopes, thereby causing the response power to be independent of frequency (i.e., is “whitened”, Fig. 2D, blue) as quantified by a white index (see methods) value near unity (Fig. 2H, left blue) as required for optimal coding. Pharmacological inactivation of feedback strongly affected tuning curves as well as temporal whitening. Indeed, we observed a strong attenuation in neural gain for all envelope frequencies tested (Fig. 2C, compare blue and purple). However, the attenuation was more pronounced for higher envelope frequencies, such as the resulting tuning curve was flat as characterized by a power law exponent near zero (Fig. 2C, purple, see inset). Such a change in tuning strongly affected whitening as response power was no longer independent of frequency (Fig. 2D, purple) as quantified by a lower white index value (Fig. 2H, left purple), which is accompanied by a decrease in sensitivity (Fig. 2H, right) indicating sub-optimal coding. These results indicate that descending input optimize neural

coding of envelopes by enhancing neural responses in a frequency dependent manner. Indeed, higher envelope frequencies are more amplified relative to lower envelope frequencies, thereby whitening neural responses to natural envelopes.

Changes in neural responses are only behaviorally relevant if they are actually decoded by downstream areas. Thus, we next investigated the effects of pharmacological inactivation of feedback pathways on behavioral responses (Fig. 2E). Under control conditions, the animal's EOD frequency tracks the envelope (Fig. 2F, blue). However, changes in EOD frequency are greater for low envelope frequencies, resulting in a behavioral gain that decreases as a function of increasing envelope frequency, in a power-law manner (Fig. 2G, blue), consistent with previous results (Metzen and Chacron, 2014). Pharmacological inactivation of feedback pathways strongly attenuated the animal's behavioral responses to envelopes (Fig. 2F, purple) in a frequency dependent manner, such that attenuation was strongest for low envelope frequencies (Fig. 2G, purple). Decreases in neural sensitivity were accompanied by decreases in behavioral sensitivity (Fig. 2H, right). We note that injection of saline alone had no effect on behavioral responses to envelopes (Fig. S2).

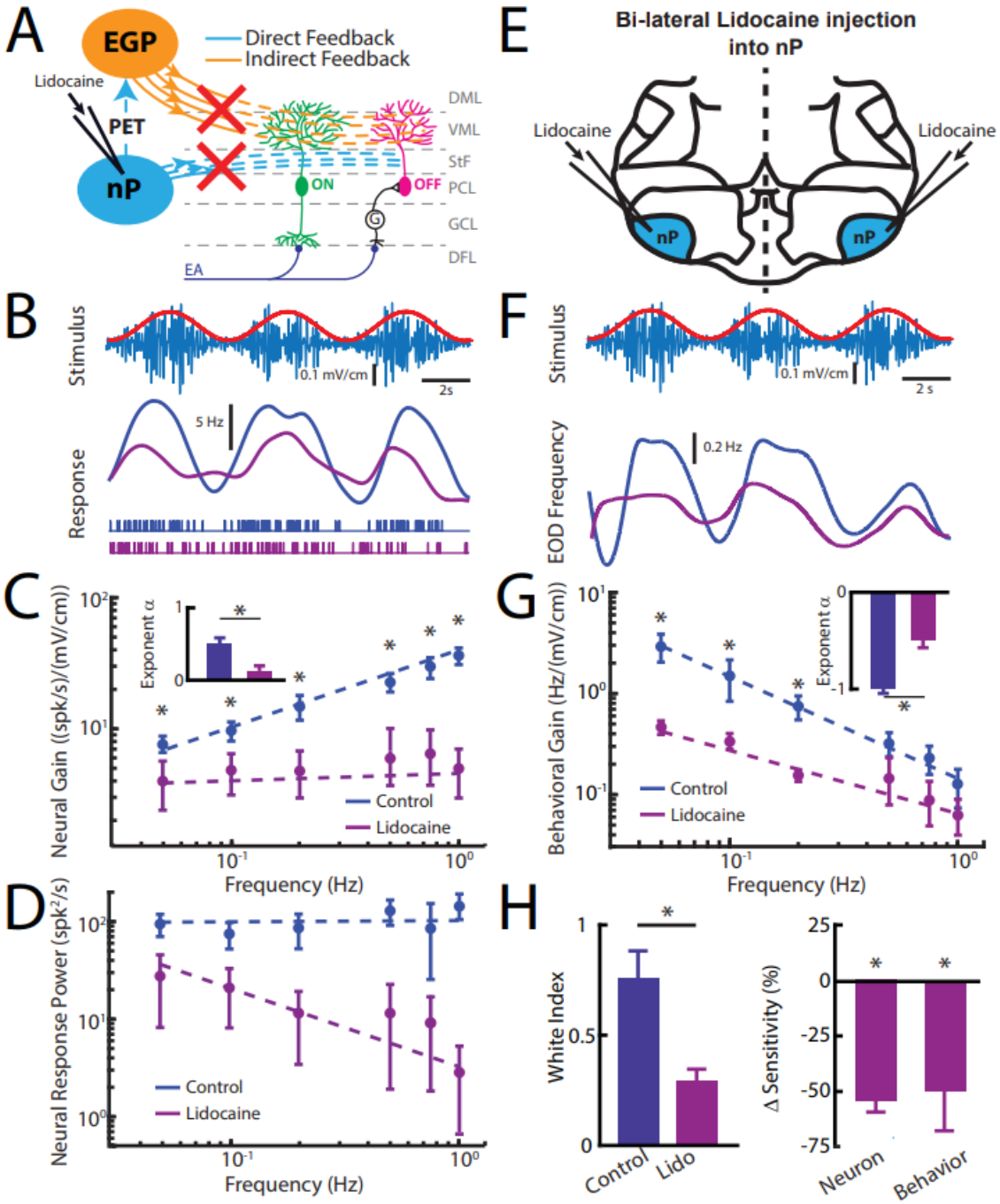

Figure 2. Descending input enhances and optimizes information transmission via whitening. A) Schematic showing relevant ELL anatomy and feedback inactivation. ON- (green) and OFF- (magenta) type ELL pyramidal cells receive feedforward input in form of excitation and di-synaptic inhibition from electrosensory afferents (EAs), respectively. Data obtained from ELL pyramidal neurons were pooled as there was no difference in envelope response between ON- and OFF-type pyramidal cells, consistent with previous results (Huang and Chacron, 2016). Both cell types also receive direct (cyan) and indirect (orange) feedback onto their apical dendrites that originate from the nucleus praeeminentialis (nP). B) Top: stimulus waveform showing the noisy AM (blue) and its sinusoidal envelope (red). Middle: Time dependent firing rate in response to the stimulus from a typical ELL pyramidal cell before (blue) and after

(purple) lidocaine application. Bottom: spiking activity from this same neuron in response to stimulation before (blue) and after (purple) lidocaine application. C) Population-averaged neural gain to sinusoidal envelopes as a function of frequency before (blue) and after (purple) lidocaine application. The dashed lines show the best power law fits to the data. Inset: Exponent before (blue) and after (purple) lidocaine injection (p = 0.0156, Wilcoxon Signed-Rank Test). ***D)*** *Population-averaged neural response power before (blue) and after (purple) lidocaine application. The dashed lines show the best power law fits to the data. E) Schematic showing that pharmacological inactivation of descending input was achieved by injecting lidocaine in both the ipsilateral and contralateral nPs. F) Top: stimulus waveform showing the noisy AM (blue) and its sinusoidal envelope (red). Bottom: Time dependent EOD frequency in response to the stimulus from a typical fish before (blue) and after (purple) lidocaine application. G) Population-averaged behavioral gain to sinusoidal envelopes as a function of frequency before (blue) and after (purple) lidocaine application. The dashed lines show the best power law fits to the data. Inset: Exponent before (blue) and after (purple) lidocaine injection (p = 0.0313, Wilcoxon Signed-Rank Test). H) Left: population-averaged white index before (blue) and after (purple) lidocaine application (p = 0.0234, Wilcoxon Signed-Rank Test). Right: population-averaged relative changes in neural (left) and behavioral (right) sensitivity following lidocaine application (neuron: p = 4.77*10^{-4}, Wilcoxon Signed-Rank Test, behavior: p = 0.002, Wilcoxon Signed-Rank Test). "*" indicates statistical significance at the p = 0.05 level.*

5.4.2 – Direct feedback enhances while indirect feedback optimizes neural responses to natural envelopes

We next investigated how direct and indirect sources of descending input contribute to determining ELL pyramidal cell and behavioral responses to envelopes. To do so, we injected 6-cyano-7-nitroquinoxaline-2,3-dione (CNQX) near the distal apical dendrites of ELL pyramidal cells (see Methods), where indirect descending input from the EGP terminates (Fig. 3A). Previous studies have shown that this manipulation effectively blocks only indirect sources of descending input within the vicinity of the ELL pyramidal cell being recorded from (Bastian, 1993; Chacron et al., 2005c). Consistent with previous results, CNQX injection increased ELL pyramidal neuron responses to AMs (Fig. S4). We found that pharmacological inactivation of indirect sources of descending input enhanced neural responses to envelopes (Fig. 3B, compare blue and green). However, neural gain was increased for low but not for high envelope frequencies, such that the resulting tuning curve was independent of frequency (Fig. 3C, green). This change in tuning antagonized optimal coding of envelopes, in that the response power spectrum was no longer independent of envelope frequency (Fig. 3D, green) as quantified by a decrease in the white index (Fig. 3H, left, green). Neural sensitivity was significantly increased (Fig. 3H, right, green). Thus, our results show that indirect sources of descending input actively

shape ELL pyramidal cell tuning to envelopes by attenuating responses to low but not high envelope frequencies, thereby optimizing coding through whitening.

In order to test the effects of the indirect feedback input on behavior, we used a different manipulation in which lidocaine was injected bilaterally within the praeeminential electrosensory tract (PET) connecting nP to EGP bilaterally (Fig. 3E). This manipulation gave rise to similar effects on ELL pyramidal cell responses than CNQX injection for both envelopes (Fig. S5) and AMs (Fig. S6). We found that pharmacological inactivation of indirect feedback input enhanced the animal's behavioral responses to envelopes (Fig. 3F, compare blue and red) only for low frequencies (Fig. 3G, compare blue and red). The behavioural response curve thus decreased more sharply as reflected by a significant decrease in the behavioral exponent (Fig. 3G, inset), leading to an increased behavioral sensitivity to envelopes only at low frequencies (Fig. 3H, right, red). Taken together, our results show that both direct and indirect feedback inputs onto ELL pyramidal cells have differential effects on envelope tuning and optimized coding. Specifically, they suggest that the function of the direct input is to enhance envelope responses independently of frequency while the indirect input selectively attenuates low frequencies, thereby optimizing coding.

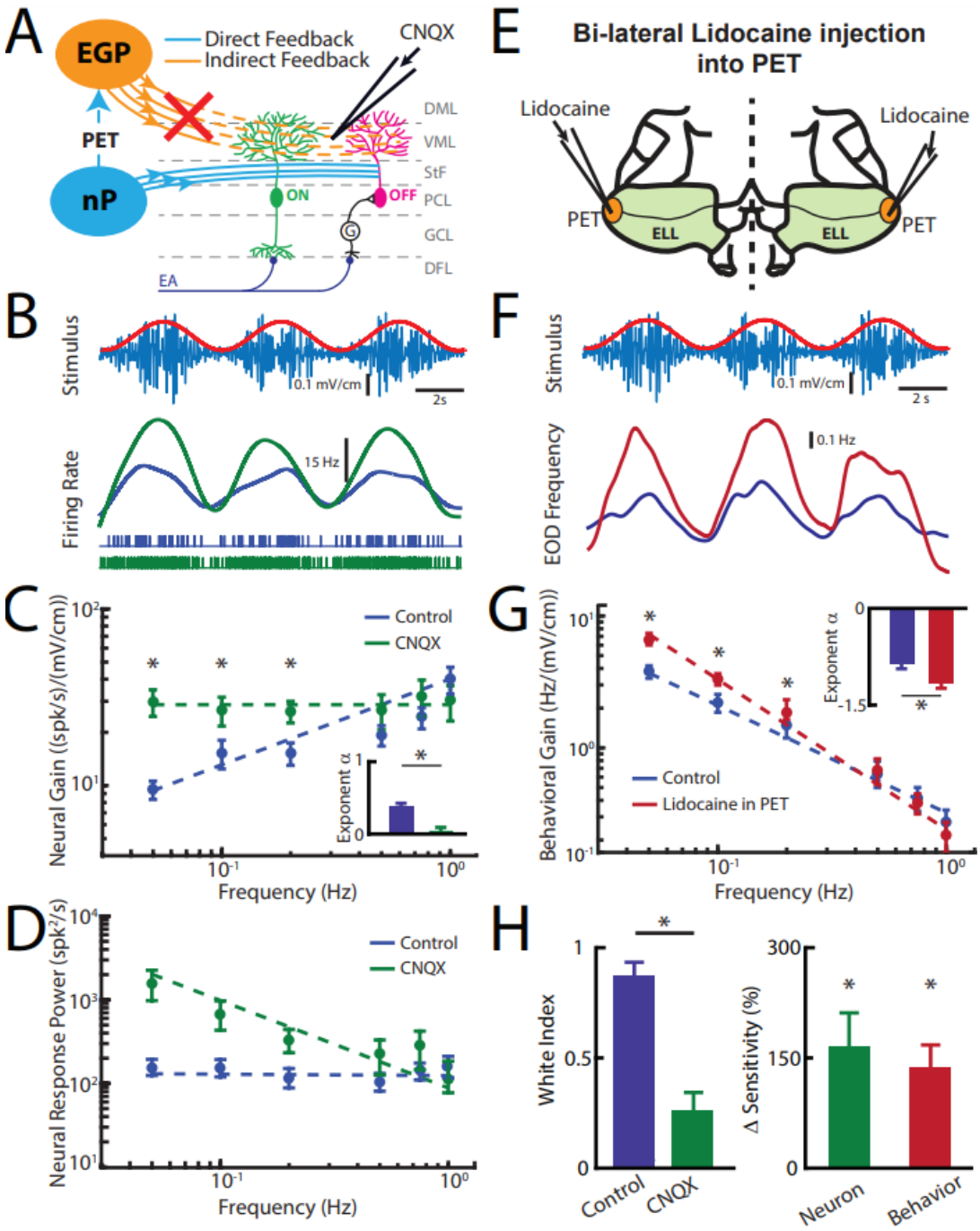

Figure 3. Direct descending input enhances while indirect input optimizes neural responses. A) Schematic showing relevant ELL anatomy. Data obtained from ELL pyramidal neurons were pooled as there is no difference in envelope response between ON- and OFF-type pyramidal cells (Huang and Chacron, 2016). Indirect feedback input from the EGP was inactivated by application of CNQX near the apical dendrites of the recorded neuron. B) Top: stimulus waveform showing the noisy AM (blue) and its sinusoidal envelope (red). Middle: Time dependent firing rate in response to the stimulus from a typical ELL pyramidal cell before (blue) and after (green) CNQX application. Bottom: spiking activity from this same neuron in

response to stimulation before (blue) and after (green) CNQX application. C) Population-averaged neural gain to sinusoidal envelopes as a function of frequency before (blue) and after (green) CNQX application. The dashed lines show the best power law fits to the data. Inset: Exponent before (blue) and after (green) CNQX injection (p = 0.0156, Wilcoxon Signed-Rank Test). D) Population-averaged neural response power before (blue) and after (green) CNQX application. The dashed lines show the best power law fits to the data. E) Schematic showing bilateral injection of lidocaine into the praeeminential electrosensory tract (PET). F) Top: stimulus waveform showing the noisy AM (blue) and its sinusoidal envelope (red). Bottom: Time dependent EOD frequency in response to the stimulus from a typical fish before (blue) and after bilateral (red) lidocaine injection. G) Population-averaged behavioral gain to sinusoidal envelopes as a function of frequency before (blue) and after (red) lidocaine injection. Inset: Exponent before (blue) and after (red) lidocaine injection (p = 0.0234, Wilcoxon Signed-Rank Test). The dashed lines show the best power law fits to the data. H) Left: population-averaged white index before (blue) and after (green) CNQX application (p = 0.039, Wilcoxon Signed-Rank Test). Right: population-averaged relative changes in neural and behavioral sensitivity following CNQX or lidocaine application (neuron: $p = 6.33*10^{-5}$, Wilcoxon Signed-Rank Test, behavior: $p = 6.74*10^{-4}$, Wilcoxon Signed-Rank Test). "" indicates statistical significance at the p = 0.05 level.*

5.4.3 – Responses of nP neurons that give rise to descending input onto ELL pyramidal cells

Finally, we investigated the nature of the descending signals that are received by ELL pyramidal cells. To do so, we recorded from nP neurons that project both directly and indirectly to ELL. Specifically, nP stellate cells project directly to ELL pyramidal cells while nP multipolar cells instead project indirectly through the EGP (Sas and Maler, 1983, 1987). Both cell types can easily be distinguished from one another based on their electrophysiological properties (Bastian and Bratton, 1990; Bratton and Bastian, 1990) (see Fig. S7). Overall, our results show that both stellate and multipolar cells responded strongly to envelopes (Fig. 4A) but showed differential frequency tuning (Fig. 4B). Specifically, stellate cell sensitivity was largely independent of envelope frequency (Fig. 4B, cyan) as quantified by a power law exponent near zero (Fig. 4D left, cyan). As such, these cells did not perform temporal whitening of natural envelopes as their response power spectra decayed with increasing frequency (Figs 4C and 4D right, cyan). These results confirm our hypothesis that the function of the direct feedback input is to enhance ELL pyramidal cell responses to envelopes independently of temporal frequency.

In contrast, multipolar cells instead displayed high-pass tuning to envelopes (Fig. 4B, orange) as quantified by a power law exponent near 0.4 (Fig. 4B, 4D left, orange) that is similar to that observed for ELL pyramidal cells (compare with Fig. 2C). As a result, we found that multipolar cells perform temporal whitening of envelopes as their response spectra was

independent of frequency (Fig. 4C, orange) as quantified by a white index near unity (Fig. 4D right, orange). Thus, our results reveal that the feedback input that is sent indirectly to ELL pyramidal cells via the EGP is already temporally whitened. This result has important implications for understanding how temporal whitening of ELL pyramidal cell responses is achieved as discussed below.

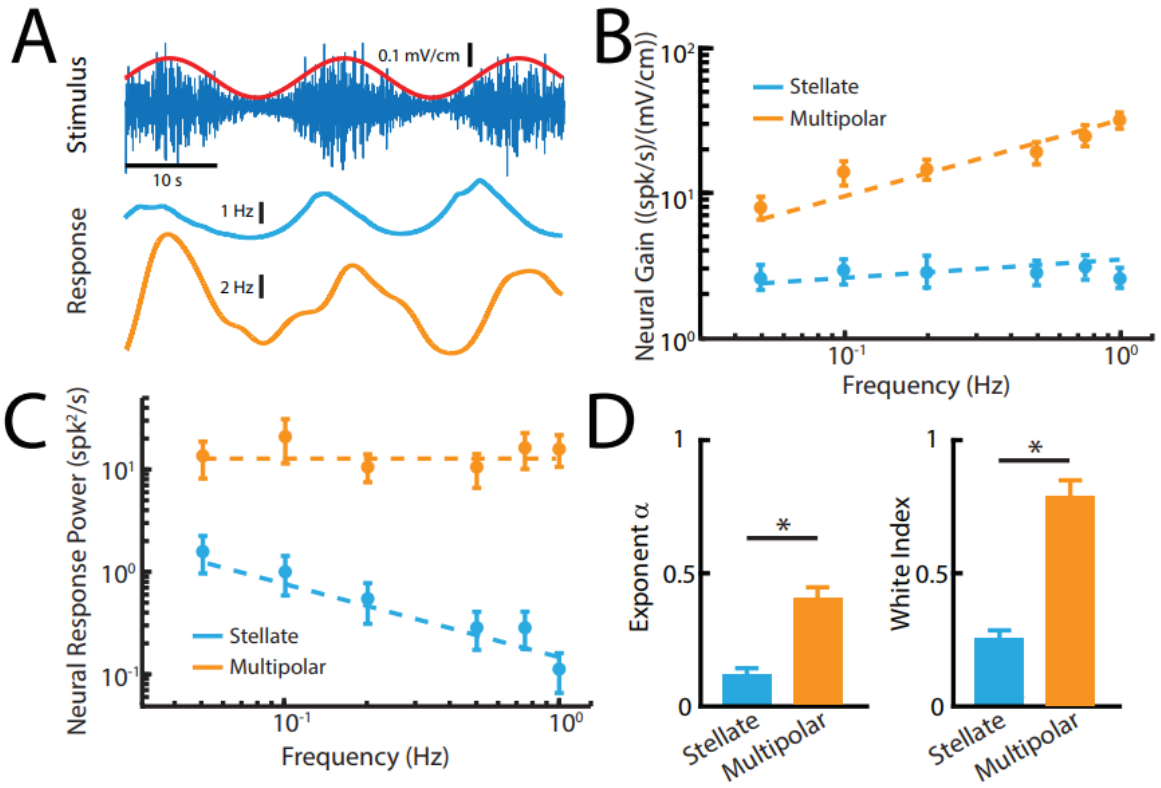

Figure 4: Only nP neurons projecting indirectly to ELL display tuning properties that are optimized to natural stimulus statistics. A) Top: stimulus waveform showing the noisy AM (blue) and its sinusoidal envelope (red). Bottom: Time dependent firing rate in response to the stimulus from typical nP stellate (cyan) and multipolar (orange) cells. B) Population-averaged neural gain as a function of frequency in response to sinusoidal envelopes for nP stellate (cyan) and multipolar (orange) cells. The dashed lines show the best power law fits to the data. C) Population-averaged neural response power for stellate (cyan) and multipolar (orange) cells. The dashed lines show the best power law fits to the data. D) Population-averaged power law exponents (left, $\chi^2 = 12$, $p = 5.32*10^{-4}$, Kruskal-Wallis ANOVA) and white index (right, $\chi^2 = 10.7$, $p = 0.0011$, Kruskal-Wallis ANOVA) values for stellate (cyan) and multipolar (orange) cells. "" indicates statistical significance at the p = 0.05 level.*

5.5 – Discussion

5.5.1 – Summary of Results

We investigated the roles of both direct and indirect sources of descending input onto ELL pyramidal cells in determining their responses to envelopes. Pharmacological inactivation of both direct and indirect sources strongly attenuated pyramidal cell and behavioral responses to envelopes. Because responses to higher envelope frequencies were more attenuated, the resulting tuning curve became independent of frequency, thereby compromising optimized coding through temporal whitening. Pharmacological inactivation of indirect input instead increased pyramidal cell and behavioral responses to envelopes. However, enhancement was observed primarily for low envelope frequencies, such that the resulting tuning curve was independent of frequency, which also compromised optimized coding through temporal whitening. Finally, we investigated the nature of the feedback signals being received both directly and indirectly by ELL pyramidal cells. Specifically, nP stellate cells that project directly to ELL displayed tuning curves that were independent of envelope frequency and did not perform temporal whitening. In contrast, nP multipolar cells that project indirectly to ELL displayed high-pass tuning and optimally encoded envelopes through temporal whitening. Thus, our results provide the first experimental evidence showing how descending pathways mediate optimized coding of stimuli by sensory neurons. While direct feedback input enhances neural responses independently of frequency, our results show that indirect feedback input selectively attenuates responses to low envelope frequencies, thereby giving rise to a high-pass tuning that opposes natural envelope statistics and optimizes coding through temporal whitening.

5.5.2 – Feedback modulation enhances responses to salient features

Our results showing that nP stellate cells projecting directly to ELL pyramidal cells enhance their responses to envelopes provide a new function for this feedback pathway. Indeed, while previous studies have suggested that the function of this feedback pathway was to enhance responses to salient stimuli (Berman and Maler, 1998, 1999; Bratton and Bastian, 1990), experimental evidence supporting this hypothesis was lacking until recently when a clear role in synthesizing responses to motion stimuli consisting exclusively of first-order stimulus features was established (Clarke and Maler, 2017). Our results show an important novel functional role for the direct feedback pathway in enhancing both neural responses to and perception of behaviorally

relevant second-order (i.e., envelope) stimuli. Interestingly, previous studies have suggested that the direct feedback pathway could function as a sensory searchlight (Berman and Maler, 1999), as originally proposed by Crick (Crick, 1984), thereby enhancing salient stimulus features and attenuating others. Our results are consistent with descending input onto ELL pyramidal cells acting in this manner but instead suggest that concerted action from both direct and indirect sources is necessary. Indeed, while the direct pathway enhances responses to envelopes independently of frequency, the indirect pathway instead selectively attenuates responses to low frequencies, thereby favoring responses to higher frequencies.

Overall, our results are consistent with previous ones showing that the tuning function of ELL pyramidal cells must be matched to natural statistics in order to optimize coding, which in turn ensures that behavioral sensitivity is greatest for frequencies at which natural stimuli contain the most power (Huang et al., 2016). Indeed, we found that feedback inactivation altered ELL pyramidal cell tuning, thereby rendering coding sub-optimal, which caused a mismatch between behavioral sensitivity and natural statistics. However, our results suggest that the relationship between ELL pyramidal cell and behavioral responses to envelopes is more complicated than previously expected. Specifically, it was assumed that changes in the neural exponent of ELL pyramidal cells alone would determine changes in the behavioral exponent. Our current results show that this is not the case as pharmacological inactivation of both direct and indirect feedback input led to similar changes in the neural tuning exponent but led to opposite changes in the behavioral tuning exponent. Thus, it is not only the tuning exponent of ELL pyramidal cells that determines the behavioral exponent, but also the overall sensitivity. Further studies are needed to better understand how information transmitted by ELL pyramidal cells is decoded by higher brain areas in order to lead to behavioral responses.

5.5.3 – The effect of the indirect feedback on neural responses to behaviourally-relevant first-order and second-order stimuli are functionally different

Previous results have demonstrated important functions for the indirect feedback pathway such as gain control (Bastian, 1986a, b) as well as cancelation of both self and externally-generated low (< 15 Hz) frequency spatially diffuse AM (i.e., first-order) stimuli (Bastian, 1986a, 1996a, b; Bastian, 1998; Bastian, 1999; Bastian et al., 2004; Chacron, 2006; Chacron et al., 2005c; Clarke and Maler, 2017), thereby allowing better detection of spatially localized stimuli (e.g., those

caused by prey) (Bastian et al., 2004; Litwin-Kumar et al., 2012). Specifically, previous studies have shown that this pathway generates a negative image of the stimulus, thereby strongly reducing ELL pyramidal cell responses. More recent studies have shed light on how short-term burst-timing dependent depression helps in sculpting this negative image in an adaptive fashion (Bol et al., 2011; Bol et al., 2013; Mejias et al., 2013). In contrast, our results have demonstrated an important new function for indirect feedback in mediating optimized coding of envelope (i.e., second-order) stimuli by selectively attenuating responses to low frequencies.

How then can the same feedback pathway mediate attenuation of responses to both low-frequency AMs and envelopes? One possibility is that in both cases it is the same mechanisms that facilitate response attenuation. This is however unlikely because of the important difference between the frequency ranges of AMs and envelopes for which responses are attenuated, as mentioned above. Specifically, while the response to a 1 Hz AM will be strongly attenuated by feedback (Bol et al., 2011), our results show that this is not the case for a 1 Hz envelope. Previous results have shown that SK1 channels strongly determine envelope but not AM tuning properties. Specifically, pharmacological inactivation of SK1 channels had minimal effects on responses to AMs (Toporikova and Chacron, 2009) but compromised optimized coding of envelopes by causing the tuning curve to be broadband (Huang et al., 2016). In fact, the effects of indirect feedback inactivation and of SK1 channel antagonists on ELL pyramidal cell tuning to envelopes were strikingly similar. We propose that indirect feedback excitation provides the necessary intracellular calcium entry that activates SK1 channels. These in turn give rise to spike frequency adaptation, thereby selectively attenuating responses to low envelope frequencies and causing the envelope tuning curve to become high-pass (Benda and Herz, 2003; Deemyad et al., 2012; Huang et al., 2016) (see (Huang and Chacron, 2017) for review). Thus, blocking indirect feedback input would strongly attenuate calcium entry via NMDA receptors, thereby effectively inhibiting SK1 channels and explaining why the effects on ELL pyramidal cell tuning to envelopes are similar to those previously observed after application of SK channel antagonists (Huang et al., 2016). The fact that calcium-permeable NMDA receptors are highly expressed within the apical dendrites of ELL pyramidal cells (Bottai et al., 1997; Harvey-Girard and Dunn, 2003), where indirect feedback input terminates (Berman and Maler, 1999) and SK1 channels are located (Ellis et al., 2008), supports our hypothesis. However, the exact mechanisms by which SK1 channels determine responses to envelopes but not AMs, though critical in order to

enable the indirect pathway to perform multiple functions, are not well-understood and should be the focus of future studies.

It is important to note that the envelope stimuli considered here are behaviorally relevant and contain important information as to the relative position between both conspecifics. Since our results show that the indirect feedback did not attenuate responses to envelopes with higher (>0.2 Hz) frequencies, it is conceivable that these could interfere with the detection of other behaviorally-relevant low frequency AM stimuli (e.g., those caused by prey) since the responses to both stimuli should be enhanced by the direct feedback pathway. This is unlikely to be the case however because: 1) the AM stimuli caused by prey are spatially localized whereas envelope stimuli are spatially diffuse and; 2) the temporal frequency content of envelopes tends to be much lower (0-1 Hz) than that of prey stimuli (0-10 Hz) (Nelson and MacIver, 1999; Stamper et al., 2013). We hypothesize that these differences in spatial extent and temporal frequency content are used by the animal to distinguish between both stimuli, but further studies are needed to verify that this is the case.

We have shown for the first time how neurons within nP that project either directly or indirectly back to ELL respond to envelopes. Stellate cells projecting directly to ELL pyramidal cells displayed broadband tuning curves. The fact that ELL pyramidal cells displayed broadband tuning curves after pharmacological inactivation of indirect descending input suggests that they perform little filtering of input from stellate cells. Interestingly, multipolar cells projecting indirectly have tuning properties that are similar to those of ELL pyramidal cells and optimize coding via temporal whitening. This result has important implications for understanding how temporal whitening of envelopes occurs in ELL pyramidal cells as it implies that the output of the nP received by EGP granule cells that project back to ELL is already temporally whitened. It is very likely that the output of nP multipolar cells, which is critical in determining ELL pyramidal cell tuning and responses to envelopes, undergoes significant filtering both by EGP granule cells to enable filtering by SK1 channels in ELL pyramidal cells. Further studies are needed to gain further understanding as to the underlying mechanisms.

5.5.4 – Implications for other sensory systems

Our results provide novel functional roles for the indirect feedback pathway in optimizing ELL pyramidal cell responses to envelopes through temporal whitening by selective attenuation of

low frequencies. It should be noted that the architecture of the indirect feedback pathway by which parallel fibers emanating from the EGP terminate onto distal ELL pyramidal cell apical dendrites shares many similarities with the cerebellum and other cerebellum-like structures (e.g., the dorsal cochlear nucleus). Studies performed in cerebellum as well as cerebellum-like structures have shown clear common functions and mechanisms mediating how such descending input in attenuating or even cancelling responses to self-generated sensory input (Bell et al., 2008; Cullen, 2011; Requarth and Sawtell, 2011; Sawtell, 2017; Singla et al., 2017; Warren and Sawtell, 2016). It is likely that our results showing that feedback input from parallel fibers in the cerebellar-like ELL mediate optimized coding of natural stimuli through whitening will be applicable to the cerebellum as well as other cerebellum-like structures.

Finally, recent results have emphasized the critical role of descending pathways, which are found ubiquitously in sensory systems (Cajal, 1909; Hollander, 1970; Ostapoff et al., 1990; Sherman and Guillery, 2002), in determining accurate sensory neural and behavioral responses to sensory input (Kwon et al., 2016; Manita et al., 2015; Takahashi et al., 2016). In particular, it was shown that feedback terminating on the apical dendrites of cortical pyramidal neurons was essential in determining both responses and perception to somatosensory input (Takahashi et al., 2016). Critically, the electrosensory system of weakly electric fish displays many documented similarities with the mammalian visual, auditory, and vestibular systems (Chacron et al., 2011; Clarke et al., 2015; Metzen et al., 2015). Thus, given that temporal whitening has been observed across sensory systems (Dan et al., 1996; Lundstrom et al., 2010; Pozzorini et al., 2013; Wang et al., 2003), it is likely that our results showing how feedback pathways mediate temporal whitening of sensory input by ELL pyramidal cells in the electrosensory system of weakly electric fish will be generally applicable to other systems.

Chapter 6

General Discussion

The primary goal of my research was to understand how envelopes are encoded and decoded in the brain in order to elicit the behavioural responses which demonstrate perception of the movement between two conspecific animals. In order to achieve this goal, I first performed a complete characterization of ELL pyramidal cell responses from various subclasses to gain an understanding of what type of responses exist to encode envelopes. It was found that a subset of those neurons could perform temporal whitening and efficiently encode envelope stimuli in an optimal manner. I also found out that other subclasses that did not perform temporal whitening served to preserve stimulus information and would work in conjunction in downstream brain areas to decode the efficiently encoded information coming from other subsets of neurons. Next, I investigated further into temporal whitening and observed exactly what would give rise to the high-pass characteristics which matched and opposed the natural stimulus statistics. In addition to making predictions with an LIF model, I tested these predictions with pharmacology to observe the direct effects on neural tuning and subsequent consequences on the animal's behaviour. Finally, I investigated the roles of feedback in generating and optimizing neural responses in the ELL, which was final piece of the puzzle which was uncovered to explain exactly where envelope responses came from in the first place. In the following sections, I will perform some general discussion of the overall projects in my dissertation.

6.1 – Integration of feedback across the three segments

From chapter 2, we know that different segments of the ELL have differential tuning curves and that temporal whitening mostly occurs for LS superficial neurons. We also know that feedback pathways are important for temporal whitening and are necessary for creating the envelope response in the first place. How do the segments then differ in their tuning responses if they are to receive similar feedback from the direct and indirect feedback pathways? One aspect that was

not discussed in the thesis is the integration of information in the TS and how that plays a role in sending information back to the ELL to modulate pyramidal cell activity in the three different segments. We can speculate that the TS is responsible for both decoding and sending different inputs back to ELL via the nP. While the nP sends similar feedback back to the three segments, how they are integrated in the dendrites could be key to the differential tuning across the segments. This could be due to what ion channels and neuromodulator receptors are co-localized with where the feedback terminates. We know from chapter 3 that SK1 channels exist on the apical dendrites of pyramidal cells in the ELL. However, the expression of the SK1 channels differ across segments, with less in CLS, and little to none in CMS. This is similarly true for superficial neurons having the most SK1 channels, and little to none in the deep neurons. Therefore, it is likely that the inputs from feedback activate either the entrance of calcium through NMDA/AMPA receptors or induce release of intracellular calcium through the Protein Kinase C (PKC) pathway to activate these SK1 channels. However, the level of activation differs due to the differential levels of expression across the three segments. This could then explain the observed differential tuning across ELL segments. This is a relatively simple hypothesis and it is likely other channels and receptors play key roles in the integration of feedback inputs. On the contrary, the feedforward integration of TS and its role in giving rise to behavioural responses would also need to be elucidated.

6.2 – Neural integrator in the midbrain for behavioural output

As mentioned above, another aspect that remains to be solved is how pyramidal cell output becomes integrated in the midbrain. Currently, it is known that there are TS neurons which respond to envelopes; however, a systematic characterization of tuning curves to neither movement nor social envelopes have been classified. It is interesting in that pyramidal cells have a high-pass tuning curve which enables temporal whitening, but ultimately the behaviour matches the statistics of the natural environment. This is to say that behavioural responses to low envelope frequencies have the highest gain and the responses to high envelope frequencies have the lowest gain. This suggests that downstream of the ELL, there is an integrator which “flips” the tuning curve to give rise to the one found in behaviour. We would need to identify TS neurons which exclusively or non-exclusively encode envelopes and explore how they are

decoding the incoming information from the ELL. One possibility is that a specific subset of TS neurons are decoding the time-dependent firing rate information coming from ELL and transforming it to feed into the nP, where this information feeds back onto the ELL to further modulate and refine responses. In contrast, another subset of TS neurons are receiving both efficiently encoded information from LS neurons in combination with the preserved copy of the stimulus coming in from CMS, to optimally decode the information through parallel processing. The difficulty in this study would be to actually identify neurons belonging to these subclasses as there are presumably over 50 cell types in the TS (Carr and Maler, 1985; Sproule et al., 2015). It is thus likely that from the vast variety of TS neurons, there are neurons which may already be integrating temporally whitened information and decoding it for behaviour by displaying a low-pass tuning curve to the envelope frequencies. However, this remains to be tested. Either way, there is a need for a neural integrator which gives rise to the signals which mediate behaviour. These neural integrators are critical to behaviour as they explain the link between primary sensory neurons and the ultimate behavioural output. One example of this is within the vestibular system, where the neural integrator exists to integrate raw signals from the otolithic organs, linear head acceleration, and eye positions and velocity inputs to elicit the vestibular ocular reflex (VOR) and all other conjugate eye movements (Dale and Cullen, 2015; Skavenski and Robinson, 1973). Whereas in our case, it is most likely that the TS takes information from all three segments (as well as other sensory pathways) and acts as a central neural integrator to generate signals necessary for behaviour.

Furthermore, one cannot discount the influence of higher brain areas such as those found in the forebrain. Previous studies have found that neurons in the forebrain are responsible for complex cognitive functions in the weakly-electric fish such as spatial navigation and memory, as well as attention (Elliott et al., 2017; Jun et al., 2016). These are all higher-level functions which have been shown extensively to influence neural tuning and behaviour. This is to say that although there are feedback projections from the TS and nP, even more modulation may come from the forebrain where these executive functions exert top-down modulation. This also introduces possibilities of stimulus-dependent or task-dependent modulation, behavioural adaptation, as well as a number of other avenues to explore regarding feedback. Models of how different higher brain areas interact with the periphery could shed light on how exactly neural responses can be altered and in turn, give rise to differential behavioural responses under different contexts.

6.3 – Implications for social envelopes

The thesis mainly focused on movement envelopes and how this type of second-order information is processed in the brain. However, as mentioned in the introduction, social envelopes also exist when there are three or more fish are either stationary or moving about around each other. However, the statistics of three fish are very complicated and thus requires much further study to understand how the electrosensory systems processes them. However, we do know that these envelope frequencies are much higher than those found in movement exclusively, and are > 1 Hz. This presents an interesting conundrum for the fish. How does a fish segregate a 4 Hz envelope from a 4 Hz first-order AM beat signal? It is likely that the fish takes into account the spectral power of the stimulus. Previous studies have shown that by the 1 Hz cutoff of the movement envelopes, the stimulus power has already decayed by three orders of magnitude (Metzen and Chacron, 2014). Furthermore, the spectral power of the envelopes is already inherently lower than those found in the first-order AM and hence would likely not be confused with the envelope. Although these two signals may be tied to one another, several lines of evidence show that first-order signals can be independently processed from second-order signals (McGillivray et al., 2012), particularly downsteam of the ELL in the TS, where these signals are subsequently decoded. However, it is unknown whether the same high-pass filtering will continue to apply to envelope frequencies > 1 Hz since social envelopes could constitute different stimulus statistics. In addition, signals > 1 Hz are often much noisier and it is likely that the brain has to employ alternative strategies in order to optimally encode those frequencies. Preliminary results from CMS recordings show that neural tuning changes for envelope frequencies > 1 Hz and thus suggest that these social envelopes are processed differentially in a separate manner. These responses remain to be tested and further studies are needed to understand how social envelopes, along with other social contexts (such as those with chirps) the fish may encounter in nature, can alter neural responses and behaviour in the wild.

6.4 – Applicability to other sensory systems

To what extent are the findings in this thesis applicable to other sensory systems? To a large extent, temporal whitening is a neural coding strategy that exists widely in the literature. For example, the classic example of (Dan et al., 1996) demonstrated that noisy or unnatural stimuli do not elicit neural responses that are temporally whitened in the lateral geniculate nucleus. Rather, only a movie (Casablanca) with natural statistics was able to elicit temporal whitening. Notably, this was performed in the adult cat visual system. Furthermore, previous studies have also found that temporal whitening performed by auditory midbrain neurons in zebra finches enhance acoustic differences between natural sounds, and thus improves discrimination between different segments of songs, which are behaviourally-relevant sounds critical for mating (Woolley et al., 2005). In addition, it was found that L2/3 neurons in the somatosensory cortex of mice were also able to perform temporal whitening using power-law adaptation, to enhance signal-to-noise ratio and thus maximize information transmission (Pozzorini et al., 2013). These results have several implications. First, these results suggest that temporal whitening is an optimal neural coding strategy which is used widely to enhance the transfer of information within any given sensory system. Second, these results suggest that temporal whitening can occur along many stages and brain areas of sensory processing. The results from this thesis suggest that temporal whitening happens relatively early on, similar to the example in the visual system, where redundant information is already filtered out before it reaches the cortex. Despite this, we must note that not all ELL pyramidal cells do perform whitening, and that the majority of deep neurons across segments and in particular the CMS, do not perform any filtering. The leading idea is that these neurons are important for preserving the stimulus statistics. Neurons which do not perform any filtering can be similarly found in other sensory systems such as in the spherical bushy cell of the ventral cochlear nucleus, whom faithfully preserve the temporal properties of the auditory nerve fiber response. Having a combination of neurons which preserve the stimulus statistics and those which serve as filters are suggestive of common parallel coding strategies. Finally, results from the auditory system and somatosensory system mentioned above suggest that temporal whitening can also take place in higher brain areas, such as a primary sensory cortex. This also has implications that perhaps neurons in the electric fish midbrain, such as subsets of TS neurons, might also be able to perform temporal whitening after integrating inputs from the three ELL segments. Despite this, it is likely that temporal whitening occurs

relatively early in sensory pathways, as further processing past primary sensory cortices become more specialized for segregating information streams. This is useful in that natural stimuli generally contains abundant forms of redundancies, all of which may not be ultimately useful for behaviour. Therefore, the findings regarding temporal whitening in my thesis contribute further evidence to these ideas.

We know that from the present studies, that SK channels are responsible for mediating the temporal whitening process described above. The question lingers as to whether and to what extent are SK channels, applicable to other systems? To answer this question, we must consider what the SK channels are actually doing to achieve temporal whitening. SK channels are mediating the AHP, which in turn determines neural excitability by controlling how fast a neuron recovers to baseline membrane potential. This process leads to spike-frequency adaptation, and the degree of spike-frequency adaptation ultimately determines the neural tuning curve in general. However, we must note that SK channels are not the only possibility in mediating spike-frequency adaptation. Spike-frequency adaptation can be achieved to a similar fashion by other channel dynamics, such as activation of Kv7 or M-channels in the electrosensory system (Deemyad et al., 2011), slow inactivation of voltage-gated sodium channels in somatosensory neurons (Fleidervish et al., 1996), sodium-dependent potassium channels in cat sensorimotor neurons (Schwindt et al., 1989), or a combination of both sodium- and calcium-dependent potassium channels found in the ferret visual system, shown to contribute to adaptation to visual contrast (Sanchez-Vives et al., 2000). The results from these studies suggest that it is not necessary to have SK channels expressed throughout the brain in all sensory systems, but rather implicates that sensory systems must utilize a strategy which enables spike-frequency adaptation to enhance encoding of natural stimuli. Therefore, it is likely that different sensory systems have evolved to utilize the available receptors and channel dynamics to adjust neural excitability in their respective systems, in order to optimize coding.

In addition to SK channels, the present studies also demonstrated that feedback is critical to generate and optimize neural responses in the ELL. To what extent does feedback play a role in general? It is well known that feedback occurs in all sensory systems, with feedback vastly outnumbering those coming from feedforward inputs. For example, the LGN in the visual system receives only ~10% of feedforward input from the retina, while ~90% of the inputs are feedback

coming from primary visual cortex V1. This seems to similarly apply to the ELL in our case. The only known feedforward input to the ELL comes from the EAs, while feedback comes from a variety of different higher brain structures such as the TS, nP, EGP, and others in the forebrain which remain to be discovered. It is also generally accepted that the prefrontal cortex sends massive top-down modulation to primary sensory areas through mechanisms which involve attention and task dependency in primates (Bichot et al., 2015; Petrides and Pandya, 2006). Thus it is not out of the realm of possibility that the weakly-electric fish also receive feedback input to the ELL from areas in the forebrain. More specifically, the ELL is designed to hold features of a cerebellar-like network. There has been extensive evidence in the weakly-electric fish literature that demonstrate this idea pertaining to cancellation of self-generated signals (Alvina and Sawtell, 2014; Requarth and Sawtell, 2011; Sawtell, 2017). Thus, it is also likely that our findings can extend beyond the electrosensory system into plasticity of other cerebellar-like networks as well as plasticity and adaptation mechanisms for learning. However, these remain to be tested with second-order stimuli such as envelopes and would be a case for future investigations.

6.5 – Future Directions

This thesis has contributed several new insights into both the electrosensory system as well as neural coding and behaviour in general. While many questions have been addressed, there are new questions that can be raised for further studies.

6.5.1 – Serotonin and its interaction with feedback input and SK channels

The studies here have addressed the cellular machinery that is present within the neural system and how it can enable the changes observed experimentally. One possible future study could be to look at how neurotransmitters modulate this system through the cellular machinery. The most prominent neurotransmitter which comes to mind is serotonin (5-HT), which has brain-wide effects due to its ubiquitous pathways extending throughout the brain. The source of 5-HT is the dorsal raphe nucleus (Rn), which is known to have projections to the ELL (Deemyad et al., 2013). Previous immunohistochemistry studies have shown that the ELL pyramidal dendrites contain 5-HT2A receptors, which are abundantly present across the hindbrain area (Marquez et

al., 2013). The remarkable finding is that the 5-HT expression patterns are quite strikingly similar to those of SK1 channels. This has several implications and have been addressed in previous studies where it was shown that exogenous and endogenous release of 5-HT downregulates SK channels. This means that the presence of 5-HT and the activation of 5-HT2A receptors leads to similar effects as blocking SK channels with UCL-1684. What remains to be discovered is how 5-HT directly modulates envelope responses. The hypothesis is that the effect of 5-HT, whether exogenously applied with a double-barrel pipette or stimulation of the Rn, will elicit a loss of high-pass tuning in pyramidal cell responses to envelopes. This would in turn lead to suboptimal coding of natural stimulus statistics and have a detrimental effect on the fish's behavioural perception. Furthermore, it is likely that serotonin will also have effects on feedback integration; however exactly how this interaction would affect neural coding is unknown at this point. Further studies are therefore needed to test these questions and elucidate the role of serotonergic modulation on envelope encoding.

6.5.2 – The nP and other electrosensory communication stimuli

The third and fourth studies show the first electrophysiology recordings of responses to second-order envelope stimuli in the nP. We had characterized how the two major cell types, stellate and multipolar cells, are tuned to low envelope frequencies <1 Hz. This exploration can be extended to other electrosensory communication stimuli such as chirps. As mentioned previously, chirps in electrocommunication are similarly important in that they signal an aggression from one fish to another. We predict that the role of feedback is not exclusively limited to envelope responses in the ELL, as the pyramidal cells in the ELL have also been shown extensively to respond to chirps. In addition, previous studies have shown that pyramidal cells are responsible for driving invariance to differential chirp stimuli, which could be due to the role of feedback from the nP neurons. The problem remains as to how chirps are so well extracted from the background first-order AM, and perhaps feedback enables this "sensory searchlight" (Crick, 1984) to enhance firing rate responses to chirps. One could imagine performing the same set of experiments involving pharmacological agents to block the direct and/or indirect feedback pathways to elucidate how chirps are encoded as well as how feedback plays a role in invariance. We can also record from the same neurons in the nP and characterize whether responses to chirps are similar

in stellate or multipolar cells as those found in the pyramidal cells in the ELL to determine whether and if so, how these responses are inherently linked.

6.5.3 – Adaptation to dynamic changes in natural stimulus statistics

The studies presented here adhere to the literature finding that the natural second-order movement envelope statistics decay in power as a function of frequency in a power-law fashion. In particular, it was found that the power-law exponent was ~-0.8. We must note that while this is true on average, there are several possibilities which could perturb this power-law to generate different stimulus statistics. For example, one could imagine that when the fish are more active during the night (because they are nocturnal), there would be higher power at the higher envelope frequencies, thereby leading to a less steep power-law decay with an exponent closer greater than -0.8. On the other hand, during the day when the fish are a lot less active, there will be higher power at the low envelope frequencies, leading to a steeper power-law decay and an exponent less than -0.8. This presents an interesting problem of whether and if so, how can the fish adapt its behavioural tuning to match those of the statistics at those given times of the day. This is a similar problem as adaptation in the visual system, where luminance can range over several orders of magnitude while only being able to encode over a few orders of magnitude (Purpura et al., 1990). Therefore, given the constraints of the electrosensory system, can the animal adapt if we alter the stimulus statistics in its environment and observe the changes that are associated with them. If so, does it use the same tools in the brain as what is observed in the studies presented here to mediate those changes? This is a logical step to take in order to elucidate how adaptation to envelopes with different stimulus statistics take place and the underlying mechanisms which enable such adaptation.

While this project is currently in progress, I would like to mention some preliminary results in order to generate some discussion below. We tested this question by generating two sets of adaptation envelope stimuli which decay in power with power-law exponents of $\alpha=0$ (active envelope) and $\alpha=-2$ (passive envelope). We used these highly extreme exponents to see exactly how far we can push the system. Preliminary results reveal that after adaptation of ~6 hours, the behavioural tuning curves were shifting in the correct direction towards the presented exponents. For example, if the adaptation stimulus with exponent $\alpha=0$ was presented continuously, the behavioural exponent shifted from $\alpha=-0.8$ towards a greater exponent with a shallower tuning

curve at α=-0.4 in a time-dependent manner. This was true also in the case when we presented α=-2 as the adaptation stimulus. We also wanted to elucidate the neural circuitry which could be mediating this adaptation process. We subsequently focused on the forebrain as there are brain areas such as the dorsal pallium (DD) and the dorsolateral pallium (DL) which show hippocampal-like circuitry akin to the Dendate Gyrus-CA3 relationship (Elliott et al., 2017), which could mediate adaptation which take place over the course of hours observed in our preliminary behaviour data. Preliminary data shows that lesioning the forebrain did not abolish the EOD frequency tracking behaviour in these fish, but did abolish the adaptation from taking place when we attempted to adapt the fish to differential stimulus statistics. We also focused on the serotonergic system as the forebrain may contact the Rn to release serotonin, which in turn would feedback onto early sensory areas (such as the ELL) to mediate adaptation. By blocking any activation of the serotonergic system by injecting 5-HT2A antagonist Ketanserin into the ELL, we observed that adaptation did not take place when we attempted to adapt the fish to differential stimulus statistics, while saline control did result in the adaptation observed earlier.

These preliminary results are promising and more work on the electrophysiology side must be completed in order to understand how neural responses are being adapted to drive the adaptation seen in behaviour. Furthermore, we can additional perform immunohistochemistry screening or qPCR to observe any changes in SK channel expression at the dendrites of pyramidal cells or mRNA levels respectively. These experiments would validate a complete characterization and circuitry of exactly how adaptation can take place in the electrosensory system and provide insight on how adaptation could take place across sensory systems in general.

6.6 – Concluding Remarks

The studies presented in this thesis have been able to provide an original contribution to both the fields of electrosensory system as well as neural coding in general. I set out to characterize envelope responses in the ELL and received an incredibly complex question of efficient and optimized coding in a neural system. With each chapter of my thesis, I uncovered more pieces of the puzzle and elucidated the underlying mechanisms which ultimately mediated the neural code of envelopes. The weakly-electric fish is truly a fascinating animal and I think that we have plenty more to learn for years to come.

While there are plenty more questions to explore in this system, I must bid farewell to the weakly-electric fish for now. As presented in my future directions sections, I am quite excited about the potential projects which could follow up on the work I completed in this dissertation. The results of these proposed studies would further help us understand the neural code of envelopes and provide useful links between molecular level processes involving channels, computations at the neural circuitry level, and behaviour and perception at the organismal level.

Reference List

Adelman, J.P., Maylie, J., and Sah, P. (2012). Small-conductance Ca2+-activated K+ channels: form and function. Annual review of physiology 74, 245-269.

Alvina, K., and Sawtell, N.B. (2014). Sensory processing and corollary discharge effects in posterior caudal lobe Purkinje cells in a weakly electric mormyrid fish. Journal of neurophysiology 112, 328-339.

Atick, J.J., and Redlich, A. (1992). What does the retina know about natural scenes. Neural Computation 4, 196-211.

Attias, H., and Schreiner, C.E. (1997). Low-order temporal statistics of natural sounds. Advances in Neural Information Processing Systems 9, 27-33.

Attneave, F. (1954). Some Informational Aspects of Visual Perception. Psychol Rev 61, 183-193.

Aumentado-Armstrong, T., Metzen, M.G., Sproule, M.K.J., and Chacron, M.J. (2015). Electrosensory Midbrain Neurons Display Feature Invariant Responses to Natural Communication Stimuli. PLoS Comput Biol 11, e1004430.

Avila-Akerberg, O., Krahe, R., and Chacron, M.J. (2010). Neural heterogeneities and stimulus properties affect burst coding in vivo. Neuroscience 168, 300-313.

Bannister, N.J., and Larkman, A.U. (1995a). Dendritic morphology of CA1 pyramidal neurones from the rat hippocampus: I. Branching patterns. Journal of Comparative Neurology 360, 150-160.

Bannister, N.J., and Larkman, A.U. (1995b). Dendritic morphology of CA1 pyramidal neurones from the rat hippocampus: II. Spine distributions. Journal of Comparative Neurology 360, 161-171.

Barlow, H. (2001). Redundancy reduction revisited. Network 12, 241-253.

Barlow, H.B. (1961). Possible principles underlying the transformation of sensory messages. In Sensory Communication, W. Rosenblith, ed. (MIT Press), pp. 217-234.

Bastian, J. (1981). Electrolocation I. How the electroreceptors of *Apteronotus albifrons* code for moving objects and other electrical stimuli. Journal of Comparative Physiology A 144, 465-479.

Bastian, J. (1986a). Gain control in the electrosensory system mediated by descending inputs to the electrosensory lateral line lobe. Journal of Neuroscience 6, 553-562.

Bastian, J. (1986b). Gain control in the electrosensory system. A role for descending projections to the lateral electrosensory lateral line lobe. Journal of Comparative Physiology A 158, 505-515.

Bastian, J. (1993). The role of amino acid neurotransmitters in the descending control of electroreception. Journal of Comparative Physiology A 172, 409-423.

Bastian, J. (1996a). Plasticity in an electrosensory system. I. General features of a dynamic sensory filter. Journal of neurophysiology 76, 2483-2496.

Bastian, J. (1996b). Plasticity in an electrosensory system. II. Postsynaptic events associated with a dynamic sensory filter. Journal of neurophysiology 76, 2497-2507.

Bastian, J. (1998). Plasticity in an electrosensory system III: Contrasting properties of spatially segregated dendritic inputs. Journal of neurophysiology 79, 1839-1857.

Bastian, J. (1999). Plasticity of feedback inputs in the apteronotid electrosensory system. The Journal of experimental biology 202, 1327-1337.

Bastian, J., and Bratton, B. (1990). Descending control of electroreception. I. Properties of nucleus praeeminentialis neurons projecting indirectly to the electrosensory lateral line lobe. The Journal of Neuroscience 10, 1226-1240.

Bastian, J., Chacron, M.J., and Maler, L. (2002). Receptive field organization determines pyramidal cell stimulus-encoding capability and spatial stimulus selectivity. The Journal of neuroscience : the official journal of the Society for Neuroscience 22, 4577-4590.

Bastian, J., Chacron, M.J., and Maler, L. (2004). Plastic and non-plastic cells perform unique roles in a network capable of adaptive redundancy reduction. Neuron 41, 767-779.
Bastian, J., and Nguyenkim, J. (2001a). Dendritic Modulation of Burst-like firing in sensory neurons. Journal of neurophysiology 85, 10-22.
Bastian, J., and Nguyenkim, J. (2001b). Dendritic modulation of burst-like firing in sensory neurons. J Neurophysiol 85, 10-22.
Bastian, J., Schniederjan, S., and Nguyenkim, J. (2001). Arginine vasotocin modulates a sexually dimorphic communication behavior in the weakly electric fish Apteronotus leptorhynchus. J Exp Biol 204, 1909-1923.
Bastos, A.M., Usrey, W.M., Adams, R.A., Mangun, G.R., Fries, P., and Friston, K.J. (2012). Canonical microcircuits for predictive coding. Neuron 76, 695-711.
Bell, C.C., Han, V., and Sawtell, N.B. (2008). Cerebellum-like structures and their implications for cerebellar function. Annual Review of Neuroscience 31, 1-24.
Benda, J., and Hennig, R.M. (2008). Spike-frequency adaptation generates intensity invariance in a primary auditory interneuron. Journal of computational neuroscience 24, 113-136.
Benda, J., and Herz, A.V. (2003). A universal model for spike-frequency adaptation. Neural Computation 15, 2523-2564.
Benda, J., Longtin, A., and Maler, L. (2005). Spike-frequency adaptation separates transient communication signals from background oscillations. The Journal of neuroscience : the official journal of the Society for Neuroscience 25, 2312-2321.
Bennett, M.V.L. (1971). Electrolocation in Fish. Ann Ny Acad Sci 188, 242-&.
Berman, N.J., and Maler, L. (1998). b Interaction of $GABA_B$-mediated inhibition with voltage-gated currents of pyramidal cells: computational mechanism of a sensory searchlight. Journal of neurophysiology 80, 3197-3213.
Berman, N.J., and Maler, L. (1999). Neural architecture of the electrosensory lateral line lobe: adaptations for coincidence detection, a sensory searchlight and frequency-dependent adaptive filtering. J Exp Biol 202, 1243-1253.
Bichot, N.P., Heard, M.T., DeGennaro, E.M., and Desimone, R. (2015). A Source for Feature-Based Attention in the Prefrontal Cortex. Neuron 88, 832-844.
Bol, K., Marsat, G., Harvey-Girard, E., Longtin, A., and Maler, L. (2011). Frequency-tuned cerebellar channels and burst-induced LTD lead to the cancellation of redundant sensory inputs. The Journal of neuroscience : the official journal of the Society for Neuroscience 31, 11028-11038.
Bol, K., Marsat, G., Mejias, J.F., Maler, L., and Longtin, A. (2013). Modeling cancelation of periodic inputs with burst-STDP and feedback. Neural networks : the official journal of the International Neural Network Society 47, 120-133.
Bottai, D., Dunn, R., Ellis, W., and Maler, L. (1997). N-Methyl-D-Aspartate receptor 1 mRNA distribution in the central nervous system of the weakly electric fish *Apteronotus leptorhynchus*. Journal of Comparative Neurology 389, 65-80.
Bratton, B., and Bastian, J. (1990). Descending control of electroreception. II. Properties of nucleus praeeminentialis neurons projecting directly to the electrosensory lateral line lobe. The Journal of Neuroscience 10, 1241-1253.
Brenner, N., Bialek, W., and de Ruyter van Steveninck, R. (2000). Adaptive rescaling maximizes information transmission. Neuron 26, 695–702.
Bullock, T.H., Hopkins, C.D., Popper, A.N., and Fay, R.R. (2005). Electroreception (New York: Springer).
Cajal, R.S. (1909). Histologie du système nerveux de l'Homme et des vertébrés (Paris: Maloine).
Carlson, B.A., and Kawasaki, M. (2006). Ambiguous encoding of stimuli by primary sensory afferents causes a lack of independence in the perception of multiple stimulus attributes (vol 26, pg 9173, 2006). Journal of Neuroscience 26, 9834-9834.

Carlson, B.A., and Kawasaki, M. (2007). Behavioral responses to jamming and 'phantom' jamming stimuli in the weakly electric fish Eigenmannia. J Comp Physiol A Neuroethol Sens Neural Behav Physiol 193, 927-941.
Carr, C.E., and Maler, L. (1985). A Golgi study of the cell types of the dorsal torus semicircularis of the electric fish Eigenmannia: functional and morphological diversity in the midbrain. The Journal of comparative neurology 235, 207-240.
Carr, C.E., and Maler, L. (1986). Electroreception in gymnotiform fish. Central anatomy and physiology. In Electroreception, T.H. Bullock, and W. Heiligenberg, eds. (New York: Wiley), pp. 319-373.
Carriot, J., Jamali, M., Cullen, K.E., and Chacron, M.J. (2017). Envelope statistics of self-motion signals experienced by human subjects during everyday activities: Implications for vestibular processing. PLoS One 12, e0178664.
Chacron, M.J. (2006). Nonlinear information processing in a model sensory system. Journal of neurophysiology 95, 2933-2946.
Chacron, M.J., and Bastian, J. (2008). Population coding by electrosensory neurons. J Neurophysiol 99, 1825-1835.
Chacron, M.J., Doiron, B., Maler, L., Longtin, A., and Bastian, J. (2003). Non-classical receptive field mediates switch in a sensory neuron's frequency tuning. Nature 423, 77-81.
Chacron, M.J., and Fortune, E.S. (2010). Subthreshold membrane conductances enhance directional selectivity in vertebrate sensory neurons. Journal of neurophysiology 104, 449-462.
Chacron, M.J., Longtin, A., and Maler, L. (2005a). Delayed excitatory and inhibitory feedback shape neural information transmission. Physical Review E 72, 051917.
Chacron, M.J., Longtin, A., and Maler, L. (2011). Efficient computation via sparse coding in electrosensory neural networks. Curr Opin Neurobiol 21, 752-760.
Chacron, M.J., Maler, L., and Bastian, J. (2005b). Electroreceptor Neuron Dynamics Shape Information Transmission. Nature Neuroscience 8, 673-678.
Chacron, M.J., Maler, L., and Bastian, J. (2005c). Feedback and Feedforward Control of Frequency Tuning to Naturalistic Stimuli. Journal of Neuroscience 25, 5521-5532.
Chacron, M.J., Toporikova, N., and Fortune, E.S. (2009). Differences in the time course of short-term depression across receptive fields are correlated with directional selectivity in electrosensory neurons. Journal of neurophysiology 102, 3270-3279.
Clarke, S.E., Longtin, A., and Maler, L. (2015). Contrast coding in the electrosensory system: parallels with visual computation. Nature reviews Neuroscience 16, 733-744.
Clarke, S.E., and Maler, L. (2017). Feedback Synthesizes Neural Codes for Motion. Curr Biol 27, 1356-1361.
Crick, F. (1984). Function of the thalamic reticular complex: the searchlight hypothesis. Proceedings of the National Academy of Sciences of the United States of America 81, 4586-4590.
Cullen, K.E. (2011). The neural encoding of self-motion. Curr Opin Neurobiol 21, 587-595.
Cumming, B.G., and Nienborg, H. (2016). Feedforward and feedback sources of choice probability in neural population responses. Curr Opin Neurobiol 37, 126-132.
Dale, A., and Cullen, K.E. (2015). Local population synchrony and the encoding of eye position in the primate neural integrator. The Journal of neuroscience : the official journal of the Society for Neuroscience 35, 4287-4295.
Dan, Y., Atick, J.J., and Reid, R.C. (1996). Efficient coding of natural scenes in the lateral geniculate nucleus: experimental test of a computational theory. The Journal of neuroscience : the official journal of the Society for Neuroscience 16, 3351-3362.
Deemyad, T., Kroeger, J., and Chacron, M.J. (2012). Sub- and suprathreshold adaptation currents have opposite effects on frequency tuning. J Physiol-London 590, 4839-4858.

Deemyad, T., Maler, L., and Chacron, M.J. (2011). Inhibition of SK and M channel-mediated currents by 5-HT enables parallel processing by bursts and isolated spikes. Journal of neurophysiology 105, 1276-1294.
Deemyad, T., Metzen, M.G., Pan, Y., and Chacron, M.J. (2013). Serotonin selectively enhances perception and sensory neural responses to stimuli generated by same-sex conspecifics. Proceedings of the National Academy of Sciences of the United States of America 110, 19609-19614.
Dong, D.W., and Atick, J.J. (1995). Statistics of natural time-varying images. Network: Comput Neural Sys, 345–358.
Drew, P.J., and Abbott, L.F. (2006). Models and properties of power-law adaptation in neural systems. Journal of neurophysiology 96, 826-833.
Dye, J. (1987). Dynamics and stimulus-dependence of pacemaker control during behavioral modulations in the weakly electric fish, Apteronotus. Journal of Comparative Physiology A-Sensory Neural & Behavioral Physiology 161, 175-185.
Elliott, S.B., Harvey-Girard, E., Giassi, A.C., and Maler, L. (2017). Hippocampal-like circuitry in the pallium of an electric fish: Possible substrates for recursive pattern separation and completion. The Journal of comparative neurology 525, 8-46.
Ellis, L.D., Maler, L., and Dunn, R.J. (2008). Differential distribution of SK channel subtypes in the brain of the weakly electric fish Apteronotus leptorhynchus. Journal of Comparative Neurology 507, 1964-1978.
Ellis, L.D., Mehaffey, W.H., Harvey-Girard, E., Turner, R.W., Maler, L., and Dunn, R.J. (2007). SK channels provide a novel mechanism for the control of frequency tuning in electrosensory neurons. Journal of Neuroscience 27, 9491-9502.
Engler, G., Fogarty, C.M., Banks, J.R., and Zupanc, G.K. (2000). Spontaneous modulations of the electric organ discharge in the weakly electric fish, Apteronotus leptorhynchus: a biophysical and behavioral analysis. Journal of comparative physiology A, Sensory, neural, and behavioral physiology 186, 645-660.
Engler, G., and Zupanc, G.K. (2001). Differential production of chirping behavior evoked by electrical stimulation of the weakly electric fish, Apteronotus leptorhynchus. Journal of comparative physiology A, Sensory, neural, and behavioral physiology 187, 747-756.
Faber, E.S., and Sah, P. (2003). Calcium-activated potassium channels: multiple contributions to neuronal function. Neuroscientist 9, 181-194.
Fairhall, A.L., Lewen, G.D., Bialek, W., and de Ruyter van Steveninck, R.R. (2001). Efficiency and ambiguity in an adaptive neural code. Nature 412, 787-792.
Fleidervish, I.A., Friedman, A., and Gutnick, M.J. (1996). Slow inactivation of Na+ current and slow cumulative spike adaptation in mouse and guinea-pig neocortical neurones in slices. J Physiol 493 (Pt 1), 83-97.
Fotowat, H., Harrison, R.R., and Krahe, R. (2013). Statistics of the Electrosensory Input in the Freely Swimming Weakly Electric Fish Apteronotus leptorhynchus. Journal of Neuroscience 33, 13758-13772.
Frank, K., and Becker, M.C. (1964). Microelectrodes for recording and stimulation. In Physical Techniques in Biological Research, W.L. Nastuk, ed. (New York: Academic), pp. 23-84.
Goldberg, J.M. (2000). Afferent Diversity and the Organisation of central vestibular pathways. Experimental Brain Research 130, 277-297.
Gussin, D., Benda, J., and Maler, L. (2007). Limits of linear rate coding of dynamic stimuli by electroreceptor afferents. Journal of neurophysiology 97, 2917-2929.
Hagedorn, M. (1986). The ecology, courtship, and mating of gymnotiform electric fish. In Electroreception, T.H. Bullock , and W. Heiligenberg, eds. (New York: Wiley).
Hagedorn, M., and Heiligenberg, W. (1985). Court and spark: electric signals in the courtship and mating of gymnotoid electric fish. Anim Behav 33, 254-265.
Harvey-Girard, E., and Dunn, R.J. (2003). Excitatory amino acid receptors of the electrosensory system: the NR1/NR2B N-methyl-D-aspartate receptor. Journal of neurophysiology 89, 822-832.

Heil, P. (2003). Coding of temporal onset envelope in the auditory system. Speech Communication 41, 123-134.
Heiligenberg, W. (1991). Neural Nets in Electric Fish (Cambridge MA: MIT Press).
Heiligenberg, W., and Dye, J. (1982). Labelling of electrosensory afferents in a gymnotid fish by intracellular injection of HRP: The mystery of multiple maps. Journal of Comparative Physiology A-Sensory Neural & Behavioral Physiology 148, 287-296.
Heiligenberg, W., Metzner, W., Wong, C.J.H., and Keller, C.H. (1996). Motor control of the jamming avoidance response of *Apteronotus leptorhynchus*: evolutionary changes of a behavior and its neuronal substrates. Journal of Comparative Physiology A-Sensory Neural & Behavioral Physiology 179, 653-674.
Hewitt, M.J., and Meddis, R. (1994). A computer model of amplitude-modulation sensitivity of single units in the inferior colliculus. J Acoust Soc Am 95, 2145-2159.
Hirschberg, B., Maylie, J., Adelman, J.P., and Marrion, N.V. (1998). Gating of recombinant small-conductance Ca-activated K+ channels by calcium. J Gen Physiol 111, 565-581.
Hitschfeld, E.M., Stamper, S.A., Vonderschen, K., Fortune, E.S., and Chacron, M.J. (2009). Effects of restraint and immobilization on electrosensory behaviors of weakly electric fish. ILAR journal / National Research Council, Institute of Laboratory Animal Resources 50, 361-372.
Hofmann, V., and Chacron, M.J. (2017). Differential receptive field organizations give rise to nearly identical neural correlations across three parallel sensory maps in weakly electric fish. PLoS Comput Biol 13, e1005716.
Hollander, H. (1970). The projection from the visual cortex to the lateral geniculate body (LGB). An experimental study with silver impregnation methods in the cat. Experimental Brain Research 10, 219-235.
Huang, C.G., and Chacron, M.J. (2016). Optimized Parallel Coding of Second-Order Stimulus Features by Heterogeneous Neural Populations. The Journal of neuroscience : the official journal of the Society for Neuroscience 36, 9859-9872.
Huang, C.G., and Chacron, M.J. (2017). SK channel subtypes enable parallel optimized coding of behaviorally relevant stimulus attributes: A review. Channels (Austin) 11, 281-304.
Huang, C.G., Zhang, Z.D., and Chacron, M.J. (2016). Temporal decorrelation by SK channels enables efficient neural coding and perception of natural stimuli. Nat Commun 7, 11353.
Hupe, J.M., James, A.C., Payne, B.R., Lomber, S.G., Girard, P., and Bullier, J. (1998). Cortical feedback improves discrimination between figure and background by V1, V2 and V3 neurons. Nature 394, 784-787.
Joris, P.X., Schreiner, C.E., and Rees, A. (2004). Neural processing of amplitude-modulated sounds. Physiol Rev 84, 541-577.
Joris, P.X., and Yin, T.C. (1992). Responses to amplitude-modulated tones in the auditory nerve of the cat. J Acoust Soc Am 91, 215-232.
Jun, J.J., Longtin, A., and Maler, L. (2016). Active sensing associated with spatial learning reveals memory-based attention in an electric fish. Journal of neurophysiology 115, 2577-2592.
Kawasaki, M. (1997). Sensory hyperacuity in the jamming avoidance response of weakly electric fish. Curr Opin Neurobiol 7, 473-479.
Khosravi-Hashemi, N., and Chacron, M.J. (2012). Bursts and isolated spikes code for opposite movement directions in midbrain electrosensory neurons. PLoS One 7, e40339.
Khosravi-Hashemi, N., and Chacron, M.J. (2014). Motion processing across multiple topographic maps in the electrosensory system. Physiological reports 2, e00253.
Khosravi-Hashemi, N., Fortune, E.S., and Chacron, M.J. (2011). Coding movement direction by burst firing in electrosensory neurons. Journal of neurophysiology 106, 1954-1968.
Klump, G.M., and Okanoya, K. (1991). Temporal modulation transfer functions in the European starling (Sturnus vulgaris): I. Psychophysical modulation detection thresholds. Hear Res 52, 1-11.

Kohler, M., Hirschberg, B., Bond, C.T., Kinzie, J.M., Marrion, N.V., Maylie, J., and Adelman, J.P. (1996). Small-conductance, calcium-activated potassium channels from mammalian brain. Science 273, 1709-1714.
Kohlrausch, A., Fassel, R., and Dau, T. (2000). The influence of carrier level and frequency on modulation and beat-detection thresholds for sinusoidal carriers. J Acoust Soc Am 108, 723-734.
Krahe, R., Bastian, J., and Chacron, M.J. (2008). Temporal processing across multiple topographic maps in the electrosensory system. Journal of neurophysiology 100, 852-867.
Krahe, R., and Maler, L. (2014). Neural maps in the electrosensory system of weakly electric fish. Curr Opin Neurobiol 24, 13-21.
Krishna, B.S., and Semple, M.N. (2000). Auditory temporal processing: responses to sinusoidally amplitude-modulated tones in the inferior colliculus. Journal of neurophysiology 84, 255-273.
Kwon, S.E., Yang, H., Minamisawa, G., and O'Connor, D.H. (2016). Sensory and decision-related activity propagate in a cortical feedback loop during touch perception. Nat Neurosci 19, 1243-1249.
Lapicque, L. (1907). Recherches quantitatives sur l'excitation électrique des nerfs traitée comme une polarisation. Journal of Physiology, Pathology, and Genetics 9, 620-635.
Larson, E.A., Metzen, M.G., and Chacron, M.J. (2014). Serotonin modulates electrosensory processing and behavior via 5-HT2-like receptors. Neuroscience 271, 108-118.
Laughlin, S. (1981). A simple coding procedure enhances a neuron's information capacity. Zeitschrift fur Naturforschung Section C: Biosciences 36, 910-912.
Lewicki, M.S. (2002). Efficient coding of natural sounds. Nature Neuroscience 5, 356-363.
Litwin-Kumar, A., Chacron, M.J., and Doiron, B. (2012). The spatial structure of stimuli shapes the timescale of correlations in population spiking activity. PLoS Comput Biol 8, e1002667.
Liu, S., Gu, Y., DeAngelis, G.C., and Angelaki, D.E. (2013). Choice-related activity and correlated noise in subcortical vestibular neurons. Nat Neurosci 16, 89-97.
Lundstrom, B.N., Fairhall, A.L., and Maravall, M. (2010). Multiple timescale encoding of slowly varying whisker stimulus envelope in cortical and thalamic neurons in vivo. Journal of Neuroscience 30, 5071-5077.
Lundstrom, B.N., Higgs, M.H., Spain, W.J., and Fairhall, A.L. (2008). Fractional differentiation by neocortical pyramidal neurons. Nature Neuroscience 11, 1335-1342.
Maler, L. (1979). The posterior lateral line lobe of certain gymnotiform fish. Quantitative light microscopy. Journal of Comparative Neurology 183, 323-363.
Maler, L. (2009a). Receptive field organization across multiple electrosensory maps. I. Columnar organization and estimation of receptive field size. Journal of Comparative Neurology 516, 376-393.
Maler, L. (2009b). Receptive field organization across multiple electrosensory maps. II. Computational analysis of the effects of receptive field size on prey localization. Journal of Comparative Neurology 516, 394-422.
Maler, L., Sas, E., Johnston, S., and Ellis, W. (1991). An atlas of the brain of the weakly electric fish *Apteronotus Leptorhynchus*. Journal of Chemical Neuroanatomy 4, 1-38.
Maler, L., Sas, E.K., and Rogers, J. (1981). The cytology of the posterior lateral line lobe of high frequency weakly electric fish (Gymnotidae): Differentiation and synaptic specificity in a simple cortex. Journal of Comparative Neurology 195, 87-139.
Malone, B.J., Scott, B.H., and Semple, M.N. (2010). Temporal codes for amplitude contrast in auditory cortex. The Journal of neuroscience : the official journal of the Society for Neuroscience 30, 767-784.
Manita, S., Suzuki, T., Homma, C., Matsumoto, T., Odagawa, M., Yamada, K., Ota, K., Matsubara, C., Inutsuka, A., Sato, M*., et al.* (2015). A Top-Down Cortical Circuit for Accurate Sensory Perception. Neuron 86, 1304-1316.

Maravall, M., Petersen, R.S., Fairhall, A.L., Arabzadeh, E., and Diamond, M.E. (2007). Shifts in coding properties and maintenance of information transmission during adaptation in barrel cortex. PLoS Biology 5, e19.
Marder, E., and Goaillard, J.M. (2006). Variability, compensation and homeostasis in neuron and network function. Nature reviews Neuroscience 7, 563-574.
Mardia, K.V., and Jupp, P.E. (1999). Directional Statistics (New York: Wiley).
Mareschal, I., and Baker, C.L., Jr. (1998). A cortical locus for the processing of contrast-defined contours. Nat Neurosci 1, 150-154.
Marquez, B.T., Krahe, R., and Chacron, M.J. (2013). Neuromodulation of early electrosensory processing in gymnotiform weakly electric fish. J Exp Biol 216, 2442-2450.
Marsat, G., Longtin, A., and Maler, L. (2012). Cellular and circuit properties supporting different sensory coding strategies in electric fish and other systems. Curr Opin Neurobiol 22, 686-692.
Marsat, G., and Maler, L. (2012). Preparing for the unpredictable: adaptive feedback enhances the response to unexpected communication signals. Journal of neurophysiology 107, 1241-1246.
Marsat, G., Proville, R.D., and Maler, L. (2009). Transient signals trigger synchronous bursts in an identified population of neurons. Journal of neurophysiology 102, 714-723.
Martinez, D., Metzen, M.G., and Chacron, M.J. (2016). Electrosensory processing in Apteronotus albifrons: implications for general and specific neural coding strategies across wave-type weakly electric fish species. Journal of neurophysiology 116, 2909-2921.
McGillivray, P., Vonderschen, K., Fortune, E.S., and Chacron, M.J. (2012). Parallel coding of first- and second-order stimulus attributes by midbrain electrosensory neurons. The Journal of neuroscience : the official journal of the Society for Neuroscience 32, 5510-5524.
Mehaffey, W.H., Maler, L., and Turner, R.W. (2008). Intrinsic frequency tuning in ELL pyramidal cells varies across electrosensory maps. Journal of neurophysiology 99, 2641-2655.
Mejias, J.F., and Longtin, A. (2012). Optimal heterogeneity for coding in spiking neural networks. Physical review letters 108, 228102.
Mejias, J.F., Marsat, G., Bol, K., Maler, L., and Longtin, A. (2013). Learning contrast-invariant cancellation of redundant signals in neural systems. PLoS Comput Biol 9, e1003180.
Metzen, M.G., and Chacron, M.J. (2014). Weakly electric fish display behavioral responses to envelopes naturally occurring during movement: implications for neural processing. The Journal of experimental biology 217, 1381-1391.
Metzen, M.G., and Chacron, M.J. (2015). Neural heterogeneities determine response characteristics to second-, but not first-order stimulus features. The Journal of neuroscience : the official journal of the Society for Neuroscience 35, 3124-3138.
Metzen, M.G., and Chacron, M.J. (2017). Stimulus background influences phase invariant coding by correlated neural activity. Elife 6, e24482.
Metzen, M.G., Hofmann, V., and Chacron, M.J. (2016a). Neural correlations enable invariant coding and perception of natural stimuli in weakly electric fish. Elife 5, e12993.
Metzen, M.G., Jamali, M., Carriot, J., Avila-Akerberg, O., Cullen, K.E., and Chacron, M.J. (2015). Coding of envelopes by correlated but not single-neuron activity requires neural variability. Proceedings of the National Academy of Sciences of the United States of America 112, 4791-4796.
Metzen, M.G., Krahe, R., and Chacron, M.J. (2016b). Burst Firing in the Electrosensory System of Gymnotiform Weakly Electric Fish: Mechanisms and Functional Roles. Front Comput Neurosci 10, 81.
Metzner, W. (1999). Neural Circuitry for Communication and Jamming Avoidance in Gymnotiform Electric Fish. J Exp Biol 202, 1365-1375.
Metzner, W., and Juranek, J. (1997). A sensory brain map for each behavior? Proceedings of the National Academy of Sciences of the United States of America 94, 14798-14803.

Meyer, T., and Olson, C.R. (2011). Statistical learning of visual transitions in monkey inferotemporal cortex. Proceedings of the National Academy of Sciences of the United States of America 108, 19401-19406.
Meyer, T., Ramachandran, S., and Olson, C.R. (2014). Statistical learning of serial visual transitions by neurons in monkey inferotemporal cortex. The Journal of neuroscience : the official journal of the Society for Neuroscience 34, 9332-9337.
Middleton, J.W., Longtin, A., Benda, J., and Maler, L. (2006). The cellular basis for parallel neural transmission of a high-frequency stimulus and its low-frequency envelope. Proceedings of the National Academy of Sciences of the United States of America 103, 14596-14601.
Nelson, M.E., and MacIver, M.A. (1999). Prey capture in the weakly electric fish Apteronotus albifrons: sensory acquisition strategies and electrosensory consequences. The Journal of experimental biology 202, 1195-1203.
Nelson, M.E., MacIver, M.A., and Coombs, S. (2002). Modeling electrosensory and mechanosensory images during the predatory behavior of weakly electric fish. Brain, behavior and evolution 59, 199-210.
Nesse, W., Maler, L., and Longtin, A. (2010). Biophysical information representation in temporally correlated spike trains. Proceedings of the National Academy of Sciences of the United States of America 107, 21973-21978.
Ostapoff, E.M., Morest, D.K., and Potashner, S.J. (1990). Uptake and retrograde transport of [^{3}H]GABA from the cochlear nucleus to the superior olive in the guinea pig. Journal of Chemical Neuroanatomy 3, 285-295.
Padmanabhan, K., and Urban, N.N. (2010). Intrinsic biophysical diversity decorrelates neuronal firing while increasing information content. Nat Neurosci 13, 1276-1282.
Petrides, M., and Pandya, D.N. (2006). Efferent association pathways originating in the caudal prefrontal cortex in the macaque monkey. The Journal of comparative neurology 498, 227-251.
Pitkow, X., and Angelaki, D.E. (2017). Inference in the Brain: Statistics Flowing in Redundant Population Codes. Neuron 94, 943-953.
Pitkow, X., Liu, S., Angelaki, D.E., DeAngelis, G.C., and Pouget, A. (2015). How Can Single Sensory Neurons Predict Behavior? Neuron 87, 411-423.
Pitkow, X., and Meister, M. (2012). Decorrelation and efficient coding by retinal ganglion cells. Nat Neurosci 15, 628-635.
Podlubny, I. (1999). Fractional differential equations : an introduction to fractional derivatives, fractional differential equations, to methods of their solution and some of their applications (San Diego: Academic Press).
Pozzorini, C., Naud, R., Mensi, S., and Gerstner, W. (2013). Temporal whitening by power-law adaptation in neocortical neurons. Nat Neurosci 16, 942-948.
Purpura, K., Tranchina, D., Kaplan, E., and Shapley, R.M. (1990). Light adaptation in the primate retina: analysis of changes in gain and dynamics of monkey retinal ganglion cells. Visual neuroscience 4, 75-93.
Rauschecker, J.P. (2015). Auditory and visual cortex of primates: a comparison of two sensory systems. The European journal of neuroscience 41, 579-585.
Requarth, T., and Sawtell, N.B. (2011). Neural mechanisms for filtering self-generated sensory signals in cerebellum-like circuits. Curr Opin Neurobiol 21, 602-608.
Rieke, F., Warland, D., de Ruyter van Steveninck, R.R., and Bialek, W. (1996). Spikes: Exploring the Neural Code (Cambridge, MA: MIT).
Risken, H. (1996). The Fokker-Planck Equation (Berlin: Springer).
Rodriguez, F.A., Chen, C., Read, H.L., and Escabi, M.A. (2010). Neural modulation tuning characteristics scale to efficiently encode natural sound statistics. Journal of Neuroscience 30, 15969-15980.
Rose, G.J. (2004). Insights into neural mechanisms and evolution of behaviour from electric fish. Nat Rev Neurosci 5, 943-951.

Rosenberg, A., and Issa, N.P. (2011). Visual Demodulation by the Y Cell Pathway. Neuron 71, 348-361.
Ruderman, D.L., and Bialek, W. (1994). Statistics of natural images: Scaling in the woods. Physical review letters 73, 814-817.
Sanchez-Vives, M.V., Nowak, L.G., and McCormick, D.A. (2000). Cellular mechanisms of long-lasting adaptation in visual cortical neurons in vitro. The Journal of neuroscience : the official journal of the Society for Neuroscience 20, 4286-4299.
Sas, E., and Maler, L. (1983). The nucleus praeeminentialis: A golgi study of a feedback center in the electrosensory system of gymnotid fish. Journal of Comparative Neurology 221, 127-144.
Sas, E., and Maler, L. (1987). The organization of afferent input to the caudal lobe of the cerebellum of the gymnotid fish *Apteronotus leptorhynchus*. Anatomy and Embryology 177, 55-79.
Saunders, J., and Bastian, J. (1984). The physiology and morphology of two classes of electrosensory neurons in the weakly electric fish *Apteronotus Leptorhynchus*. Journal of Comparative Physiology A 154, 199-209.
Savard, M., Krahe, R., and Chacron, M.J. (2011). Neural heterogeneities influence envelope and temporal coding at the sensory periphery. Neuroscience 172, 270-284.
Sawtell, N.B. (2017). Neural Mechanisms for Predicting the Sensory Consequences of Behavior: Insights from Electrosensory Systems. Annual review of physiology 79, 381-399.
Sayles, M., Fullgrabe, C., and Winter, I.M. (2013). Neurometric amplitude-modulation detection threshold in the guinea-pig ventral cochlear nucleus. J Physiol 591, 3401-3419.
Scheich, H., Bullock, T.H., and Hamstra, R.H. (1973). Coding properties of two classes of afferent nerve fibers: high frequency electroreceptors in the electric fish, Eigenmania. Journal of neurophysiology 36, 39-60.
Schulz, D.J., Goaillard, J.M., and Marder, E. (2006). Variable channel expression in identified single and electrically coupled neurons in different animals. Nat Neurosci 9, 356-362.
Schwindt, P.C., Spain, W.J., and Crill, W.E. (1989). Long-lasting reduction of excitability by a sodium-dependent potassium current in cat neocortical neurons. Journal of neurophysiology 61, 233-244.
Shannon, R.V., Zeng, F.G., Kamath, V., Wygonski, J., and Ekelid, M. (1995). Speech recognition with primarily temporal cues. Science 270, 303-304.
Shannon, R.V., Zeng, F.G., and Wygonski, J. (1998). Speech recognition with altered spectral distribution of envelope cues. J Acoust Soc Am 104, 2467-2476.
Sherman, S.M., and Guillery, R.W. (2002). The role of the thalamus in the flow of information to the cortex. Philosophical Transactions of the Royal Society of London - Series B: Biological Sciences 357, 1695-1708.
Shumway, C. (1989). Multiple electrosensory maps in the medulla of weakly electric Gymnotiform fish. I. Physiological differences. Journal of Neuroscience 9, 4388-4399.
Simmonds, B., and Chacron, M.J. (2015a). Activation of parallel fiber feedback by spatially diffuse stimuli reduces signal and noise correlations via independent mechanisms in a cerebellum-like structure. PLoS Comput Biol 11, e1004034.
Simmonds, B., and Chacron, M.J. (2015b). Activation of parallel fiber feedback by spatially diffuse stimuli simultaneously reduces signal and noise correlations via independent mechanisms in a cerebellum-like structure. PLoS Computational Biology 11, e1004034.
Simoncelli, E.P., and Olshausen, B.A. (2001). Natural image statistics and neural representation. Annual Review of Neuroscience 24, 1193-1216.
Singla, S., Dempsey, C., Warren, R., Enikolopov, A.G., and Sawtell, N.B. (2017). A cerebellum-like circuit in the auditory system cancels responses to self-generated sounds. Nat Neurosci 20, 943-950.
Skavenski, A.A., and Robinson, D.A. (1973). Role of abducens neurons in vestibuloocular reflex. Journal of neurophysiology 36, 724-738.

Smirnakis, S.M., Berry, M.J., Warland, D.K., Bialek, W., and Meister, M. (1997). Adaptation of retinal processing to image contrast and spatial scale. Nature 386, 69-73.
Sproule, M.K., and Chacron, M.J. (2017). Electrosensory neural responses to natural electro-communication stimuli are distributed along a continuum. PLoS One 12, e0175322.
Sproule, M.K., Metzen, M.G., and Chacron, M.J. (2015). Parallel sparse and dense information coding streams in the electrosensory midbrain. Neurosci Lett 607, 1-6.
Stamper, S.A., Carrera, G.E., Tan, E.W., Fugere, V., Krahe, R., and Fortune, E.S. (2010). Species differences in group size and electrosensory interference in weakly electric fishes: implications for electrosensory processing. Behavioral Brain Research 207, 368-376.
Stamper, S.A., Fortune, E.S., and Chacron, M.J. (2013). Perception and coding of envelopes in weakly electric fishes. J Exp Biol 216, 2393-2402.
Stamper, S.A., Madhav, M.S., Cowan, N.J., and Fortune, E.S. (2012). Beyond the Jamming Avoidance Response: weakly electric fish respond to the envelope of social electrosensory signals. J Exp Biol 215, 4196-4207.
Takahashi, N., Oertner, T.G., Hegemann, P., and Larkum, M.E. (2016). Active cortical dendrites modulate perception. Science 354, 1587-1590.
Theunissen, F.E., and Elie, J.E. (2014). Neural processing of natural sounds. Nature reviews Neuroscience 15, 355-366.
Toporikova, N., and Chacron, M.J. (2009). Dendritic SK channels gate information processing *in vivo* by regulating an intrinsic bursting mechanism seen *in vitro*. Journal of neurophysiology 102, 2273-2287.
Tripathy, S.J., Padmanabhan, K., Gerkin, R.C., and Urban, N.N. (2013). Intermediate intrinsic diversity enhances neural population coding. Proceedings of the National Academy of Sciences of the United States of America 110, 8248-8253.
van Kerkoerle, T., Self, M.W., Dagnino, B., Gariel-Mathis, M.A., Poort, J., van der Togt, C., and Roelfsema, P.R. (2014). Alpha and gamma oscillations characterize feedback and feedforward processing in monkey visual cortex. Proceedings of the National Academy of Sciences of the United States of America 111, 14332-14341.
Viemeister, N.F. (1979). Temporal modulation transfer functions based upon modulation thresholds. J Acoust Soc Am 66, 1364-1380.
Vonderschen, K., and Chacron, M.J. (2011). Sparse and dense coding of natural stimuli by distinct midbrain neuron subpopulations in weakly electric fish. Journal of neurophysiology 106, 3102-3118.
Wang, X., and Sachs, M.B. (1995). Transformation of temporal discharge patterns in a ventral cochlear nucleus stellate cell model: implications for physiological mechanisms. Journal of neurophysiology 73, 1600-1616.
Wang, X.J., Liu, Y., Sanchez-Vives, M.V., and McCormick, D.A. (2003). Adaptation and temporal decorrelation by single neurons in the primary visual cortex. Journal of neurophysiology 89, 3279-3293.
Warren, R., and Sawtell, N.B. (2016). A comparative approach to cerebellar function: insights from electrosensory systems. Curr Opin Neurobiol 41, 31-37.
Wessel, R., Koch, C., and Gabbiani, F. (1996). Coding of time-varying electric field amplitude modulations in a wave-type electric fish. Journal of neurophysiology 75, 2280-2293.
Woolley, S.M.N., Fremouw, T.E., Hsu, A., and Theunissen, F.E. (2005). Tuning for spectro-temporal modulations as a mechanism for auditory discrimination of natural sounds. Nature Neuroscience 8, 1371-1379.
Xu, Z., Payne, J.R., and Nelson, M.E. (1996). Logarithmic time course of sensory adaptation in electrosensory afferent nerve fibers in a weakly electric fish. Journal of neurophysiology 76, 2020-2032.
Yu, N., Hupe, G., Garfinkle, C., Lewis, J.E., and Longtin, A. (2012a). Coding conspecific identity and motion in the electric sense. PLoS Comput Biol 8, e1002564.

Yu, N., Hupe, G.J., Garfinkle, C., Lewis, J.E., and Longtin, A. (2012b). Coding Conspecific Identity and Motion in the Electric Sense. PLoS Computational Biology 8, e1002564.
Zakon, H., Oestreich, J., Tallarovic, S., and Triefenbach, F. (2002). EOD modulations of brown ghost electric fish: JARs, chirps, rises, and dips. Journal of physiology, Paris 96, 451-458.
Zhang, Z.D., and Chacron, M.J. (2016). Adaptation to second order stimulus features by electrosensory neurons causes ambiguity. Sci Rep 6, 28716.
Zhao, H.B., and Liang, Z.A. (1997). Temporal encoding and transmitting of amplitude and frequency modulations in dorsal cochlear nucleus. Hear Res 106, 83-94.
Zohary, E., Shadlen, M.N., and Newsome, W.T. (1994). Correlated neuronal discharge rate and its implications for psychophysical performance. Nature 370, 140-143.
Zupanc, G.K.H., and Maler, E. (1993). Evoked Chirping in the Weakly Electric Fish Apteronotus-Leptorhynchus - a Quantitative Biophysical Analysis. Can J Zool 71, 2301-2310.

Supplementary Materials

Supplementary figures for Chapter 3

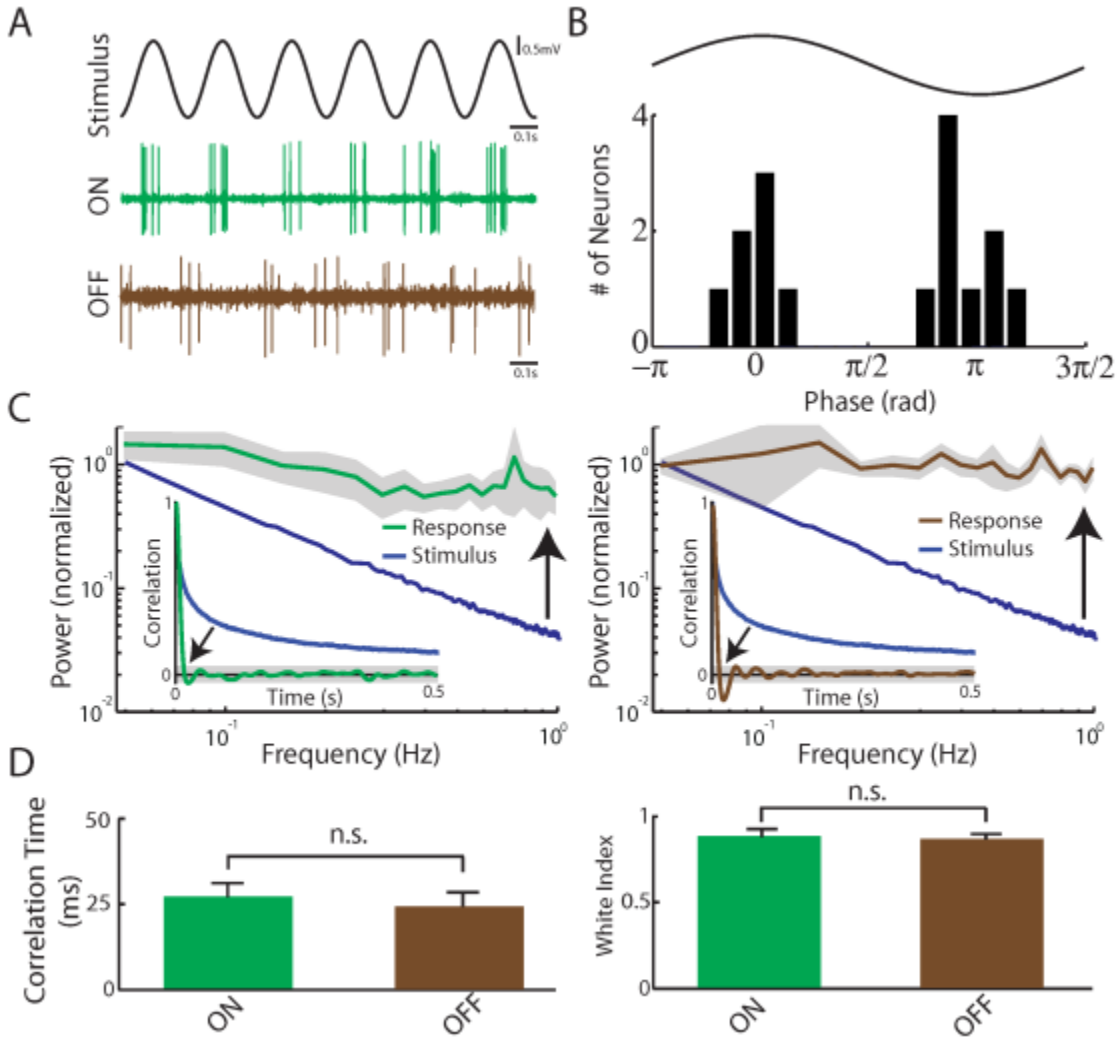

Supplementary Figure 1. ON and OFF-type ELL pyramidal cells display similarresponses to second order attributes of natural electrosensory stimuli. A) Example responses of example ON-type (green) and OFF-type (brown) ELL pyramidal cells to a 4 Hz sinusoidal AM (black). B) Distribution of stimulus phase for which ELL pyramidal cells in our dataset fired preferentially. The distribution is clearly bimodal (Hartigan's dip test, p=0.0167) with ON-type cells firing preferentially near the maximum of the stimulus (phase 0) and OFF-type cells firing preferentially near the minimum (phase π). C) The population-averaged response power spectrum (green) for ON (left) and (brown) OFF (right) type cells was relatively constant as compared to that of the envelope stimulus (blue). Insets: The population-averaged response autocorrelation function (green) for ON (left) and (brown) OFF (right) type cells decayed to zero much faster than that of the stimulus (blue). D) Population-averaged correlation times (left) and white index (right) for ON (green) and OFF (brown) type cells. No significant differences were observed between correlation time (Wilcoxon rank-sum test, p>0.05, n.s., N=14) or white index values (Wilcoxon rank-sum test, p>0.05, n.s., N=14).

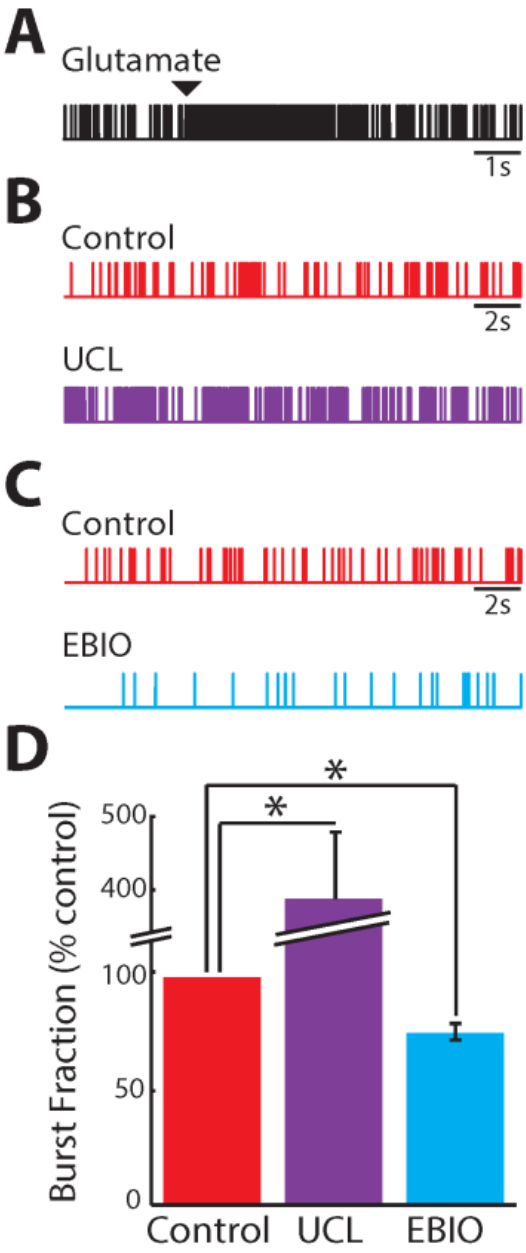

Supplementary Figure 2: UCL and EBIO application have opposite effects on pyramidal neuron baseline activity. A) Glutamate ejection causes rapid increases in pyramidal neuron firing rate, indicating that the pharmacology electrode is close to the neuron from which we are recording. B) Baseline activity under control (top) and after UCL application (bottom) from a typical pyramidal neuron. C) Same as B for EBIO application. D) Populationaveraged burst fractions under baseline (control) and after UCL and EBIO application, respectively. Burst fraction was significantly different between control and UCL (Wilcoxon rank-sum test, $p<0.05$, $N=6$) and between control and EBIO (Wilcoxon rank-sum test, $p<0.05$, $N=6$).

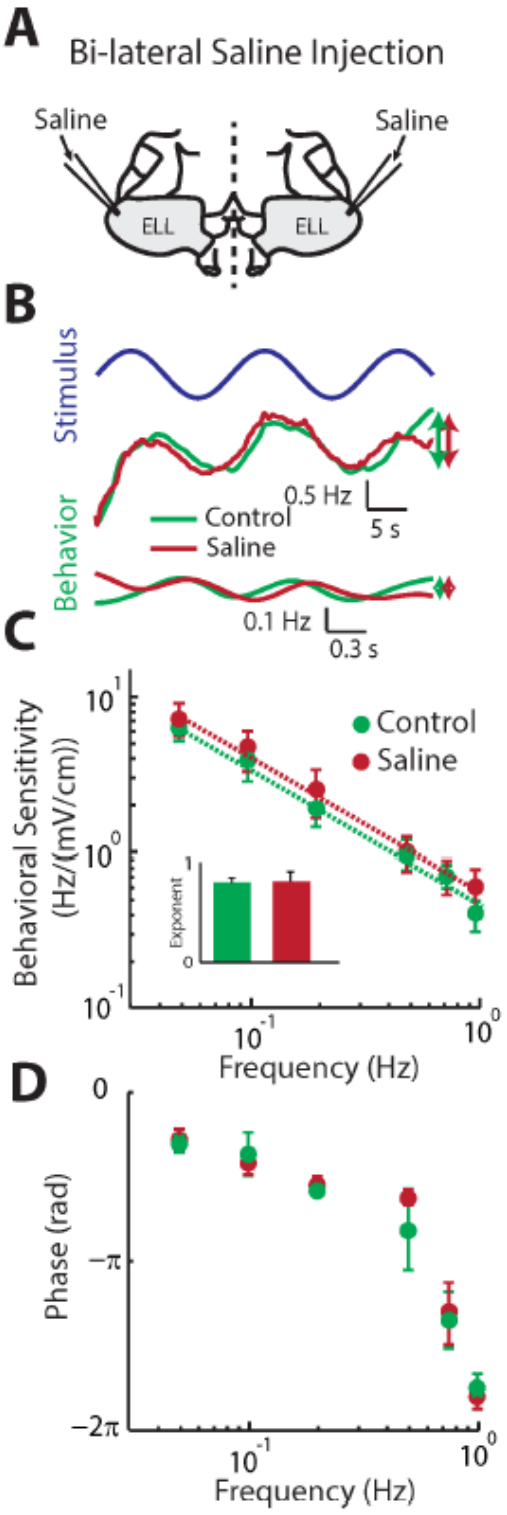

Supplementary Figure 3: *Saline injection does not significantly alter behavioral responses to envelope stimuli.* A) Schematic showing the bilateral saline injection. B) *Top:* Low (*left)* and high (*right*) frequency envelope stimuli. *Bottom:* Corresponding behavioral responses before (green) and after (red) saline injection. C) Population-averaged behavioral sensitivity before (green) and after (red) saline injection. The dashed lines show the best power law fits to the data. Inset: Population-averaged power law exponents for before (green) and after saline injection (red) (N=3). D) Population-averaged phase lag before (green) and after (red) saline injection
(N=3).

Supplementary figures for Chapter 4

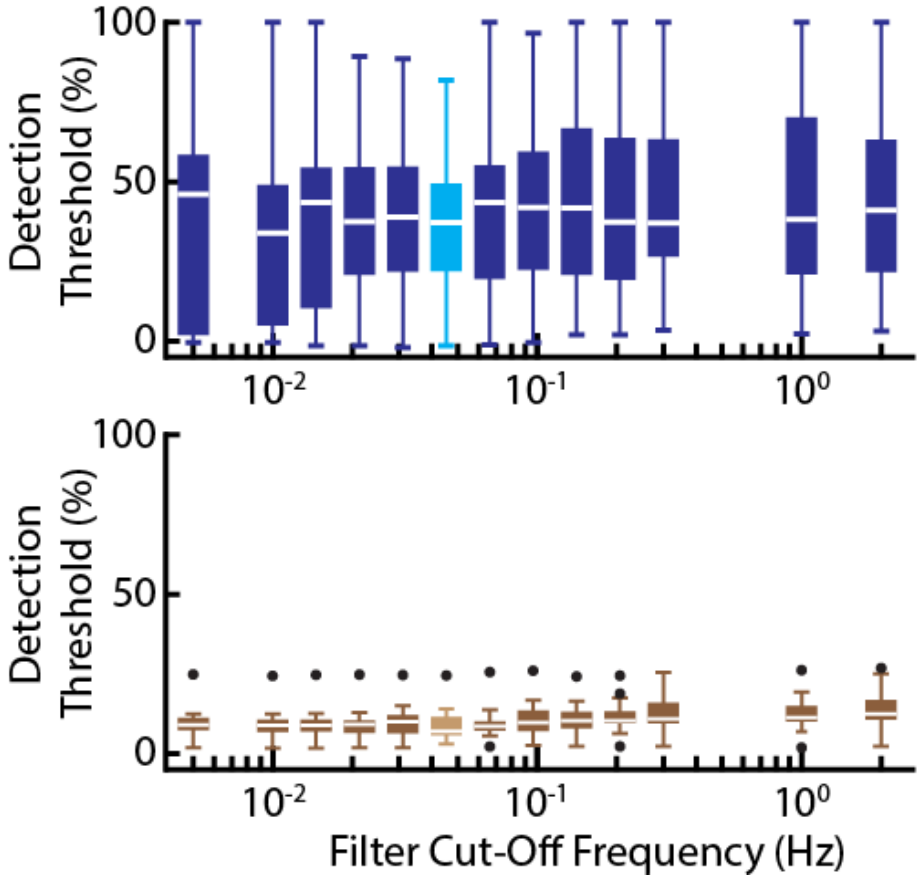

Supplemental Figure 1. Filter settings do not affect detection threshold values obtained for EAs and behavior. Detection thresholds as a function of filter cut-off frequency for EAs (blue) and behavior (brown). Light blue and light brown data points indicate the values obtained for a cut-off frequency of 0.05 Hz as used in this study. Detection thresholds did not differ significantly for different filter cut-off frequencies (EAs: Kruskal-Wallis, df = 12, p = 0.999 with Bonferroni correction; behavior: Kruskal-Wallis, df = 12, p = 0.6162 with Bonferroni correction).

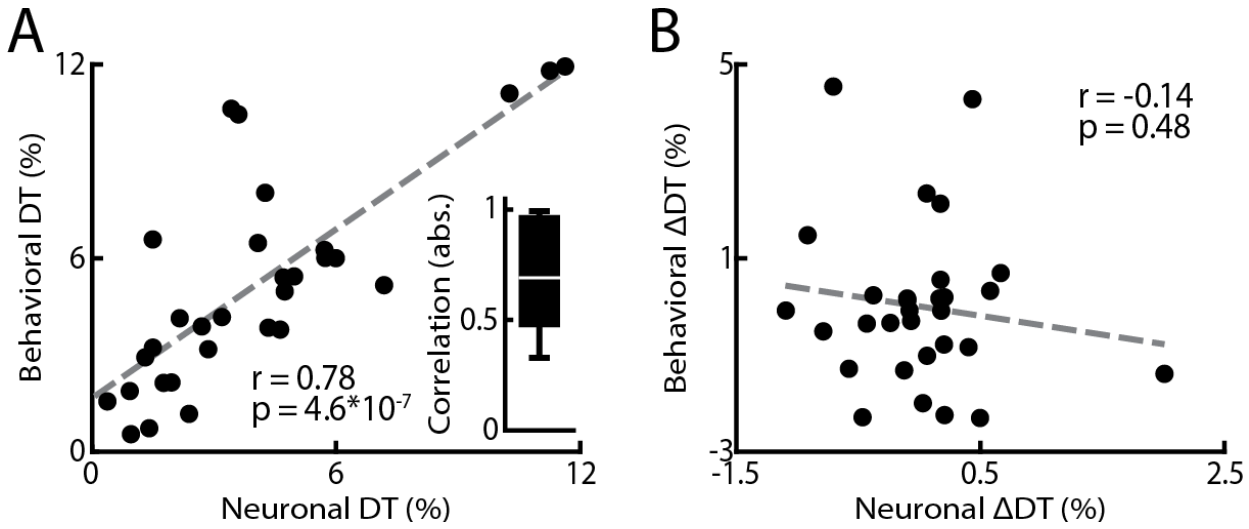

*Supplementary Figure 2. Neuronal and behavioral detection threshold values are strongly correlated but not their residuals. A) The detection threshold values of PCells and behavior are strongly positively correlated as indicated by a high r-value (Pearson's rho: r = 0.93; p = 4.6*10^{-7}) The inset shows a whisker-box of the correlation coefficient obtained for each pair. B) The residuals of neuronal and behavioral detection threshold values obtained for repetitive stimulation (three repetitions) are not significantly correlated (Pearson's rho: r = -0.14, p = 0.48).*

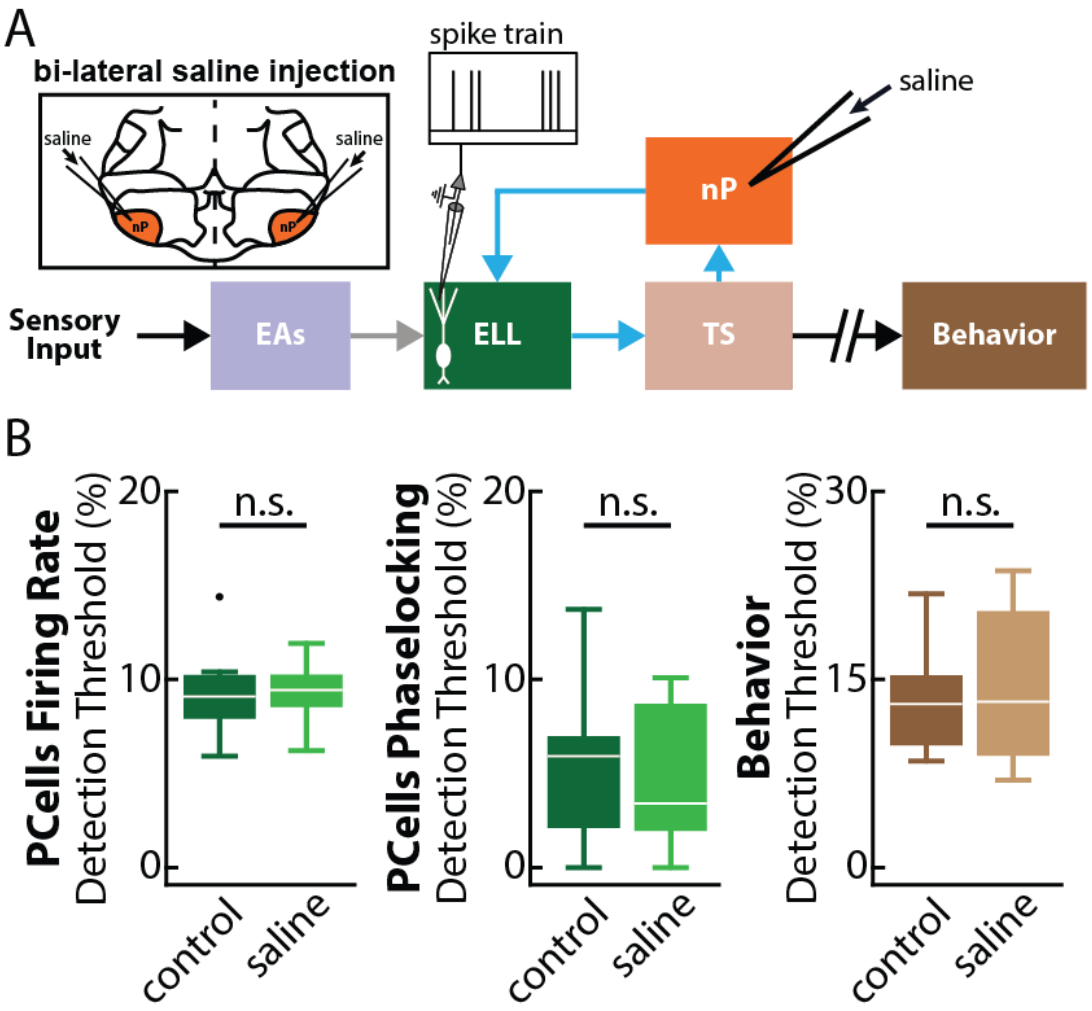

Supplemental Figure 3. Saline injection into nP does not affect neuronal and behavioral detection thresholds. A) Relevant anatomy diagram showing the main brain areas considered. Recordings were made from individual PCells. B) Left: PCell firing rate detection threshold values did not change after saline injection (control: 9.4±1.0%, saline: 9.3±0.7%; Wilcoxon sign rank test, n = 7; p = 0.94). Middle: PCell vector strength detection threshold values did not change after saline injection (control: 5.4±1.7%, saline: 4.8±1.5%; Wilcoxon sign rank test, n = 7; p = 0.59). Right: Behavioral detection threshold values did not change after saline injection (control: 13.1±1.5%, saline: 13.1±2.2%; Wilcoxon sign rank test, n = 8; p = 0.95). "ns" indicates no significant difference.

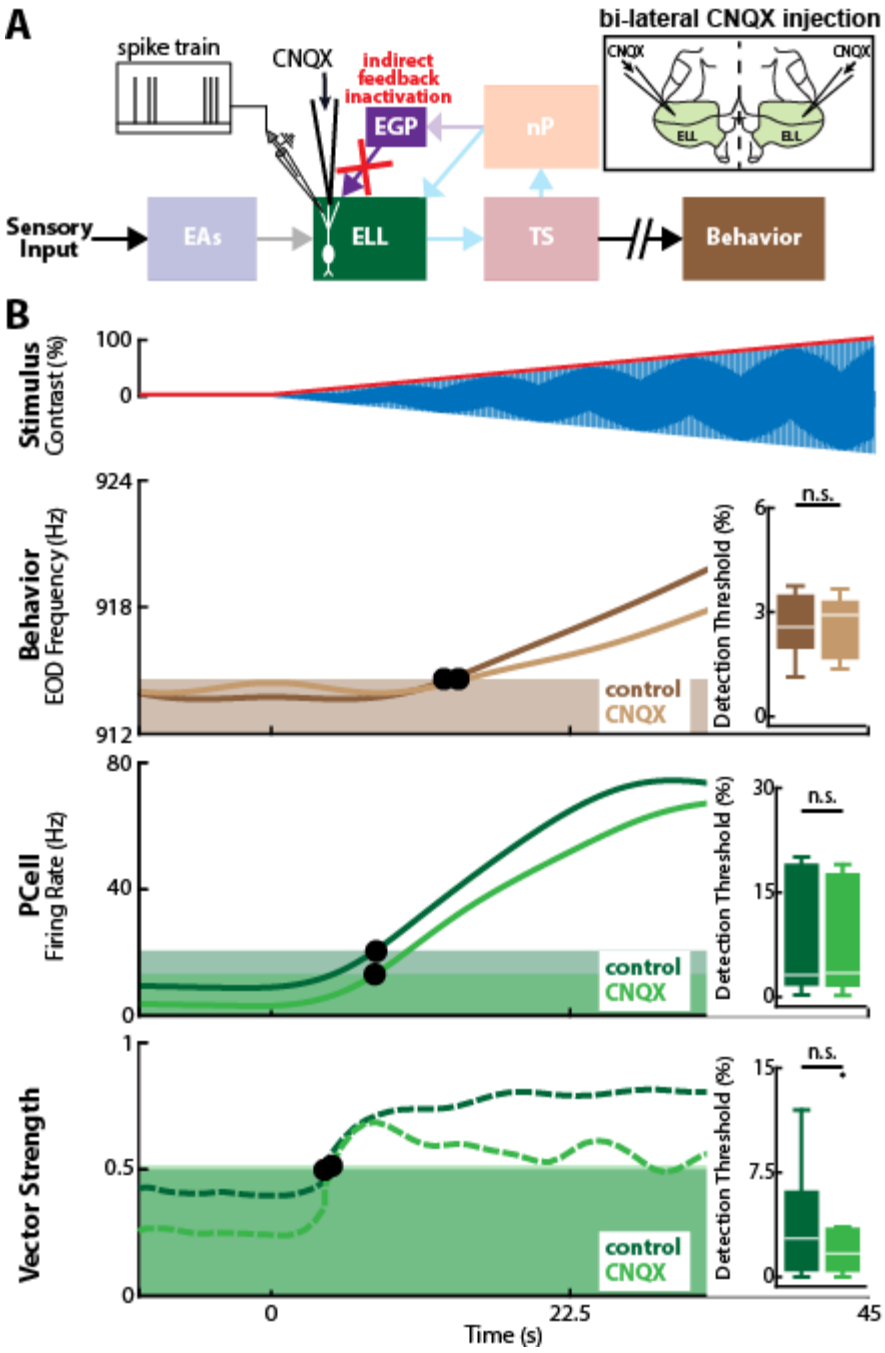

Supplementary Figure 4. Inactivating the indirect feedback pathway does not alter detection thresholds observed for either central electrosensory neurons or from the organism. a) Relevant anatomy diagram showing the main brain areas considered. Recordings were made from individual PCells. Right inset: bilateral injection of the non-NMDA glutamate receptor antagonist CNQX near the apical dendrites of ELL pyramidal cells in the molecular layer near the cell being recorded from as well as to test the effects on behavior. b) Top: Example behavioral responses to increasing contrast (top) before (dark brown) and after (light brown) bilateral CNQX injection. Middle: example firing rate responses to increasing contrast from an example ELL pyramidal neuron (dark green) and after (light green) bilateral CNQX injection.

*Bottom: example time-varying vector strength responses to increasing contrast from the same ELL pyramidal neuron (dark green) and after (light green) bilateral CNQX injection. We found that both behavioral (top, inset, control: 2.6±0.4%; CNQX: 2.5±0.4%, Wilcoxon sign rank test, n = 7, p = 0.81) and neural (firing rate: middle inset, control: 8.5±3.2%; CNQX: 8.1±3.0%, Wilcoxon sign rank test, n = 8, p = 0.31; vector strength: bottom inset, control: 3.8±1.5%; CNQX: 3.2±1.7%, Wilcoxon sign rank test, n = 8, p = 0.55) detection thresholds were not affected by CNQX injections. Note that previous studies have shown that saline injection within the molecular layer does not affect behavioral responses (Deemyad et al., 2013; Huang et al., 2016; Larson et al., 2014). As a positive control, we note that injection of CNQX significantly decreased the baseline (i.e., in the absence of stimulation) firing rates of ELL pyramidal cells (control: 12.75±1.98 spk*s^{-1}; CNQX: 6.79±1.18 spk*s^{-1}, Wilcoxon sign rank test, n = 8, N = 3 fish, p = 0.0078), which is consistent with previous results (Bastian and Nguyenkim, 2001a; Chacron and Bastian, 2008). "ns" indicates no significant difference.*

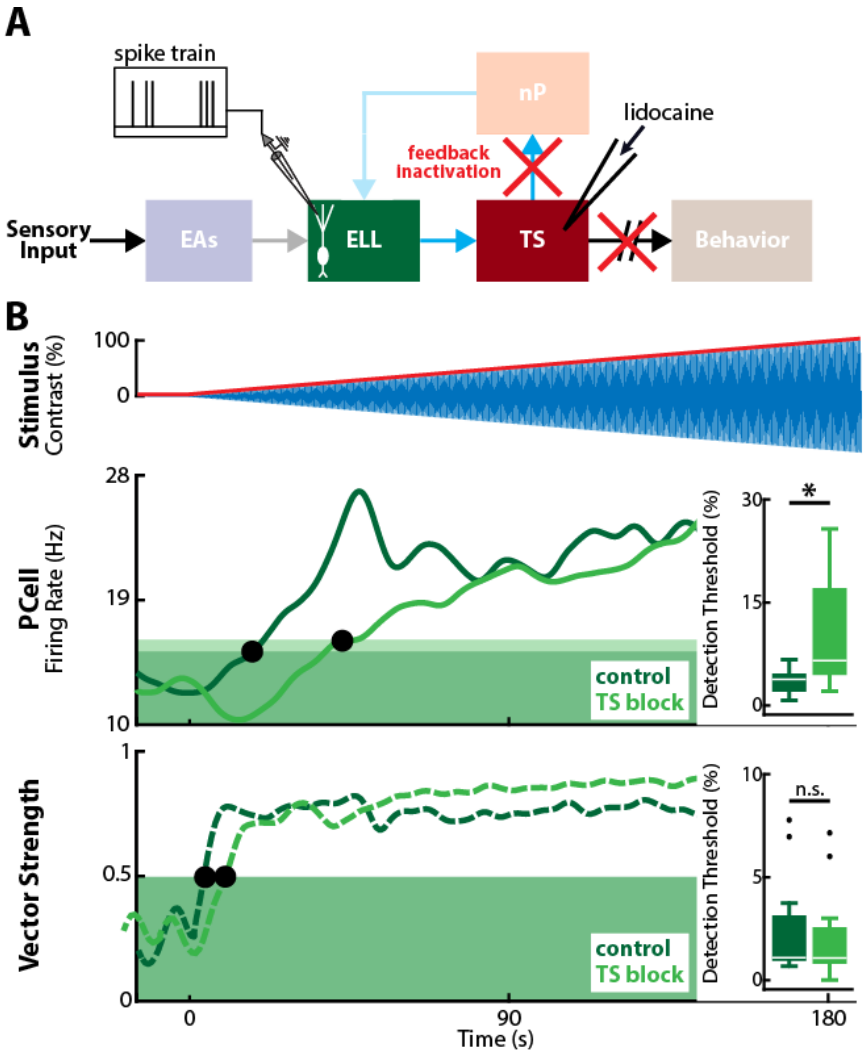

Supplementary Figure 5. Inactivating the direct feedback pathway by injecting Lidocaine into TS significantly increases firing rate detection thresholds but does not affect phase locking detection

thresholds. A) Relevant anatomy diagram showing the main brain areas considered. Lidocaine was injected in TS while recordings were made from individual PCells within the contralateral ELL. B) Top: example firing rate responses to increasing contrast (top) from an example ELL pyramidal neuron (dark green) and after (light green) Lidocaine injection. Bottom: example time-varying vector strength responses to increasing contrast (top) from the same ELL pyramidal neuron (dark green) and after (light green) unilateral Lidocaine injection into the contralateral TS. We found that firing rate detection thresholds significantly increased after Lidocaine application (middle inset, control: 3.6±0.5%; Lidocaine: 13.6±4.9%, Wilcoxon sign rank test, n = 12, N = 5 fish, $p = 4.88*10^{-4}$). In contrast, vector strength detection thresholds were not significantly altered by Lidocaine injections into the contralateral TS (bottom inset: control: 2.4±0.7%; Lidocaine: 2.1±0.7%, Wilcoxon sign rank test, n = 12, p = 0.42). We note that these results are qualitatively similar to those obtained by injecting Lidocaine into nP thereby blocking STCells (compare with Fig. 5). "ns" indicates no significant difference.

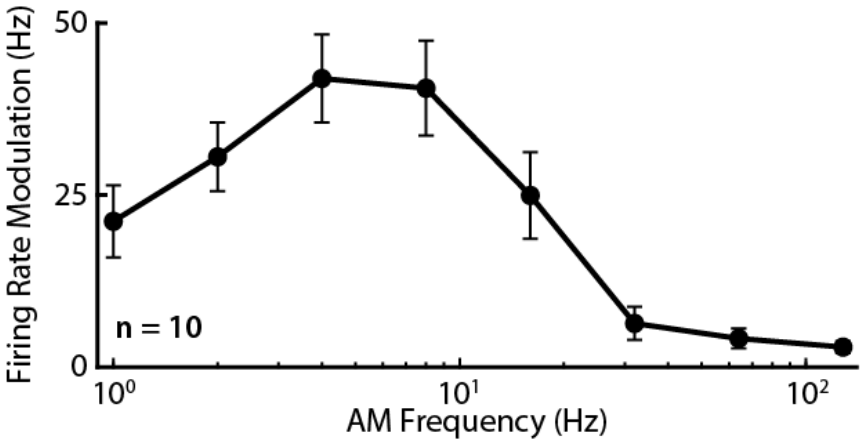

Supplementary Figure 6. Identifying nP stellate cells based on previous characterization. Response profile of our nP stellate cell population (n = 10) to different sinusoidal AM frequencies. The firing rate modulation peaks around 4-8 Hz and is negligible for AM frequencies > 32 Hz. This is similar to that reported previously for stellate cells (Bratton and Bastian, 1990) and strongly differs from properties of other neuron types within nP (Bastian and Bratton, 1990).

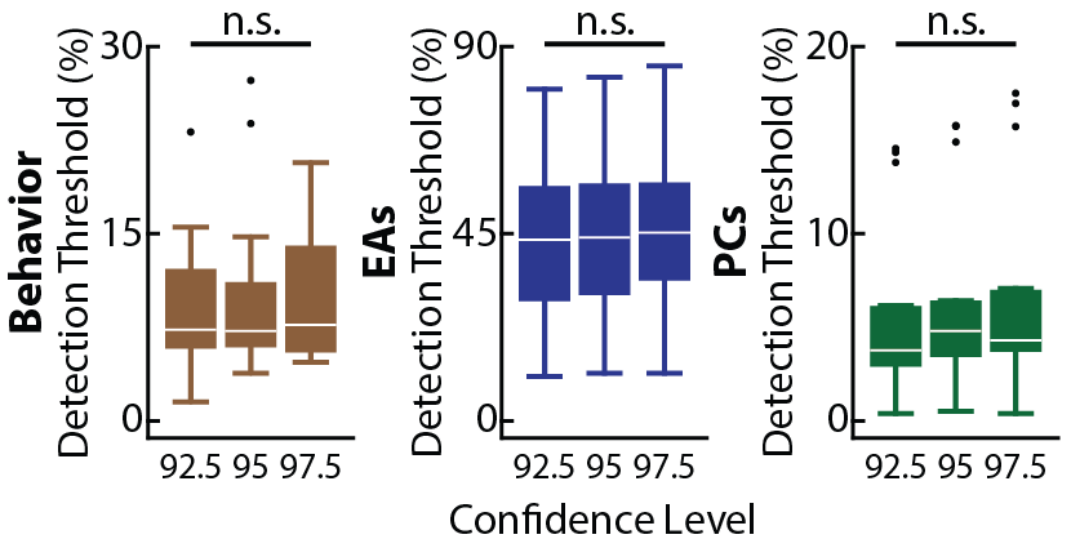

Supplementary Figure 7. Detection threshold values are similar for different response levels. No significant differences were seen for behavior (brown, left), EAs (blue, middle), and PCells (green, right) when altering the significance level (Kruskal-Wallis, df = 2; Behavior: p = 0.99; EAs: p = 0.99; PCells: p > 0.66 with Bonferroni correction).

Supplementary Figures for Chapter 5

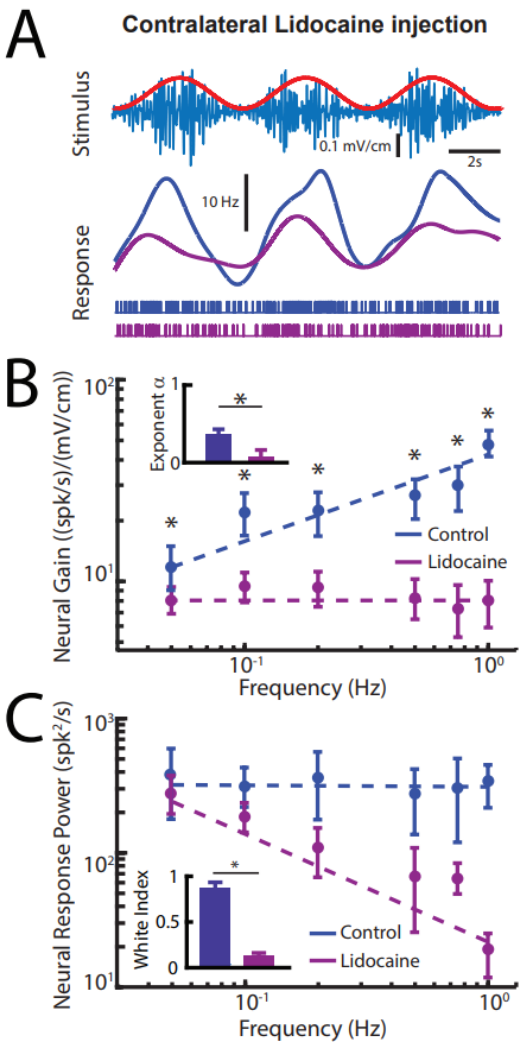

Supplementary Figure 1. Unilateral injection of lidocaine in contralateral nP gives rise to effects qualitatively similar to those observed when injecting bilaterally. A) Top: stimulus waveform showing the noisy AM (blue) and its sinusoidal envelope (red). Middle: Time dependent firing rate in response to the stimulus from a typical ELL pyramidal cell before (blue) and after (purple) contralateral lidocaine application. Bottom: spiking activity from this same neuron in response to stimulation before (blue) and after (purple) lidocaine application. B) Population-averaged neural gain to sinusoidal envelopes as a function of frequency before (blue) and after (purple) lidocaine application. The dashed lines show the best power law fits to the data. Inset: Exponent before (blue) and after (purple) lidocaine application ($p = 0.0039$, Wilcoxon Signed-Rank Test). C) Population-averaged neural response power before (blue) and after (purple) lidocaine application. The dashed lines show the best power law fits to the data. Inset: White index for neural response power before (blue) and after (purple) lidocaine application ($p = 0.0156$, Wilcoxon Signed-Rank Test).

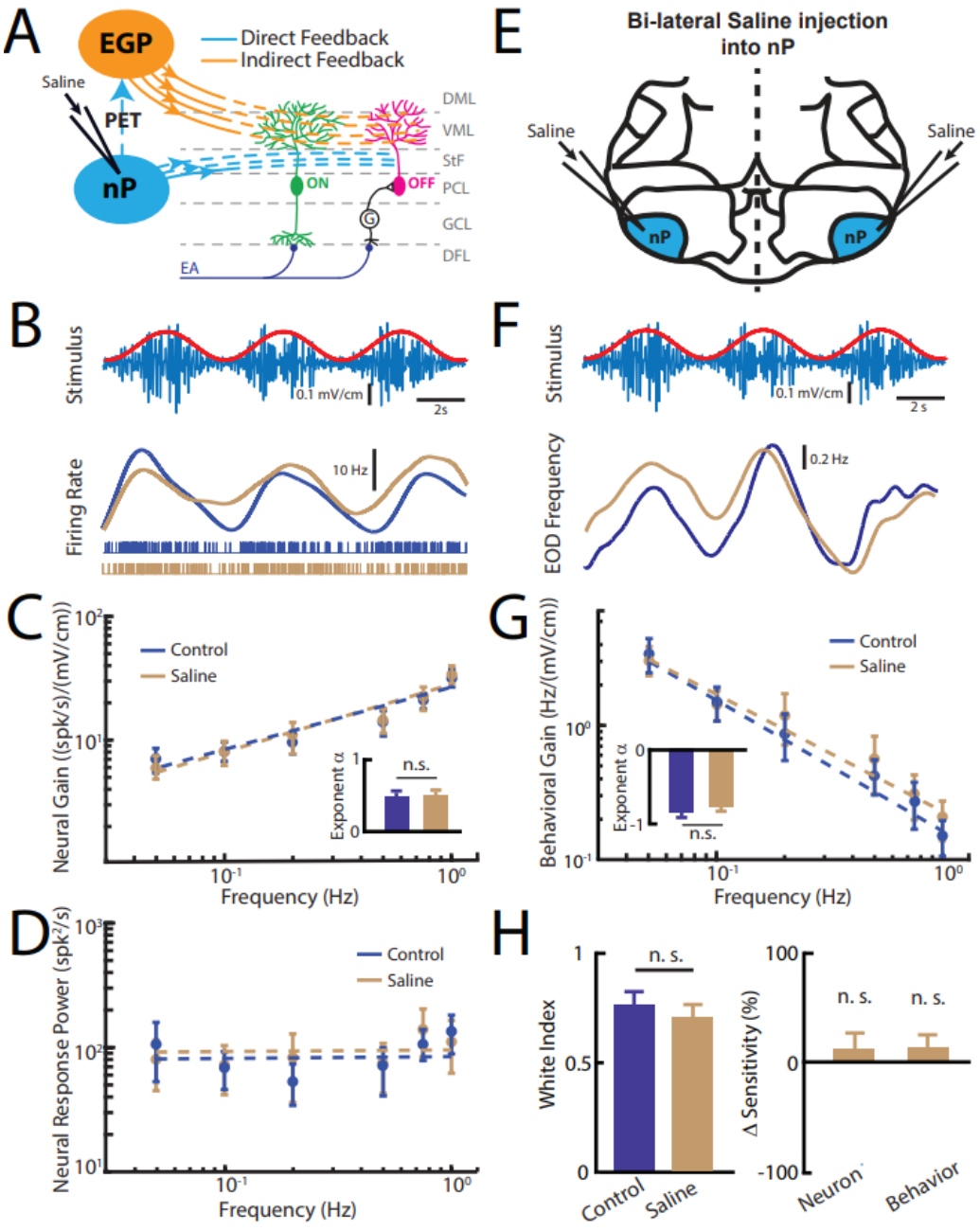

Supplementary Figure 2. Saline injection has no effect on ELL pyramidal cell tuning properties and optimized coding of natural stimuli. A) Schematic showing the relevant ELL anatomy. Data obtained from ELL pyramidal neurons were pooled as there is no difference in envelope response between ON- and OFF-type pyramidal cells (Huang and Chacron, 2016). Saline injection was performed into nP. B) Top: stimulus waveform showing the noisy AM (blue) and its sinusoidal envelope (red). Middle: Time dependent firing rate in response to the stimulus from a typical ELL pyramidal cell before (blue) and after (brown) saline application. Bottom: spiking activity from this same neuron in response to stimulation before (blue) and after (brown) saline application. C) Population-averaged neural gain to sinusoidal envelope stimulation as a function of frequency before (blue) and after (brown) saline application. The dashed lines show the best power law fits to the data. Inset: Exponent before (blue) and after (brown) saline injection. No

significant changes were observed (p = 0.641 Wilcoxon Signed-Rank Test). D) Population-averaged neural response power before (blue) and after (brown) saline application. The dashed lines show the best power law fits to the data. E) Schematic showing bilateral injection of saline during behavioral experiments. F) Top: stimulus waveform showing the noisy AM (blue) and its sinusoidal envelope (red). Bottom: Time dependent EOD frequency in response to the stimulus from a typical fish before (blue) and after (brown) saline application. G) Population-averaged behavioral gain to sinusoidal envelopes as a function of frequency before (blue) and after (brown) saline application. The dashed lines show the best power law fits to the data. Inset: Exponent before (blue) and after (brown) saline injection. No significant changes were observed (p = 0.938, Wilcoxon Signed-Rank Test). H) Left: population-averaged white index before (blue) and after (brown) saline application. No significant changes were observed (p = 0.547, Wilcoxon Signed-Rank Test). Right: population-averaged relative changes in neural and behavioral sensitivities following saline application. No significant changes were observed (neuron: p = 0.710, Wilcoxon Signed-Rank Test, behavior p = 0.750, Wilcoxon Signed-Rank Test). "n. s." indicates no significant difference.

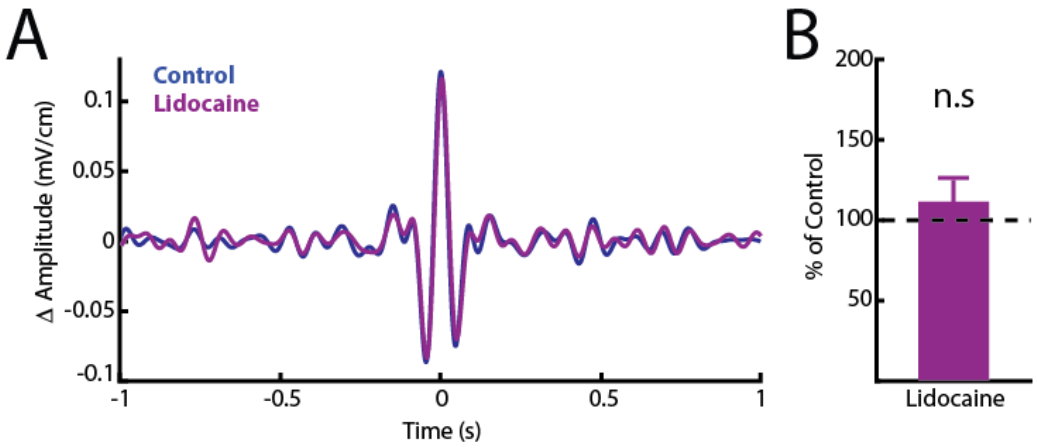

Supplementary Figure 3. Bilateral lidocaine injection does not affect ELL pyramidal cell responses to AMs. A) Spike-triggered average (STA) of the noisy AM stimulus waveform before (blue) and after (purple) bilateral lidocaine injection from an example ELL pyramidal cell. B) Population-averaged STA amplitudes before and after injection were not significantly different from one another (p = 0.469, Wilcoxon Signed-Rank Test).

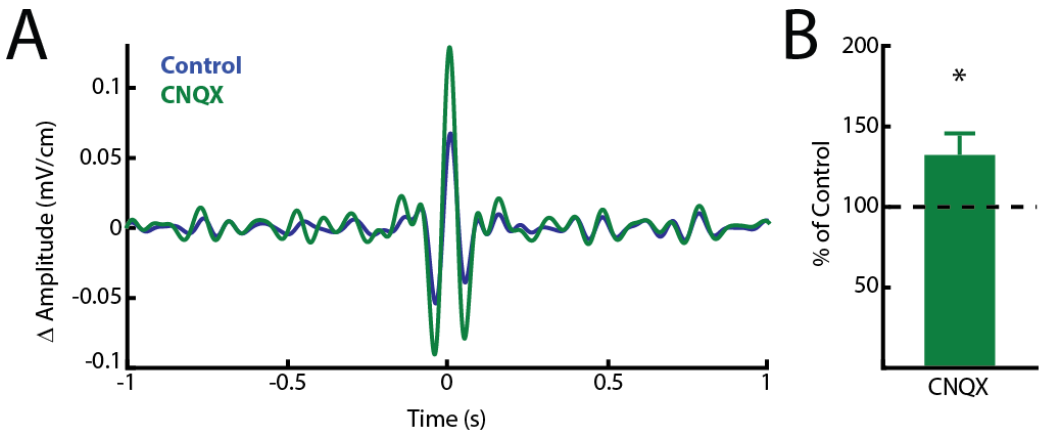

Supplementary Figure 4. CNQX injection increases ELL pyramidal cell responses to AMs, consistent with previous results (Bastian et al., 2004; Clarke and Maler, 2017). A) Spike-triggered average (STA) of the noisy AM stimulus waveform before (blue) and after (green) CNQX injection from an example ELL pyramidal cell. B) Population-averaged STA amplitude was significantly lower before CNQX injection (p = 0.008, Wilcoxon Signed-Rank Test).

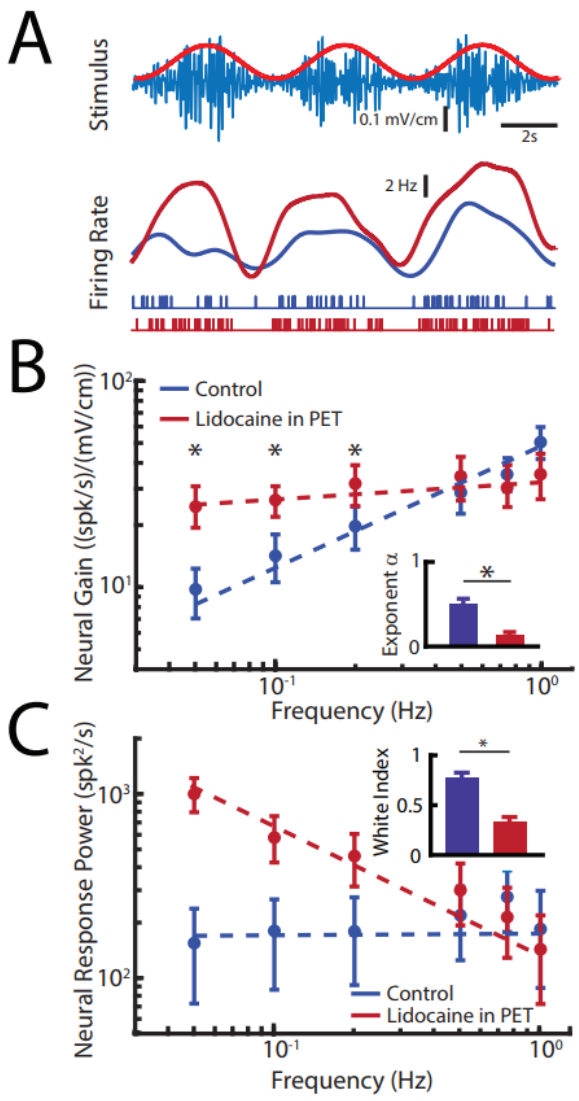

Supplementary Figure 5. Lidocaine injection within the PET gives rise to effects on ELL pyramidal cell responses to envelopes that are qualitatively similar to those observed when injecting CNQX. A) Top: stimulus waveform showing the noisy AM (blue) and its sinusoidal envelope (red). Middle: Time dependent firing rate in response to the stimulus from a typical ELL pyramidal cell before (blue) and after (red) PET lidocaine injection. Bottom: spiking activity from this same neuron in response to stimulation before (blue) and after (red) PET lidocaine injection. B) Population-averaged neural gain to sinusoidal envelopes as a function of frequency before (blue) and after (red) PET lidocaine injection. The dashed lines show the best power law fits to the data. Inset: Exponent before (blue) and after (red) lidocaine injection (p = 0.0039, Wilcoxon Signed-Rank Test). C) Population-averaged neural response power before (blue) and after (red) PET lidocaine injection. The dashed lines show the best power law fits to the data. Inset: White index for neural response power, p = 0.0273, Wilcoxon Signed-Rank Test).

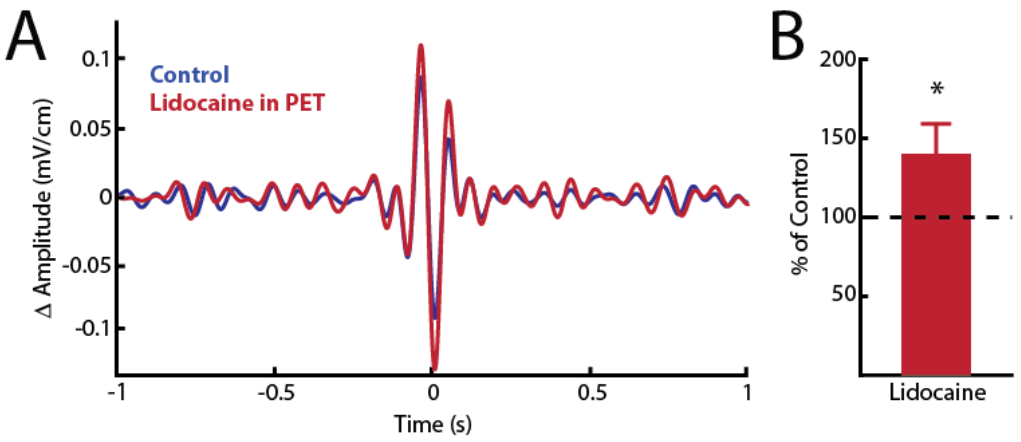

Supplementary Figure 6. PET lidocaine injection increases ELL pyramidal cell responses to AMs, consistent with previous results (Bastian, 1986a). A) Spike-triggered average (STA) of the noisy AM stimulus waveform before (blue) and after (red) PET lidocaine injection from an example ELL pyramidal cell. B) Population-averaged STA amplitude was significantly lower before PET lidocaine injection (p = 0.0391, Wilcoxon Signed-Rank Test).

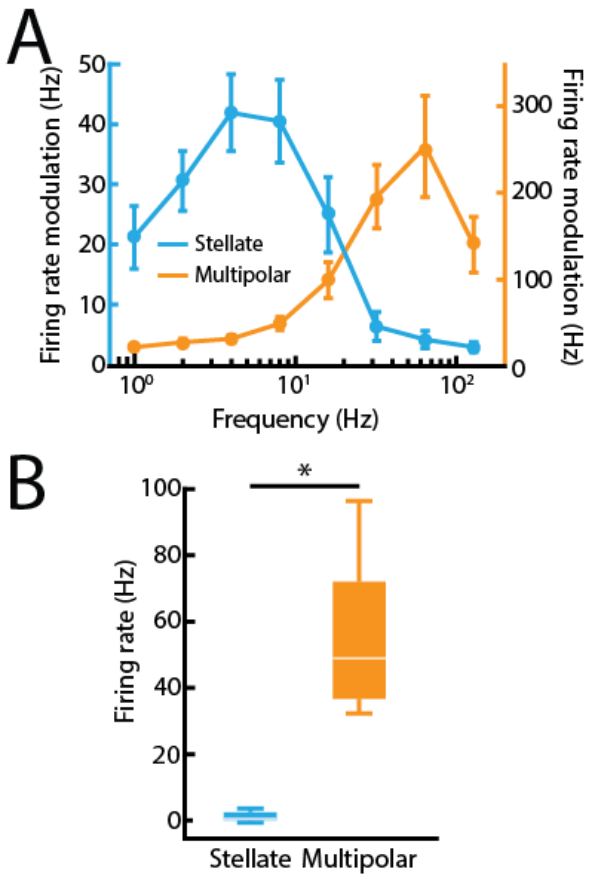

Supplementary Figure 7. nP stellate and multipolar cells have different electrophysiological properties. A) Cyan: AM frequency tuning curve for nP stellate cells. Note that the tuning curve rapidly drops off at higher frequencies >32 Hz due to a lack of responses to those frequencies. Orange: AM frequency tuning curve for nP multipolar cells. Note that the multipolar cells in contrast respond to the higher frequencies >32 Hz. The tuning curves are in agreement with previous studies. B) Whisker-boxplot of baseline firing rate distribution of stellate (cyan) and multipolar (orange) cells recorded from. Note that multipolar cells have significantly higher baseline firing rates than stellate cells ($\chi^2 = 12$, $p = 5.32*10^{-4}$, Kruskal-Wallis ANOVA). Overall, values were in agreement with those of previous studies (Bastian and Bratton, 1990; Bratton and Bastian, 1990). "" indicates statistical significance at the p = 0.05 level.*